





# Density Functional Studies of Transition-Metal Catalyzed Reactions

Inaugural – Dissertation

zur

Erlangung des Doktorgrades der  
Mathematisch-Naturwissenschaftlichen Fakultät  
der Heinrich-Heine-Universität Düsseldorf

vorgelegt von

Debasis Koley

aus Uttarpara (Indien)

Düsseldorf 2005

Gedruckt mit der Genehmigung der Mathematisch-Naturwissenschaftlichen Fakultät der  
Heinrich-Heine Universität Düsseldorf

Referent: Univ.-Prof. Dr. Walter Thiel

Korreferentin: Univ.-Prof. Dr. Christel Marian

Tag der mündlichen Prüfung:

09.11.2005

## Abstract

Density functional theory (DFT) has been used to study the mechanism of three transition-metal catalyzed reactions: Suzuki cross-coupling, Heck olefination, and zirconocene-mediated olefin polymerization. The DFT calculations generally employed the BP86 functional, basis sets of medium size, and a small-core pseudopotential for the metal. Full catalytic cycles were computed, with complete optimization of all intermediates and transition states.

The standard Suzuki cross-coupling reaction starts with an oxidative addition of an aryl halide to a palladium(0) catalyst. The calculations confirm the presence of three-coordinate anionic palladium(0) species as proposed by Amatore and Jutand, but do not provide any evidence for the existence of the postulated five-coordinate palladium(II) complexes. Instead the decisive intermediate is a four-coordinate structure, with linear coordination of the aryl halide *via* a hypervalent halogen atom, which can then rearrange without significant barriers to enter a catalytic cycle dominated by *cis*-configured palladium(II) complexes.

For the Suzuki cross-coupling between phenyl boronic acid and acetic anhydride, multiple interconnected catalytic cycles have been studied that start from the neutral  $\text{Pd}(\text{PMe}_3)_2$  molecule, the two-coordinate anionic  $[\text{Pd}(\text{PMe}_3)\text{OAc}]^-$  complex, and the three-coordinate anionic  $[\text{Pd}(\text{PMe}_3)_2\text{OAc}]^-$  complex. The initial oxidative addition is easier on the anionic pathways because of the higher propensity to coordinate to carbon electrophiles. There are two competing pathways for the subsequent transmetalation step, both of which involve anionic palladium(II) monophosphine complexes, with *cis* or *trans* arrangement of the acetate ligands. The final reductive elimination step is rather facile in each case. Overall, the anionic pathways are favored over the neutral pathways in the chosen model system.

Palladium(0) complexes of Staab-type proton sponges derived from quino[7,8-*h*]quinolines have recently been identified as excellent catalysts for Heck olefination. These proton sponges have been characterized computationally with regard to structure, basicity, electronic properties, and complexation by palladium(II) and palladium(0). The catalytic activity of the palladium(0) complexes in Heck olefination reactions is consistent with the computed relative energies of the intermediates in a plausible catalytic cycle.

A previously proposed single-center, two-state kinetic model for zirconocene-catalyzed ethylene polymerization has been explored computationally by considering different conformers and isomers of the propyl group in the cations  $[\text{L}_2\text{Zr-Pr}]^+$  ( $\text{L}=\text{Cp}$ ,  $\text{Cp}^*$ ;  $\text{Pr} = n\text{-propyl}$ ) corresponding to two catalysts with different observed rate orders. The calculations suggest that equilibria involving such conformers and isomers cannot account for the requirements of this kinetic model, implying that interactions with counterions would need to be considered.

For all three investigated types of reaction, the DFT calculations provide detailed mechanistic insight. The computational results for the Suzuki cross-coupling reactions call for a reevaluation of some commonly accepted mechanistic notions.



## Zusammenfassung

Mit Hilfe der Dichtefunktionaltheorie (DFT) ist der Mechanismus von drei Übergangsmetall-katalysierten Reaktionen untersucht worden: Suzuki-Kupplung, Heck-Olefinierung und Olefin-Polymerisierung. Bei den DFT Rechnungen wurden in der Regel das BP86 Funktional, mittelgroße Basissätze und ein Pseudopotential am Metallatom verwendet. Meist wurden komplette katalytische Zyklen berechnet, mit vollständiger Optimierung aller Intermediate und Übergangszustände.

Die normale Suzuki-Kupplungsreaktion beginnt mit der oxidativen Addition eines Arylhalogenids an einen Palladium(0)-Katalysator. Die Rechnungen bestätigen, dass dabei dreifach koordinierte anionische Palladium(0)-Spezies auftreten, wie von Amatore und Jutand vorgeschlagen, sie geben jedoch keinerlei Hinweise auf die Existenz der postulierten fünffach koordinierten Palladium(II)-Komplexe. Stattdessen findet man als entscheidendes Intermediat eine vierfach koordinierte Spezies, mit einer linearen Anordnung des Arylhalogenids über ein hypervalentes Halogenatom, welche dann ohne signifikante Barrieren umlagern und in einen katalytischen Zyklus mit vorwiegend *cis*-konfigurierten Palladium(II)-Komplexen übergehen kann.

Für die Suzuki-Kupplung zwischen Phenylboronsäure und Acetanhydrid sind mehrere, untereinander vernetzte katalytische Zyklen untersucht worden, die vom neutralen  $\text{Pd}(\text{PMe}_3)_2$  Molekül, vom zweifach koordinierten  $[\text{Pd}(\text{PMe}_3)\text{OAc}]^-$  Anion und vom dreifach koordinierten  $[\text{Pd}(\text{PMe}_3)_2\text{OAc}]^-$  Anion ausgehen. Die anfängliche oxidative Addition ist in den anionischen Systemen einfach möglich, weil diese eine hohe Affinität zu Elektrophilen aufweisen. Für die folgende Transmetallierung findet man zwei konkurrierende Reaktionswege, bei denen jeweils anionische Palladium(II)-Monophosphin-Komplexe auftreten, mit *cis* oder *trans* Anordnung der Acetat-Liganden. Die abschliessende reduktive Eliminierung verläuft in allen Fällen relativ leicht. Insgesamt sind in dem gewählten Modellsystem die anionischen gegenüber den neutralen Reaktionspfaden bevorzugt.

Palladium(0)-Komplexe von Protonschwämmen des Staab-Typs, welche sich vom 4,9-Dichlorchino[7,8-*h*]chinolin herleiten, haben sich als exzellente Katalysatoren für die Heck-Olefinierung erwiesen. Diese Verbindungen sind mittels DFT Rechnungen charakterisiert worden, im Hinblick auf Struktur, Basizität, elektronische Eigenschaften und Komplexierung mit Palladium(II) und Palladium(0). Eine katalytische Aktivität der Palladium(0)-Komplexe bei der Heck-Olefinierung steht im Einklang mit den berechneten relativen Energien von Intermediaten in einem plausiblen katalytischen Zyklus.

Ein literaturbekanntes Einzentren-Zweizustands-Modell für die Kinetik der Zirconocen-katalysierten Ethen-Polymerisation ist durch DFT-Rechnungen an Konformeren und Isomeren der Kationen  $[\text{L}_2\text{Zr-Pr}]^+$  ( $\text{L}=\text{Cp}$ ,  $\text{Cp}^*$ ;  $\text{Pr} = n$ -propyl) überprüft worden, welche als aktive Spezies für zwei Katalysatoren ( $\text{L}=\text{Cp}$ ,  $\text{Cp}^*$ ) mit experimentell unterschiedlichen Reaktionsordnungen angesehen werden. Die Rechnungen deuten darauf hin, dass Gleichgewichte zwischen solchen Konformeren und Isomeren nicht die in dem kinetischen Modell verlangten Bedingungen erfüllen, so dass man auch Wechselwirkungen mit Gegenionen berücksichtigen muss.

Bei allen untersuchten Reaktionstypen vermitteln die durchgeführten DFT Rechnungen detaillierte mechanistische Einblicke. Die erhaltenen Ergebnisse für die Suzuki-Reaktion legen die Überprüfung und Revision einiger mechanistischer Vorstellungen nahe.





*We have a habit in writing articles published in scientific journals to make the work as finished as possible, to cover all the tracks, to not worry about the blind alleys or describe how you had the wrong idea first, and so on. So there isn't any place to publish, in a dignified manner what you actually did in order to do the work....*

(Richard Feynmann, In the Nobel Foundation, *Nobel Lectures*, Physics 1963-1970

Nobel Lecture, 11 December **1965**.)

*To my didama, ma, and bapi.*

## ACKNOWLEDGEMENTS

I would like to express my profound gratefulness to Prof. Dr. Walter Thiel, for providing me the opportunity and support to carry out research in a most intriguing and inspiring field of science. I am highly indebted for his amicable and candid attitude, his help and accessibility for discussions and his encouragement.

I am also grateful to Prof. Dr. C. Marian for kindly accepting to act as co-referee for this thesis.

I convey my earnest regards to Prof. Dr. Lukas Gooßen for introducing me to a most captivating and enthralling project on mechanistic studies of palladium chemistry. I am also grateful to Prof. Dr. Vidar Jensen for his kind behavior and patience to unfold and comprehend the underlying chemistry in metallocene-catalyzed polymerization reactions.

It is my pleasure to thank my colleagues of the Thiel group for ensuring a sociable atmosphere with lots of excitement and stimulating discussions. Particularly, I would like to thank Dr. Michael Bühl, Dr. Holger Hermann, Dr. Sergei Vyboishchikov, Dr. Klaus Angermund, Dr. Hans Martin Senn, and Dr. Jürgen Breidung for scientific help and advice.

Special thanks go to Nikolaj, Martin, Uli, Marco, Maya and Aiping for lots of fun with unscientific, hilarious discussions. My special regards are conveyed to Jens Paetzold and Lars Winkel for providing a helping hand during my lab work.

My greatest gratitude is also conveyed to Masimoni, Shivaniji and Amritji for providing me with hand made, delicious, appetizing Indian dishes which I missed a lot.

I thank the computer department of the MPI Mülheim, especially Horst Lenk, Mr. Boll and Mr. Angenendt, for help in solving hardware and software problems. Thanks to Axel for helping me to install the graphic card in my notebook and his most friendly behavior and attitude.

I am obliged to the Max-Planck-Gesellschaft and Deutsche Forschungsgemeinschaft for financial support during my research tenure.







## Contents

### **Chapter 1.** Introduction

1.1	Suzuki cross-coupling.....	1
1.2	Palladium complexes of proton sponges as catalysts in Heck olefination.....	3
1.3	Olefin polymerization.....	5
1.4	Quantum mechanical methods.....	7
1.4.1	<i>Ab Initio</i> Theory.....	7
1.4.2	Density Functional Theory.....	10
1.5	Geometry optimization.....	13
1.5.1	Minima.....	13
1.5.2	Transition States.....	13
1.5.3	Intrinsic Reaction Coordinates.....	14
1.6	Continuum Solvation Models.....	14
1.7	Population analysis.....	16
	<b>Bibliography</b> .....	19

### **Chapter 2.** Mechanistic Pathways for Oxidative Addition of Aryl Halides to Palladium(0) Complexes: A DFT Study.

2.1	Introduction.....	27
2.2	Computational Details.....	31
2.3	Results and Discussion.....	32
2.3.1	Catalytically active species.....	32
2.3.2	The coordination of aryl halides to palladium(0) species.....	35
2.3.3	The mechanism of oxidative addition to anionic palladium(0) species.....	39
2.3.4	The cleavage of the carbon-iodine bond: Path A.....	44
2.3.5	The cleavage of the carbon-iodine bond: Path B.....	48
2.4	<i>Cis-trans</i> isomerization.....	49

2.5	Conclusions.....	54
2.6	Supporting Information.....	56
	<b>Bibliography.....</b>	<b>58</b>
 <b>Chapter 3.</b> The Palladium-Catalyzed Cross-Coupling Reactions of Carboxylic Anhydrides with Arylboronic Acids: A DFT Study.		
3.1	Introduction.....	65
3.2	Computational Details.....	69
3.3	Results.....	70
3.3.1	Oxidative addition and ligand exchange.....	70
3.3.1.1	Neutral cycle.....	70
3.3.1.2	Anionic cycle.....	74
3.3.2	Transmetalation.....	78
3.3.3	Reductive elimination.....	81
3.3.3.1	Neutral cycle.....	82
3.3.3.2	Anionic cycle.....	85
3.4	Discussion and Conclusion.....	87
3.5	Supporting Information.....	91
	<b>Bibliography.....</b>	<b>103</b>
 <b>Chapter 4.</b> Palladium Monophosphine Intermediates in Catalytic Cross-Coupling Reactions: A DFT Study.		
4.1	Introduction.....	109
4.2	Computational Details.....	113
4.3	Results.....	114
4.3.1	Outline of the catalytic cycles.....	114
4.3.2	Oxidative addition and ligand exchange starting from the anionic monophosphine complex <b>19</b> .....	116
4.3.3	Oxidative addition starting from the anionic diphosphine complex <b>1</b> .....	121



4.3.4	An alternative transmetalation pathway.....	123
4.3.5	Reductive elimination under formation of the anionic monophosphine complex.....	126
4.4	Discussion and Conclusions.....	130
4.5	Supporting Information.....	136
	<b>Bibliography.....</b>	<b>146</b>
<b>Chapter 5.</b>	<b>Density Functional Study of Proton Sponges: Proton Affinity, Structural Behavior and Palladium Complexes.</b>	
5.1	Introduction.....	153
5.2	Computational Details.....	155
5.3	Results and Discussion.....	156
5.3.1	Ligands.....	156
5.3.1.1	Structural features.....	156
5.3.1.2	Conjugate acids and proton affinity.....	159
5.3.1.3	Strain energy.....	163
5.3.1.4	Bader analysis.....	165
5.3.2	Complexes.....	167
5.3.2.1	Palladium(II) complexes.....	167
5.3.2.2	Palladium(0) complexes.....	169
5.3.3	Heck olefination by palladium(0) complexes.....	171
5.3.3.1	Oxidative addition.....	173
5.3.3.2	Coordination of styrene.....	173
5.3.3.3	Insertion.....	174
5.3.3.4	$\beta$ -Hydride elimination.....	175
5.3.3.5	Discussion.....	176
5.4	Conclusions.....	178
5.5	Supporting Information.....	180

<b>Bibliography</b> .....	186
<b>Chapter 6.</b> DFT Investigation of the Single-Center, Two-State Model for the Broken Rate Order of Transition Metal Catalyzed Olefin Polymerization.	
6.1     Introduction.....	193
6.1.1     The single-center, two-state model.....	195
6.1.2     The strategy.....	195
6.2     Computational Details.....	197
6.3     Results and Discussion.....	199
6.3.1     Primary alkyl cations.....	199
6.3.2     Frontside olefin coordination and insertion.....	202
6.3.3     Backside olefin coordination and insertion.....	206
6.3.4     Comparison to the single-center, two-state model.....	208
6.3.5     Comparison to experiment.....	209
6.3.6     Isomerization of the primary alkyl cations.....	210
6.4     Conclusion.....	215
6.5     Supporting Information.....	216
<b>Bibliography</b> .....	219
<b>Chapter 7.</b> Regiocontrolled Ru-catalyzed addition of carboxylic acids to alkynes: practical protocols for the synthesis of vinyl esters.	
7.1     Introduction.....	231
7.2     Mechanism.....	236
7.3     Conclusion.....	239
7.4     Experimental Section.....	240
<b>Bibliography</b> .....	250
<b>Chapter 8.</b> Summary	
List of Abbreviations and Symbols	





## INTRODUCTION

*No science has ever made more rapid progress in a shorter time than chemistry.*

(Martin Heinrich Kloppe, 1791, First Professor of Chemistry at the University of Berlin)

Few other fields in chemistry have developed as rapidly as organometallic chemistry in the past two decades. Transition-metal catalyzed reactions provide an ever increasing arsenal of versatile transformations for chemical synthesis, and there are numerous experimental and theoretical investigations that attempt to explore and understand the underlying mechanisms. In this thesis I have employed computational methods, in particular density functional theory (DFT), to study three classes of organometallic reactions, namely Suzuki cross-coupling, Heck olefination, and zirconocene-catalyzed olefin polymerization. This chapter gives an introductory overview over these three areas and outlines the applied computational methods.

### 1.1 Suzuki cross-coupling

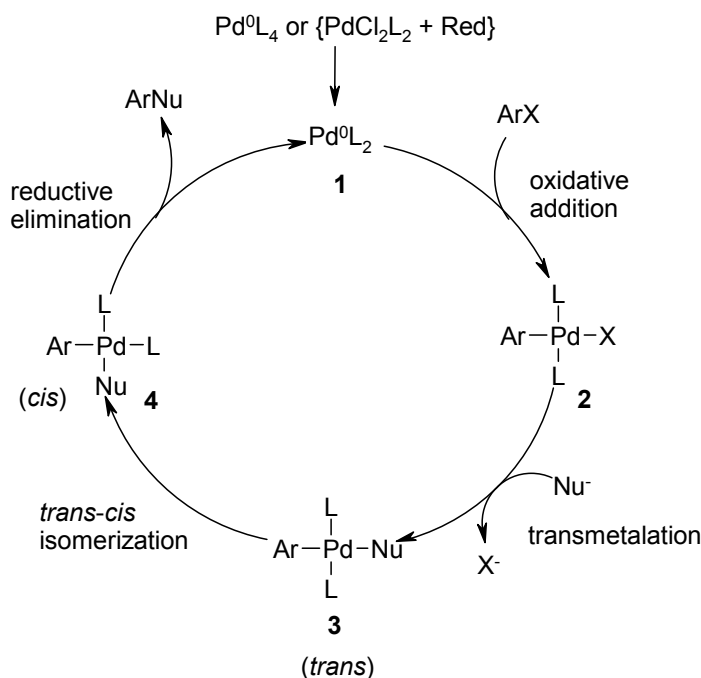
The palladium-catalyzed cross-coupling reaction between organoboron compounds and aryl halides or triflates is widely known as Suzuki-Miyaura coupling. It provides a powerful and general methodology for the formation of C—C bonds in organometallic chemistry.[1] A general catalytic cycle for the cross-coupling reaction of organometallics, which involves oxidative addition-transmetalation-isomerization-reductive elimination sequences, is depicted in Scheme 1.1.

Oxidative addition is often the rate-determining step in this catalytic cycle. The relative reactivity depends on the nature of X in the aryl substrate and decreases in the order of  $I > OTf > Br \gg Cl$ . A wide range of palladium(0) catalysts or precursors can be used for cross-coupling reactions.  $Pd(PPh_3)_4$  is most commonly employed, but  $PdCl_2(PPh_3)_2$  and  $Pd(OAc)_2$  in combination with  $PPh_3$  or other phosphine ligands are also efficient since they are stable to air and can readily be reduced to the active palladium(0) complexes.[2] The oxidative addition step has been investigated thoroughly both from the experimental and theoretical side. According to the classical mechanism (Scheme 1.1) aryl halides add oxidatively to coordinatively unsaturated  $Pd^0L_2$  complexes. This simple concept has recently been challenged by experimental findings that counterions of the palladium(II) precatalysts and added metal

salts exert a significant influence on catalytic activity, and mechanistic alternatives have been proposed that take such counterions into account and involve five-coordinate intermediates.[3] We have therefore studied the mechanism for oxidative addition of aryl halides to palladium(0) complexes by detailed DFT calculations and found a new pathway that has not been considered before (Chapter 2).

The subsequent transmetalation step is less well understood. The reaction mixtures are quite complex because they contain not only the reactants, but also bases, coordinating solvent, and sometimes further additives.[1] The ease of transmetalation depends on the chosen organometallic system and reaction conditions, and it has been reported that the addition of sodium hydroxide or other bases has a remarkable effect on the transmetalation rate of organoboron reagents with metal halides.[4,5,6]

**Scheme 1.1. Generalized mechanism for palladium(0) catalyzed cross-coupling reaction.**



Given the overall complexity of Suzuki cross-coupling reactions, the lack of theoretical studies on their mechanism is not surprising. We have chosen to focus not on the classic Suzuki biaryl synthesis with aryl halides, but on the conceptually very similar cross-coupling of carboxylic anhydrides with boronic acids which has been investigated experimentally by the Gooßen group in our institute. As smallest viable model system, we have selected the reaction of acetic anhydride with phenylboronic acid in the presence of a palladium(II) acetate/trimethylphosphine catalyst, where the acetate ion plays a triple role as leaving group, base, and counterion. For this model system, we have computed complete catalytic cycles (including oxidative addition, transmetalation, and reductive elimination). Chapter 3 reports

the results for the neutral  $\text{Pd}(\text{PMe}_3)_2$  and the anionic  $[\text{Pd}(\text{PMe}_3)_2\text{OAc}]^-$  catalyst, and Chapter 4 describes the cycle for the anionic monophosphine complex  $[\text{Pd}(\text{PMe}_3)\text{OAc}]^-$  as well as several interconnections between the catalytic cycles. Taken together, these calculations provide the first comprehensive mechanistic study of a cross-coupling reaction.

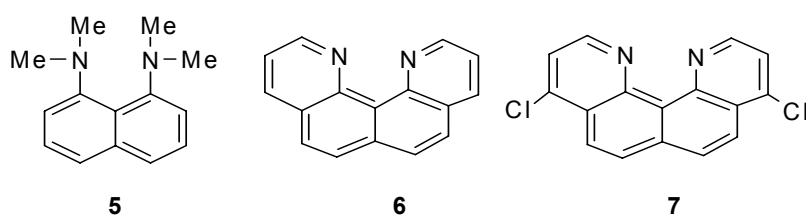
## 1.2 Palladium complexes of proton sponges as catalysts in Heck olefination

The success of organometallic chemistry is rooted in the opportunity to select and tailor the optimal ancillary ligands at the metal center for any given reaction or transformation. Strong organic bases are an efficient choice for ligands in various transition metal catalyzed transformations.

The design and synthesis of strong organic bases has long been an active field of research in organic chemistry.[7] With a  $\text{p}K_a$  value around 12, 1,8-*bis*(dimethylamino)naphthalene **5** (Scheme 1.2) is an exceptionally strong base, in comparison with other aromatic amines. It forms strong ionic complexes, with a cationic hydrogen bond  $[\text{N}-\text{H}\cdots\text{N}]^+$ , and is a prototypical example of so-called “proton sponges”. However, **5** is not a good choice as a ligand for transition metal complexes,[8] since the methyl groups shield the nitrogen atoms sterically, thereby reducing the thermodynamic stability of the complexes.

Staab *et al.*[9] prepared a different type of “proton sponge”, quino[7,8-*h*]quinoline **6**, which is a comparatively strong base with a  $\text{p}K_a$  value of 12.8. More recently, Wüstefeld *et al.*[10] synthesized the dichloro derivative **7** which can act as a unique ligand in metal complexes. The platinum and palladium complexes of **7** are highly stable and can be used as catalysts in various organometallic reactions.

### Scheme 1.2. The structures of various well known “proton sponges”

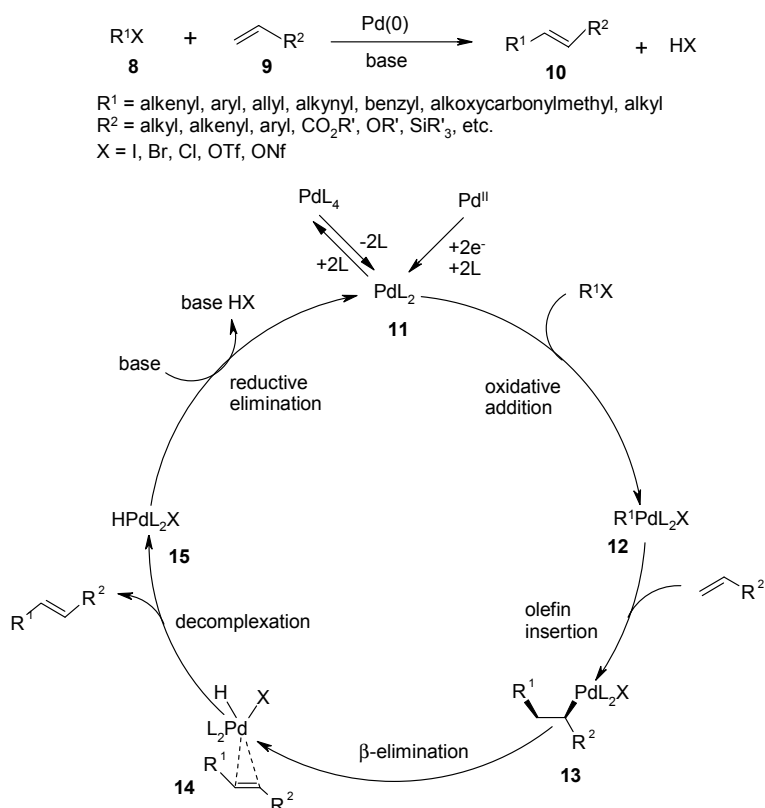


We have performed a thorough DFT study of these proton sponges (Scheme 1.2) to gain a better understanding of their structural and electronic properties. Chapter 5 summarizes the results and analyzes the high basicities of these compounds in terms of intramolecular hydrogen bonding in the conjugate acid, the relief of strain upon protonation and other factors. It also reports on the corresponding palladium(II) and palladium(0) complexes of **7** and related proton sponges, the latter being excellent catalysts for Heck reactions.[11,12]

Scheme 1.3 displays the currently accepted catalytic cycle for Heck olefination. A catalytically active, coordinatively unsaturated palladium(0) complex **11** is normally generated *in situ* from a stable palladium complex or salt such as  $\text{Pd}(\text{OAc})_2$ . After oxidative addition of an aryl or alkenyl halide or sulfonate[13] an electrophilic palladium(II) complex **12** is formed. Olefin insertion into the  $\text{Pd}-\text{R}^1$  bond leads to a  $\sigma$ -alkyl complex **13**. This complex normally undergoes a  $\beta$ -hydride elimination to give the  $\pi$ -alkene complex **14**, but side reactions are also possible.[14,15] Decomplexation of **14** affords the olefin product and the hydridopalladium species **15** which then regenerates the catalyst **11** by a base-induced reductive elimination, thus completing the catalytic cycle.

We have characterized the key intermediates in this cycle for the Heck reaction between phenylbromide and styrene using the palladium(0) complex of proton sponge **7** as the catalyst (Chapter 5).

### Scheme 1.3. Mechanism for Heck olefination





### 1.3 Olefin polymerization

After the discovery of the titanium chloride catalyzed polymerization of ethylene by Ziegler[16] and the stereoselective polymerization of propene by Natta,[17] a lot of effort has been spent to elucidate the mechanism of the Ziegler-Natta polymerizations of olefins.[18] Kaminsky *et al.*[19] discovered the first homogeneous Group-IV metallocene-based catalyst: dichlorozirconocene, when treated with a large excess of methylalumoxane (MAO), catalyzes the polymerization of ethylene to high-density polyethylene. Moreover, stereorigid racemic *ansa-bis*(indenyl)zirconium dichloride and ethyl-bridged fluorenylcyclopentadienylzirconium dichloride can each be activated by MAO to produce highly *isotactic*[20] and *syndiotactic*[21] polypropene, respectively, from propene. Experimental studies by Jordan have shown that the active species is cationic and monomeric.[22] The exact role of MAO is still under debate, but it is generally accepted that MAO acts first as a methylating agent and then as the anionic counterion in the reaction. In the basic Cossée-Arlman mechanism,[23] the approaching olefin binds to the vacant coordination site, forming a  $\pi$ -complex, and insertion takes place in a four-membered transition state, leading to a polymer chain with two more carbon atoms and a new vacant site for further olefin attack. Brookhart and Green[24] have refined this mechanism by taking the possible agostic interactions into account (Scheme 1.4)

The propagation rate law for a single-site Cossée mechanism is first-order with respect to catalyst concentration  $[C]$  and monomer concentration  $[M]$ :

$$R_p = k_p [C][M] \quad (1.5.0)$$

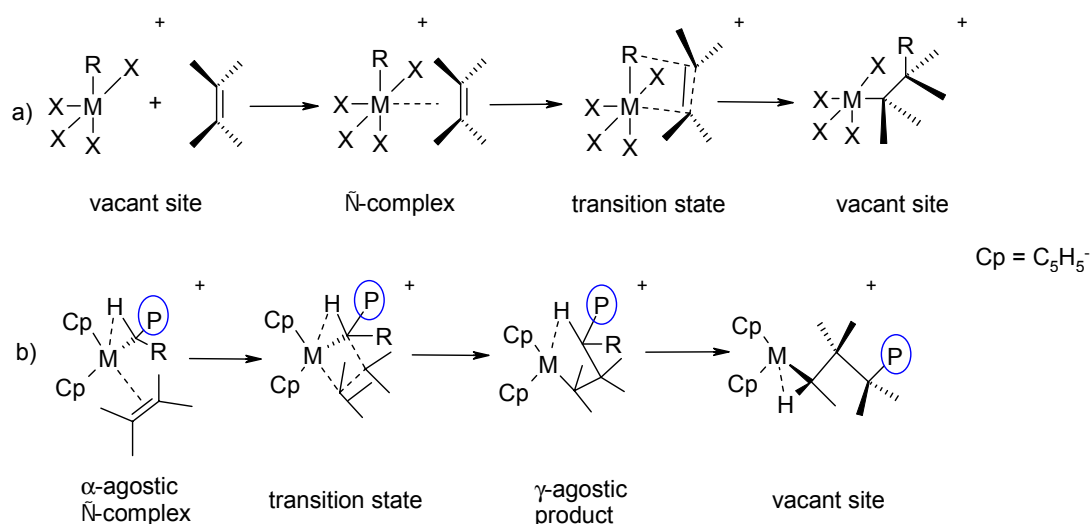
However, in many cases, eqn. (1.5.0) does not hold and the reaction rate order in  $[M]$  is higher than one for propene,[25] ethene,[26] styrene,[27] and diene[28] polymerization.

There are several kinetic models in the literature that may explain these observed broken rate orders, including the “trigger mechanism” by Ystenes[29] and the “single-center two-state catalyst” model by Fait *et al.*[25(b),30] In the latter, the catalyst is assumed to be in equilibrium between two states, and it is postulated that (a) the two states differ in their propagation rate constants (a faster propagating state  $C_{\text{fast}}$  and a slower one  $C_{\text{slow}}$ ), (b) the two states are interconverting and their interconversion does not involve the monomer, and (c) monomer insertion transforms a slow state into a fast one (Scheme 1.5). The propagation rate law according to this kinetic scheme will be:

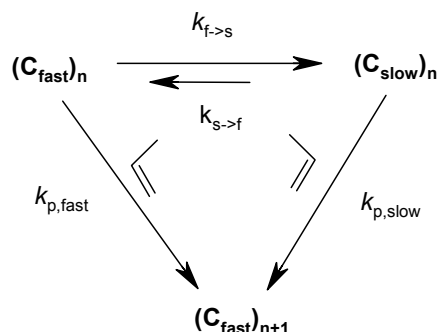
$$\frac{R_p}{[C]} = \frac{\left\{ \left( k_{f \rightarrow s} + \frac{k_{p,fast} k_{s \rightarrow f}}{k_{p,slow}} \right) [M] + k_{p,fast} [M]^2 \right\}}{\left( \frac{k_{f \rightarrow s} + k_{s \rightarrow f}}{k_{p,slow}} \right) + [M]} \quad (1.5.1)$$

Eqn. (1.5.1) reduces to a first-order rate law for  $k_{s \rightarrow f} \gg k_{f \rightarrow s}$ , or  $k_{p,slow} [M] \gg k_{f \rightarrow s}, k_{s \rightarrow f}$ , for which  $R_p \approx k_{p,fast} [C][M]$ . On the other hand we can have second-order kinetics with  $R_p \approx k_{p,fast} [C][M]^2$ , when  $k_{p,fast} [M] \gg k_{f \rightarrow s} \gg k_{p,slow} [M] \gg k_{s \rightarrow f}$ .

**Scheme 1.4. The Cossée-Arlman (a) and Brookhart-Green (b) mechanism**



**Scheme 1.5. Scheme for the interconversion of fast and slow centers**



Hence, a reaction order higher than 1 in monomer concentration is achieved when the slow state of the catalytic center is energetically more stable than the fast one and the

interconversion rate between the fast and the slow center is intermediate between their respective chain propagation rates.

We have performed a DFT study on different conformers and isomers of the alkyl cations  $[L_2Zr-Pr]^+$  ( $L = Cp, Cp^*$ ;  $Pr = n$ -propyl), corresponding to two catalysts with experimentally recorded rate orders ( $n$ ) for ethylene polymerization of different magnitudes, in order to explore the single-center, two-state kinetic model for olefin polymerization (Chapter 6).

## 1.4 Quantum mechanical methods

*To understand an observable means being able to predict, albeit qualitatively, the results that a perfectly reliable calculation would yield for that observable.*

(Roald Hoffmann, *Acc. Chem. Res.* **1971**, 4, pages 1-9)

### 1.4.1 *Ab Initio* Theory

Quantum methods are used for the theoretical investigation of molecular properties which depend on the electronic structure of the system. The basis of these methods is the time-independent nonrelativistic *Schrödinger equation*:<sup>[31]</sup>

$$H\Psi = E\Psi \quad (1.4.0)$$

where  $H$  is the Hamiltonian operator,  $E$  the energy and  $\Psi$  the wavefunction of the system under consideration. However, we have to make approximations to solve eqn. (1.4.0) either analytically or numerically for systems of interest.

The *Born-Oppenheimer* approximation<sup>[32]</sup> simplifies the general molecular problem by separating nuclear and electronic motions. This approximation is reasonable since the mass of a typical nucleus is thousands of times greater than that of an electron. The nuclei move very slowly with respect to the electrons, and the electrons react essentially instantaneously to changes in nuclear position. Thus, the electron distribution within a molecular system depends on the positions of the nuclei and not on their velocities. Hence the application of the *Born-Oppenheimer* approximation yields the electronic *Schrödinger equation*:

$$H_{el}\Psi_{el} = E_{el}\Psi_{el} \quad (1.4.1)$$

The electronic Hamiltonian operator of the system is defined as (in a.u.):

$$H_{el} = -\sum_{i=1}^N \frac{1}{2} \nabla_i^2 - \sum_{i=1}^N \sum_{A=1}^M \frac{Z_A}{r_{iA}} + \sum_{i=1}^N \sum_{j>i}^N \frac{1}{r_{ij}} \quad (1.4.2)$$

where the terms describe the kinetic energy of the electrons, the electron-nuclear interaction, and the electron-electron Coulomb repulsion, respectively. To obtain the total energy of the system within the *Born-Oppenheimer* approximation, we have to include the Coulombic nucleus-nucleus interaction term:

$$E_{tot} = E_{el} + \sum_{A=1}^M \sum_{B>A}^M \frac{Z_A Z_B}{R_{AB}} \quad (1.4.3)$$

A many-electron wavefunction can be approximated as Slater determinant, which is composed of one-electron functions, so-called spin-orbitals. With the assumption that each electron moves in the “effective field” due to the nuclei and N–1 electrons, the N-electron eigenvalue problem is reduced to N one-electron eigenvalue problems. Taking the orthogonality of the spin orbitals into account, we arrive at the *Hartree-Fock* equations (in canonical form):[33]

$$F\psi_i = \epsilon_i \psi_i \quad (1.4.4)$$

where  $F$  is an effective one-electron operator,  $\psi_i$  a spin-orbital and  $\epsilon_i$  the respective orbital energy. For a closed-shell system the Fock operator is written as:

$$F = H^{core} + \sum_{i=1}^{N/2} \{2J_i - K_i\} \quad (1.4.5)$$

where  $J_i$  and  $K_i$  are the Coulomb and exchange operator respectively.  $H^{core}$  is the core Hamiltonian operator, which represents the kinetic energy of the electrons and the electron-nuclear interaction.

The *Hartree-Fock* eigenfunctions  $\psi_i$  can be expressed by a linear combination of atomic orbitals (LCAO)  $\phi_\mu$  (“basis functions”):

$$\psi_i = \sum_{\mu} c_{\mu i} \phi_{\mu} \quad (1.4.6)$$

which leads to the generalized eigenvalue problem (*Roothaan-Hall* equation):[34]

$$FC = SCE \quad (1.4.7)$$

where  $F$  corresponds to the Fock matrix,  $C$  is the orbital coefficient matrix,  $S$  the overlap matrix and  $E$  the diagonal matrix of orbital energies.

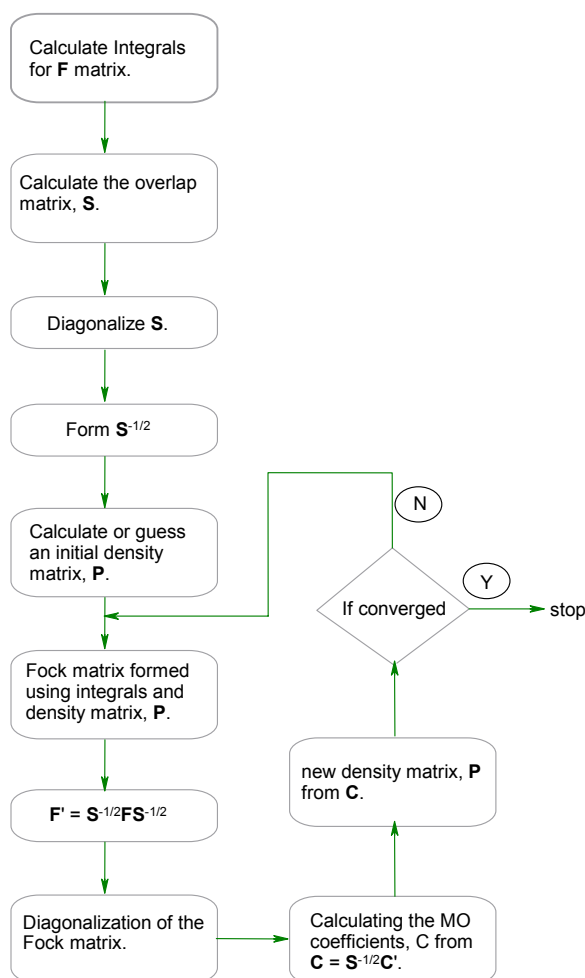
The *Roothaan-Hall* equations have a non-trivial solution only if the following secular equation is satisfied:

$$\det|F - \epsilon_i S| = 0 \quad (1.4.8)$$

This equation cannot be solved directly because the Fock matrix elements  $F_{ij}$  involve Coulomb and exchange integrals which themselves depend on the spatial wavefunctions. So we have to use a self-consistent (SCF) field approach, which iteratively improves the coefficients  $C_{ja}$  until convergence has been reached. Scheme 1.6 below represents the schematic diagram for solving the *Roothaan-Hall* equations.

The correlated *ab initio* methods go beyond the *Hartree-Fock* approximation, and include the effects of electron correlation by a variety of techniques, for instance by perturbation theory or by variational theory. These methods are accurate and widely used by quantum chemists today. However, there are practical limitations, because the computational effort is extremely high for large molecules.

**Scheme 1.6. Flowchart for solving *Roothaan-Hall* equations**



### 1.4.2 Density Functional Theory

An alternative to *ab initio* methods that has been growing in popularity over the past decade is density functional theory (DFT).

In wavefunction-based *ab initio* theory we calculate the full N-electron wavefunction, whereas DFT focuses on the total energy and the one-electron density distribution. One of the most important reasons for the success of DFT is that it includes the electron correlation in an effective manner. The central underlying idea is the relationship between total energy and electron density. In 1964, Hohenberg and Kohn showed that the electron density  $\rho(r)$  uniquely defines the ground-state energy  $E$  and other properties of a system.[35] Therefore,  $E$  is a unique functional of  $\rho(r)$ .

In DFT the energy functional is written as a sum of two terms:

$$E[\rho(r)] = \int V_{ext}(r)\rho(r)dr + F[\rho(r)] \quad (1.4.9)$$

The first term arises from the interaction of the electrons with an external potential  $V_{ext}(r)$ .  $F[\rho(r)]$  is the sum of the kinetic energy of the electrons and the contribution from interelectronic interactions. There is a constraint on the electron density as the number of electrons (N) is fixed. In order to minimize the energy, this constraint is introduced as Lagrangian multiplier  $(-\mu)$ , leading to:

$$\frac{\delta}{\delta\rho(r)} [E[\rho(r)] - \mu \int \rho(r)dr] = 0 \quad (1.4.10)$$

$$\left( \frac{\delta E[\rho(r)]}{\delta\rho(r)} \right)_{V_{ext}} = \mu \quad (1.4.11)$$

where  $\mu$  is the chemical potential of the electrons for a given external potential. According to Kohn and Sham[36] the term  $F[\rho(r)]$  in eqn. (1.4.9) can be approximated by:

$$F[\rho(r)] = E_{KE}[\rho(r)] + E_H[\rho(r)] + E_{XC}[\rho(r)] \quad (1.4.12)$$

where  $E_{KE}[\rho(r)]$  is the kinetic energy of a system of non-interacting electrons with the same density  $\rho(r)$  as the real system.  $E_H[\rho(r)]$  is the electron-electron Coulombic energy, and the so-called exchange-correlation functional  $E_{XC}[\rho(r)]$  contains contributions from exchange and correlation (plus kinetic energy corrections). Kohn-Sham orbitals  $\psi_i(r)$  are introduced to

evaluate the kinetic energy  $E_{KE}[\rho(r)]$ . The full expression for the energy of an N-electron system within the Kohn-Sham scheme reads:

$$E[\rho(r)] = \sum_{i=1}^N \int \psi_i(r) \left( -\frac{\nabla^2}{2} \right) \psi_i(r) dr + \frac{1}{2} \iint \frac{\rho(r_1)\rho(r_2)}{|r_1 - r_2|} dr_1 dr_2 + E_{xc}[\rho(r)] - \sum_{A=1}^M \int \frac{Z_A}{|r - R_A|} \rho(r) dr \quad (1.4.13)$$

The density  $\rho(r)$  of the system is obtained from the Kohn-Sham orbitals:

$$\rho(r) = \sum_{i=1}^N |\psi_i(r)|^2 \quad (1.4.14)$$

A variational treatment leads to the one-electron Kohn-Sham equations:

$$\left\{ -\frac{\nabla^2}{2} - \left( \sum_{A=1}^M \frac{Z_A}{r_{1A}} \right) + \int \frac{\rho(r_2)}{r_{12}} dr_2 + V_{xc}[r_1] \right\} \psi_i(r_1) = \varepsilon_i \psi_i(r_1) \quad (1.4.15)$$

where  $\varepsilon_i$  are the orbital energies.  $V_{xc}$  is known as the exchange-correlation potential, which is the derivative of the exchange-correlation energy with respect to the electron density. The Kohn-Sham equations are solved self-consistently: an initial guess of the density is fed to eqn. (1.4.14) from which a set of orbitals are obtained, leading to an improved density, which is used for the second iteration, and so on until convergence is achieved.

The exchange-correlation functional is *a priori* unknown in density functional theory. The simplest approximation considers the homogeneous, uniform electron gas, where the electron density is constant throughout the space. The exchange-correlation energy for the uniform electron gas can be written as:

$$E_{xc}^{LDA} = E_x^{LDA} + E_c^{LDA} \quad (1.4.16)$$

The first term, comprising the exchange energy, has the form,

$$E_x^{LDA} = -\frac{9}{4\alpha_{ex}} \left[ \frac{3}{4\pi} \right]^{\frac{1}{3}} \sum_r \int [\rho_1^r(r_1)]^{\frac{4}{3}} dr_1 \quad (1.4.17)$$

where  $\alpha_{ex}$  is the exchange scale factor, with the theoretical value of 2/3. The second term, the correlation energy, is represented as,

$$E_c^{LDA} = \int \rho_1(r_1) \varepsilon_c[\rho_1^\alpha(r_1), \rho_1^\beta(r_1)] dr_1 \quad (1.4.18)$$

where  $\varepsilon_c[\rho_1^\alpha, \rho_1^\beta]$  represents the correlation energy per electron with  $\rho_1^\alpha$  and  $\rho_1^\beta$  being the respective  $\alpha$ - and  $\beta$ - spin densities. Ceperley and Alder[37] determined the correlation energy of a uniform electron gas using Monte Carlo methods. In order to use these results in DFT calculations, suitable analytic interpolations have been determined by Vosko, Wilk and Nusair (VWN).[38] The representation of the exchange-correlation energy by eqns. (1.4.16-1.4.18) has been coined the local density approximation (LDA).

The most notorious shortcoming of the LDA is its tendency to overestimate binding energies. The obvious reason is that the electron distribution in molecules is far from a uniform electron gas. To remedy some of the deficiencies in LDA, the functionals have been refined by considering the gradient of the charge density,  $\nabla\rho(r)$ , in corrections to the LDA:

$$E_{xc}[\rho] = \int \rho \varepsilon_{xc}(\rho) F(\rho, \nabla\rho) dr \quad (1.4.19)$$

where  $F(\rho, \nabla\rho)$  is termed a gradient or ‘non-local’ correction, since the potential now depends not only on the electron density, but also on its gradient.[39]

The resulting GGA (generalized gradient approximation) functionals offer significant improvements over LDA and are widely used in computational chemistry. One prominent example is the BP86 functional[40,41] which has become the workhorse for many applications in organometallic chemistry.

The performance of GGA functionals can often be further improved by the admixture of some Hartree-Fock exchange, typically of the order of 20%. The most popular of the hybrid functionals is B3LYP[40,42,43] which is currently the preferred choice for DFT calculations in organic chemistry.

Further information about the merits of different functionals can be found in reviews and monographs on DFT.[39,44]



## 1.5 Geometry optimization

### 1.5.1 Minima

Stable molecules and intermediates in reactions correspond to minima on the potential energy surface, the lowest one being the *global energy minimum*. From a mathematical standpoint, a function  $f$ , which depends on one or more independent variables,  $x_1, x_2, \dots, x_i$ , has a minimum when the first derivative of the function with respect to each of the variables is zero and the second derivatives are all positive:

$$\frac{\partial f}{\partial x_i} = 0; \frac{\partial^2 f}{\partial x_i^2} > 0 \quad (1.5.0)$$

The function to be optimized and its derivatives are calculated with a finite precision, which depends on the computational implementation. In practice the geometry optimization is considered converged if the gradient is reduced below a suitable “cut-off” value. There are a number of well-established optimization methods for finding minima which are usually classified by the required input information: Zero-order methods need only the values of the function itself (*e.g.*, grid searches), first-order methods make use of the function and its gradient (*e.g.*, steepest descent and conjugate gradient methods), and second-order methods require the function as well as the first and second derivatives (*e.g.*, Newton-Raphson methods). With increasing order, the computational effort in the quantum-chemical calculation and the rate of convergence in the geometry optimization normally both increase so that a compromise is needed for best overall performance. We generally use for energy optimization first-order quasi-Newton methods with BFGS updating as implemented in the Gaussian code.[45]

### 1.5.2 Transition States

Transition states are generally much more difficult to locate than minima, because one needs to find a maximum in one (and only one) direction, and minima in all other directions.

At a first-order saddle point, the first derivatives of the potential function with respect to the coordinates are all zero, and the energy passes through a maximum (negative curvature) for movement along the pathway that connects two minima, but is minimal for displacements in all other directions perpendicular to the path (positive curvature). The linear synchronous transit algorithm (LST),[46] which searches for a maximum along a linear path between reactants and products, is one of the methods to get near to the transition state, but it often leads to structures with two or more negative eigenmodes. This problem is effectively handled by using the

quadratic synchronous transit method (QST),[46] where the algorithm searches for a maximum along a parabola connecting reactants and products, and for a minimum in all directions perpendicular to the parabola. Later, Bell and Crighton refined this approach, by looking for a maximum along a parabolic path between the reactants and products,[47] while a minimum is found in the space conjugate (rather than orthogonal) to the path. A more recent variation of QST, implemented by Peng and Schlegel,[48] uses a circle arc instead of a parabola for interpolation and follows the tangent to the circle for guiding the search towards the TS region. This approach is called Synchronous Transit-Guided Quasi Newton (STQN) method. We have used this method as implemented in Gaussian program package[45] for locating transition states.

### 1.5.3 Intrinsic Reaction Coordinates

In a given coordinate system, a reaction path is defined as a steepest descent path or minimum energy path (MEP) from the transition state down to the reactants and products. If mass-weighted Cartesian coordinates are used, then this path is known as intrinsic reaction coordinate (IRC). Tracing the IRC in both directions establishes which minima are connected by a given transition state. Many different algorithms have been suggested for determining reaction paths. Widely used is the one by Gonzalez and Schlegel,[49] which is efficient and reliable, and remains stable even at larger step sizes. We have used this algorithm as implemented in the Gaussian code[45] whenever an IRC calculation was deemed necessary to confirm the nature of a given transition state.

## 1.6 Continuum Solvation Models

One of the greatest challenges for computational chemist is to model organometallic reactions in a solvent environment, so as to mimic the reality in a reaction flask. Solvent molecules may directly interact with the solute, as in the case of ester hydrolysis, or they may not directly affect the solute but provide an environment that alters the behavior of the solute. The latter case can be described by continuum solvation models.

The solvation free energy ( $\Delta G_{sol}$ ) is the free energy change to transfer a molecule from vacuum to solvent, which is represented as:

$$\Delta G_{sol} = \Delta G_{elec} + \Delta G_{vdw} + \Delta G_{cav} \quad (1.6.0)$$

$\Delta G_{elec}$  represents the electrostatic part, arising due to the polarization of the medium under constant dielectric  $\epsilon_s$ .  $\Delta G_{vdw}$  is the van der Waals interaction between the solute and the solvent, which can further be divided into a repulsive term and an attractive dispersion term.

$\Delta G_{cav}$  is the free energy required for cavity formation. Only  $\Delta G_{elec}$  is treated by continuum solvation models.

In 1920, Born derived the electrostatic component of the free energy of solvation for placing a charge within a spherical solvent cavity,[50] which is obtained as the difference in the work done in charging the ion in the dielectric and *in vacuo*:

$$\Delta G_{elec} = -\frac{q^2}{2a} \left( 1 - \frac{1}{\epsilon_s} \right) \quad (1.6.1)$$

where  $q$  is the charge on the ion and  $a$  is the radius of the cavity. Onsager later extended this model to a dipole in a spherical cavity.[51] We now introduce the concept of the “reaction field”. If we consider an isotropic liquid with solvent molecules undergoing random thermal motion, the average electric field at any point will be zero. However, the presence of solute will change this net orientation and hence the field induced by the introduction of the solute is referred as the “reaction field”. In the “self-consistent reaction field method (SCRF)” method the reaction field is incorporated into quantum mechanics by considering it as a perturbation of the Hamiltonian for an isolated molecule:

$$H_{tot} = H_o + H_{RF} \quad (1.6.2)$$

where  $H_o$  is the Hamiltonian of the isolated molecule, and  $H_{RF}$  is the perturbation due to the reaction field[52]. The latter is given by

$$H_{RF} = -\hat{\mu}^T \frac{2(\epsilon_s - 1)}{(2\epsilon_s + 1)a^3} \langle \psi | \hat{\mu} | \psi \rangle \quad (1.6.3)$$

where  $\hat{\mu}$  is the dipole moment operator and  $\hat{\mu}^T$  is its transpose. The electrostatic contribution to the solvation free energy is obtained after solving for the wavefunction  $\psi$  of the modified Hamiltonian:

$$\Delta G_{elec} = \langle \psi | H_{tot} | \psi \rangle - \langle \psi_o | H_o | \psi_o \rangle + \frac{(\epsilon_s - 1)}{(2\epsilon_s + 1)a^3} \mu^2 \quad (1.6.4)$$

The third term in eqn. (1.6.4) represents the work done in creating the charge distribution of the solute within the cavity in the dielectric medium.

The disadvantage of the original SCRF method is the use of a spherical cavity to represent all molecules. In 1981, Tomasi *et al.*[53] devised a method for generating a realistic cavity shape of a molecule, using the van der Waals radii of the atoms of the solute. They coined this

approach as “polarizable continuum” method (PCM), which has been implemented in various quantum mechanical programs. In PCM,  $\Delta G_{elec}$  is computed numerically, because of the non-analytical nature of the cavity shape. Since the wavefunction of the solute extends beyond the cavity, there are slight complications in PCM which can be handled in an approximate manner by scaling the charge distribution on the surface so that it is equal and opposite to the charge of the solute. Later, in 1993, Klamt and Schüürmann introduced COSMO (“conductor-like screening model”) as an interesting variant of the PCM method.[54] In this model, the cavity is considered to be surrounded by a conductor with infinite dielectric constant, which greatly simplifies the treatment of the screening effects and allows for an *a posteriori* correction to account for the finite dielectricity constant. COSMO is implemented in various quantum mechanical packages (*e.g.*, Gaussian[45] and Turbomole[55]). We have used COSMO to incorporate bulk solvation effects in our calculations.

## 1.7 Population analysis

In population analysis the electron density is partitioned among the nuclei, such that each nucleus is associated with a specific number of electrons and a net atomic charge. We have used two out of many possible definitions, following Mulliken[56] and Weinhold.[57]

In Mulliken population analysis,[56] the electrons are divided between the atoms according to the degree to which different atomic orbital basis functions contribute to the total wavefunction. The starting point of this analysis is the equation which relates the total number of electrons to the density matrix and to the overlap integral.

$$N = \sum_{\mu=1}^K P_{\mu\mu} + 2 \sum_{\mu=1}^K \sum_{\nu=\mu+1}^K P_{\mu\nu} S_{\mu\nu} \quad (1.7.0)$$

Assuming that the basis functions are centered on atomic nuclei, the number of electrons associated with a particular atom can be obtained by summing over all basis functions centered on that atom. The net charge associated with an atom A is then given by:

$$N = Z_A - \sum_{\mu=1}^K P_{\mu\mu} + \sum_{\mu=1; \mu \text{ on } A}^K \sum_{\nu=1; \nu \neq \mu}^K P_{\mu\nu} S_{\mu\nu} \quad (1.7.1)$$

This population scheme is simple, but can depend strongly on the basis set, and a balanced basis set is needed to obtain meaningful results.

Natural Bond Orbital (NBO) analysis is used as a technique for studying hybridization and covalency effects in polyatomic wavefunctions.[57] The NBO for a localized  $\sigma$  bond  $\sigma_{AB}$

between atoms A and B is formed from orthonormal hybrids  $h_A$ ,  $h_B$  (natural hybrid orbitals or NHOs):

$$\sigma_{AB} = C_A h_A + C_B h_B \quad (1.7.2)$$

Natural hybrid orbitals are composed of natural atomic orbitals (NAOs), optimized for the chosen wavefunction. *Ab initio* wavefunctions transformed to NBO form are found to be consistent with Lewis structures and with the Pauling-Slater-Coulson picture of polarization and bond hybridization.[58] The transformation to NBOs provides orbitals, which are unoccupied and can be used to describe non-covalency effects.

These antibonds  $\sigma^*_{AB}$  are represented as:

$$\sigma^*_{AB} = C_B h_A - C_A h_B \quad (1.7.3)$$

Deleting these orbitals from the basis set and then recalculating the total energy gives the energy associated with the antibonds. Hence, we can decompose the total energy  $E$  into components contributing for both covalent and noncovalent effects:

$$E = E_{\sigma\sigma} + E_{\sigma\sigma^*} \quad (1.7.4)$$

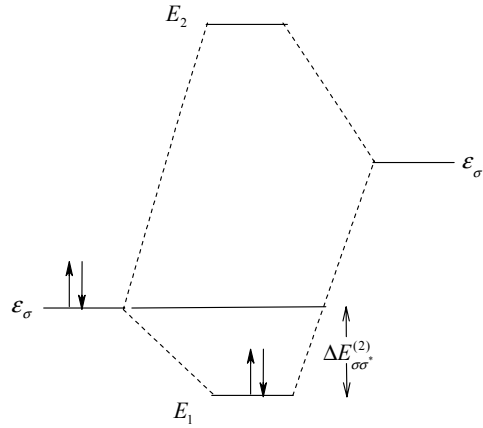


**Figure 1.1.** Perturbative donor-acceptor interaction, involving a filled orbital  $\sigma$  and an unfilled orbital  $\sigma^*$ .

Figure 1.2 displays the interaction of a filled  $\sigma$  orbital with the unfilled antibonding  $\sigma^*$  orbitals of the Lewis structure. Estimates for the energy lowering  $\Delta E_{\sigma\sigma^*}^{(2)}$  can be obtained from second-order perturbation theory:

$$\Delta E_{\sigma\sigma^*}^{(2)} = -2 \frac{\langle \sigma | \hat{F} | \sigma^* \rangle^2}{\epsilon_{\sigma^*} - \epsilon_\sigma} \quad (1.7.5)$$

where  $\epsilon_\sigma$  and  $\epsilon_{\sigma^*}$  are NBO orbital energies, and  $\hat{F}$  is the Fock operator. The NBO perturbative analysis (eqn. 1.7.4) allows one to apply qualitative ideas of valence theory to describe the noncovalent energy lowering.

As the noncovalent delocalization effects (eqn. 1.7.4) are associated with  $\sigma \rightarrow \sigma^*$  interactions between donor and acceptor orbitals, it can be appropriate to describe them as being of “donor-acceptor”, “charge transfer”, or generalized “Lewis base-Lewis acid” type. The quantity of charge  $q$  transferred in such interactions is given by:

$$q \cong \frac{|\Delta E_{\sigma\sigma^*}^{(2)}|}{\epsilon_{\sigma^*} - \epsilon_\sigma} \quad (1.7.6)$$

The amount of charge transferred is typically much less than that required for formation of an ion pair. Hence, in a nutshell, NBO analysis emphasizes the importance of quantum mechanical orbital interaction and exchange effects in the non-covalent regime. We have mainly used NBO analysis (rather than Mulliken analysis) for the interpretation of the computational results.

## Bibliography

- [1] N. Miyaura, A. Suzuki. "Palladium-Catalyzed Cross-Coupling Reactions of Organoboron Compounds." *Chem. Rev.* **1995**, 95, 2457-2483.
- [2] (a) R. McCrindle, G. Ferguson, G. J. Arsenault, A. J. McAlees, D. K. Stephanson, "Formation and Characterisation of Enamine Complexes of Palladium(II)chloride. Crystal Structure Analysis of Di- $\mu$ -chlorodichlorobis[2-(NN-di-isopropylimino)ethyl-C]-dipalladium(II)." *J. Chem. Res. (S)* **1984**, 360-361. (b) C. Amatore, A. Jutand, M. A. M'Barki, "Evidences for the Formation of Zerovalent Palladium from Pd(OAc)<sub>2</sub> and Triphenylphosphine." *Organometallics* **1992**, 11, 3009-3013.
- [3] C. Amatore, A. Jutand, "Anionic Pd(0) and Pd(II) Intermediates in Palladium-Catalyzed Heck and Cross-Coupling Reactions." *Acc. Chem. Res.* **2000**, 33, 314-321.
- [4] J. B. Honeycutt, J. M. Riddle, "Triethylborane as an Alkylating Agent in Both Organic and Aqueous Media." *J. Am. Chem. Soc.* **1959**, 81, 2593-2593.
- [5] J. H. Gardner, P. Borgstrom, "A Method of Coupling Organic Radicals by Means of the Grignard Reagent." *J. Am. Chem. Soc.* **1929**, 51, 3375-3377.
- [6] H. C. Brown, N. C. Hebert, C. H. Snyder, "The Reaction of Triethylborane with Oxides of Silver, Gold, and Platinum-A New Convenient Route To Noble Metal Alkyls and to Free Radical Chemistry." *J. Am. Chem. Soc.* **1961**, 83, 1001-3377.
- [7] (a) F. Hibbert, "Proton transfer from intramolecularly hydrogen-bonded acids." *Acc. Chem. Res.* **1984**, 17, 115-120. (b) H. A. Staab, T. Saupe, "'Proton Sponges" and the Geometry of Hydrogen Bonds: Aromatic Nitrogen Bases with Exceptional Basicities." *Angew. Chem., Int. Ed. Engl.* **1988**, 27, 865-879. (c) R. W. Alder, "Intrabridgehead chemistry." *Tetrahedron* **1990**, 46, 683-713.
- [8] R. W. Alder, P. S. Bowman, W. R. S. Steele, D. R. Winterman, "The Remarkable Basicity of 1,8-Bis(dimethylamino)naphthalene." *Chem. Commun.* **1968**, 723-724.
- [9] M. A. Zirnstein, H. A. Staab, "Quino[7,8-*h*]quinoline, a New Type of "Proton Sponge."" *Angew. Chem., Int. Ed. Engl.* **1987**, 26, 460-461.

- [10] H. U. Wüstefeld, W. C. Kaska, F. Schüth, G. D. Stucky, X. Bu, B. Krebs, "Transition Metal Complexes with the Proton Sponge 4,9-Dichloroquino[7,8-*h*]quinoline: Highly Twisted Aromatic Systems and an Extreme "Out-of-Plane" Position of the Coordinated Transition Metal Atom." *Angew. Chem., Int. Ed. Engl.* **2001**, *40*, 3182-3184.
- [11] T. Mizoroki, K. Mori, "Arylation of Olefin with Aryl Iodide Catalyzed by Palladium." *Bull Chem Soc Jpn.* **1971**, *44*, 581-581.
- [12] R. F. Heck, J. P. Nolley, "Palladium-Catalyzed Vinylic Hydrogen Substitution Reactions with Aryl, Benzyl, and Styryl Halides." *J. Org. Chem.* **1972**, *37*, 2320-2322.
- [13] (a) C. Amatore, F. Pflüger, "Mechanism of Oxidative Addition of Palladium(0) with Aromatic Iodides in Toluene, Monitored at Ultramicroelectrodes." *Organometallics* **1990**, *9*, 2276-2282. (b) A. Jutand, A. Mosleh, "Rate and Mechanism of Oxidative Addition of Aryl Triflates to Zerovalent Palladium Complexes. Evidence for the Formation of Cationic (Ö-Aryl)palladium Complexes." *Organometallics* **1995**, *14*, 1810-1817. (c) P. Cianfriglia, V. Narducci, C. L. Sterzo, E. Viola, "Mechanism of the Palladium-Catalyzed Metal-Carbon Bond Formation. Isolation of Oxidative Addition and Transmetalation Intermediates." *Organometallics* **1996**, *15*, 5220-5230.
- [14] A. C. Albéniz, P. Espinet, Y-S. Lin, "Cyclization versus Pd-H Elimination-Readdition: Skeletal Reaggrangement of the Products of Pd-C<sub>6</sub>F<sub>5</sub> Addition to 1,4-Pentadienes." *J. Am. Chem. Soc.* **1996**, *118*, 7145-7152, and references therein.
- [15] A. Hessian, W. Müllers. "Stereochemie der palladium-katalysierten Disproportionierung des 1,2-Dihydronaphthalins." *Chem. Ber.* **1980**, *113*, 19-23.
- [16] K. Ziegler, E. Holzkamp, H. Breil, H. Martin, "Das Mülheimer Normaldruck-Polyäthylen-Verfahren." *Angew. Chem.* **1955**, *67*, 541.
- [17] G. Natta, P. Pino, P. Corradini, F. Danusso, E. Mantica, G. Mazzanti, G. Moraglio, "Crystalline High Polymers Of  $\alpha$ -Olefins." *J. Am. Chem. Soc.* **1995**, *77*, 1708-1710.
- [18] H.-H. Brintzinger, D. Fischer, R. Mülhaupt, B. Rieger, R. M. Waymouth, "Stereospecific Olefin Polymerization with Chiral Metallocene Catalysts." *Angew. Chem., Int. Ed. Engl.* **1995**, *34*, 1143-1170.



- [19] A. Andresen, H. -G. Cordes, J. Herwig, W. Kaminsky, A. Merck, R. Mottweiler, J. Pein, H. Sinn, H. -J. Vollmer, "Halogen - Free Soluble Ziegler Catalysts for the Polymerization of Ethylene. Control of Molecular Weight by Choice of Temperature." *Angew. Chem., Int. Ed. Engl.* **1976**, *15*, 630-632.
- [20] W. Kaminsky, K. Külper, H. -H. Brintzinger, F. R. W. P. Wild. "Polymerization of Propene and Butene with a Chiral Zirconocene and Methylalumoxane as Cocatalyst." *Angew. Chem., Int. Ed. Engl.* **1985**, *24*, 507-508.
- [21] J. A. Ewen, R. L. Jones, A. Razavi, J. D. Ferrara. "Syndiospecific propylene polymerizations with Group IVB metallocenes." *J. Am. Chem. Soc.* **1988**, *110*, 6255-6256.
- [22] (a) R. F. Jordan, "Cationic metal alkyl olefin polymerization catalysts (SYMP)." *J. Chem. Educ.* **1988**, *65*, 285-289. (b) Y. W. Alelynuas, R. F. Jordan, S. F. Echols, S. L. Borkowsky, P. K. Bradley, "Acetonitrile insertion reactions of zirconium complexes  $(C_5H_4R)_2Zr(R)(L)^+$ ." *Organometallics* **1991**, *10*, 1406-1416. (c) P. G. Gassman, M. R. Callstrom, "Isolation, and partial characterization by XPS, of two distinct catalysts in the Ziegler-Natta polymerization of ethylene." *J. Am. Chem. Soc.* **1987**, *109*, 7875-7876. (d) R. F. Jordan, C. S. Bajgur, R. Willett, B. Scott, "Ethylene polymerization by a cationic dicyclopentadienyl zirconium(IV) alkyl complex." *J. Am. Chem. Soc.* **1986**, *108*, 7410-7411.
- [23] (a) P. Cossée, "Ziegler-Natta Catalysis I. Mechanism of Polymerization of  $\alpha$ -Olefins with Ziegler-Natta Catalyst." *J. Catal.* **1964**, *3*, 80-88. (b) E. J. Arlman, "Ziegler-Natta Catalysis II. Surface Structure of Layer-Lattice Transition Metal Chlorides." *J. Catal.* **1964**, *3*, 89-98. (c) E. J. Arlman, P. Cossée, "Ziegler-Natta Catalysis III. Stereospecific Polymerization of Propene with the catalyst system  $TiCl_3-AlEt_3$ ." *J. Catal.* **1964**, *3*, 99-104.
- [24] M. Brookhart, M. L. H. Green, "Carbon---hydrogen-transition metal bonds." *J. Organomet. Chem.* **1983**, *250*, 395-408.
- [25] (a) J. A. Ewen, M. J. Elder, R. J. Jones, S. Curtis, H. N. Cheng, "Catalytic Olefin Polymerization, Studies in Surface Science and Catalysis." T. Keii, K. Soga, Eds., Elsevier, New York, **1990**, page 439. (b) L. Resconi, A. Fait, F. Piemontesi, M. Colonna, H. Rychlicki, R. Ziegler, "Effect of Monomer Concentration on Propene Polymerization with the *rac*-[Ethylenebis(1-indenyl)zirconium Dichloride/Methylaluminoxane Catalyst." *Macromolecules* **1995**, *28*, 6667-6676.

- [26] J. C. W. Chien, Z. Yu, M. M. Marques, J. C. Flores, M. D. Rausch, "Polymerization of Olefins and Diolefins Catalyzed by Monocyclopentadienyl Titanium Complexes Containing a (Dimethylamino)ethyl Substituent and Comparison with *ansa*-Zirconocene Systems." *J. Polym. Sci.: Part A: Polym. Chem.* **1998**, *36*, 319-328.
- [27] P. Longo, L. Olivia, A. Grassi, C. Pellicchia, "Behaviour of homogeneous catalysts for propene polymerization in methylene chloride." *Makromol. Chem.* **1989**, *190*, 2357-2361.
- [28] (a) B. A. Dolgoplosk, "Stereospecific catalysis of diene polymerization and copolymerization and the mechanism of stereoregulation." *Vysokomol. Soedin., Ser. A* **1971**, *13*, 325-347. (b) E. S. Novikova, O. P. Parenago, V. M. Frolov, B. A. Dolgoplosk, "Kinetics of butadiene polymerization under the influence of the catalytic system  $\pi$ -crotyl(allyl)nickel halide-chloral." *Kinet. Katal.* **1976**, *17*, 928-934.
- [29] (a) M. Ystenes, "The Trigger Mechanism for Polymerization of  $\alpha$ -Olefins with Ziegler-Natta Catalysts: A New Model Based on Interaction of Two Monomers at the Transition State and Monomer Activation." *J. Catal.* **1991**, *129*, 383. (b) M. Ystenes, "Predictions from the Trigger Mechanism for Ziegler-Natta Polymerization of  $\alpha$ -olefins." *Makromol. Chem. Macromol. Symp.* **1993**, *66*, 71-82.
- [30] A. Fait, L. Resconi, G. Guerra, P. Corradini, "A Possible Interpretation of the Nonlinear Propagation Rate Laws for Insertion Polymerizations: A Kinetic Model Based on a Single-Center, Two-State Catalyst." *Macromolecules* **1999**, *32*, 2104-2109.
- [31] E. Schrödinger, "Quantisierung als Eigenwertproblem." *Ann. Phys.* **1926**, *79*, 361-376.
- [32] M. Born, R. Oppenheimer, "Zur Quantentheorie der Molekeln." *Ann. Phys.* **1927**, *84*, 457-484.
- [33] (a) D. R. Hartree, "The Wave Mechanics of an Atom with a Non-Coulomb Central Field. Part I. Theory and Methods." *Proc. Cambridge. Philos. Soc.* **1928**, *24*, 89-110. (b) V. Fock, "Näherungsmethode zur Lösung des quantenmechanischen Mehrkörperproblems." *Z. Physik* **1928**, *61*, 126-148.
- [34] (a) J. C. C. Roothaan, "New Developments in Molecular Orbital Theory." *Rev. Mod. Phys.* **1951**, *23*, 69-89. (b) G. G. Hall, "The Molecular Orbital Theory of Chemical Valency VIII. A Method for Calculating Ionization Potentials." *Proc. R. Soc, London* **1951**, *A205*, 541-552.

- [35] P. Hohenberg, W. Kohn, "Inhomogeneous Electron Gas." *Phys. Rev.* **1964**, *B136*, 864-871.
- [36] W. Kohn, L. J. Sham, "Self-consistent Equations Including Exchange and Correlation Effects." *Phys. Rev.* **1965**, *A140*, 1133-1138.
- [37] D. M. Ceperley, B. J. Alder, "Ground State of the Electron Gas by a Stochastic Method." *Phys. Rev. Lett.* **1980**, *45*, 566-569.
- [38] S. H. Vosko, L. Wilk, M. Nusair, "Accurate Spin-dependent Electron Liquid Correlation Energies for Local Spin Density Calculations: A Critical Analysis." *Can. J. Phys.* **1980**, *58*, 1200-1211.
- [39] For detailed expositions of DFT formalism and functionals see, R. G. Parr, W. Yang, "Density-Functional Theory of Atoms and Molecules." Oxford University Press, New York, **1989**.
- [40] A. D. Becke, "Density-functional exchange-energy approximation with correct asymptotic behaviour." *Phys. Rev. A* **1988**, *38*, 3098-3100.
- [41] J. P. Perdew, "Density-functional approximation for the correlation energy of the inhomogeneous electron gas." *Phys. Rev. B* **1986**, *33*, 8822-8824.
- [42] A. D. Becke, "Density-functional thermochemistry. III. The role of exact exchange." *J. Chem. Phys.* **1993**, *98*, 5648-5652.
- [43] C. Lee, W. Yang, R. G. Parr, "Development of the Colle-Salvetti correlation-energy formula into a functional of the electron density." *Phys. Rev. B* **1988**, *37*, 785-789.
- [44] (a) T. Ziegler, "Approximate Density Functional Theory as a Practical Tool in Molecular Energetics and Dynamics." *Chem. Rev.* **1991**, *91*, 651-667. (b) W. Koch, M. C. Holthausen, "A Chemist's Guide to Density Functional Theory." Wiley-VCH Verlag GmbH, Weinheim, **2000**.
- [45] Gaussian 03, Revision B.01, M. J. Frisch, G. W. Trucks, H. B. Schlegel, G. E. Scuseria, M. A. Robb, J. R. Cheeseman, J. A. Montgomery, Jr., T. Vreven, K. N. Kudin, J. C. Burant, J. M. Millam, S. S. Iyengar, J. Tomasi, V. Barone, B. Mennucci, M. Cossi, G. Scalmani, N. Rega, G. A. Petersson, H. Nakatsuji, M. Hada, M. Ehara, K. Toyota, R. Fukuda, J. Hasegawa, M. Ishida, T. Nakajima, Y. Honda, O. Kitao, H. Nakai, M. Klene, X. Li, J. E.

Knox, H. P. Hratchian, J. B. Cross, C. Adamo, J. Jaramillo, R. Gomperts, R. E. Stratmann, O. Yazyev, A. J. Austin, R. Cammi, C. Pomelli, J. W. Ochterski, P. Y. Ayala, K. Morokuma, G. A. Voth, P. Salvador, J. J. Dannenberg, V. G. Zakrzewski, S. Dapprich, A. D. Daniels, M. C. Strain, O. Farkas, D. K. Malick, A. D. Rabuck, K. Raghavachari, J. B. Foresman, J. V. Ortiz, Q. Cui, A. G. Baboul, S. Clifford, J. Cioslowski, B. B. Stefanov, G. Liu, A. Liashenko, P. Piskorz, I. Komaromi, R. L. Martin, D. J. Fox, T. Keith, M. A. Al-Laham, C. Y. Peng, A. Nanayakkara, M. Challacombe, P. M. W. Gill, B. Johnson, W. Chen, M. W. Wong, C. Gonzalez, and J. A. Pople, Gaussian, Inc., Pittsburgh PA, **2003**.

[46] T. A. Halgren, W. N. Lipscomb, "The synchronous-transit method for determining reaction pathways and locating molecular transition states." *Chem. Phys. Lett.* **1977**, *49*, 225-232.

[47] S. Bell, J. S. Crighton, "Locating transition states." *J. Chem. Phys.* **1984**, *80*, 2464-2475.

[48] C. Peng, H. B. Schlegel, "Combining Synchronous Transit and Quasi-Newton Methods to Find Transition States." *Israeli. J. Chem.* **1993**, *33*, 449-454.

[49] (a) C. Gonzalez, H. B. Schlegel, "An improved algorithm for reaction path following." *J. Chem. Phys.* **1989**, *90*, 2154-2161. (b) C. Gonzalez, H. B. Schlegel, "Reaction path following in mass-weighted internal coordinates." *J. Phys. Chem.* **1990**, *94*, 5523-5527.

[50] M. Born, "Volumen und Hydratationswärme der Ionen." *Z. Physik* **1920**, *1*, 45-48.

[51] L. Onsager, "Electric Moments of Molecules in Liquids." *J. Am. Chem. Soc.* **1936**, *58*, 1486-1493.

[52] O. Tapia, O. Goscinski, "Self-Consistent Reaction Field Theory of Solvent Effects." *Mol. Phys.* **1975**, *29*, 1653-1661.

[53] (a) S. Miertus, E. Scrocco, J. Tomasi, "Electrostatic Interaction of a Solute with a Continuum-A Direct Utilization of *Ab Initio* Molecular Potentials for the Provision of Solvent Effects." *Chem. Phys.* **1981**, *55*, 117-129. (b) J. Tomasi, M. Persico, "Molecular Interactions in Solution: An Overview of Methods Based on Continuous Distribution of the Solvent." *Chem. Rev.* **1994**, *94*, 2027-2094.

[54] (a) A. Klamt, G. Schüürmann, "COSMO: A New Approach to Dielectric Screening in Solvents with Explicit Expressions for the Screening Energy and its Gradient." *J. Chem. Soc.*

*Perkin Trans. 2.* **1993**, 799-805. (b) A. Klamt, V. Jonas, T. Bürger, J. C. W. Lohrenz, "Refinement and Parametrization of COSMO-RS." *J. Phys. Chem. A* **1998**, *102*, 5074-5085. (c) A. Schäfer, A. Klamt, D. Sattel, J. C. W. Lohrenz, F. Eckert, "COSMO Implementation in TURBOMOLE: Extension of an efficient quantum chemical code towards liquid systems." *Phys. Chem. Chem. Phys.* **2000**, *2*, 2187-2193.

[55] R. Ahlrichs, M. Bär, M. Häser, H. Horn, C. Kölmel, "Electronic structure calculations on workstation computers: The program system turbomole." *Chem. Phys. Lett.* **1989**, *162*, 165-169.

[56] R. S. Mulliken, "Electronic Population Analysis on LCAO-MO Molecular Wave Functions I." *J. Chem. Phys.* **1955**, *23*, 1833-1846.

[57] (a) J. P. Foster, F. Weinhold, "Natural hybrid orbitals." *J. Am. Chem. Soc.* **1980**, *102*, 7211-7218. (b) A. E. Reed, R. B. Weinstock, F. Weinhold, "Natural population analysis." *J. Chem. Phys.* **1985**, *83*, 735-746.

[58] (a) L. Pauling, "The nature of the chemical bond. Application of results obtained from the quantum mechanics and from a theory of paramagnetic susceptibility to the structure of molecules." *J. Am. Chem. Soc.* **1931**, *53*, 1367-1400. (b) J. C. Slater, "Directed valence in polyatomic molecules." *Phys. Rev.* **1931**, *37*, 481-489; (c) C. A. Coulson, "Valence", 2<sup>nd</sup> ed., Oxford University Press, London, **1952**.









## Mechanistic Pathways for Oxidative Addition of Aryl Halides to Palladium(0) Complexes: A DFT Study.

*In principle one could go ahead and calculate each molecule...However...even if the results were in excellent agreement with experiment, the resultant predictability would not necessarily imply understanding. True understanding implies a knowledge of the various physical factors, the mix of different physical mechanisms, that go into making an observable.*

(Roald Hoffmann, Accounts of Chemical Research, Interaction of Orbitals through Space and through Bonds (page 2), Volume 4, Number 1 **1971**)

### 2.1 Introduction

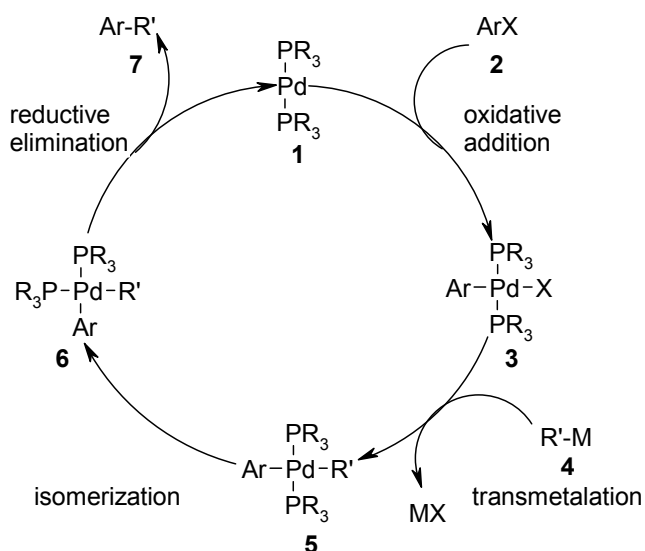
Palladium-catalyzed cross-coupling reactions such as Suzuki reactions, Heck olefinations, Stille couplings or Buchwald-Hartwig aminations have become indispensable tools of modern organic synthesis.[1,2,3,4] The initiating step of all these transformations is the oxidative addition of aryl halides to palladium(0) complexes. In many cases, it is believed to be rate-determining[5] so that it is essential to understand its detailed mechanism and the factors which influence its efficiency.

Therefore, this oxidative addition step has been the subject of extensive investigations including experimental studies on model systems,[6] kinetic measurements[7,8] and quantum chemical calculations.[9,10,11] Originally, it was proposed that the catalytically active palladium species are coordinatively unsaturated complexes of the Pd(0)L<sub>2</sub> type **1**. [8] According to the “textbook mechanism” depicted in Scheme 2.1, aryl halides **2** oxidatively add to such species giving rise to *trans*-configured complexes **3**, which have been isolated and characterized.[8] Complex **3** acts as the starting point for further steps of the catalytic transformations: In the case of C—C coupling reactions, a transmetalation step follows, leading to structure **5**. Due to the *trans*-geometry of this intermediate, an isomerization to compound **6** is necessary before the product can be liberated *via* reductive elimination.

Most of the computational studies are based on this mechanistic concept. A series of calculations were performed by Bickelhaupt *et al.* to further elucidate the elemental steps of

the catalytic cycle.[9] They reported on three different types of mechanisms for C—X oxidative addition to a bare  $d^{10}$  metal center: a concerted *cis* oxidative addition of palladium to the C—Cl bond, a backside nucleophilic substitution on the *ipso* carbon ( $S_N2$  approach) and a radical mechanism *via* a single electron transfer (SET).[9] In their calculations, the concerted mechanism for the oxidative insertion *via* a three-membered transition state was favored. Diefenbach and Bickelhaupt emphasized the quantitative significance of relativistic effects in C—X addition reactions.[9] Sundermann *et al.* postulate the formation of a  $\eta^2$ -phenyl iodide palladium(0) complex as a starting point for the oxidative addition of the aryl iodide *via* a nonplanar and perpendicular transition state.[10]

### Scheme 2.1. The “textbook mechanism” for cross-coupling reactions

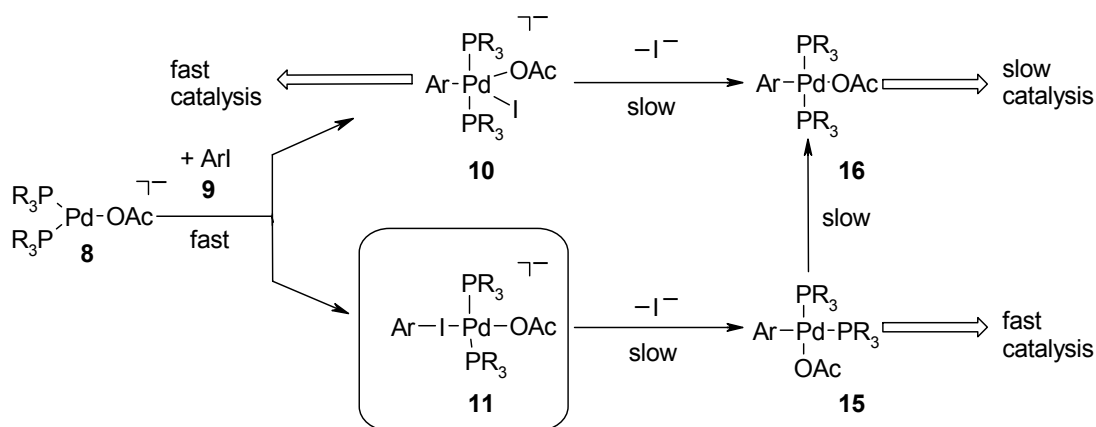


In recent years, the significance of this “textbook mechanism” for palladium-catalyzed reactions has been questioned, since it does not agree with some important experimental findings, especially the pronounced influence that counterions of the palladium(II) pre-catalysts and added metal salts have on catalytic activities.[8] Furthermore, isolated *trans*-complexes **3** have been found to react only very slowly with organometallic reagents, while catalytic cross coupling reactions with the same reagents proceed much faster.[7,12] This is expected, since the isomerization from *cis* to *trans* should be very slow. Moreover, Espinet *et al.* observed that the oxidative addition of aryl iodides initially leads to *cis*-complexes, which then isomerize to the more stable intermediate *trans*-complexes **3**. [7]

Amatore and Jutand found that in the reaction of palladium(II) salts with phosphines, three-coordinate anionic palladium(0) complexes **8** are formed instead of the expected  $Pd(0)L_2$  **1** (Scheme 2.2). The counterion of the pre-catalyst remains bound to palladium and affects its

reactivity. Kinetic studies indicate that upon addition of phenyl iodide (**9a**, Ar = phenyl) to the three-coordinate complex **8b** (R = phenyl), a new species forms quantitatively within seconds, while the solution remains free of iodide and acetate anions. If no further reagent is added, the four-coordinate *trans*-complex **16b** (R, Ar = phenyl) is detected several minutes later. In order to rationalize these findings, Amatore and Jutand proposed a radically different reaction mechanism *via* three- and five-coordinate palladium species starting from the five-coordinate structure **10**.<sup>[8]</sup> However, a dominating role of five-coordinate palladium species would seem doubtful as only few five-coordinate palladium complexes are known which contain constraining polydentate ligands.<sup>[13]</sup> Furthermore it is hard to see why the formation of **10**, which requires the cleavage of a strong C–I bond and the formation of two new bonds, should happen within seconds, while the release of an iodide ion to yield the stable *trans*-complex **16** should be so much slower.

### Scheme 2.2. Alternative pathways for the oxidative addition reaction



Since many experimental findings can be rationalized with the reaction mechanism suggested by Amatore and Jutand, we decided to use it as a starting point for theoretical studies using DFT calculations (BP86/LANL2DZ).<sup>[14,15,16,17]</sup> We first concentrated on the three- and five-coordinate intermediates and could indeed verify the stability of the three-coordinate anionic complexes **8**. However, despite thorough searches we did not find any evidence for an energy minimum of a five-coordinate anionic complex **10**. Instead, we located a stable minimum for an entirely different structure **11**, in which the aryl iodide linearly coordinates to palladium *via* the iodine atom.<sup>[18]</sup> Furthermore, we were able to show a possible reaction pathway for the oxidative addition of the aryl iodide starting from this intermediate giving rise to the *cis*-configured complex **15**. The key findings of our calculations were disclosed in a preliminary communication.<sup>[19]</sup> Herein we present further theoretical studies on the structure

and stability of the key intermediates and discuss alternative pathways for the oxidative addition of aryl halides to anionic palladium(0) species.

## 2.2 Computational Details

All calculations were performed with the Gaussian98 and Gaussian03 program packages.[14] The density functional calculations (DFT) with the BP86 functional[15] employed a basis set of double- $\zeta$  quality, which is denoted LANL2DZ in Gaussian. For the heavy elements (*e.g.* Pd, P, and I) effective core potentials (ECPs)[16] with the corresponding basis set were used while the light elements (C, H, O) were described by a Dunning/Huzinaga full double- $\zeta$  basis set.[17] Geometries were fully optimized, normally without symmetry constraints. Harmonic force constants were computed at the optimized geometries to characterize the stationary points as minima or saddle points. Zero-point vibrational corrections were determined from the harmonic vibrational frequencies to convert the total energies  $E_e$  to ground state energies  $E_0$ . The rigid-rotor harmonic-oscillator approximation was applied for evaluating the thermal and entropic contributions. Transition states were located from a linear transit scan, in which the reaction coordinate was kept fixed at different distances while all other degrees of freedom were optimized. After the linear transit search, the transition states were optimized using the default Berny algorithm implemented in Gaussian98. The nature of transition states **[12a-13a]**<sup>‡</sup>, **[13a-14a]**<sup>‡</sup> and **[14a-15a]**<sup>‡</sup> was verified by following the intrinsic reaction coordinates. Single point solvent calculations were performed on the optimized gas-phase geometries for all the intermediates and transition states involved in the whole process. We employed the CPCM model,[20] which is an implementation of the conductor-like screening solvation model (COSMO)[21] in Gaussian03. THF was used as solvent with UAKS (United Atom Topological Model) radii scheme for the respective atoms (Pd, H, C, O, P, I). For further validation, single-point calculations were performed at the optimized BP86/LANL2DZ geometries employing larger basis sets: Using quasirelativistic pseudopotentials,[22,23] Pd and I were described by (8s7p5d)/[6s5p3d][22] and SDB-cc-pVTZ[24] valence basis sets, respectively; the aug-cc-pVTZ basis[25] was employed for O, P and C, and the cc-pVDZ[26] basis for all H atoms. The relative energies derived from these BP86/EXT single-point calculations ( $E_{EXT}$ ) are included in the respective tables, together with the corresponding BP86/LANL2DZ results. Tables 2.2 to 2.5 document the energetics required for various steps, including  $\Delta E_e$  (change in electronic energy);  $\Delta E_0$  (change in electronic plus zero-point energy);  $\Delta H_{298}$  (change in thermal enthalpies);  $\Delta G_{298}$  (change in free energies),  $\Delta E_{sov}$  (change in electronic energy including solvent effects) and  $\Delta E_{EXT}$  (change in BP86/EXT single-point electronic energy). We find only minor variations in the computed DFT energies upon basis set extension ( $\Delta E_e$  vs.  $\Delta E_{EXT}$ ), in agreement with a recent systematic benchmark study on the oxidative addition of methane to palladium.[27] The charge distribution around the metal center was analyzed using Weinhold's

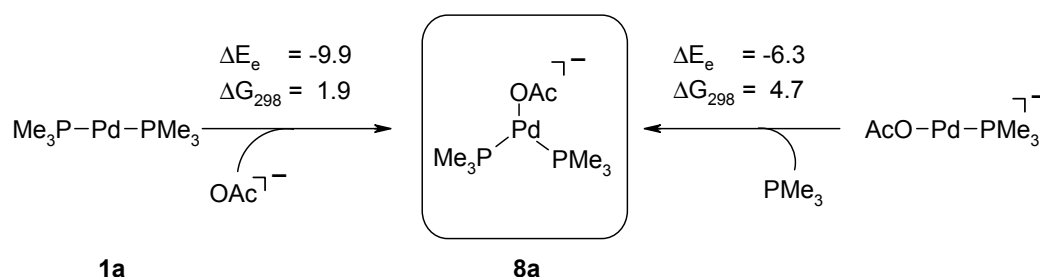
NPA approach.[28] Wiberg bond indices (WBIs) were also calculated to quantify covalent interactions in the complexes.[29] Contour maps were drawn with the Molden program package.[30]

## 2.3 Results and Discussion

### 2.3.1 Catalytically active species

In order to identify the most likely starting point for the oxidative addition step, we calculated the properties of several coordinatively unsaturated palladium(0)phosphine species at the BP86/LANL2DZ level of theory. Initially,  $\text{PMe}_3$  was used as phosphine ligand to reduce the computational effort. Energy minima were found for the “classical”  $\text{d}^{10}$   $\text{Pd}(\text{PMe}_3)_2$  complex (**1a**), for an anionic, three-coordinate complex  $[\text{Pd}(\text{PMe}_3)_2\text{OAc}]^-$  (**8a**) as proposed by Amatore and Jutand, and for a coordinatively unsaturated anionic  $[\text{Pd}(\text{PMe}_3)\text{OAc}]^-$  complex similar to that observed by Hartwig *et al.* for sterically crowded phosphines (Scheme 2.3). The structural information is summarized in Figure 2.1.

**Scheme 2.3. Comparison of several palladium(0) species (BP86/LANL2DZ, kcal/mol)**



The two phosphines in **1a** are oriented staggered with respect to each other in an essentially collinear P—Pd—P arrangement. The Pd—O bond is shorter in  $[\text{Pd}(\text{PMe}_3)\text{OAc}]^-$  (2.100 Å) than in **8a** (2.319 Å) indicating a stronger palladium-acetate bond in the former complex.

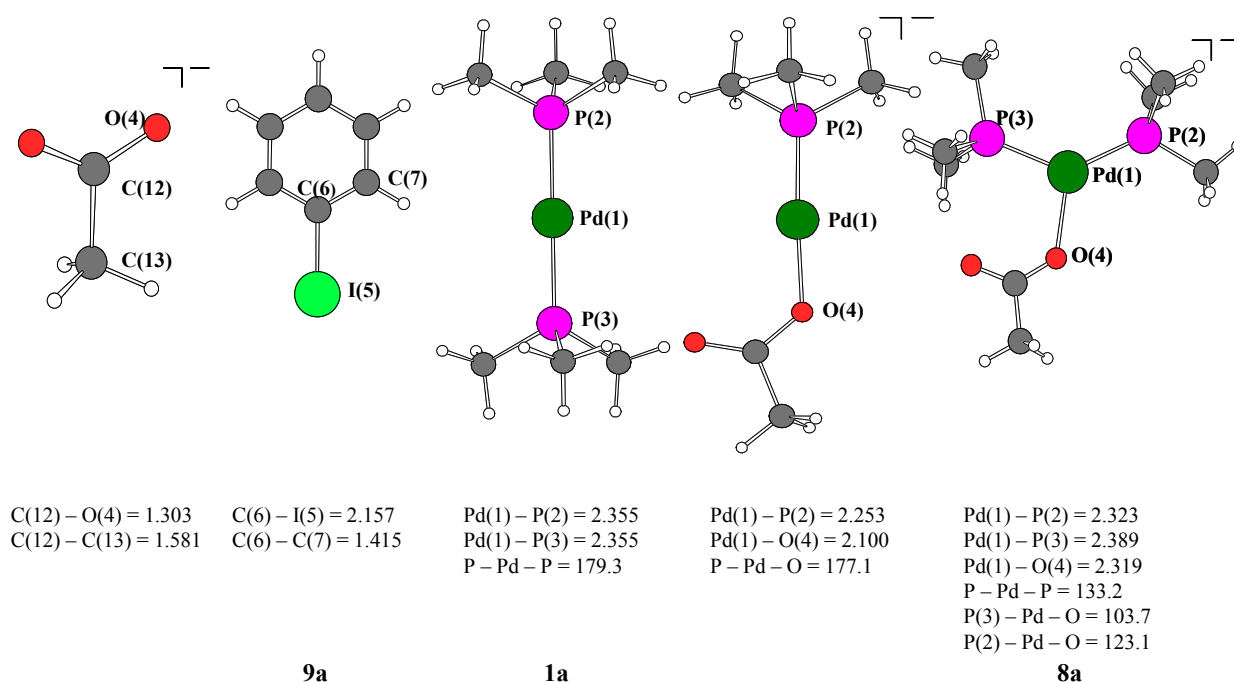


**Figure 2.1.** Optimized structures of the starting materials (BP86/LANL2DZ) with selected bond lengths (in Å) and angles (in deg).

In **8a**, the palladium is in a distorted trigonal planar environment. The P–Pd–P angle amounts to 133.2° and the two phosphines are oriented staggered to each other. Due to interactions between the carboxylic oxygen of the acetate ligand and hydrogen atoms of one PMe<sub>3</sub> ligand, the acetate lies almost within the P Pd P plane, and the two P–Pd–O angles differ by almost 20° (103.7° vs. 123.1°). The complexation reactions leading to **8a** (Scheme 2.3) are computed to be exothermic, by –9.9 kcal/mol from **1a** and –6.3 kcal/mol from [Pd(PMe<sub>3</sub>)OAc]<sup>–</sup>. They are slightly endergonic at 298 K (by 1.9 and 4.7 kcal/mol, respectively) because of the entropic penalty for gas-phase association reactions.

To get further evidence for the existence of anionic palladium(0) species of the Jutand-type, we performed additional calculations on the more realistic [Pd(PPh<sub>3</sub>)<sub>2</sub>OAc]<sup>–</sup> system **8b**. Geometry optimization at the BP86/LANL2DZ level led to an energy minimum for **8b** with a structure similar to that of **8a**.

The larger steric demand of the PPh<sub>3</sub> ligands in **8b** compared with the PMe<sub>3</sub> ligands in **8a** causes a twisted (P(2)–Pd–O(4)–C = 67.8°) orientation of the acetate ligand relative to the P Pd P plane and a larger P–Pd–P angle (136.6° vs. 132.2°). The carboxylic oxygen of the acetate interacts only weakly with one of the phenyl hydrogen atoms in **8b**. Compared with **8a**, the environment of palladium is more symmetrical in **8b** (P–Pd–O angles of 109.2° and 113.5°; Pd–P bond lengths of 2.368 and 2.365 Å). The shorter Pd–O bond (2.304 Å instead of 2.319 Å) suggests that the acetate ligand is more strongly bound in **8b** than in **8a**, and the

calculated dissociation energy is indeed significantly higher (−21.8 vs. −9.9 kcal/mol, BP86/LANL2DZ).

Three-coordinate anionic species were also found with chloride ligands: Both  $[\text{Pd}(\text{PMe}_3)_2\text{Cl}]^-$  (**8c**) and  $[\text{Pd}(\text{PPh}_3)_2\text{Cl}]^-$  (**8d**) are energy minima on the BP86/LANL2DZ potential energy surface. Again, **8c** is rather distorted around palladium, while **8d** is more symmetrical. In a recent B3LYP/LACVP\* study,[31] stable structures were identified for **8d** and  $[\text{Pd}(\text{PH}_3)_2\text{Cl}]^-$  (**8e**), but no minimum was found for **8c**. In order to clarify this discrepancy, we performed further B3LYP/LACVP\* calculations.

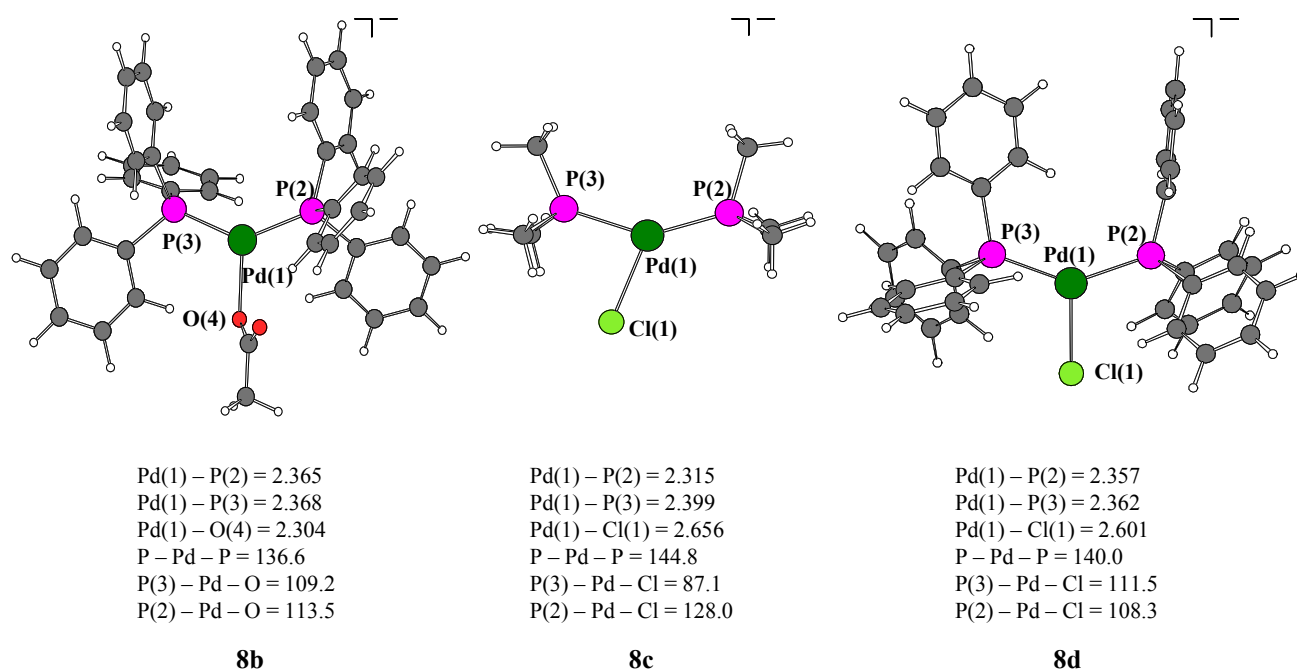


**Figure 2.2.** Optimized structures of **8b**, **8c** and **8d** (BP86/LANL2DZ). Selected bond lengths (in Å) and angles (in deg).

We confirm the published results[31] for **8d** and **8e**. B3LYP/LACVP\* geometry optimization of **8c** leads to dissociation of chloride when starting from an initial symmetric structure similar to **8e**, and to a local minimum when starting from the distorted BP86/LANL2DZ structure of **8c**, so that the B3LYP/LACVP\* and BP86/LANL2DZ are actually consistent with each other. Given the doubts on whether  $\text{PMe}_3$  is a suitable model ligand in three-coordinate palladium complexes,[31] we have carried out further calculations on **8a** at the BP86/LACVP\*, BP86/EXT, and MP2/LANL2DZ levels which invariably give energy minima with distorted geometries (similar to the BP86/LANL2DZ structure of **8a** shown in Figure 2.1). Unless noted otherwise, all results in the following sections refer to BP86/LANL2DZ by default.



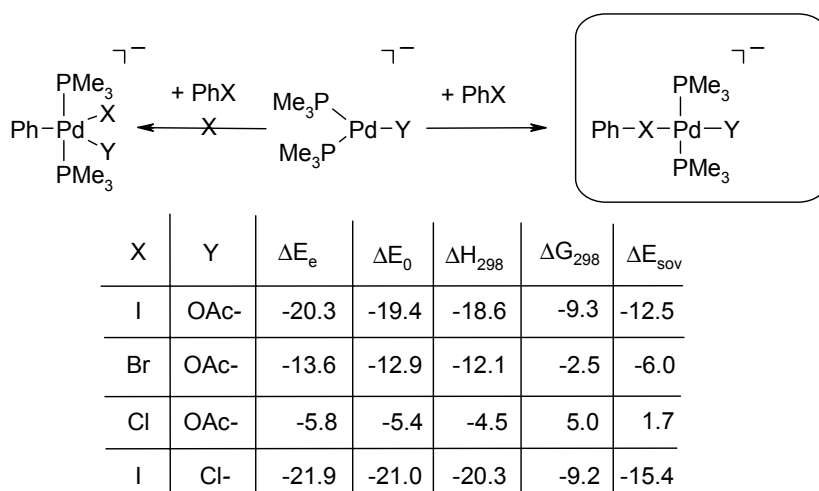
### 2.3.2 The coordination of aryl halides to palladium(0) species

After these studies on three-coordinate anionic palladium(0) species, we investigated possible structures for the initial product of the oxidative addition of phenyl iodide **9a** to these compounds. We first focused on five-coordinate complexes as proposed by Amatore and Jutand.[8] However, despite intensive searches starting from compounds **8a**, **8c** and **8b**, we did not find any energy minima for five-coordinate palladium species containing both a phenyl and an iodide ligand. For any chosen starting geometry, all investigated palladium-species with five ligands immediately lost one of them to form stable four-coordinate complexes.[10] Gradually approaching a phenyl iodide molecule to the three-coordinate species **8a** and slowly cleaving the C—I bond also did not lead to stable structures. In alternative attempts, we started out from a square planar complex and brought a fifth ligand closer to the metal center. In this case, one of the other ligands dissociated upon the formation of the new bond. Solely by freezing the palladium-ligand bonds or certain bond angles during optimization, we were able to minimize the energies of such constrained five-coordinate structures. However, as soon as the restrictions were removed, one of the ligands dissociated.

To make sure that these failures were not due to gas phase effects, we also tried to optimize the geometry of selected five-coordinate species in a solvent (THF) using the COSMO methodology as implemented in TURBOMOLE.[21,32] However, these calculations gave analogous results. In view of all these futile attempts, we have serious doubts that such five-coordinate palladium(0) species with monodentate ligands can exist in the gas phase or in solution and that they could be decisive intermediates in catalytic processes.

In the course of these calculations, we discovered that the phenyl iodide molecule is strongly attracted to the anionic palladium species giving rise to an intermediate with entirely different geometry: Almost independent of the orientation of these two fragments, a gradual approach leads to the formation of a four-coordinate square planar complex (**11a**) in which the phenyl iodide linearly coordinates to the palladium center (Scheme 2.4). Geometry optimizations of several pre-coordination complexes (*e.g.* van der Waals gas-phase adducts) produce the same energy minimum.

## Scheme 2.4. Energetics (kcal/mol) for the coordination of the phenyl halide



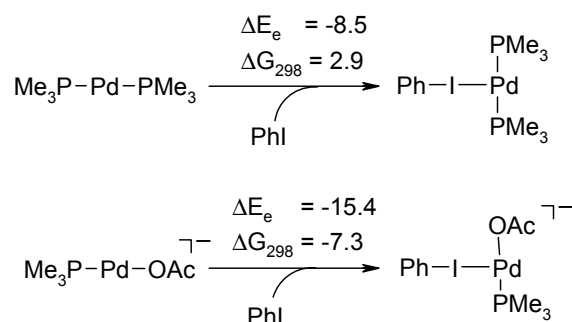
The formation of **11a** is highly exothermic and exergonic ( $\Delta E_e = -20.3$  kcal/mol,  $\Delta G_{298} = -9.3$  kcal/mol) with respect to the starting materials (**8a** and **9a**) and occurs without a significant energy barrier. Therefore, this complex should be formed rapidly under experimental conditions, without giving rise to free acetate or iodide ions. This is fully consistent with the experimental findings by Amatore and Jutand, that almost immediately after addition of phenyl iodide to a solution of an anionic palladium(0) complex both compounds disappear, but neither free acetate nor iodine can be detected.[8]

To validate the stability of the intermediate **11a**, we recalculated its structure with a significantly larger basis set (BP86/EXT, see computational details) and also found an energy minimum. With **8a**, **9a** and **11a** fully optimized at the BP86/EXT level, the reaction **8a** + **9a**  $\rightarrow$  **11a** is predicted to be highly exothermic ( $\Delta E_e = -14.5$  kcal/mol). Furthermore, structure **11a** remained stable during a full solvent optimization (THF) using the COSMO methodology (BP86/LANL2DZ). Finally, we confirmed that the coordination of phenyl iodide is more favorable than a possibly competing coordination of donor ligands, such as THF: All attempts to optimize the geometry of an adduct between **8a** and a single THF molecule resulted in the dissociation of this additional ligand from the metal center. Therefore, the direct formation of **11a** is likely to occur also under experimental conditions in a polar solvent such as THF.

The formation of such a four-coordinate adduct is also possible when starting from the anionic palladium species **8c** containing a chloride instead of an acetate ligand ( $\Delta E_e = -21.9$  kcal/mol,  $\Delta G_{298} = -9.2$  kcal/mol). The coordination of a phenyl iodide molecule to the coordinatively unsaturated anionic monophosphine complex  $[\text{Pd}(\text{PMe}_3)\text{OAc}]^-$  is also quite exergonic ( $\Delta G_{298} = -7.3$  kcal/mol). In contrast to this, the coordination of phenyl iodide to the neutral complex  $\text{Pd}(\text{PMe}_3)_2$  **1a** yielding a T-shaped structure is much less favorable ( $\Delta G_{298} = 2.9$  kcal/mol)

(Scheme 2.5). These differences may help to explain the different performance of catalysts generated *in situ* from different palladium(II) or palladium(0) precursors.

**Scheme 2.5. Coordination of phenyl iodide to palladium(0) species**



It is particularly interesting to investigate whether structures of the general formula **11** are also stable for phenyl bromide or phenyl chloride, since these halides are widely used in catalytic processes. The formation of a four-coordinate species of type **11** is possible for phenyl bromide ( $\Delta E_e = -13.6$  kcal/mol,  $\Delta G_{298} = -2.6$  kcal/mol), while the formation of an adduct between **8a** and phenyl chloride is still exothermic, but no longer exergonic ( $\Delta E_e = -5.8$  kcal/mol,  $\Delta G_{298} = 5.0$  kcal/mol). This agrees with the experimental finding that catalytic reactions involving aryl chloride require special conditions, *i.e.* the use of sterically highly demanding electron-rich ligands. Under these conditions, alternative reaction pathways *via* coordinatively unsaturated anionic palladium species similar to **7a** might become prevailing.[6]

The palladium(0) intermediates **11a-d** are almost square planar complexes with linearly bound aryl halides. They can be best seen as “ate” complexes of iodine,[18] since upon complexation of phenyl iodide to the  $[\text{Pd}(\text{PMe}_3)_2\text{OAc}]^-$  fragment **8a**, the electron density at the phenyl iodide is increased by  $0.505 e$  ( $0.249 e$  at I), mainly due to a charge transfer from the Pd metal into the antibonding  $\sigma^*(\text{C}-\text{I})$  orbital. During this complexation, the C—I bond is elongated by as much as  $0.279 \text{ \AA}$  (13%) and the length of the palladium-acetate bond is increased from  $2.319 \text{ \AA}$  in **8a** to  $2.436 \text{ \AA}$  (5%) in **11a**. Only little changes are observed for the Pd—P bonds while the P—Pd—P bond angle increases from  $133.2^\circ$  to  $174.2^\circ$ .

The bonding situation within the linear “Pd(1)—I(5)—C(6)” framework. The bonding pattern in **11a** is somewhat analogous to that in the hypervalent linear species  $\text{I}_3^-$ . [33] In accordance with the  $\sigma$  interaction in an  $\text{I}_3^-$  ion, we observe in KS-HOMO-13 ( $E = -0.160$  au), KS-HOMO ( $E = -0.012$  au) and KS-LUMO ( $E = 0.062$  au) a bonding, nonbonding and antibonding interaction, respectively, along the Pd—I—C framework (Figure 2.3) where “HOMO-*n*” represents the *n*<sup>th</sup> occupied orbital below KS-HOMO. The anti-bonding palladium-acetate interaction in KS-

HOMO (involving  $d_{x^2-y^2}$  at Pd and  $p_x$  at O(4)) becomes more pronounced in the course of the rearrangement **11a**  $\rightarrow$  **12a** with the dissociation of acetate.

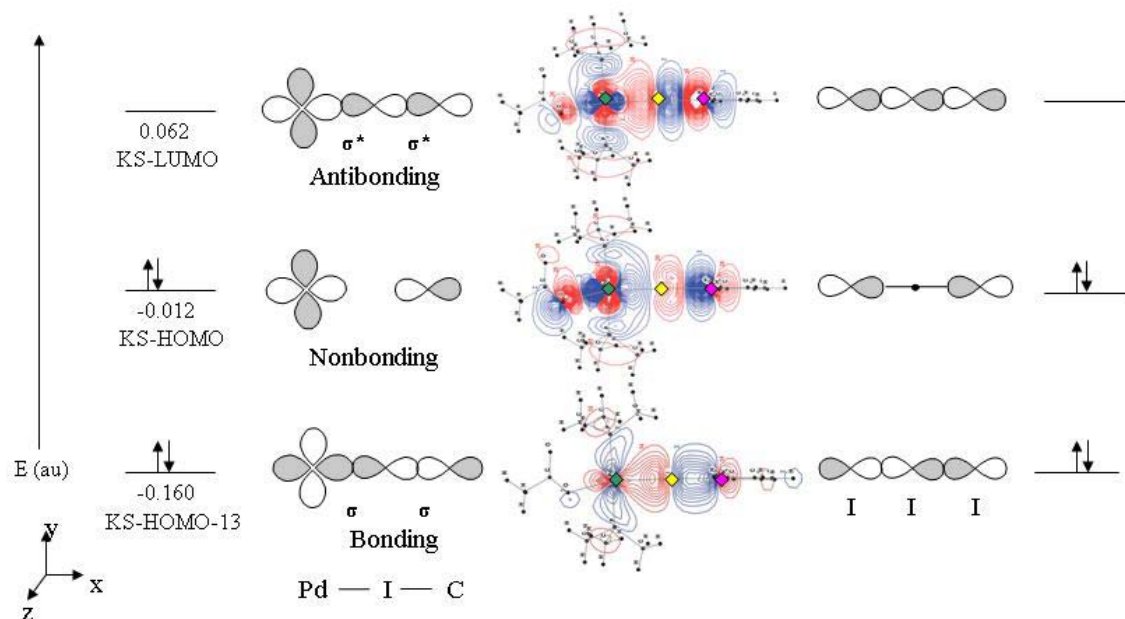


**Figure 2.3.** Contour maps of some important KS-MOs for intermediate **11a** (BP86/LANL2DZ). Given on the left are Kohn-Sham orbital energies (in au). Contour values are 0.00,  $\pm 0.007$ ,  $\pm 0.014$ ,  $\pm 0.021$ ,  $\pm 0.028$ , ..... (in  $e^{1/2} \text{ au}^{-3/2}$ ). Blue and red lines represent positive and negative values, respectively. Pd(1), I(5) and C(6) are marked by green, yellow and pink diamonds respectively. Schematic orbital diagrams are included for the  $\text{I}_3^-$  anion.

**Table 2.1.** Electron density  $\rho_b$ , Laplacian of the electron density  $\nabla^2\rho_b$ , principal curvatures  $\chi_i$  and ellipticities  $\varepsilon$  at bond critical points in the four-coordinate intermediate **11a**. All values in au

	Pd–P(2)	Pd–P(3)	Pd–O	Pd–I	I–C
$\rho_b$	0.077	0.078	0.041	0.037	0.068
$\nabla^2\rho_b$	0.147	0.145	0.191	0.062	0.036
$\chi_1$	-0.063	-0.064	-0.038	-0.023	-0.056
$\chi_2$	-0.063	-0.062	-0.038	-0.023	-0.053
$\chi_3$	0.272	0.21	0.267	0.108	0.146
$\varepsilon$	0.001	0.023	0.009	0.016	0.053

Analysis of the electron density[34] in **11a** yields (3, -1) bond critical points for Pd–P(2), Pd–P(3), Pd–O(4), Pd–I(5), and I(5)–C(6). In the bonds involving palladium, the electron densities  $\rho_b$  at these points are relatively small, and the low ellipticities  $\varepsilon$  indicate a rather

cylindrical electron density distribution (Table 2.1). The Laplacian  $\nabla^2\rho_b$  of the electron density (Figure 2.4) identifies regions where the density is locally concentrated ( $\nabla^2\rho_b < 0$ ) or depleted ( $\nabla^2\rho_b > 0$ ). It assumes positive values at the bond critical points (Table 2.1) which is commonly regarded as evidence for closed-shell rather than covalent interactions.[34]

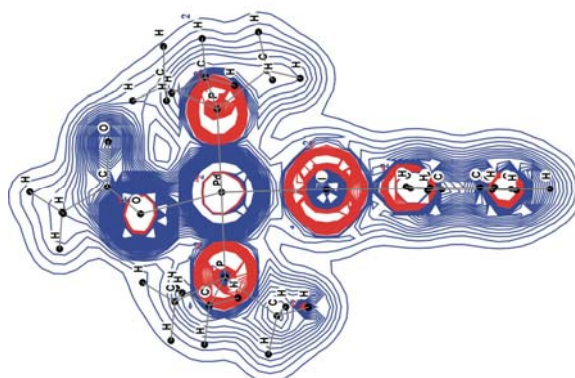
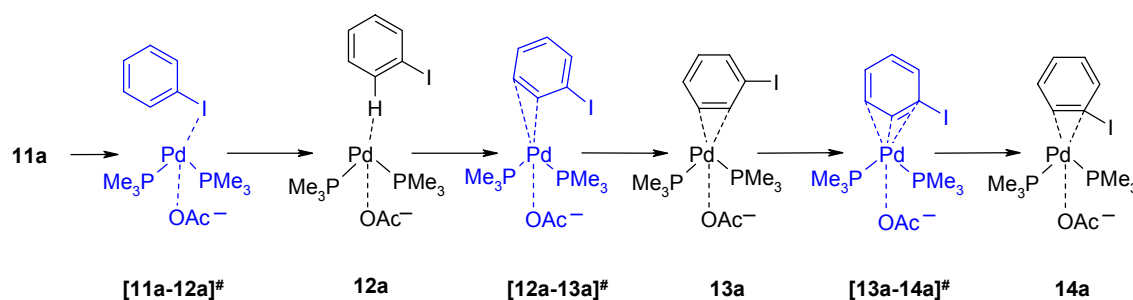


**Figure 2.4.** The Laplacian of the electron density for intermediate **11a**. The contour values are 0.00,  $\pm 0.007$ ,  $\pm 0.014$ ,  $\pm 0.021$ ,  $\pm 0.028$ ,..... Blue and red lines represent negative and positive values, respectively.

### 2.3.3 The mechanism of oxidative addition to anionic palladium(0) species

While the formation of **11a** from aryl iodide and the anionic palladium(0) complex **8a** should proceed very rapidly, the actual oxidative addition reaction can be expected to be a rather complicated process, since the phenyl iodide has to turn around before a cleavage of the C—I bond can be initiated.

#### Scheme 2.6. Reaction pathway from **11a** to **14a**



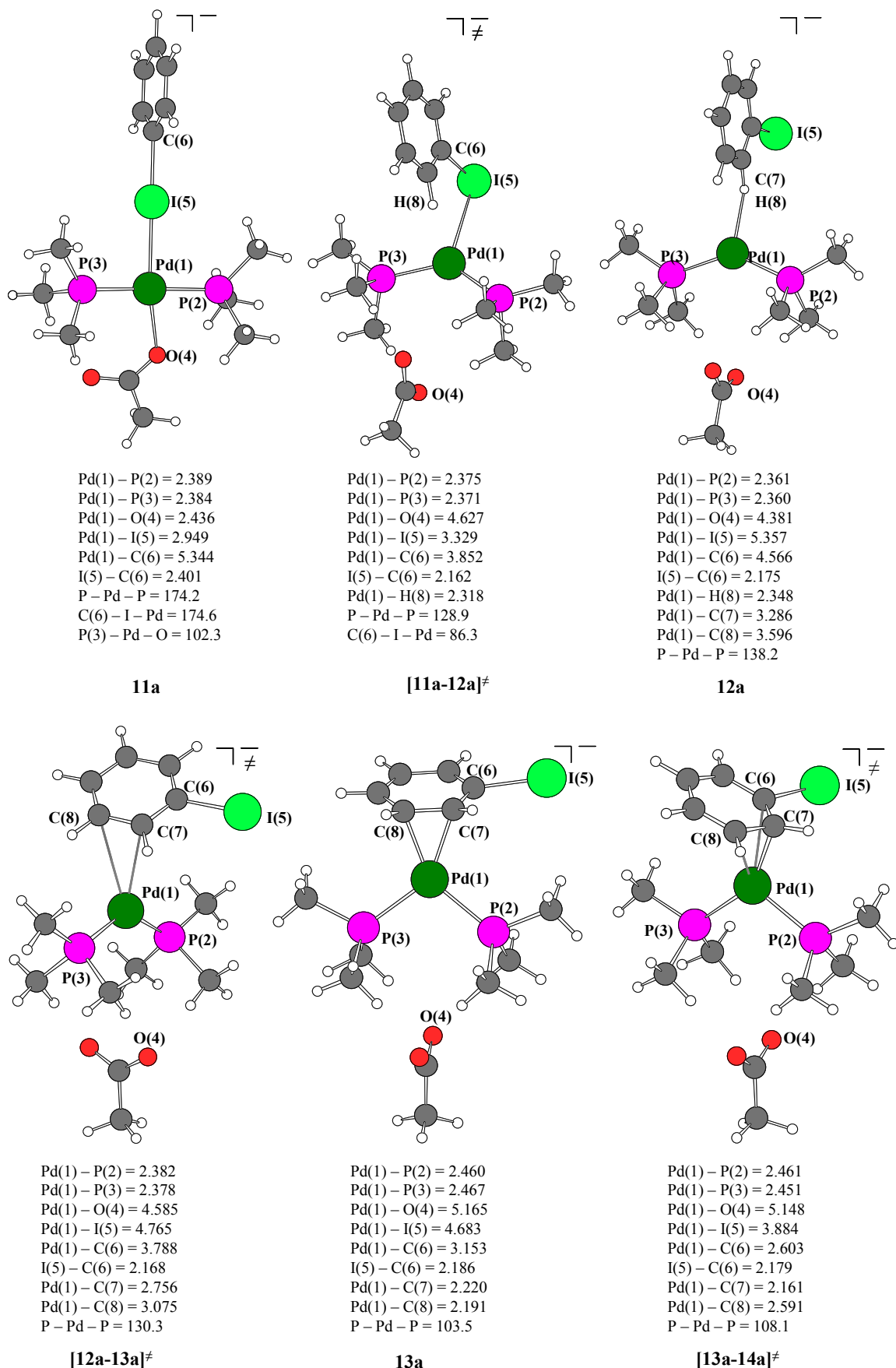
According to our calculations this rearrangement is a multistep process leading to the  $\pi$ -complex **14a**, which is the starting point of the actual C—X cleaving step (Scheme 2.6). The energetics of this sequence is summarized in Table 2.2. It is evident that in contrast to the initial coordination of the aryl iodide, this process requires significant activation energy.

**Table 2.2. Energetics (kcal/mol) for the coordination of phenyl iodide to an anionic palladium(0) species 8a as shown in Scheme 2.6**

Reaction Step	$8a + 9a \rightarrow 11a$	$11a \rightarrow [11a-12a]^{\ddagger}$	$[11a-12a]^{\ddagger} \rightarrow 12a$	$12a \rightarrow [12a-13a]^{\ddagger}$	$[12a-13a]^{\ddagger} \rightarrow 13a$	$13a \rightarrow [13a-14a]^{\ddagger}$	$[13a-14a]^{\ddagger} \rightarrow 14a$
$\Delta E_e$	-20.3	12.6	-1.8	2.2	-10.3	6.7	-9.9
$\Delta E_0$	-19.4	12.5	-1.6	1.8	-9.8	6.3	-9.2
$\Delta H_{298}$	-18.6	11.5	-0.8	1.3	-9.8	6.0	-8.9
$\Delta G_{298}$	-9.3	15.1	-4.2	2.4	-6.8	6.9	-9.9
$\Delta E_{\text{soV}}$	-12.5	9.2	-0.7	2.3	-9.7	6.9	-9.8
$\Delta E_{\text{EXT}}$	-15.2	9.7	-0.5	1.9	-9.3	7.6	-9.5

The calculated geometries of the intermediates and transition states and some of their important structural features are shown in Figure 2.5.

Starting from intermediate **11a**, a linear transit search shortening the C(6)—Pd(1) distance led to the discovery of intermediate **12a**. One of the characteristic features of **12a** is the presence of a C—H interaction with palladium while both the Pd—P distances are almost equivalent (Figure 2.5). Reaching the corresponding transition state  $[11a-12a]^{\ddagger}$  requires only a moderate activation of 12.6 kcal/mol ( $\Delta E_e$ ), and this is already the highest energy barrier in the whole process of the oxidative addition. The imaginary frequency at the transition state reflects the incoming motion of H(8) towards palladium(1) and simultaneous removal of iodine(5). The flatness of the potential energy surface in this region is manifested in the low imaginary frequency of  $[11a-12a]^{\ddagger}$  (25  $\text{icm}^{-1}$ ).



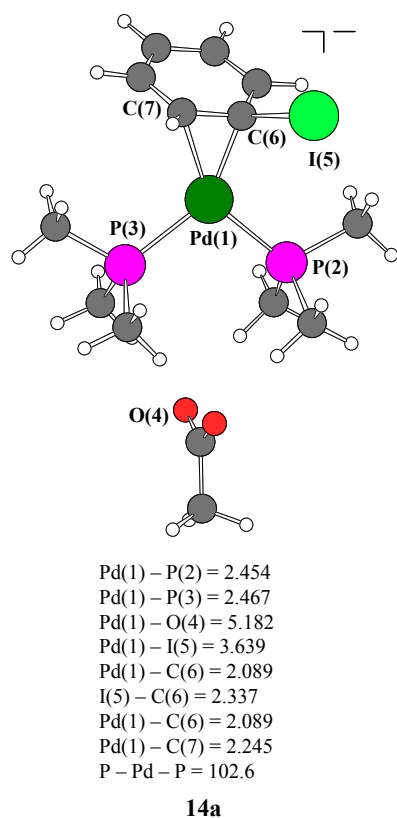


**Figure 2.5.** Optimized structures of intermediates **9a** to **14a** including selected bond lengths (in Å) and angles (in deg).

Concurrently with the approach of the phenyl iodide, an early dissociation of the acetate is observed; in  $[\mathbf{11a-12a}]^{\ddagger}$  the Pd–O(4) distance already amounts to 4.627 Å. A weak bonding interaction of both H(8) and I(5) with palladium can be considered, similar to that observed by Bickelhaupt *et al.* for methyl chloride complexes.[9] The interaction of H(8) with the metal center in  $[\mathbf{11a-12a}]^{\ddagger}$  is manifested in an elongated C(7)–H(8) bond distance (1.115 Å). According to the second-order perturbational NBO analysis, there is a weak donor-acceptor interaction between a d orbital of the palladium and the  $\sigma^*(\text{C(7)–H(8)})$  bond orbital (accounting for ~ 4 kcal/mol). Figure 2.6 shows the KS-LUMO for  $[\mathbf{11a-12a}]^{\ddagger}$ , in which a bonding orbital interaction between Pd(1), H(8) and C(5)–I(6) is visible.

Compared to  $[\mathbf{11a-12a}]^{\ddagger}$ , the intermediate **12a** is only –1.8 kcal/mol ( $\Delta E_e$ ) lower in energy. The rearrangement from **12a** to **13a** through the transition state  $[\mathbf{12a-13a}]^{\ddagger}$  requires an activation energy of only 2.2 kcal/mol ( $\Delta E_e$ ). The mode corresponding to the only imaginary frequency of  $[\mathbf{12a-13a}]^{\ddagger}$  indicates a wagging motion of the phenyl iodide moiety towards the metal center.



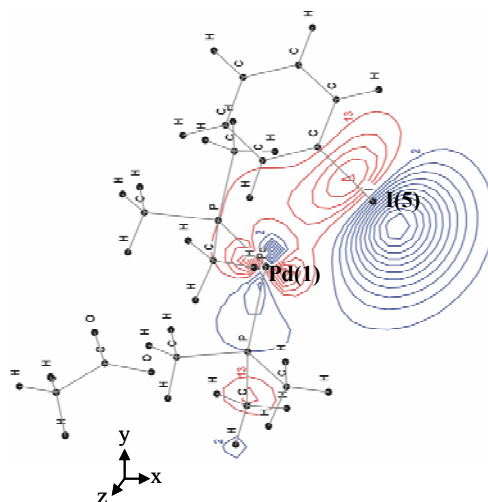


**Figure 2.6.** KS-LUMO for  $[11a-12a]^\ddagger$ . Contour values are 0.00,  $\pm 0.007$ ,  $\pm 0.014$ ,  $\pm 0.021$ ,  $\pm 0.028$ ,.....(in  $e^{1/2} \text{ au}^{-3/2}$ ). Blue and red lines represent negative and positive values, respectively.

$\pi$ -Complexes of type **13a** with  $\eta^2$ -bonding of palladium to the C(7)—C(8)  $\pi$ -bond have been discussed for various organometallic reactions.[9,10,11,19] The NBO analysis of **13a** reveals an electron donation from the  $\pi(\text{C}(7)\text{—C}(8))$  bond orbital to the bonding s-orbital, along with a back donation from the  $d_\pi$ -orbital of the metal to the  $\pi^*(\text{C}(7)\text{—C}(8))$  bond orbital. The presence of the electron-rich trimethyl phosphine ligands increases the electron density on the metal center, and thus enhances the electron donating ability. In the  $\eta^2$ -palladium(0)  $\pi$ -complex **13a**, both the C(8)—Pd(1) and C(7)—Pd(1) bond distances are much shorter than in the transition state  $[12a-13a]^\ddagger$  (Figure 2.5), and the P—Pd—P bond angle decreases by  $26.7^\circ$ , concomitant with the increase of the Pd-acetate distance by almost 0.6 Å. Obviously, the P—Pd—P angle is very sensitive to the position of the acetate: moving the acetate out of the coordination zone of palladium allows for smaller angles.

From intermediate **13a**, the reaction continues *via* transition state ( $[13a-14a]^\ddagger$ ) to another  $\pi$ -complex **14a**. This complex is more stable than **13a** and an ideal precursor for the C—I cleavage reaction. The transition state  $[13a-14a]^\ddagger$  has activation energy of 6.7 kcal/mol ( $\Delta E_c$ ) and is characterized by a single imaginary frequency ( $68 \text{ i cm}^{-1}$ ). The imaginary mode describes the simultaneous breaking of the C(8)—Pd(1) bond and the formation of the C(6)—Pd(1) bond. There is a considerable increase in the C(8)—Pd(1) distance (by 0.400 Å) in  $[13a-14a]^\ddagger$  as compared to **13a**, while both the C(6)—Pd(1) and C(7)—Pd(1) distances are shortened (by 0.550 and 0.059 Å).

A closer look at the  $\eta^3$ -transition state ( $[\mathbf{13a-14a}]^\ddagger$ ) reveals a perpendicular orientation of the C(8)—C(7)—C(6) plane with respect to the P—Pd—P plane. The elongated C(7)—C(8) and C(7)—C(6) distances (1.457 Å and 1.451 Å) in the phenyl group reflect the loss of double bond character in this 3-center bond. Interestingly, both in **13a** and **14a**, the  $\eta^2$ -bonding axis is coplanar with the P—Pd—P plane. Hence, during the reaction the square-planar geometry of the reactant (**13a**) changes to a quasi-tetrahedral transition state ( $[\mathbf{13a-14a}]^\ddagger$ ) and then back to the square-planar product (**14a**). Recently, a similar type of “ring-hopping” transition state has been discussed by Reinhold *et al.* while studying the C—F bond activation in  $M(\text{H}_2\text{PCH}_2\text{CH}_2\text{PH}_2)(\text{C}_6\text{F}_6)$  ( $M = \text{Ni}$  and  $\text{Pt}$ ) complexes.[35]

The product **14a** is stabilized by bonding and back-bonding interactions between palladium and the C(6)—C(7) moiety. The latter are clearly visible in KS-HOMO–2 (see Figure 2.7) involving  $d_{xy}$  at palladium and  $\pi^*$  at C(6)—C(7).

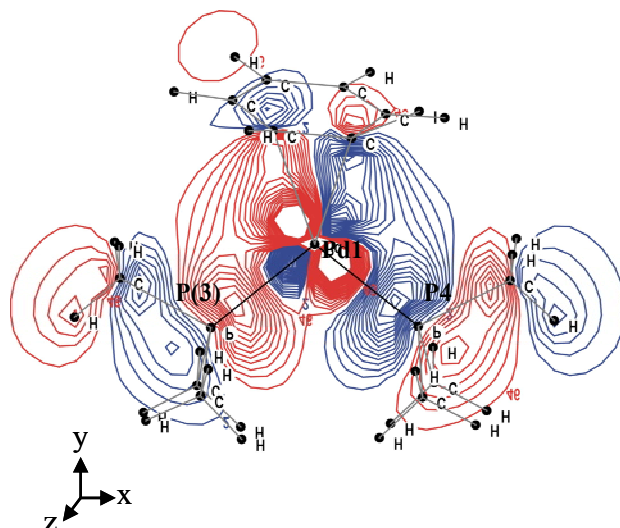
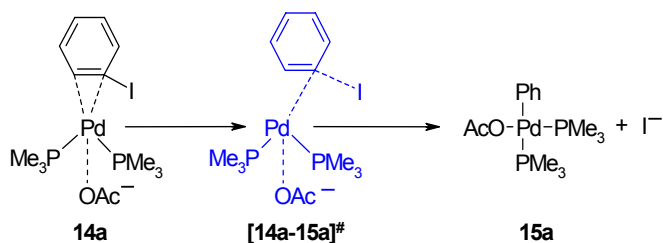


**Figure 2.7.** Kohn-Sham HOMO–2 orbital of **14a**. Contour values are 0.00,  $\pm 0.007$ ,  $\pm 0.014$ ,  $\pm 0.021$ ,  $\pm 0.028$ ,.....(in  $e^{1/2} \text{ au}^{-3/2}$ ). Blue and red lines represent negative and positive values, respectively.

### 2.3.4 The cleavage of the carbon-iodine bond: Path A

We have identified two possible pathways for the cleavage of the C—I bond in **14a**, leading to two different species (**15a** and **18a**). In both of them, the phosphines are located *cis* to each other. We could not identify a pathway leading directly to the more stable *trans* compound **3a**. This is consistent with experimental findings by Espinet *et al.* They added  $\text{C}_6\text{Cl}_2\text{F}_3\text{I}$  to  $\text{Pd}(\text{PPh}_3)_4$  at room temperature and observed, that initially, *cis*- $[\text{Pd}(\text{C}_6\text{Cl}_2\text{F}_3)\text{I}(\text{PPh}_3)_2]$  was formed, which upon heating rearranged to the *trans*-isomer.[7]

## Scheme 2.7. The cleavage of the carbon-iodine bond with removal of the iodide



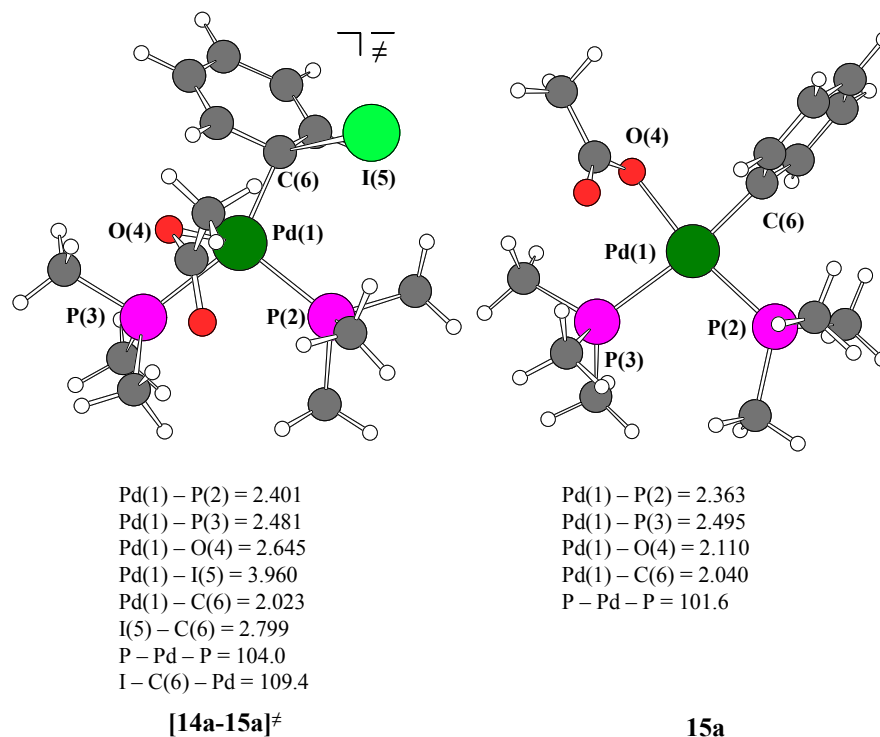
In **14a**, the acetate is held by long-range electrostatic interactions in the complex. When we decreased the palladium-acetate distance, the C(6)–I(5) distance started to increase and finally, the C–I bond broke and the iodide dissociated giving rise to the palladium(II) complex **15a**. The transition state (**[14a-15a]**<sup>‡</sup>) has an activation barrier of only 8.5 kcal/mol ( $\Delta E_e$ , Table 2.3). When going from **14a** to **[14a-15a]**<sup>‡</sup>, the coordination of the phenyl ring changes from  $\eta^2$  to  $\eta^1$ , and the acetate coordinates to the newly available position. In the transition state, the Pd(1)–O(4) and C(6)–I(5) distances amount to 2.645 Å and 2.799 Å, respectively, and the C(6)–I(5) bond becomes highly polarized: The NPA charge on I(5) is increased from –0.074 in **14a** to –0.464 *e* in **[14a-15a]**<sup>‡</sup> (reflecting the formation of an iodide anion). The imaginary mode of 48 *icm*<sup>–1</sup> in **[14a-15a]**<sup>‡</sup> represents the simultaneous incoming of acetate and removal of I(5) from Pd(1).

Table 2.3. Energetics (kcal/mol) for path A as represented in Scheme 2.7

Reaction Step	<b>14a</b> → <b>[14a-15a]</b> <sup>‡</sup>	<b>[14a-15a]</b> <sup>‡</sup> → <b>15a</b>
$\Delta E_e$	8.5	-20.9
$\Delta E_0$	8.2	-19.0
$\Delta H_{298}$	7.9	-18.7
$\Delta G_{298}$	10.3	-27.7
$\Delta E_{\text{sov}}$	6.8	-42.5
$\Delta E_{\text{EXT}}$	10.6	-16.6

In the presence of a polar solvent, the generation of solvated iodide will be more facile than in the gas phase. Indeed, COSMO calculations performed in a solvent field (THF), reduce the

energy difference between **14a** and  $[14a-15a]^{\ddagger}$  to 6.8 kcal/mol ( $\Delta E_{\text{sov}}$ ) and increase the subsequent energy release to  $-42.5$  kcal/mol ( $\Delta E_{\text{sov}}$ ).



**Figure 2.8.** Optimized structures of  $[14a-15a]^{\ddagger}$  and **15a** including selected bond lengths (in Å) and angles (in deg).

The final product **15a** (Figure 2.8) of the oxidative addition is a neutral, square planar  $d^8$  palladium(II) complex. The P–Pd–P angle is  $101.6^\circ$  and the Pd(1)–P(2) distance is greater than the Pd(1)–P(3) distance, due to the strong *trans* influence of the phenyl group. During the reactions discussed in previous sections (*vide supra*), the acetate is close to the metal in **11a**,  $[14a-15a]^{\ddagger}$  and **15a**. In all other species, it is a remote ligand, which remains in proximity to the hydrogen atoms of a  $\text{PMe}_3$  group. In solution, one may expect that these weak gas-phase interactions will not survive and that acetate will be solvated.[19]

### 2.3.5 The cleavage of the carbon-iodine bond: Path B

Looking for an alternative C–I cleavage, we performed a linear transit scan decreasing the Pd(1)–I(5) distance in **14a**. In this case, the iodine remained bound to the palladium, while the acetate was liberated giving rise to complex **17a**. Since the transition state  $[14a-17a]^{\ddagger}$  has a slightly lower energy ( $\Delta E_e = 2.6$  kcal/mol,  $\Delta G_{298} = 3.2$  kcal/mol) in comparison to  $[14a-15a]^{\ddagger}$  this pathway might be kinetically favored. When going from **14a** to  $[14a-17a]^{\ddagger}$  the C(6)–I(5)

distance increases by 0.35 Å, while the Pd(1)—I(5) distance decreases by an amount of 0.23 Å. In  $[14a-17a]^{\ddagger}$  the iodine atom is oriented such that the C(6)—I(5) axis is almost perpendicular to the P—Pd—P plane, with the C(6)—C(7)  $\eta^2$  coordination diminishing as iodine approaches.

### Scheme 2.8. Path B

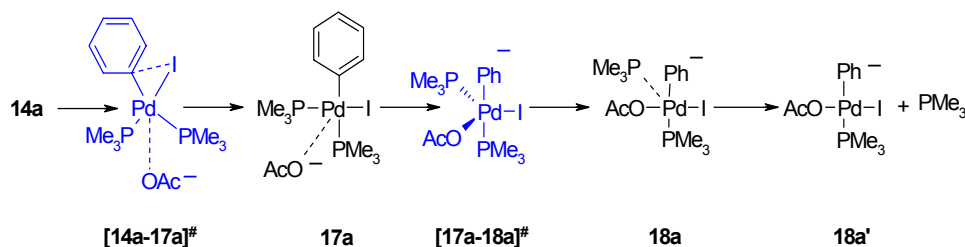
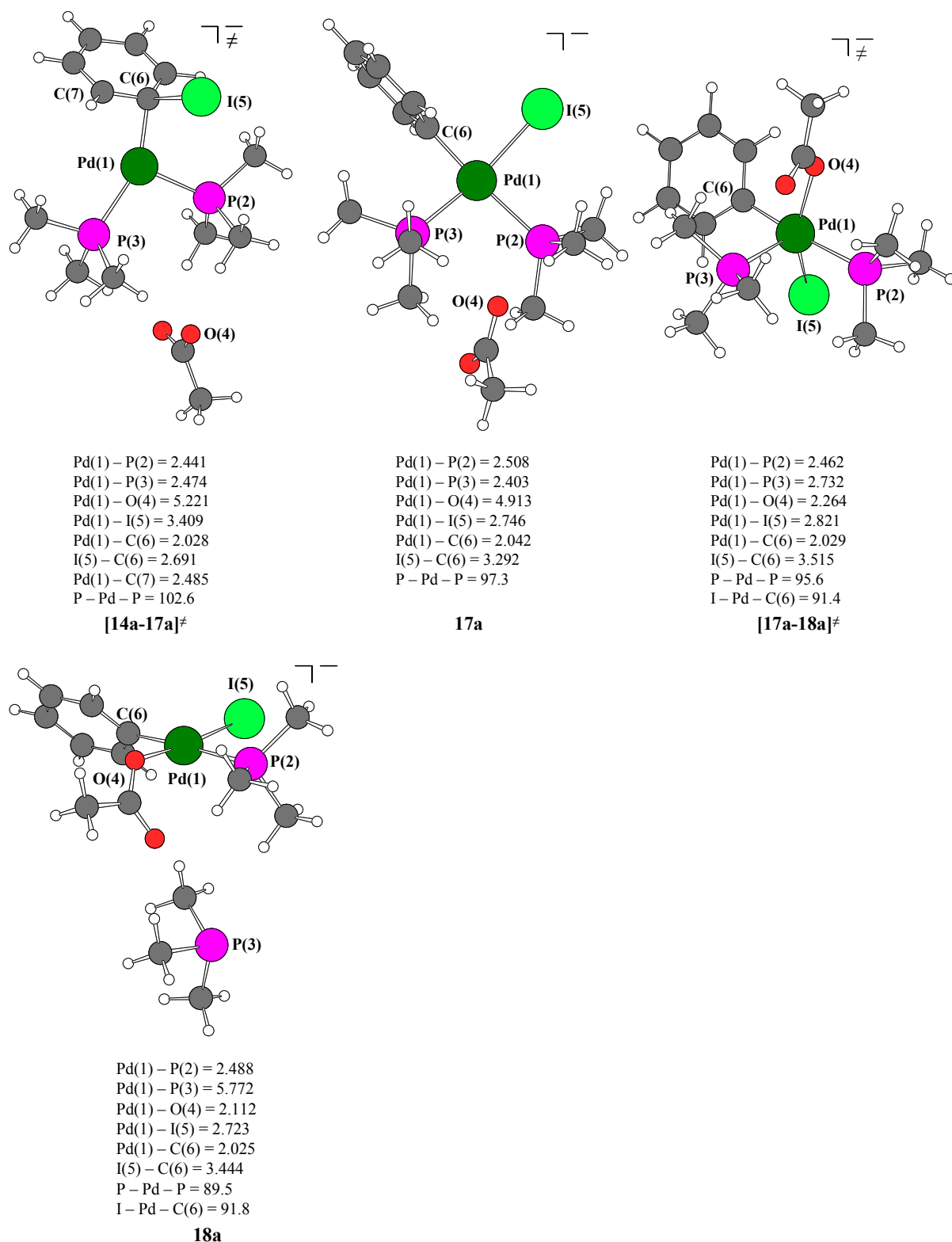


Table 2.4. Energetics (kcal/mol) for path B as represented in Scheme 2.8

Reaction Step	$14a \rightarrow [14a-17a]^{\ddagger}$	$[14a-17a]^{\ddagger} \rightarrow 17a$	$17a \rightarrow [17a-18a]^{\ddagger}$	$[17a-18a]^{\ddagger} \rightarrow 18a$
$\Delta E_e$	2.6	-34.7	12.7	-7.6
$\Delta E_0$	2.7	-33.1	11.1	-7.2
$\Delta H_{298}$	2.3	-33.0	11.3	-6.6
$\Delta G_{298}$	3.2	-32.4	11.4	-9.9
$\Delta E_{\text{soV}}$	2.1	-34.9	13.5	-6.5
$\Delta E_{\text{EXT}}$	4.7	-35.2	17.3	-5.2

Several groups performed similar calculations on H—H and C—H  $\sigma$ -bond activation reactions of metal phosphine complexes  $M(PH_3)_2$  ( $M = Pd, Pt$ )[36,37] and found that the oxidative addition proceeds through an approach of the substrate parallel to the P—Pd—P plane. This appears reasonable since the electron back-donation to the  $\sigma^*$  orbital, that promotes bond breaking, occurs from the  $d_{\parallel}$  orbital in the P—Pd—P plane, and is thus facilitated by electron-donating phosphine ligands. However, other types of transition states for  $\sigma$ -bond activation have also been reported. Sakaki *et al.* found a largely twisted transition state for the activation of C—C and C—Si  $\sigma$  bonds on the  $Pt(PH_3)_2$  complex.[38] Recently, Matsubara *et al.* explained the activation of the C—Sn  $\sigma$ -bond of  $HC\equiv C-SnH_3$  on the  $Pd(PH_3)_2$  complex, through a non-planar, perpendicular approach.[39] Senn *et al.* described a transition state similar to  $[14a-17a]^{\ddagger}$ , where the orientation of the ligands around the palladium center is quasi-tetrahedral.[11]



**Figure 2.9.** Optimized structures of complexes [14a-17a]<sup>‡</sup>, 17a, [17a-18a]<sup>‡</sup> and 18a. Selected bond lengths (in Å) and angles (in deg).

Formation of 17a from [14a-17a]<sup>‡</sup> is highly exothermic by –34.7 kcal/mol ( $\Delta E_e$ ). Complex 17a shows the usual square-planar environment around the metal center with P–Pd–P and I–Pd–C(6) bond angles of 97.3° and 85.5°, respectively. The *trans* influence of the phenyl

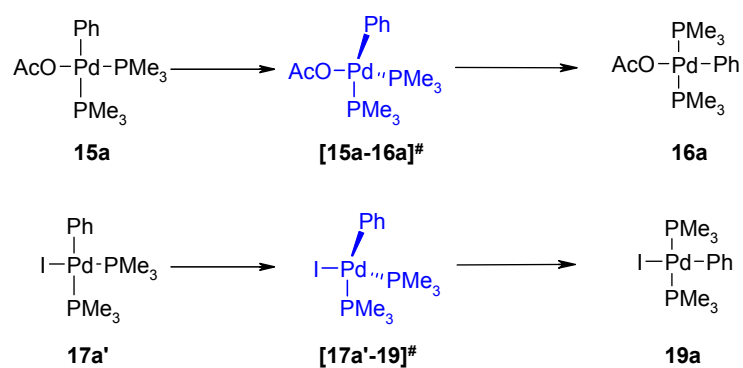
group is also prominent in **17a**, and leads to a longer P(2)—Pd(1) distance. After direct coordination of I(5) to Pd(1), the NPA charge on the metal center is decreased by 0.032 *e*.

Bringing the acetate closer to palladium in a linear transit scan results in the dissociation of one of the phosphines *via* a five-coordinated transition state (**[17a-18a]<sup>‡</sup>**) with acetate and I(5) lying in the equatorial position. The dissociation of iodine might be thermodynamically favorable in solution, but in the gas phase it is endergonic. We observe that the gradual incoming of the acetate from **17a** affords a new intermediate **18a** *via* the transition state **[17a-18a]<sup>‡</sup>**. The gas-phase activation barrier is 12.7 kcal/mol ( $\Delta E_e$ ), which slightly increases to 13.5 kcal/mol ( $\Delta E_{\text{sov}}$ ) in THF.

In **[17a-18a]<sup>‡</sup>**, the Pd(1)—P(3) distance is very large (2.732 Å), indicating that the dissociation of the phosphine is well advanced. The product **18a** is a usual, square-planar palladium(II) complex, with a relatively long Pd(1)—P(2) bond (*i.e.* 2.488 Å), due to the *trans* influence of phenyl group. The second PMe<sub>3</sub> group is completely dissociated and is 5.772 Å away from palladium.

## 2.4 *Cis-trans* isomerization

Three different mechanisms are usually considered for a *cis-trans* isomerization in square planar complexes: the associative pathway,[40] the Berry pseudo-rotation mechanism,[41] and the dissociative pathway.[42] Which of them is most favorable depends on the nature of the solvent, the electronic effects of the ligands and the temperature. Recently, Casado *et al.* performed elaborate kinetic studies on the *cis-trans* isomerization of PdRX(PPh<sub>3</sub>)<sub>2</sub> (R = Aryl, X = halide). They proposed two phosphine (*i.e.* PPh<sub>3</sub>) dependent and two phosphine independent associative pathways. On the basis of their kinetic measurements they rule out dissociative pathways *via* three-coordinate intermediates.[7]

Scheme 2.9. *Cis-trans* isomerizationTable 2.5. Energetics (kcal/mol) for *cis-trans* isomerization

Reaction step	$17a' \rightarrow [17a'-19a]^\ddagger$	$[17a'-19a]^\ddagger \rightarrow 19a$	$15a \rightarrow [15a-16a]^\ddagger$	$[15a-16a]^\ddagger \rightarrow 16a$
$\Delta E_c$	19.5	-28.8	21.4	-32.5
$\Delta E_0$	18.4	-27.2	20.4	-31.3
$\Delta H_{298}$	18.5	-27.4	20.4	-31.3
$\Delta G_{298}$	17.9	-26.0	20.2	-31.5
$\Delta E_{\text{soV}}$	20.2	-27.2	23.7	-31.9
$\Delta E_{\text{EXT}}$	22.4	-32.0	24.3	-33.3



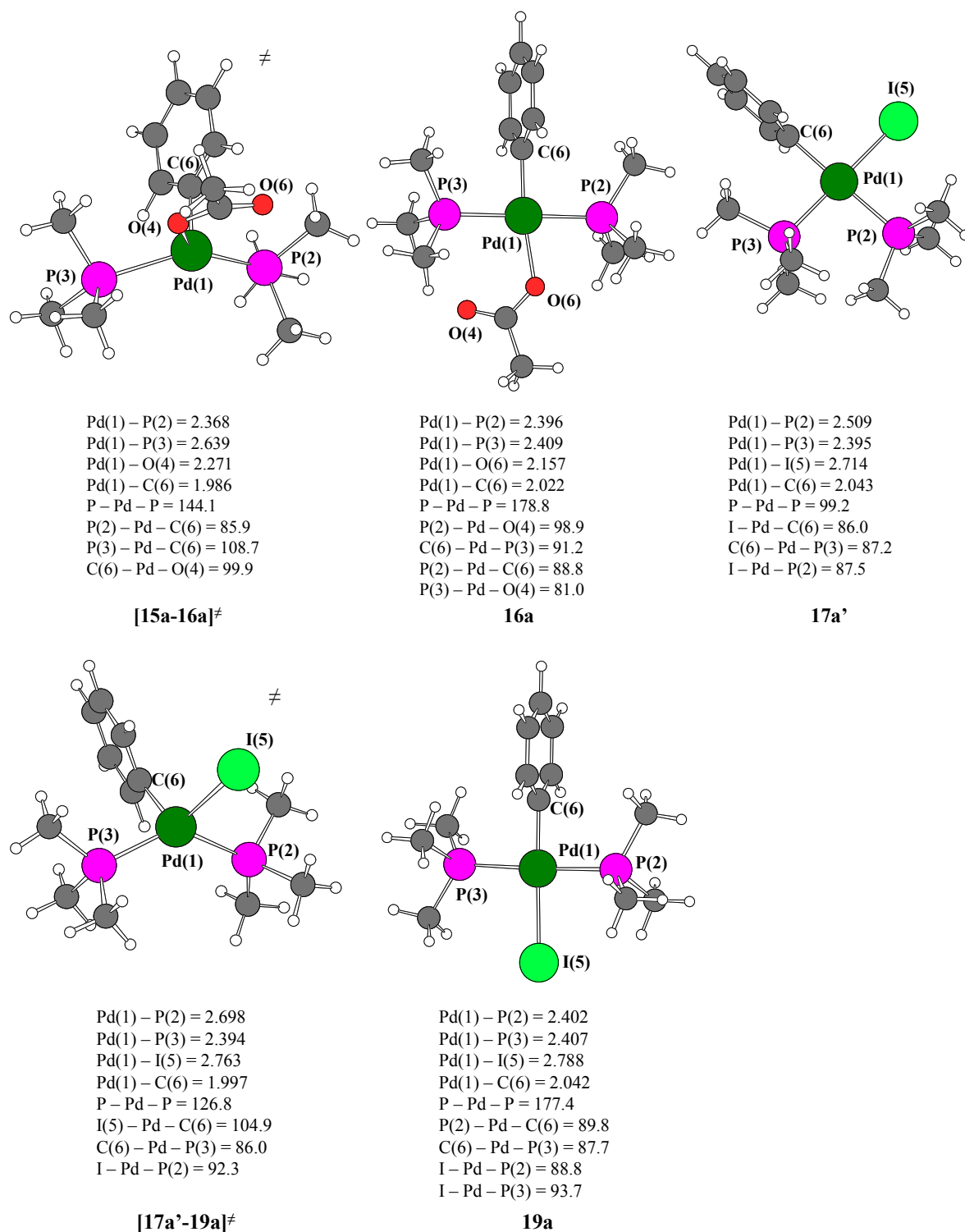


**Figure 2.10.** Optimized structures for complexes [15a-16a]<sup>‡</sup>, 16a, 17a', [17a'-19a]<sup>‡</sup> and 19a. Selected bond distances (in Å) and angles (in deg) are given.

We have calculated a single-step mechanism for the transformation of *cis*-complex 17a' (*i.e.* 17a without the loosely attached AcO<sup>−</sup>) to its *trans* counterpart (19a). In solution, the acetate, which is electrostatically attached to the metal complex in 17a, (Figure 2.9) is expected to be solvated, thereby facilitating its dissociation to form 17a' (17a → 17a' + OAc<sup>−</sup>; ΔE<sub>e</sub> = 32.3

kcal/mol,  $\Delta G_{298} = 17.1$  kcal/mol and  $\Delta E_{\text{sov}} = 1.7$  kcal/mol) therefore **17a'** may serve as a simple model for the situation in solution.

The *cis-trans* isomerization is displayed in Scheme 2.9. The activation barrier in the gas phase is 19.5 kcal/mol ( $\Delta E_e$ ). The structural parameters for the transition state (**[17a'-19a]**<sup>‡</sup>) indicate a quasi-tetrahedral species, arising from an intramolecular rearrangement, which can be viewed as a rotation of C(6)—Pd—I moiety relative to P—Pd—P with concomitant opening of the respective angles. The Pd(1)—C(6) bond length of 1.997 Å in **[17a'-19a]**<sup>‡</sup> is shorter than the values found for **17a'** (2.043 Å) and **19a** (2.042 Å) respectively. The P(2)—Pd(1) bond is longer (2.509 Å) than the P(3)—Pd(1) bond (2.394 Å), due to the higher *trans*-effect of the phenyl group in **17a'**. For the same reason, the Pd(1)—I(5) bond is longer (2.788 Å) in **19a** than in **17a'**. We also studied a similar *cis-trans* isomerization reaction starting from the *cis*-complex **15a**. The latter eventually connects (Figure 2.10) to a quasi-tetrahedral transition state (**[15a-16a]**<sup>‡</sup>), which then affords the *trans*-complex **16a**. The activation barrier for isomerization of **15a** to **16a** is 21.4 kcal/mol ( $\Delta E_e$ ) (Table 2.5).

The lowering of palladium d orbital population is consistent with the process of oxidative addition reaction. Figure 2.11 illustrates the atomic population of the key atoms involved in the oxidative addition process, while Table 2.6 lists selected NPA charges and Wiberg bond indices for various complexes and intermediates. The drastic increase of I(5) population in **11a**, with the concomitant lowering of the palladium population, reflects the charge transfer from palladium to the I(5)—C(6) bond. In the species after **11a**, the I(5) population drastically decreases, because there is no direct coordination to the metal center and hence the charge transfer is not present. The rise of the I(5) population from **14a** onwards is due to the generation of an iodide anion by heterolytic dissociation.

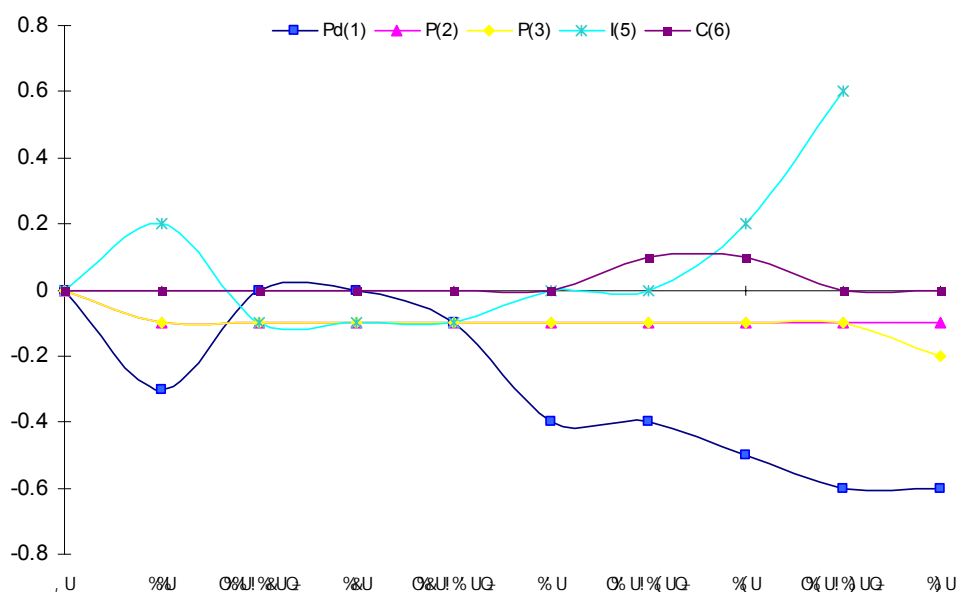


**Figure 2.11.** Natural population changes of selected atoms during Pd–I oxidative addition to **8a**. Positive and the negative signs represent decreases and increases in population, respectively, relative to **8a**.

**Table 2.6.** NPA charges (*e*) for key atoms and Wiberg bond indices for complexes (**8a**–**16a**)

No.	NPA charges								
	Pd(1)	P(2)	P(2)Me <sub>3</sub>	P(3)	P(3)Me <sub>3</sub>	I(5)	O(4)	O(4)Ac <sup>−</sup>	C(6)
<b>8a</b>	0.005	0.700	-0.103	0.729	-0.017	–	-0.782 <sup>+</sup>	-0.876	–
<b>11a</b>	0.044	0.824	0.158	0.812	0.159	-0.099	-0.791	-0.856	-0.222
<b>11a'</b>	-0.044	0.742	0.099	0.734	0.080	0.058	-0.786	-0.911	-0.208
<b>[11a-12a]<sup>+</sup></b>	-0.167	0.734	0.065	0.730	0.064	0.168	-0.785	-0.914	-0.217
<b>12a</b>	-0.253	0.760	0.112	0.760	0.112	0.111	-0.781	-0.919	-0.210
<b>[12a-13a]<sup>+</sup></b>	-0.121	0.740	0.085	0.723	0.064	0.109	-0.777	-0.913	-0.207
<b>13a</b>	0.165	0.749	0.113	0.751	0.108	0.068	-0.778	-0.909	-0.185
<b>[13a-14a]<sup>+</sup></b>	0.169	0.724	0.070	0.729	0.085	0.099	-0.788	-0.912	-0.275
<b>14a</b>	0.237	0.772	0.153	0.763	0.138	-0.074	-0.778	-0.907	-0.299
<b>[14a-15a]<sup>+</sup></b>	0.363	0.816	0.188	0.783	0.129	-0.464	-0.817	-0.873	-0.175
<b>15a</b>	0.387	0.893	0.356	0.795	0.232	–	-0.718	-0.667	-0.193
<b>[14a-17a]<sup>+</sup></b>	0.289	0.830	0.248	0.751	0.148	-0.399	-0.784	-0.903	–
<b>17a</b>	0.257	0.799	0.213	0.899	0.355	-0.534	–	-0.901	-0.206
<b>[17a-18a]<sup>+</sup></b>	0.496	0.822	0.170	0.764	0.077	-0.615	-0.747	-0.769	-0.512
<b>18a</b>	0.440	0.807	0.169	0.689	-0.014	-0.538	-0.699	-0.689	-0.166

## Chapter 2. Oxidative Addition of Aryl Halides to Palladium(0) Complexes: A DFT Study

<b>17a'</b>	0.242	0.767	0.196	0.876	0.334	-0.473	—	—	-0.814
<b>[17a'-19a]<sup>+</sup></b>	0.375	0.670	0.067	0.855	0.321	-0.608	—	—	-0.086
<b>19a</b>	0.236	0.885	0.360	0.888	0.363	-0.589	—	—	-0.277
<b>[15a-16a]<sup>+</sup></b>	0.444	0.706	0.358	0.879	0.115	—	-0.823	-0.805	-0.062
<b>16a</b>	0.348	0.894	0.369	0.902	0.367	—	-0.787	-0.745	-0.204

---

Wiberg bond indices.

	Pd(1)—P(2)	Pd(1)—P(3)	Pd(1)—O(4)	C(6)—I(5)	Pd(1)—I(5)	Pd(1)—C(6)
<b>8a</b>	0.528	0.384	0.125*	—	—	—
<b>11a</b>	0.371	0.404	0.084	0.552	0.328	—
<b>11a'</b>	0.358	0.369	0.001	0.717	0.329	0.134
<b>[11a-12a]<sup>+</sup></b>	0.437	0.423	0.003	0.971	0.079	0.023
<b>12a</b>	0.457	0.459	0.003	0.978	0.007	0.009
<b>[12a-13a]<sup>+</sup></b>	0.418	0.435	0.003	0.980	0.009	0.028
<b>13a</b>	0.326	0.308	0.001	0.964	0.009	0.042
<b>[13a-14a]<sup>+</sup></b>	0.293	0.352	0.001	0.699	0.016	0.126
<b>14a</b>	0.317	0.319	0.001	0.797	0.110	0.342
<b>[14a-15a]<sup>+</sup></b>	0.348	0.290	0.046	0.414	0.163	0.458
<b>15a</b>	0.444	0.297	0.251	—	—	0.509
<b>[14a-17a]<sup>+</sup></b>	0.352	0.327	0.001	0.468	0.176	0.449
<b>17a</b>	0.313	0.403	0.002	0.123	0.347	0.480
<b>[17a-18a]<sup>+</sup></b>	0.295	0.173	0.173	0.109	0.523	0.559
<b>18a</b>	0.291	0.001	0.265	0.119	0.416	0.564
<b>17a'</b>	0.291	0.378	—	—	0.374	0.499
<b>[17a'-19a]<sup>+</sup></b>	0.182	0.393	—	—	0.339	0.679
<b>19a</b>	0.375	0.369	—	—	0.313	0.489
<b>[15a-16a]<sup>+</sup></b>	0.220	0.444	0.134	—	—	0.714
<b>16a</b>	0.380	0.363	0.015*	—	—	0.562

\*In this case O(6) is coordinated to Pd(1); Pd(1)—O(6) = 0.198

## 2.5 Conclusions

In this work we have explored several reaction pathways for oxidative addition reactions of aryl halides to palladium(0) species. Our results confirm that three-coordinate anionic palladium(0) species as proposed by Amatore and Jutand should be stable and can indeed serve as starting points for catalytic reactions. However, we did not find any evidence for the existence of the proposed five-coordinate palladium(II) complexes. Instead, stable four-

coordinate intermediates were found, in which the aryl halides coordinate linearly to the palladium *via* the halide atom. There is no significant energy barrier for the formation of these species, which is consistent with the experimental findings that within seconds after the addition of iodobenzene to a Pd-catalyst, neither the initial palladium(0) species nor free iodide or acetate is detectable.

Furthermore, we have identified two energetically feasible reaction pathways for the actual C—X cleavage reaction starting from these adducts, confirming that such hypervalent halide species might indeed be the initial intermediates formed in catalytic reactions. In the more favorable one, the acetate counterion initially bound to the palladium-catalyst remains at the catalytic center, while the halide originating from the substrate is liberated. Both reaction pathways lead to the formation of *cis* configured palladium(II) complexes. Therefore, a subsequent *cis-trans*-isomerization of these complexes is necessary. This reaction requires significantly more activation than the oxidative addition reaction, confirming that such isomerizations are unfavorable steps in palladium chemistry.

In conclusion, some fundamental steps of palladium catalyzed cross-coupling reactions have been elucidated. In our forthcoming chapters we are focusing on further catalytic steps such as transmetalation and reductive elimination reactions.

## **2.6 Supporting Information**

### **Contents:**

**Table 2.S1.** Absolute energies (hartree) from BP86/LANL2DZ calculations.

**Table 2.S1.** Absolute energies (hartree) from BP86/LANL2DZ calculations.

No.	E <sub>e</sub>	E <sub>0</sub>	H <sub>298</sub>	G <sub>298</sub>	E <sub>sov</sub>
<b>8a</b>	-607.881301	-607.610489	-607.585842	-607.667950	-607.940782
<b>9a</b>	-243.025510	-242.937435	-242.930485	-242.968672	-243.028047
<b>11a</b>	-850.939210	-850.578854	-850.546031	-850.651409	-850.988715
<b>[11a-12a]<sup>‡</sup></b>	-850.919111	-850.558888	-850.527631	-850.627270	-850.974042
<b>12a</b>	-850.921901	-850.561383	-850.528952	-850.634030	-850.975142
<b>[12a-13a]<sup>‡</sup></b>	-850.918319	-850.558476	-850.526870	-850.630133	-850.971472
<b>13a</b>	-850.934655	-850.574101	-850.542458	-850.640999	-850.986859
<b>[13a-14a]<sup>‡</sup></b>	-850.923911	-850.564064	-850.532836	-850.630018	-850.975809
<b>14a</b>	-850.939706	-850.578700	-850.546997	-850.645792	-850.991435
<b>[14a-15a]<sup>‡</sup></b>	-850.926165	-850.565612	-850.534472	-850.629343	-850.980665
<b>15a</b>	-839.454556	-839.090886	-839.061612	-839.151650	-839.464231
<b>[14a-17a]<sup>‡</sup></b>	-850.935574	-850.574396	-850.543316	-850.640772	-850.988127
<b>17a</b>	-850.990831	-850.627114	-850.595985	-850.692393	-851.043691
<b>[17a-18a]<sup>‡</sup></b>	-850.970546	-850.609377	-850.577986	-850.674187	-851.022167
<b>18a</b>	-850.982619	-850.620798	-850.588514	-850.689885	-851.032077
<b>[15a-16a]<sup>‡</sup></b>	-839.420532	-839.058348	-839.029167	-839.119427	-839.426422
<b>16a</b>	-839.472299	-839.108228	-839.078986	-839.169699	-839.477266
<b>17a'</b>	-622.440368	-622.125765	-622.099816	-622.184102	-622.449258
<b>[17a'-19a]<sup>‡</sup></b>	-622.409325	-622.096392	-622.070340	-622.155510	-622.417049
<b>19a</b>	-622.455176	-622.139798	-622.114077	-622.196901	-622.460405
<b>Iodide(I<sup>-</sup>)</b>	-11.504977	-11.504978	-11.502617	-11.521826	-11.584167
<b>PMe<sub>3</sub></b>	-126.244239	-126.133517	-126.125524	-126.163505	-126.245755

E <sub>e</sub>	Electronic energy
E <sub>0</sub>	Total energy plus zero-point vibrational energy
H <sub>298</sub>	Enthalpy at 298 K
G <sub>298</sub>	Gibbs free enthalpy at 298 K
E <sub>sov</sub>	Total energy plus CPCM solvation energy (THF)

## Bibliography

- [1] (a) N. Miyaura, "Metal-Catalyzed Cross-Coupling Reactions." F. Diederich, P. J. Stang, Eds., Wiley-VCH, New York, 2<sup>nd</sup> Edition. **2004**. (b) N. Miyaura, A. Suzuki, "Palladium-Catalyzed Cross-Coupling Reactions of Organoboron Compounds." *Chem. Rev.* **1995**, *95*, 2457-2483.
- [2] (a) A. De Meijere, F. E. Meyer, "Fine Feathers Make Fine Birds: The Heck Reaction in Modern Garb." *Angew. Chem., Int. Ed. Engl.* **1995**, *33*, 2379-2411. (b) I. P. Beletskaya, A. V. Cheprakov, "The Heck Reaction as a Sharpening Stone of Palladium Catalysis." *Chem. Rev.* **2000**, *100*, 3009-3066.
- [3] J. K. Stille, "The Palladium-Catalyzed Cross-Coupling Reactions of Organotin Reagents with Organic Electrophiles." *Angew. Chem., Int. Ed. Engl.* **1986**, *25*, 508-524.
- [4] (a) J. P. Wolfe, H. Tomori, J. P. Sadighi, J. Yin, S. L. Buchwald, "Simple, Efficient Catalyst System for the Palladium-Catalyzed Amination of Aryl Chlorides, Bromides, and Triflates." *J. Org. Chem.* **2000**, *65*, 1158-1174. (b) A. Ehrentraut, A. Zapf, M. Beller, "Progress in the Palladium-Catalyzed  $\alpha$ -Arylation of Ketones with Chloroarenes." *Adv. Synth. Catal.* **2002**, *344*, 209-217 and references therein.
- [5] J. K. Stille, K. S. Y. Lau, "Mechanisms of oxidative addition of organic halides to Group 8 transition-metal complexes." *Acc. Chem. Res.* **1977**, *10*, 434-442.
- [6] (a) A. H. Roy, J. F. Hartwig, "Directly Observed Reductive Elimination of Aryl Halides from Monomeric Arylpalladium(II) Halide Complexes." *J. Am. Chem. Soc.* **2003**, *125*, 13944-13945. (b) J. P. Stambuli, M. Bühl, J. F. Hartwig, "Synthesis, Characterization, and Reactivity of Monomeric, Arylpalladium Halide Complexes with a Hindered Phosphine as the Only Dative Ligand." *J. Am. Chem. Soc.* **2002**, *124*, 9346-9347.
- [7] (a) A. L. Casado, P. Espinet, "Mechanism of the Stille Reaction. 1. The Transmetalation Step. Coupling of  $R^1I$  and  $R^2SnBu_3$  Catalyzed by *trans*-[PdR<sup>1</sup>IL<sub>2</sub>] ( $R^1 = C_6Cl_2F_3$ ;  $R^2 =$  Vinyl, 4-Methoxyphenyl; L = AsPh<sub>3</sub>)." *J. Am. Chem. Soc.* **1998**, *120*, 8978-8985. (b) A. L. Casado, P. Espinet, "On the Configuration Resulting from Oxidative Addition of RX to Pd(PPh<sub>3</sub>)<sub>4</sub> and the Mechanism of the *cis*-to-*trans* Isomerization of [PdRX(PPh<sub>3</sub>)<sub>2</sub>] Complexes (R = Aryl, X = Halide)<sup>†</sup>." *Organometallics* **1998**, *17*, 954-959. (c) P. Espinet, A. M. Echavarren, "The Mechanisms of the Stille Reactions." *Angew. Chem., Int. Ed. Engl.* **2004**, *43*, 4704-4734.



- [8] (a) C. Amatore, A. Jutand, "Anionic Pd(0) and Pd(II) Intermediates in Palladium-Catalyzed Heck and Cross-Coupling Reactions." *Acc. Chem. Res.* **2000**, *33*, 314-321. (b) C. Amatore, M. Azzabi, A. Jutand, "Rates and mechanism of the reversible oxidative of (Z)- and (E)-1,2-dichloroethylene to low-ligated zerovalent palladium." *J. Am. Chem. Soc.* **1991**, *113*, 1670-1677. (c) C. Amatore, A. Jutand, A. Suarez, "Intimate mechanism of oxidative addition to zerovalent palladium complexes in the presence of halide ions and its relevance to the mechanism of palladium-catalyzed nucleophilic substitutions." *J. Am. Chem. Soc.* **1993**, *115*, 9531-9541.
- [9] (a) F. M. Bickelhaupt, T. Ziegler, P. R. von Schleyer, "Oxidative Insertion as Frontside SN2 Substitution: A Theoretical Study of the Model Reaction System Pd + CH<sub>3</sub>Cl." *Organometallics* **1995**, *14*, 2288-2296. (b) A. Diefenbach, F. M. Bickelhaupt, "Oxidative addition of Pd to C—H, C—C and C—Cl bonds: Importance of relativistic effects in DFT calculations." *J. Chem. Phys.* **2001**, *115*, 4030-4040. (c) K. Albert, P. Gisdakis, N. Rösch, "On C—C Coupling by Carbene-Stabilized Palladium Catalysts: A Density Functional Study of the Heck Reaction." *Organometallics* **1998**, *17*, 1608-1616. (d) M. Jakt, L. Johannissen, H. S. Rzepa, D. A. Widdowson, A. Wilhelm, "A computational study of the mechanism of palladium insertion into alkynyl and aryl carbon-fluorine bonds." *J. Chem. Soc., Perkin Trans. 2* **2002**, 576-581.
- [10] A. Sundermann, O. Uzan, J. M. L. Martin, "Computational Study of a New Heck Reaction Mechanism Catalyzed by Palladium(ii/iv) Species." *Chem. Eur. J.* **2001**, *7*, 1703-1711.
- [11] H. M. Senn, T. Ziegler, "Oxidative Addition of Aryl Halides to Palladium(0) Complexes: A Density-Functional Study Including Solvation." *Organometallics* **2004**, *23*, 2980-2988.
- [12] (a) J. F. Fauvarque, A. Jutand, "Arylation of the Reformatsky Reagent Catalyzed by Zerovalent Complexes of Nickel and Palladium." *J. Organomet. Chem.* **1977**, *132*, C17-C19. (b) J. F. Fauvarque, A. Jutand, "Action de divers nucléophiles sur des organopalladiques." *Bull. Soc. Chim. Fr.* **1976**, 765-770.
- [13] (a) S. Hansson, P. O. Norrby, M. P. T. Sjögren, B. Åkermark, M. E. Cucciolito, F. Giordano, A. Vitagliano, "Effects of phenanthroline type ligands on the dynamic processes of ( $\eta^3$ -Allyl)palladium Complexes. Molecular Structure of (2,9-Dimethyl-1,10-

phenanthroline)[(1,2,3- $\eta$ )-3-methyl-2-butenyl]-chloropalladium.” *Organometallics* **1993**, *12*, 4940-4948. (b) M. Bröring, C. D. Brandt, “A five coordinate Pd<sup>II</sup> complex stable in solution and in the solid state.” *Chem. Commun.* **2003**, 2156-2157.

[14] Gaussian 03, Revision B.01, M. J. Frisch, G. W. Trucks, H. B. Schlegel, G. E. Scuseria, M. A. Robb, J. R. Cheeseman, J. A. Montgomery, Jr., T. Vreven, K. N. Kudin, J. C. Burant, J. M. Millam, S. S. Iyengar, J. Tomasi, V. Barone, B. Mennucci, M. Cossi, G. Scalmani, N. Rega, G. A. Petersson, H. Nakatsuji, M. Hada, M. Ehara, K. Toyota, R. Fukuda, J. Hasegawa, M. Ishida, T. Nakajima, Y. Honda, O. Kitao, H. Nakai, M. Klene, X. Li, J. E. Knox, H. P. Hratchian, J. B. Cross, C. Adamo, J. Jaramillo, R. Gomperts, R. E. Stratmann, O. Yazyev, A. J. Austin, R. Cammi, C. Pomelli, J. W. Ochterski, P. Y. Ayala, K. Morokuma, G. A. Voth, P. Salvador, J. J. Dannenberg, V. G. Zakrzewski, S. Dapprich, A. D. Daniels, M. C. Strain, O. Farkas, D. K. Malick, A. D. Rabuck, K. Raghavachari, J. B. Foresman, J. V. Ortiz, Q. Cui, A. G. Baboul, S. Clifford, J. Cioslowski, B. B. Stefanov, G. Liu, A. Liashenko, P. Piskorz, I. Komaromi, R. L. Martin, D. J. Fox, T. Keith, M. A. Al-Laham, C. Y. Peng, A. Nanayakkara, M. Challacombe, P. M. W. Gill, B. Johnson, W. Chen, M. W. Wong, C. Gonzalez, and J. A. Pople, Gaussian, Inc., Pittsburgh PA, **2003**.

[15] (a) A. D. Becke, “Density-functional exchange-energy approximation with correct asymptotic behaviour.” *Phys. Rev. A* **1988**, *38*, 3098-3100. (b) J. P. Perdew, “Density-functional approximation for the correlation energy of the inhomogeneous electron gas.” *Phys. Rev. B* **1986**, *33*, 8822-8824.

[16] T. H. Dunning, Jr., P. J. Hay, “Modern Theoretical Chemistry”, H. F. Schaefer III, Eds., Plenum, New York, **1976**, Vol. 3, page 1.

[17] P. J. Hay, W. R. Wadt, “*Ab initio* effective core potentials for molecular calculations. Potentials for K to Au including the outermost core orbitals.” *J. Chem. Phys.* **1985**, *82*, 299-310.

[18] G. Boche, M. Schimeczek, J. Cioslowski, P. Piskorz, “The Role of Ate Complexes in Halogen(Metalloid)-Metal Exchange Reactions: A Theoretical Study.” *Eur. J. Org. Chem.* **1998**, 1851-1860 and references therein.

[19] L. J. Gooßen, D. Koley, H. Hermann, W. Thiel, “The mechanism of the oxidative addition of aryl halides to Pd-catalysts: a DFT investigation.” *Chem. Commun.* **2004**, 2141-2143.

- [20] (a) V. Barone, M. Cossi, "Quantum Calculations of Molecular Energies and Gradients in Solutions by a Conductor Solvent Model." *J. Phys. Chem. A* **1998**, *102*, 1995-2001. (b) M. Cossi, N. Rega, G. Scalmani, V. Barone, "Energies, Structures, and Electronic Properties of Molecules in Solution with the C-PCM Solvation Model." *J. Comput. Chem.* **2003**, *24*, 669-681.
- [21] A Klamt, G. Schüürmann, "COSMO: A New Approach to Dielectric Screening in Solvents with Explicit Expressions for the Screening Energy and its Gradient." *J. Chem. Soc. Perkin Trans 2.* **1993**, 799-805. (b) A. Schäfer, A. Klamt, D. Sattel, J. C. W. Lohrenz, F. Eckert, "COSMO Implementation in TURBOMOLE: Extension of an efficient quantum chemical code towards liquid systems." *Phys. Chem. Chem. Phys.* **2000**, *2*, 2187-2193..
- [22] D. Andrae, U. Häußermann, M. Dolg, H. Stoll, H. Preuß, "Energy-adjusted ab initio pseudopotentials for the second and third row transition elements." *Theor. Chim. Acta* **1990**, *77*, 123-141.
- [23] A. Bergner, M. Dolg, W. Küchle, H. Stoll, H. Preuß, "Ab initio energy-adjusted pseudopotential for elements of group 13 through 17." *Mol. Phys.* **1993**, *80*, 1431-1441.
- [24] J. M. L. Martin, A. Sundermann, "Correlation consistent valence basis sets for use with the Stuttgart-Dresden-Bonn relativistic effective core potentials: The atoms Ga-Kr and In-Xe." *J. Chem. Phys.* **2001**, *114*, 3408-3420.
- [25] (a) T. H. Dunning Jr., "Gaussian basis sets for use in correlated molecular calculations. I. The atoms boron through neon and hydrogen." *J. Chem. Phys.* **1989**, *90*, 1007-1023. (b) R. A. Kendall, T. H. Dunning Jr., R. J. Harrison, "Electron affinities of the first-row atoms revisited. Systematic basis sets and wave functions." *J. Chem. Phys.* **1992**, *96*, 6796-6806. (c) D. E. Woon, T. H. Dunning Jr., "Gaussian basis sets for use in correlated molecular calculations. III. The atoms aluminium through argon." *J. Chem. Phys.* **1993**, *98*, 1358-1371.
- [26] K. A. Peterson, D. E. Woon, T. H. Dunning Jr., "Benchmark calculations with correlated molecular wave functions. IV. The classical barrier height of the  $\text{H}+\text{H}_2\rightarrow\text{H}_2+\text{H}$  reaction." *J. Chem. Phys.* **1994**, *100*, 7410-7415.
- [27] G. T. de Jong, M. Sola, L. Visscher, F. M. Bickelhaupt, "Ab initio benchmark study for the oxidative addition of  $\text{CH}_4$  to Pd: Importance of basis-set flexibility and polarization." *J. Chem. Phys.* **2004**, *121*, 9982-9992.

- [28] (a) A. E. Reed, L. A. Curtiss, F. Weinhold, "Intermolecular Interactions from a Natural Bond Orbital, Donor-Acceptor Viewpoint." *Chem. Rev.* **1998**, *88*, 899-926. (b) E. D. Glendening, A. E. Reed, J. E. Carpenter, Weinhold, F. *NBO Version 3.1*.
- [29] K. B. Wiberg, "Application of the Pople-Santry-Segal CNDO method to the cyclopropylcarbinyl and cyclobutyl cation and to bicyclobutane." *Tetrahedron* **1968**, *24*, 1083-1096.
- [30] G. Schaftenaar, J. H. Noordik, "Molden: a pre- and post-processing program for molecular and electronic structures." *J. Comput. -Aided Mol. Des.* **2000**, *14*, 123-134.
- [31] S. Kozuch, S. Shaik, A. Jutand, C. Amatore, "Active Anionic Zero-Valent Palladium Catalysts: Characterization by Density Functional Calculations." *Chem. Eur. J.* **2004**, *10*, 3072-3080.
- [32] R. Ahlrichs, M. Bär, M. Häser, H. Horn, C. Kölmel, "Electronic structure calculations on workstation computers: The program system turbomole." *Chem. Phys. Lett.* **1989**, *162*, 165.
- [33] D. F. Shriver, P. W. Atkins, C. H. Langford, "Inorganic Chemistry" 2<sup>nd</sup> Edition, Oxford University Press, Oxford, **1994**.
- [34] (a) R. F. W. Bader, "A quantum theory of molecular structure and its applications." *Chem. Rev.* **1991**, *91*, 893-928. (b) R. F. W. Bader, P. L. A. Popelier, T. A. Keith, "Theoretical Definition of a Functional Group and the Molecular Orbital Paradigm." *Angew. Chem., Int. Ed. Engl.* **1994**, *33*, 620-631. (c) R. F. W. Bader, C. F. Matta, "Bonding to Titanium." *Inorg. Chem.* **2001**, *40*, 5603-5611. (d) R. F. W. Bader, C. F. Matta, F. Cortés-Guzmán, "Where To Draw the Line in Defining a Molecular Structure." *Organometallics* **2004**, *23*, 6253-6263.
- [35] M. Reinhold, J. E. McGrady, R. N. Perutz, "A Comparison of C—F and C—H Bond Activation by Zerovalent Ni and Pt: A Density Functional Study." *J. Am. Chem. Soc.* **2004**, *126*, 5268-5276.
- [36] (a) J. J. Low, W. A. Goddard III, "Theoretical Studies of Oxidative Addition and Reductive Elimination:  $\text{H}_2 + \text{Pt}(\text{PH}_3)_2 \rightarrow \text{Pt}(\text{H})_2(\text{PH}_3)_2$ ." *J. Am. Chem. Soc.* **1984**, *106*, 6928-6937. (b) S. Obara, K. Kituara, K. Morokuma, "Reaction Mechanisms of Oxidative Addition [ $\text{H}_2 + \text{Pt}^0(\text{PH}_3)_2 \rightarrow \text{Pt}^{\text{II}}(\text{H})_2(\text{PH}_3)_2$ ] and Reductive Elimination [ $\text{Pt}^{\text{II}}(\text{H})(\text{CH}_3)(\text{PH}_3)_2 \rightarrow \text{CH}_4 + \text{Pt}^0(\text{PH}_3)_2$ ]. Ab Initio MO Study." *J. Am. Chem. Soc.* **1984**, *106*, 7482-7492.

- [37] (a) J. J. Low, W. A. Goddard III, "Reductive Coupling of H, H—C, and C—C Bonds from Palladium complexes." *J. Am. Chem. Soc.* **1984**, *106*, 8321-8322. (b) J. J. Low, W. A. Goddard III, "Theoretical Studies of Oxidative Addition and Reductive Elimination. 2. Reductive Coupling of H—H, H—C, and C—C Bonds from Palladium and Platinum Complexes<sup>†</sup>." *Organometallics* **1996**, *5*, 609-622. (c) J. J. Low, W. A. Goddard III, "Theoretical studies of oxidative addition and reductive elimination. 3. C—H and C—C reductive coupling from palladium and platinum bis(phosphine) complexes." *J. Am. Chem. Soc.* **1986**, *108*, 6115-6128.
- [38] S. Sakaki, N. Mizoe, Y. Musashi, B. Biswas, M. Sugimoto, "Is a Transition State Planar or Nonplanar in Oxidative Additions of C—H, Si—H, C—C, and Si—C  $\sigma$ -Bonds to Pt(PH<sub>3</sub>)<sub>2</sub>? A Theoretical Study." *J. Phys. Chem. A* **1998**, *102*, 8027-8036.
- [39] (a) T. Matsubara, "Density Functional Study on the Mechanism of the Oxidative Addition of the Highly Polarized Sn—C  $\sigma$ -Bond to the (LH<sub>3</sub>)(L'H<sub>3</sub>)Pd and (LH<sub>2</sub>C<sub>2</sub>H<sub>4</sub>LH<sub>2</sub>)Pd (L, L' = N, P, As, Sb) Complexes." *Organometallics* **2003**, *22*, 4286-4296. (b) T. Matsubara, K. Hirao, "Importance of the Apical Site of the (H<sub>2</sub>PC<sub>2</sub>H<sub>4</sub>PH<sub>2</sub>)Pd Complex on the Elementary Reactions. A Density Functional Study." *Organometallics* **2002**, *21*, 2662-2673.
- [40] F. Basolo, G. Pearson, "Mechanism of Inorganic Reactions." 2<sup>nd</sup> Edition, Wiley, New York, **1967**.
- [41] (a) G. K. Anderson, R. J. Cross, "Isomerisation mechanisms of square-planar complexes." *Chem. Soc. Rev.* **1980**, *9*, 185-215. (b) R. S. Berry, "Correlation of Rates of Intramolecular Tunneling Processes, with Application to Some Group V Compounds." *J. Chem. Phys.* **1960**, *32*, 933-938.
- [42] (a) F. Ozawa, T. Ito, Y. Nakamura, A. Yamamoto, "Mechanism of Thermal Decomposition of *trans*- and *cis*-Dialkylbis(tertiaryphosphine)palladium(II). Reductive Elimination and *trans* to *cis* Isomerization." *Bull. Chem. Soc. Jpn.* **1981**, *54*, 1868-1880. (b) R. S. Pavonessa, W. C. Troglor, "Solvent-Dependent Reactions of Carbon Dioxide with a Platinum(II) Dihydride. Reversible Formation of a Platinum(II) Formatehydride and a Cationic Platinum(II) Dimer, [Pt<sub>2</sub>H<sub>3</sub>(PEt<sub>3</sub>)<sub>4</sub>][HCO<sub>2</sub>]." *J. Am. Chem. Soc.* **1982**, *104*, 3529-3530.









## The Palladium-Catalyzed Cross-Coupling Reaction of Carboxylic Anhydrides with Arylboronic Acids: A DFT Study.

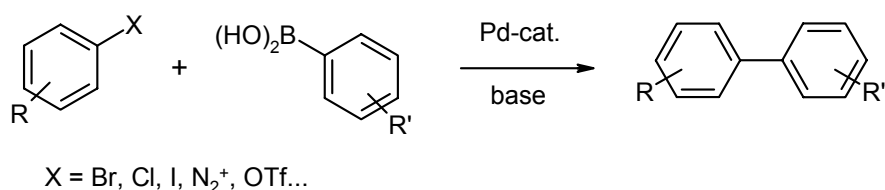
*The true student will seek evidence to establish fact rather than confirm his own concept of truth, for truth exists whether it is discovered or not*

(Melven Calvin, Chemical Evolution, Chapter 11, page 252)

### 3.1 Introduction

Palladium-catalyzed cross-coupling reactions of arylboronic acids are powerful synthetic tools broadly applied throughout research laboratories and industrial production.[1] The most prominent example is the Suzuki coupling of aryl halides with arylboronic acids, which due to its high selectivity and the mild reaction conditions is the method of choice for the synthesis of biaryls (Scheme 3.1). In the last decades, numerous related palladium-catalyzed couplings have been developed, *e.g.* for the synthesis of dienes,[2] arylacetic acids[3] or arylketones.[4]

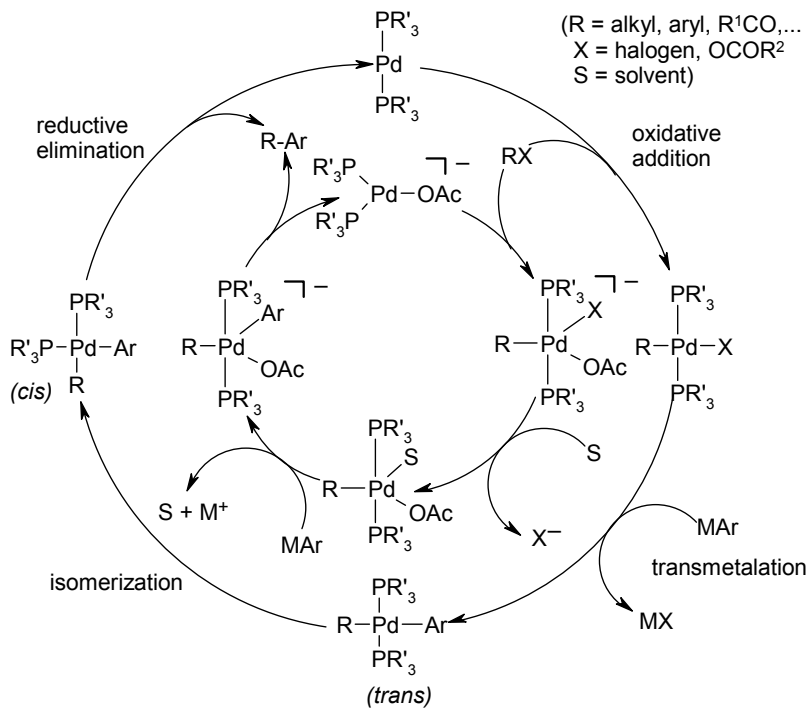
#### Scheme 3.1. Suzuki biaryl synthesis



Despite their enormous synthetic importance, the mechanism of such reactions is still not fully understood. The initially proposed catalytic cycle (“textbook mechanism”) consists of an oxidative addition of the aryl halide to a coordinatively unsaturated  $\text{Pd}(0)\text{L}_2$  species, followed by a transmetalation step in which the aryl residue is transferred from boron to palladium, and finally a reductive elimination to provide the biaryl product (Scheme 3.2).[1] Unfortunately, this mechanism provides no explanation for the pronounced influence exerted on catalytic activities by counterions, originating from either palladium(II) pre-catalysts or added metal salts.[5] One way to rationalize these effects is *via* the more complex reaction mechanism proposed by Amatore and Jutand, which involves an additional, faster catalytic cycle that starts from a three-coordinate anionic  $[\text{Pd}(0)\text{L}_2\text{X}]^-$  species and involves five-coordinate palladium(II) intermediates.[5] However, while the existence of anionic  $[\text{Pd}(0)\text{L}_2\text{X}]^-$  species could

meanwhile be confirmed both spectroscopically and by theoretical studies,[6,7] there still is no proof for the existence of five-coordinate intermediates.[6,8]

**Scheme 3.2. “Textbook” (outer cycle) and “Amatore-Jutand” (inner cycle) mechanisms for cross-coupling reactions**

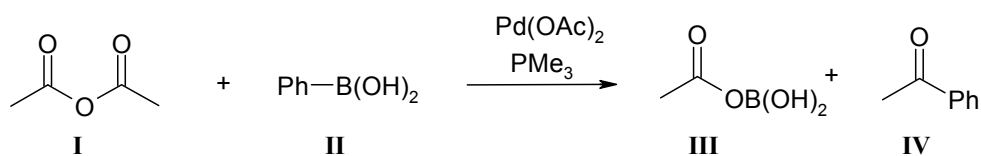


In-depth mechanistic studies as well as theoretical calculations on Suzuki coupling are difficult since the reaction mixtures tend to be extremely complex. In most protocols, the catalysts are generated *in situ* from palladium(II) salts and phosphine ligands, and the reaction mixtures not only contain arylboronic acids and aryl halides but also bases, coordinating solvents, and sometimes further additives.[1] Thus, a great variety of palladium species can potentially be formed, which all must be considered as possible intermediates in the catalytic process. This complexity, especially in the later stages of the reaction, is probably the main reason why there are very only few mechanistic studies on the Suzuki coupling,[1a,9] in contrast to related reactions such as hydroborations[10] or Heck olefinations.[11]

In this article, we use density functional theory (DFT) to investigate the mechanism of palladium-catalyzed cross-coupling reactions. We have chosen to focus not on the classic Suzuki biaryl synthesis, but on the conceptually very similar cross-coupling of carboxylic anhydrides with boronic acids.[4] This aryl ketone synthesis, itself of high synthetic interest and versatility, is believed to proceed *via* an analogous mechanism (Scheme 3.2,  $R = COMe$ ,  $X = OCOMe$ ), and the similarity between the oxidative addition of aryl halides and anhydrides is already well-documented.[12]

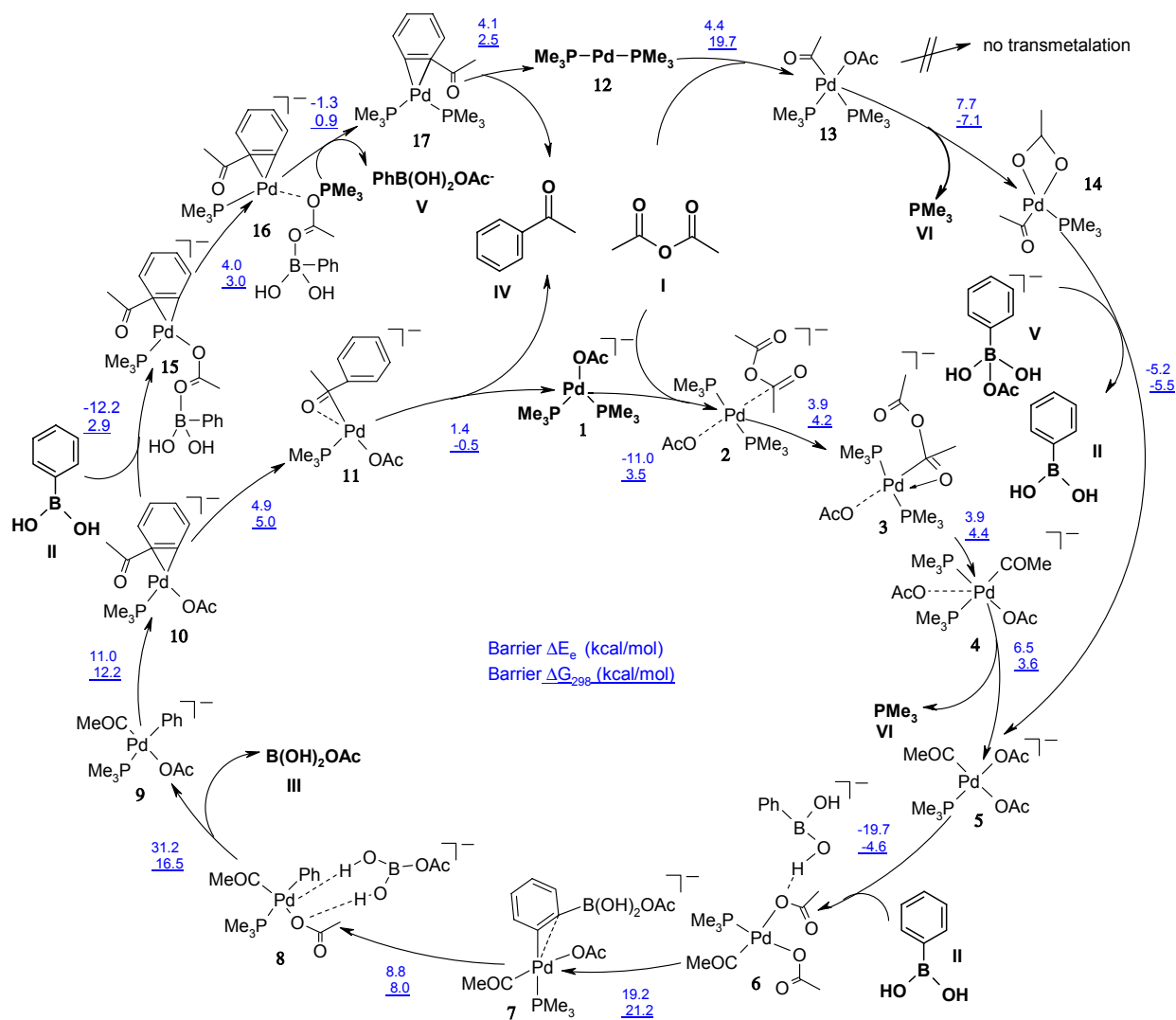
While this coupling reaction contains all important features of the Suzuki biaryl synthesis, it can be reduced to much greater simplicity without becoming unrealistic: The most elementary but still experimentally viable model system is the reaction of acetic anhydride with phenylboronic acid in the presence of a palladium(II)acetate/trimethylphosphine catalyst (Scheme 3.3). In this reaction, the acetate ion plays a triple role as the leaving group, the base, and the counterion in the palladium(II) precursor, so that the overall number of possible intermediates is greatly reduced.

**Scheme 3.3. Cross-coupling of acetic anhydride with phenylboronic acid**



Using density functional theory (BP86/6-31G\*), we have computed two full catalytic cycles for this model reaction, one starting from a neutral  $\text{Pd}(0)\text{L}_2$  complex, and the other one from the “Jutand-type” anionic  $[\text{Pd}(0)\text{L}_2\text{X}]^-$  species (Scheme 3.4). These are the first complete catalytic cycles that have been calculated for the coupling of carbon electrophiles with boronic acids, and to the best of our knowledge, they are also the first computational studies on transmetalation reactions of boronic acids in general. To minimize the computational effort, we have chosen the ligand to be trimethylphosphine ( $\text{L} = \text{PMe}_3$ ) which is smaller and more electron-rich than the triarylphosphines that are commonly used in experimental studies.[12] In contrast to the corresponding triarylphosphine complexes, palladium(0) complexes of  $\text{PMe}_3$  undergo facile oxidative addition reactions with anhydrides even at room temperature.[12] For this reason, the calculations for our model system are expected to yield a rather low barrier for the oxidative addition and a relatively high barrier for the reductive elimination compared with the systems investigated experimentally. However, once a viable reaction pathway for this model system has been identified, it can serve as the starting point for studies on more realistic systems with larger phosphine ligands.

**Scheme 3.4.** Main intermediates of the calculated catalytic cycles starting either from a neutral or an anionic palladium species



The general features of the calculated cycles shown in Scheme 3.4 are consistent with the proposed mechanisms outlined in Scheme 3.2. However, there are also some striking differences: While the “textbook mechanism” mainly proceeds *via trans*-configured palladium(II)diphosphine complexes (Scheme 3.2), *cis*-configured intermediates dominate in the calculated catalytic cycles (Scheme 3.4). Moreover, according to the proposition of Amatore and Jutand, the anionic pathway involves five-coordinate species, whereas we find only four-coordinate intermediates, in qualitative agreement with related calculations on the oxidative addition of aryl halides to anionic palladium(0) complexes.[6,8] Interestingly, the transmetalation step is predicted to proceed *via* the same pathway for both catalytic cycles (Scheme 3.4).

### 3.2 Computational Details

All calculations were performed with the Gaussian98 and Gaussian03 suites of programs.[13] The DFT calculations employed the BP86 functional[14,15] using the standard 6-31G\* basis[16] for all atoms, except for palladium which was described by the LANL2DZ valence basis set in combination with the corresponding effective core potential.[17] Geometries were fully optimized, normally without symmetry constraints. Harmonic force constants were computed at the optimized geometries to characterize the stationary points as minima or saddle points. Zero-point vibrational corrections were determined from the harmonic vibrational frequencies to convert the total energies  $E_e$  to ground-state energies  $E_0$ . The rigid-rotor harmonic-oscillator approximation was applied for evaluating the thermal and entropic contributions that are needed to derive the enthalpies  $H_{298}$  and Gibbs free enthalpies  $G_{298}$  at 298 K. Transition states were located from a linear transit scan in which the reaction coordinate was kept fixed at different distances while all other degrees of freedom were optimized. After the linear transit search the transition states were optimized using the default Berny algorithm implemented in the Gaussian code.[13] In critical cases, the nature of a given transition state was analyzed by IRC (Intrinsic Reaction Coordinate) computations.

For further validation, single-point BP86 calculations were performed at the optimized BP86/6-31G\* geometries employing a larger basis set (EXT): Palladium was described by a Stuttgart-Dresden quasirelativistic pseudopotential and the associate (8s7p5d)/[6s5p3d] valence basis set,[18] the 6-31+G\* basis was employed for B, C, O, and P, and the 6-31G\*\* basis for all H atoms[16] (abbreviated as BP86/EXT). Single-point solvent calculations were performed at the optimized gas-phase geometries for all the intermediates and transition states, using the CPCM[19] approach, which is an implementation of the conductor-like screening solvation model (COSMO)[20] in Gaussian03; THF was chosen as solvent (dielectric constant  $\epsilon = 7.58$ ) with UAHF (United Atom Hartree-Fock) radii for the respective atoms (Pd, H, B, C, O, P). The charge distribution around the metal center was analyzed using Weinhold's NPA (Natural Population Analysis) approach.[21]

### 3.3 Results

Figure 3.1 shows the starting materials and products of the reactions studied. For these molecules and all other relevant species, we optimized the geometry in the gas phase and calculated the electronic energy ( $E_e$ ), the energy with zero-point vibrational corrections ( $E_0$ ), the thermal enthalpy at 298 K ( $H_{298}$ ), the Gibbs free energy at 298 K ( $G_{298}$ ), and the energy with a continuum solvent model ( $E_{\text{sov}}$ ) respectively, all at the BP86/6-31G\* level of theory.

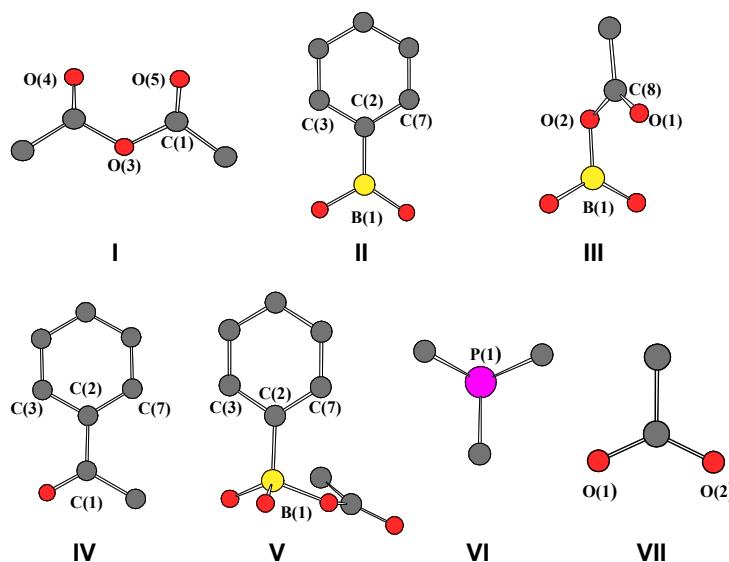


**Figure 3.1.** Starting materials and products involved in both pathways. BP86/6-31G\* optimized structures are shown, with hydrogens removed for clarity. Color code: C gray, O red, B yellow, P violet.

For each segment of the catalytic cycles, *i.e.*, oxidative addition, transmetalation, and reductive elimination, we evaluated the changes in electronic energy ( $\Delta E_e$ ) and Gibbs free energy ( $\Delta G_{298}$ ) for the optimized gas-phase geometries. The BP86/6-31G\* results were validated by calculating single-point energies of the resulting intermediates and transition states with a larger basis set ( $\Delta E_{\text{EXT}}$ ). Finally, a solvent field was applied to account for bulk solvent effects ( $\Delta E_{\text{sov}}$ ). The figures that display energy profiles for reaction steps will show these four quantities.

#### 3.3.1 Oxidative addition and ligand exchange

##### 3.3.1.1 Neutral cycle

The classic catalytic cycle for a cross-coupling reaction starts from the coordinatively unsaturated palladium(0)diphosphine  $d^{10}$ -complex **12**,<sup>[1]</sup> which has a linear geometry, with the methyl groups of the  $\text{PMe}_3$  ligands in an eclipsed arrangement (Figure 3.2).<sup>[6,7]</sup> Oxidative addition of acetic anhydride directly leads to the *cis*-configured complex **13** ( $\Delta E_e = -9.8$

kcal/mol,  $\Delta G_{298} = 6.2$  kcal/mol). Only moderate activation ( $\Delta E_e = 4.4$  kcal/mol,  $\Delta G_{298} = 19.7$  kcal/mol) is required to reach the transition state  $[12-13]^\ddagger$ . In this transition state, the palladium is already in a four-coordinate, planar environment, the C(1)—O(4) distance of the acetic anhydride is elongated by 0.194 Å, and the imaginary mode ( $92 \text{ i cm}^{-1}$ ) involves further stretching of the C(1)—O(4) bond. The resulting intermediate **13** has a square-planar coordination, with the phosphine *trans* to the acyl group being more distant from Pd than the other one (Pd(1)—P(1) = 2.483 Å, Pd(1)—P(2) = 2.292 Å). This is as expected since the acyl group has a significantly stronger *trans*-effect than the acetyl group.[22] The oxidative nature of the addition reaction is obvious from the decrease of the NPA charge on Pd(1) by 0.311 *e* in going from **12** to **13**.

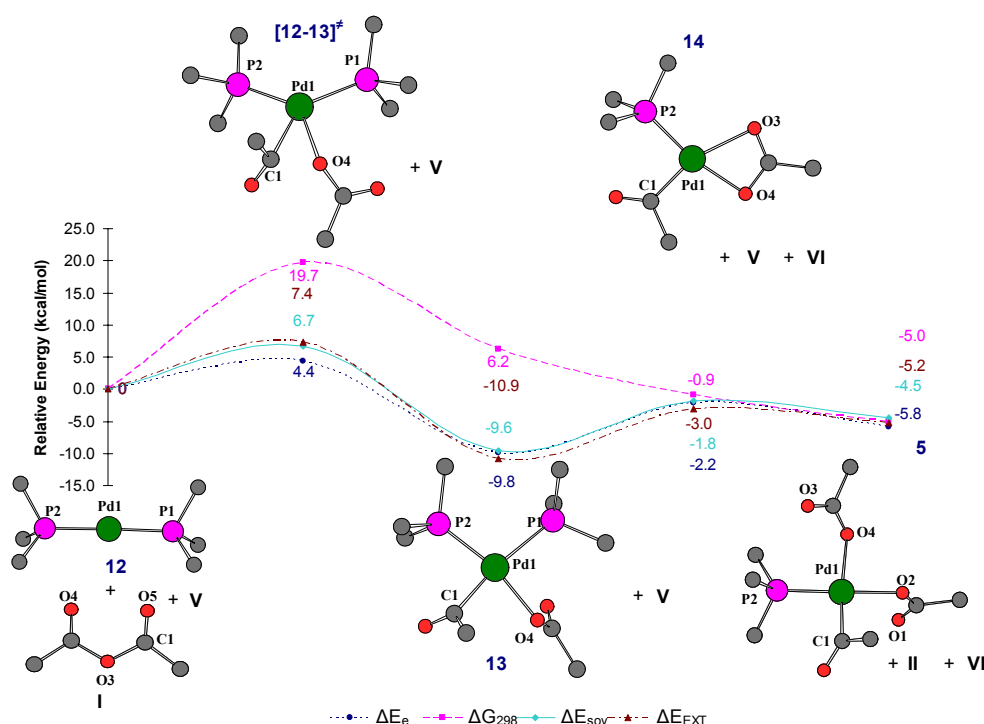


**Figure 3.2.** Energy profile for oxidative addition and ligand exchange: neutral pathway starting from Pd(PMe<sub>3</sub>)<sub>2</sub> (**12**). Conventions see Figure 3.1.

Despite several attempts, we did not find any energetically feasible pathway for an oxidative addition leading directly to a *trans*-configured palladium(II) complex. The fact that products isolated from oxidative addition reactions are usually *trans*-configured does not disprove that *cis*-complexes such as **13** are formed initially. Espinet *et al.* observed experimentally that the oxidative addition of aryl halides to palladium(0) complexes initially leads to *cis*-complexes, which in the absence of further reagents slowly rearrange to the *trans*-isomers.[23]

There has been a long-standing debate about the most plausible starting point for the ensuing transmetalation step.[24] The main question is whether a transmetalation can occur with two phosphines coordinated to the palladium center, or whether dissociation of one of the phosphines is required.[23,25] The observation that transmetalation of organoboron compounds can be inhibited by adding excess phosphine suggests such a dissociative mechanism. For organotin compounds, kinetic investigations by Hartwig and coworkers give further evidence for a reaction channel in which the phosphine dissociates prior to the transmetalation step.[26] Our results also support a dissociative mechanism: In careful searches starting from various different geometries, we were unable to identify a reaction pathway for the addition of phenylboronic acid to palladium(II)diphosphine compounds such as **13**. [25] In contrast, we found several possible reaction channels for the transmetalation of palladium(II)monophosphine complexes, the most favorable of them starting from the anionic complex **5**. Therefore, additional steps had to be considered that transform the initial addition product **13** into **5**.

Our calculations showed that the most favorable pathway for the exchange of one of the phosphine ligands of **13** begins with the dissociation of the more distant phosphine under formation of **14**. In this intermediate, the acetate is coordinated to the palladium in a bidentate fashion with Pd(1)—O(4) and Pd(1)—O(3) bond distances of 2.179 Å and 2.310 Å, respectively. Due to this bidentate coordination of the acetate, the step is only slightly endothermic, and the increased entropy makes it exergonic ( $\Delta E_e = 7.7$  kcal/mol,  $\Delta G_{298} = -7.1$  kcal/mol).

In principle, intermediate **14** could serve as a starting point for a transmetalation reaction with the hypervalent boron species  $[\text{PhB}(\text{OH})_2\text{OAc}]^-$  (**V**) similar to that proposed by Miyaura and Suzuki for base-assisted transmetalation reactions.[27] However, explorations of such pathways indicate substantial barriers that are around 15 kcal/mol higher than those discussed below. This is probably related to the fact that the transfer of the acetate from **V** to **14** is calculated to be exergonic, so that at least in the gas phase it is energetically more favorable to first transfer the acetyl group of compound **V** to the palladium under formation of intermediate **5** ( $\Delta E_e = -3.6$  kcal/mol,  $\Delta G_{298} = -4.1$  kcal/mol) prior to the transmetalation. Therefore, the transmetalation of **14** and **V** was not considered further.

The reaction step **14**  $\rightarrow$  **5** is extremely exothermic (by more than 30 kcal/mol) if free acetate is used, with almost no activation barrier involved ( $\Delta E_e < 3$  kcal/mol). However, we consider it more reasonable to assume that the acetate will coordinate to the Lewis-acidic boronic acid whenever it is liberated within the reaction cycle, and we therefore chose to generate **5** from **14**



by acetyl transfer from **V** (see Figure 3.2). Compound **5** is our favored starting point for the transmetalation. However, alternative pathways cannot yet be completely ruled out and remain under investigation.

Basis set extension has only a very minor effect on the calculated reaction profile ( $\Delta E_{\text{EXT}}$  vs.  $\Delta E_{\text{e}}$ , Figure 3.2) and the relative energies calculated for THF as the solvent using the CPCM model also show very similar trends as those in the gas phase. We have also performed such additional calculations for all subsequent reaction steps (see Figures 3.2-3.7). However, we will not further comment on them unless they differ significantly from the standard gas-phase BP86/6-31G\* results.

Within the overall oxidative addition pathway, the initial addition of the anhydride to the palladium-catalyst is generally expected to be rate-determining under the standard experimental conditions.[12] The computed activation barrier for this step is rather low, partly because we have chosen to use the small and electron-rich trimethylphosphine ligand in the calculations (rather than triarylphosphines).

Selected structural parameters of all intermediates and transition states of the oxidative addition/ligand exchange sequence are summarized in Table 3.1. Selected NPA charges and dipole moments are given in Table 3.2 and more detailed structural data is available in the Supporting Information.

**Table 3.1. Optimized geometric parameters for complexes 12 to 14. Bond distances are given in Ångström and bond angles in degrees.**

No.	Pd—P(1)	Pd—P(2)	Pd—C(1)	Pd—O(4)	Pd—O(3)	P—Pd—P
<b>12</b>	2.922	2.991	—	—	—	178.6
<b>[12-13]*</b>	2.441	2.280	2.215	2.344	3.639	122.9
<b>13</b>	2.483	2.292	2.048	2.164	3.005	102.3
<b>14</b>	—	2.272	1.988	2.179	2.310	—

**Table 3.2. NPA charges (*e*) for key atoms and dipole moments (in Debye) for complexes 12 to 14.**

No.	Pd(1)	P(1)Me <sub>3</sub>	P(2)Me <sub>3</sub>	C(1)	O(4)	O(3)	μ (D)
<b>12</b>	-0.333	0.166	0.166	–	–	–	0.083
<b>[12-13]*</b>	0.133	0.112	0.189	0.555	-0.621	-0.578	3.725
<b>13</b>	0.311	0.180	0.314	0.390	-0.725	-0.672	6.565
<b>14</b>	0.342	–	0.379	0.428	-0.704	-0.681	3.508

### 3.3.1.2 Anionic cycle

An alternative catalytic pathway for the oxidative addition was sought starting from the complex  $[\text{Pd}(\text{PMe}_3)_2\text{OAc}]^-$  (**1**), in order to determine whether such “Jutand-type” anionic palladium(0) species would give rise to a more favorable overall mechanism. According to Amatore and Jutand, an oxidative addition to such anionic species should result in the formation of five-coordinate palladium(II) species.[5] However, in analogy to our theoretical studies on the oxidative addition of aryl halides,[6] we did not find any evidence for the existence of such intermediates. Instead, upon bringing acetic anhydride (**I**) into the proximity of the anionic palladium(0) catalyst **1**, the van der Waals-adduct **2** is formed in a barrierless reaction. In this species, the electron-poor carbonyl carbon of the incoming acetic anhydride interacts with the electron-rich palladium center ( $\Delta E_e = -11.0$  kcal/mol,  $\Delta G_{298} = 3.5$  kcal/mol,  $\Delta E_{\text{sov}} = -5.7$  kcal/mol). While palladium is calculated to be almost neutral ( $0.004 e$ ) in **1**, it has a negative charge of  $-0.244 e$  in complex **2** (Table 3.3), mostly due to charge transfer from the two phosphine ligands, which allows for an attractive electrostatic interaction with the positively charged carboxylic carbon C(1) ( $0.802 e$ ).

Intermediate **2** has an almost planar geometry around palladium, with the acetate and the anhydride residues oriented perpendicular to the P–Pd–P plane. Compared to **1**, the Pd–O(1) distance is significantly increased (Pd(1)–O(1) =  $4.183 \text{ \AA}$  in **2** vs.  $2.327 \text{ \AA}$  in **1**), and the P–Pd–P bond angle has widened by more than  $10^\circ$  (Figure 3.3). The Pd(1)–C(1) distance of  $3.735 \text{ \AA}$  is quite large, but already within the range of a weak interaction. Two hydrogen atoms of the anhydride appear to interact with the palladium center (Pd–H<sub>1</sub> =  $2.626 \text{ \AA}$ , Pd–H<sub>2</sub> =  $2.519 \text{ \AA}$ , C–H<sub>1</sub> =  $1.118 \text{ \AA}$ , C–H<sub>2</sub> =  $1.122 \text{ \AA}$ ) causing a slight distortion of the coordination geometry.

Starting from compound **2**, the oxidative addition proceeds in two steps. In an exergonic reaction ( $\Delta E_e = -7.3$  kcal/mol,  $\Delta G_{298} = -4.8$  kcal/mol), intermediate **3** is formed *via* an

energetically low-lying transition state  $[2-3]^\ddagger$  ( $\Delta E_e = 3.9$  kcal/mol,  $\Delta G_{298} = 4.2$  kcal/mol, confirmed by IRC calculations), with an imaginary-frequency mode ( $52\text{ i cm}^{-1}$ ) that reflects the gradual approach of C(1) towards the palladium center. In intermediate **3**, the anhydride is bound by a  $\eta^2$  type interaction between the C(1)—O(5) carbonyl double bond and the palladium (Pd(1)—C(1) = 2.085 Å, Pd(1)—O(5) = 2.216 Å), the C(1)—O(5) bond being elongated from 1.209 Å in **1** to 1.285 Å in **3**. The second carboxylic oxygen O(4) of the anhydride is almost in an axial position with respect to the metal center, with a distance Pd(1)—O(4) = 2.929 Å that allows for a weak interaction. In contrast, the acetate ligand is far away from the metal center (Pd(1)—O(1) = 5.143 Å) and acts as a weakly bound spectator ligand.

During the transition from **2** via  $[2-3]^\ddagger$  to **3**, there are significant changes in the atomic charges of palladium and of the carboxy group indicating that this reaction is already part of the oxidative addition. Almost 0.5  $e$  are transferred from the metal centre (Pd(1) =  $-0.244\text{ }e$  in **2**, Pd(1) =  $0.241\text{ }e$  in **3**) to the carboxy group (C(1) =  $0.802\text{ }e$  in **2**, C(1) =  $0.458\text{ }e$  in **3**; O(5) =  $-0.544\text{ }e$  in **2**, O(5) =  $-0.642\text{ }e$  in **3**).

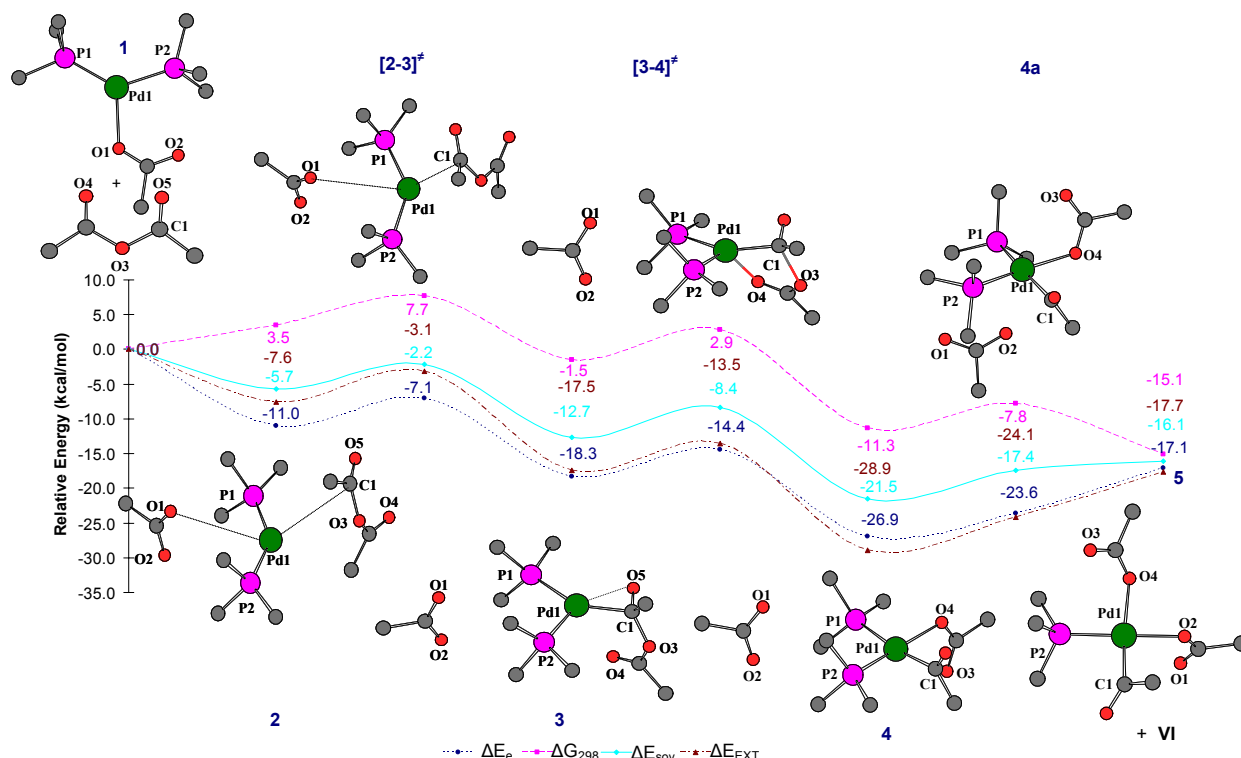


**Figure 3.3.** Energy profile for oxidative addition and ligand exchange: anionic pathway starting from  $[\text{Pd}(\text{PMe}_3)_2\text{OAc}]^-$ . Conventions see Figure 3.1.

In the next step, the bond between C(1) and O(3) in **3** is broken to form the oxidative addition product **4** via the transition state  $[3-4]^\ddagger$ , and further electron density is transferred from the

metal and the phosphine ligands to C(1) and O(4) (C(1) = 0.458 *e* in **3** and 0.381 *e* in **4**; O(4) = -0.585 *e* in **3** and -0.706 *e* in **4**) but not to O(5) (O(5) = -0.527 *e* in **4**).

The transition state [**3-4**]<sup>‡</sup> contains a five-membered ring in which O(4) approaches palladium from an axial direction. The imaginary mode (106 *icm*<sup>-1</sup>) involves this approach of O(4) with simultaneous C(1)—O(3) bond breaking. At the same time, the Pd(1)—C(1) bond is shortened while the Pd(1)—O(5) distance increases (change from  $\eta^2$  to  $\eta^1$  coordination, reinstating the double bond character between C(1) and O(5)). The activation energy for the formation of the *cis* configured complex **4** is low ( $\Delta E_e = 3.9$  kcal/mol,  $\Delta G_{298} = 4.4$  kcal/mol), and the overall reaction from **3** to **4** is exergonic ( $\Delta E_e = -8.6$  kcal/mol,  $\Delta G_{298} = -9.8$  kcal/mol).

As in the case of the neutral pathway, an alternative mechanism leading to the corresponding *trans*-complex was not found, and all attempts failed to accomplish a transmetalation starting from a diphosphine complex (*i.e.*, **4** or **4a**). However, the replacement of one of the phosphine ligands by acetate is easily achieved. Internal rotation around the Pd(1)—O(4) bond in **4** leads to a less stable conformer **4a**, where the orientation of the bound acetate ligand is more suitable for the substitution of a phosphine ligand by the spectator acetate ligand (Figure 3.3). In contrast to **4**, the oxygen atom O(3) is at the opposite side of the spectator acetate ligand and thereby facilitates its approach in **4a**. Gradual removal of any one of the two phosphines from **4a** prompts the spectator acetate ligand to coordinate to the palladium replacing the phosphine. The representation in Figure 3.3 is slightly simplified as this substitution involves additional intermediates.[28]

Since the Pd(1)—P(1) bond is weaker than the Pd(1)—P(2) bond, the P(1)Me<sub>3</sub> ligand is displaced, and an intermediate **5** is formed in which the two acetate groups are oriented *cis* to each other. This requires less activation energy ( $\Delta E_e = 8.5$  kcal/mol,  $\Delta G_{298} = 7.5$  kcal/mol) than the alternative formation of the *trans*-diacetate complex, as the removal of the other phosphine P(2)Me<sub>3</sub> from **4a** would be more endothermic ( $\Delta E_e = 12.9$  kcal/mol,  $\Delta G_{298} = 11.5$  kcal/mol).

The structural parameters of all intermediates and transition states of the anionic pathway are summarized in Table 3.3, selected NPA charges and dipole moments are given in Table 3.4. More detailed structural data is available in the Supporting Information.

**Table 3.3. Optimized geometric parameters for complexes 1 to 5. Bond distances are given in Ångström and bond angles in degrees.**

No.	Pd–P(1)	Pd–P(2)	Pd–C(1)	Pd–O(1)	Pd–O(2)	Pd–O(4)	Pd–O(5)	P–Pd–P
<b>1</b>	2.247	2.307	–	2.327	3.535	–	–	132.2
<b>2</b>	2.291	2.299	3.735	4.183	4.218	5.006	1.214	142.6
<b>[2-3]<sup>†</sup></b>	2.314	2.317	2.590	4.233	4.267	4.512	1.223	140.3
<b>3</b>	2.403	2.297	2.085	5.143	5.144	2.929	1.285	105.2
<b>[3-4]<sup>†</sup></b>	2.433	2.291	2.047	5.115	5.195	2.454	1.248	104.3
<b>4</b>	2.484	2.308	2.031	5.191	5.338	2.184	1.223	99.7
<b>4a</b>	2.459	2.285	2.031	4.226	3.162	2.195	1.227	103.7
<b>5</b>	–	2.274	1.997	3.059	2.147	2.215	1.231	

**Table 3.4. NPA populations for key atoms and dipole moments (in Debye) for the intermediates 1 to 5.**

No.	Pd(1)	P(1)Me <sub>3</sub>	P(2)Me <sub>3</sub>	O(1)	O(2)	C(1)	O(4)	O(3)	μ (D) <sup>a</sup>
<b>1</b>	0.004	-0.115	-0.054	-0.754	-0.729	–	–	–	–
<b>AcOAc(I)</b>	–	–	–	–	–	0.799	-0.509	-0.585	3.739
<b>2</b>	-0.244	0.075	0.094	-0.745	-0.748	0.802	-0.523	-0.583	–
<b>[2-3]<sup>†</sup></b>	-0.088	0.097	0.054	-0.740	-0.747	0.713	-0.546	-0.581	–
<b>3</b>	0.241	0.089	0.156	-0.751	-0.743	0.458	-0.585	-0.572	–
<b>[3-4]<sup>†</sup></b>	0.299	0.185	0.106	-0.753	-0.741	0.406	-0.665	-0.601	–
<b>4</b>	0.305	0.159	0.266	-0.749	-0.739	0.381	-0.706	-0.674	–
<b>4a</b>	0.345	0.145	0.307	-0.757	-0.743	0.375	-0.734	-0.669	–
<b>5</b>	0.426	–	0.254	-0.658	-0.734	0.393	-0.721	-0.714	–
<b>P(1)Me<sub>3</sub></b>	–	0.000	–	–	–	–	–	–	1.394

<sup>a</sup> The (origin-dependent) dipole moment is not reported for the anions.

Overall, we have identified valid reaction pathways for the oxidative addition of acetic anhydride to both a neutral and an anionic palladium(0) species. For both pathways, the calculated energy profiles seem reasonable (Figure 3.2 and 3.3). Although one has to be careful when comparing the energies of the two pathways with each other (*vide infra*), our results suggest that the anionic pathway for the oxidative addition is energetically more favorable than the neutral one: Starting from the anionic species **1**, the highest free energy barrier ( $\Delta G_{298} = 7.7$  kcal/mol) of the oxidative addition sequence is found to be significantly lower than that of the

neutral pathway ( $\Delta G_{298} = 19.7$  kcal/mol). This is consistent with the experimental finding that catalysts generated *in situ* from palladium(II)acetate show a higher activity than preformed palladium(0)phosphine complexes.[5]

### 3.3.2 Transmetalation

As mentioned earlier, all our attempts to identify a transmetalation pathway starting from diphosphine complexes failed. For example, approaching phenylboronic acid to **13** from various angles resulted in high energies and ultimate dissociation of one of the phosphines. The same outcome was observed when starting from the corresponding *trans*-configured complex  $[\text{Pd}(\text{PMe}_3)_2(\text{OAc})(\text{COMe})]^-$ . [29] In contrast, several plausible pathways for transmetalation reactions of monophosphine complexes such as **5** were found.

While optimizing the geometry of compound **5**, we discovered an energetically almost degenerate rotamer **5a** which proved to be more suitable for the following reaction. In **5a**, the two  $\text{sp}^2$ -hybridized oxygen atoms of the acetyl groups (O(3) and O(1)) are pointing out of the coordination plane into the same direction, while they are on opposite sides in intermediate **5**.

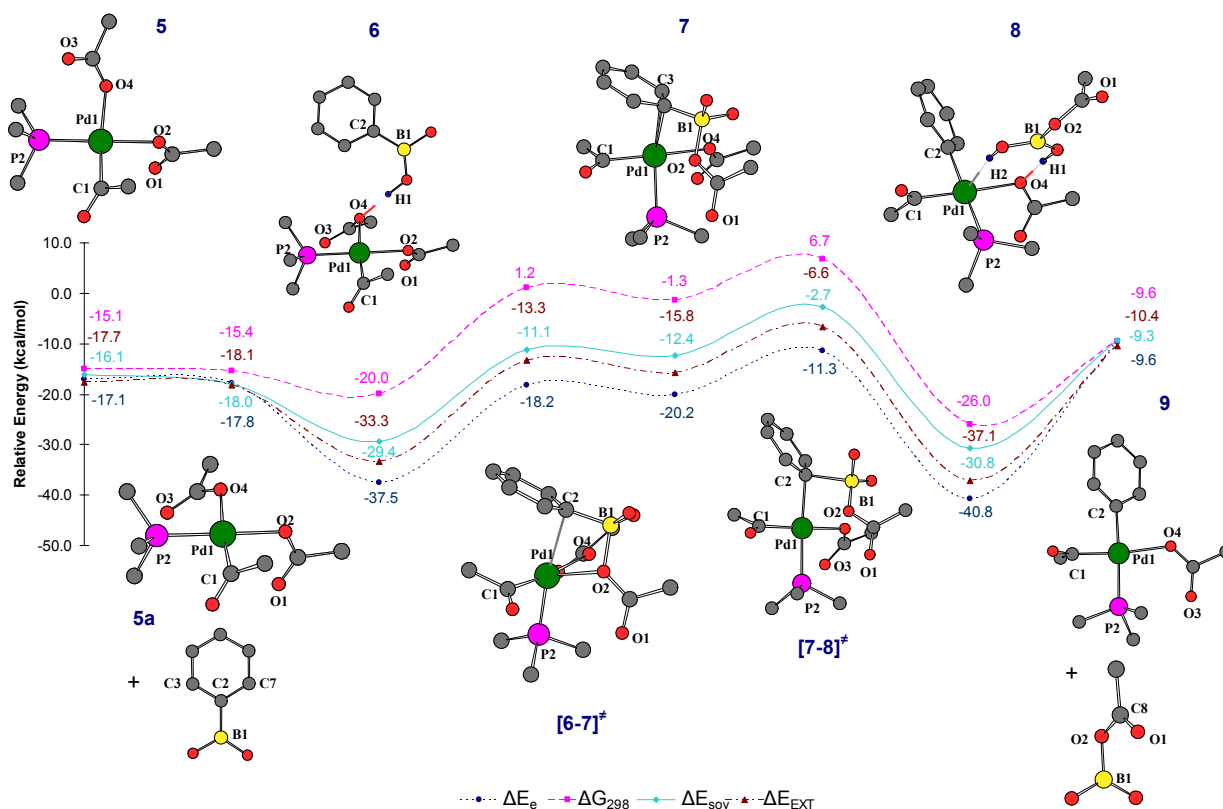


**Figure 3.4.** Energy profile for the transmetalation reaction involving intermediates **5** to **9**. Relative energies are given with respect to the anionic pathway (Figure 3.3). Conventions see Figure 3.1.

Bringing a molecule of boronic acid  $\text{PhB(OH)}_2$  (**II**) closer to the palladium center of **5a** affords the stable adduct **6** in a barrierless reaction. In this pre-coordination complex, one OH group of the boronic acid forms a hydrogen bond to O(4), which carries the most negative charge of all oxygen atoms ( $\text{O(4)} = -0.781 e$ ,  $\text{O(3)} = -0.679 e$ ,  $\text{O(2)} = -0.732 e$  and  $\text{O(1)} = -0.665 e$ ). The bridging hydrogen bond is responsible for the high stability of **6** in comparison to **5a** and  $\text{PhB(OH)}_2$  ( $\Delta E_e = -19.7 \text{ kcal/mol}$ ,  $\Delta G_{298} = -4.6 \text{ kcal/mol}$ ). Consequently, a deep valley interrupts the smooth energy profile of the reaction causing a high energy barrier for the following step. It should be stressed, however, that these results come from gas-phase calculations and do not reflect the situation in solution where the boronic acid will form hydrogen bonds either to a reaction partner (as in **6**) or to an external partner, *i.e.* a solvent molecule. In our gas-phase model calculations, the former are included, but the latter are not. For a realistic assessment of the situation in solution, these interactions with an external partner should be taken into account. On the basis of calculations on model systems consisting of water, THF and boronic acid, the energy arising from a hydrogen bond between the boronic acid and a solvent molecule was estimated to be around  $-10 \text{ kcal/mol}$  ( $\Delta E_e$ ).<sup>[30]</sup> Subtracting this value from the calculated relative energy of **6** of  $-37.5 \text{ kcal/mol}$  (Figure 3.4) leads a much smoother and, as we think, much more realistic reaction profile. For the same reason,  $-20 \text{ kcal/mol}$  will be subtracted from the calculated value of  $-40.8 \text{ kcal/mol}$  in intermediate **8**, with its two internal hydrogen bonds.

The conversion of intermediate **6** into intermediate **7** is decisive within the transmetalation process since it involves the first direct coordination of the phenyl group to the palladium, initially by an  $\eta^2$  bond to the C(2)–C(3) bond. We have located the corresponding transition state **[6-7]**<sup>‡</sup>, and confirmed by IRC calculations that it connects **6** and **7**. It contains a four-membered ring formed by the atoms Pd(1), C(2), B(1) of the boronic acid, and O(2) of the acetate ligand. The imaginary mode ( $40 \text{ i cm}^{-1}$ ) shows the simultaneous approach of the phenyl group towards the palladium along with an elongation of the O(2)–Pd(1) bond. Similar four-membered cyclic transition states have been postulated for other palladium-catalyzed reactions. For example, Napolitano *et al.* found a cyclic transition state for the transmetalation in a B3LYP/LANL2DZ calculation performed on Stille couplings,<sup>[25]</sup> and Matos *et al.* proposed a similar geometry for the transfer of alkyl groups from alkylboranes to palladium complexes on the basis of NMR studies.<sup>[31]</sup> Our computed transmetalation mechanism is consistent with experimental work performed by Miyaura who suggested that transmetalation with *oxo*-palladium(II) complexes may involve a rate-determining coordination of the RO (R = COMe) ligand to the boron atom.<sup>[27]</sup>

In the complex **7**, the phenyl group is coordinated *via* a  $\eta^2$  bond, as can be seen by the short palladium-carbon distances (Pd(1)—C(2) = 2.549 Å and Pd(1)—C(3) = 2.448 Å) and the increase in the C(2)—C(3) bond distance (1.432 Å in **7** vs. 1.414 Å in PhB(OH)<sub>2</sub>) (Figure 3.4). The formation of  $\eta^2$   $\pi$ -complexes like **7** preceding the insertion of a transition metal into an aryl—X bond is not uncommon in palladium chemistry. For example, such intermediates were also found in oxidative addition reactions of aryl halides with palladium(0) complexes,[8,11,32] the calculated intermediates structurally resembling intermediate **7**.

Gradual elongation of the C(2)—B bond of **7** leads to intermediate **8**, in which the C(2)—B bond is cleaved. The transition state [**7-8**]<sup>‡</sup> (confirmed by IRC) reveals an elongated carbon-boron bond (C(2)—B = 2.122 Å in [**7-8**]<sup>‡</sup>, and 1.663 Å in **7**). The imaginary mode (254 *icm*<sup>-1</sup>) indicates a stretching of the C(2)—B(1) bond in the transition state. The activation barrier is moderate ( $\Delta E_e$  = 8.8 kcal/mol,  $\Delta G_{298}$  = 8.0 kcal/mol).

A hydrogen-bonding stabilization similar to that observed in intermediate **6** is seen in **8**, giving rise to a very low energy of this intermediate. Again, this effect is expected to be much less pronounced under experimental conditions, where all species are solvated. Removal of the borate leads to the square planar intermediate **9**, in which the phenyl and acetyl groups are oriented *cis* to each other. Hence, the reductive elimination can proceed directly from **9**, without any requirement of further isomerization.

The structural parameters of all intermediates and transition states of the common transmetalation step are summarized in Table 3.5. Selected NPA charges and dipole moments are given in Table 3.6 and more detailed structural data is available in the Supporting Information.

**Table 3.5. Optimized geometric parameters for complexes 5a to 9. Bond distances are given in Ångström and bond angles in degrees.**

No.	Pd—P(2)	Pd—C(1)	Pd—O(2)	Pd—O(4)	Pd—C(2)	C(2)—B1	C(1)—Pd—P(2)
<b>5a</b>	2.281	1.989	2.150	2.203	—	—	—
<b>6</b>	2.285	1.981	2.129	2.267	5.446	1.586	90.7
[ <b>6-7</b> ] <sup>‡</sup>	2.293	1.979	2.486	2.238	2.817	1.654	89.6
<b>7</b>	2.315	1.987	3.066	2.231	2.549	1.663	86.8
[ <b>7-8</b> ] <sup>‡</sup>	2.317	1.983	2.794	2.259	2.245	2.122	88.3
<b>8</b>	2.383	1.989	5.372	2.253	2.076	4.686	91.8
<b>9</b>	2.395	1.987	—	2.232	2.086	—	91.5



**Table 3.6. NPA populations for key atoms and dipole moments (in Debye) for the species 5a to 9.**

No.	Pd(1)	P(2)Me <sub>3</sub>	O(1)	O(2)	C(1)	O(4)	O(3)	B(1)	C(2)	$\mu$ (D) <sup>a</sup>
<b>II</b>	–	–	–	–	–	–	–	1.107	-0.424	1.255
<b>5a</b>	0.425	0.246	-0.655	-0.731	0.397	-0.726	-0.713	–	–	–
<b>6</b>	0.443	0.279	-0.665	-0.732	0.398	-0.726	-0.713	–	–	–
<b>[6-7]<sup>†</sup></b>	0.473	0.275	-0.654	-0.710	0.419	-0.776	-0.683	1.084	-0.349	–
<b>7</b>	0.455	0.329	-0.666	-0.689	0.407	-0.774	-0.682	1.083	-0.335	–
<b>[7-8]<sup>†</sup></b>	0.416	0.266	-0.626	-0.712	0.397	-0.773	-0.676	1.172	-0.422	–
<b>8</b>	0.313	0.200	-0.574	-0.709	0.372	-0.759	-0.654	1.223	-0.273	–
<b>III</b>	–	–	-0.565	-0.730	–	–	–	1.283	–	2.592
<b>9</b>	0.329	0.153	–	–	0.362	-0.719	-0.714	–	-0.251	–

<sup>a</sup> The (origin-dependent) dipole moment is not reported for the anions.

### 3.3.3 Reductive elimination

The traditional mechanism for cross-coupling reactions has been derived from the known geometries of isolable palladium complexes, and thus involves *trans*-configured palladium(II)diphosphine species as intermediates (Scheme 3.2). One of the strongest arguments against this proposed mechanism is that the reductive elimination of the cross-coupling products Pd(PR'<sub>3</sub>)<sub>2</sub>RAr from a *trans*-configured diphosphine intermediate would require an additional *cis-trans* isomerization, which can be expected to be strongly endothermic. Amatore and Jutand have pointed out that if this mechanism were true, the isomerization step should be rate-determining.[5] Since this is in contrast to experimental findings, they went on to propose their alternative catalytic cycle involving five-coordinate palladium complexes (Scheme 3.2).

According to our calculated mechanism, which does not invoke any five-coordinate intermediates, the acyl and phenyl groups are already positioned *cis* to each other in the intermediate **9** which is set up for reductive elimination. Due to the close proximity of these groups, the reductive elimination of the product acetophenone proceeds smoothly, as expected from experimental findings.

We calculated two possible pathways for this final step in the catalytic cycle, one giving rise to the neutral Pd(PMe<sub>3</sub>)<sub>2</sub> species (**12**), and the other one reinstating the anionic [Pd(PMe<sub>3</sub>)<sub>2</sub>OAc]<sup>–</sup> (**1**) complex. In both cases, starting from **9**, reductive elimination is initiated by the formation

of a bond between the aryl and the acyl group, leading to a  $\eta^2$ - $\pi$ -complex of palladium with acetophenone (**10**). In the corresponding transition state **[9-10]<sup>‡</sup>** ( $\Delta E_e = 11.0$  kcal/mol,  $\Delta G_{298} = 12.2$  kcal/mol) the C(1)—C(2) distance is already reduced to 1.965 Å, and the imaginary mode (280  $\text{cm}^{-1}$ ) indicates a further shortening of this distance. The Pd(1)—P(2) bond length in **[9-10]<sup>‡</sup>** is reduced by 0.097 Å, which may arise from the fact that the phenyl group is no longer positioned *trans* to the phosphine ligand.

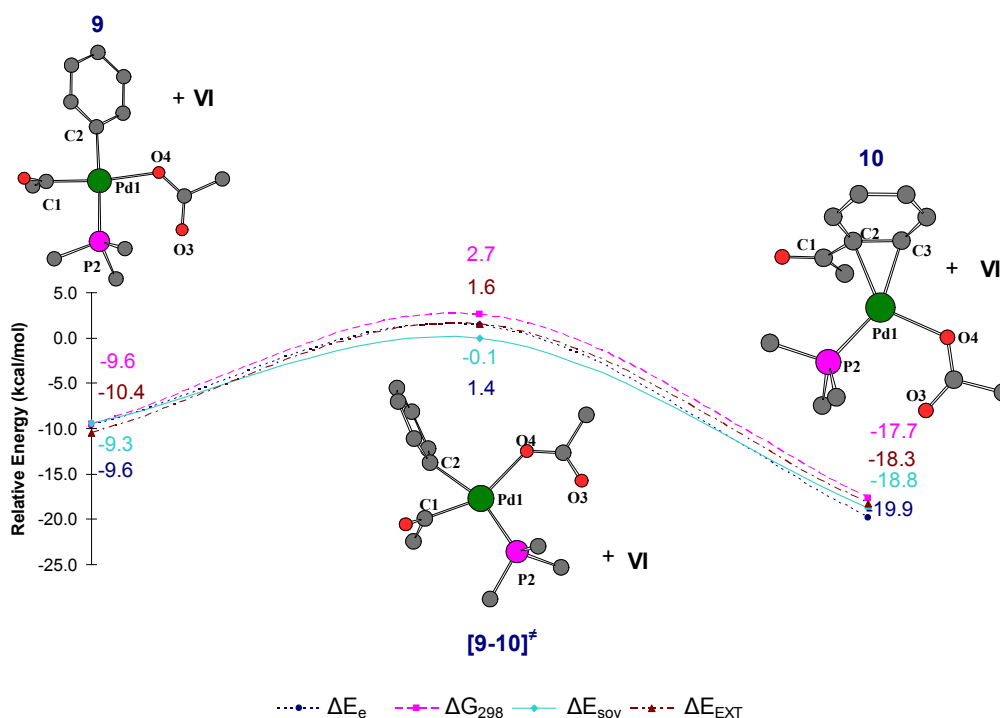


**Figure 3.5.** Energy profile from intermediate **9** to **10**. Conventions see Figures 3.1 and 3.4.

We also tested whether the approach of a second  $\text{PMe}_3$  ligand to compound **9** would give rise to an alternative pathway for the reductive elimination of acetophenone but found that in this case the other phosphine, not the acetate or the acetophenone, left the coordination sphere of the palladium.

In the relatively stable intermediate **10** ( $\Delta E_e = -10.3$  kcal/mol,  $\Delta G_{298} = -8.2$  kcal/mol with respect to **9**), the phenyl moiety of the newly formed acetophenone remains closely bound to the palladium *via* an  $\eta^2$  coordination of the aromatic double bond adjacent to the acyl group (C(2)—Pd(1) = 2.226 Å and C(3)—Pd(1) = 2.205 Å; Figure 3.5).

### 3.3.3.1 Neutral cycle

In order to complete the catalytic cycle, the coordinated acetophenone has to be released from complex **10**, and the  $\text{Pd}(\text{PMe}_3)_2$  species **12** has to be regenerated. Although this process requires several steps, they are all energetically very similar and involve only negligible

activation barriers. As before, the  $[\text{PhB}(\text{OH})_2\text{OAc}]^-$  species is used as a carrier for the acetate anion, which is transferred back to the palladium in step **10**  $\rightarrow$  **15**. In this way, unrealistically high barriers are avoided, and one obtains a more accurate view on the relative energies of the intermediates within the catalytic cycle. Under the authentic reaction conditions used in the catalysis, the acetate probably coordinates not only to the boron species in solution but also to the polar solvent. Therefore, such ligand exchange reactions are difficult only in gas-phase calculations, while they should be facile in solution. Coordination of the boronic acid to the most electronegative oxygen of the acetate ligand results in the formation of the intermediate **15**, in which the Pd(1)—O(4) bond distance is larger than in **10** (2.323 Å vs. 2.231 Å). Starting from this complex, the de-coordination of the anionic boron species **V** does not require much energy, and the gradual elongation of Pd(1)—O(4) bond results in the formation of an adduct **16**, where the Pd(1)—O(4) distance is as long as 4.761 Å. Reaching the corresponding transition state **[15-16]**<sup>‡</sup>, which has a Pd(1)—O(4) distance of 3.095 Å, requires only little activation ( $\Delta E_e = 4.0$  kcal/mol,  $\Delta G_{298} = 3.0$  kcal/mol). If a phosphine is brought close to this coordinatively unsaturated complex, it immediately binds to the palladium, while the  $[\text{PhB}(\text{OH})_2\text{OAc}]^-$  species completely leaves the coordination sphere.

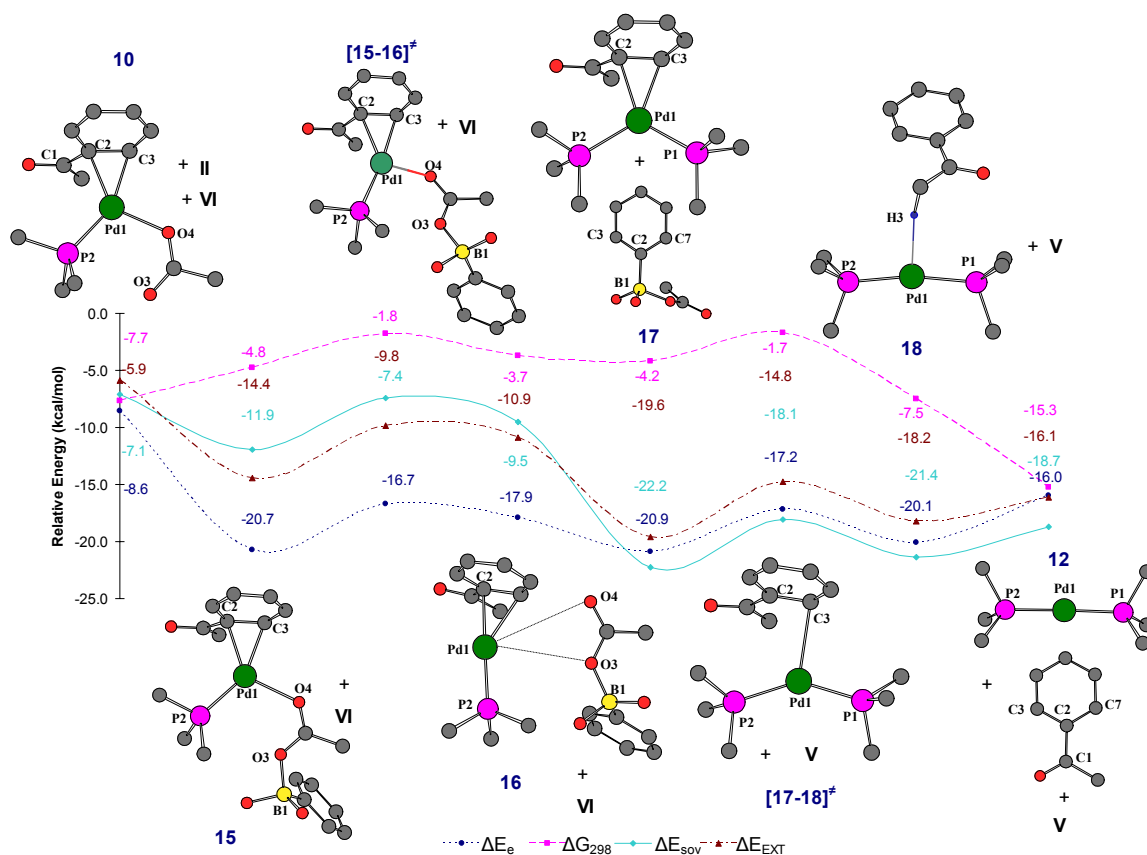


**Figure 3.6.** Energy profile for reductive elimination reaction involving the liberation of acetophenone and the regeneration of the neutral complex **12**. Relative energies are given with respect to the neutral pathway (Figure 3.2). Conventions see Figure 3.1.

Due to the strong electron-donating ability of the phosphine, the ligand exchange (**16** → **17**) causes a loosening of the coordination of the acetophenone ( $C(2)-Pd(1) = 2.309 \text{ \AA}$ ,  $C(3)-Pd(1) = 2.300 \text{ \AA}$ ). As a result, the subsequent removal of the phenyl group from **17** easily cleaves the Pd–C bond *via* the transition state [**17-18**]<sup>‡</sup>. The imaginary mode ( $40 \text{ icm}^{-1}$ ) involves the movement of the phenyl group away from the metal center. Interestingly, the acetophenone does not fully dissociate but remains loosely bound to **18** *via* one of the hydrogens ( $Pd(1)-H(3) = 2.353 \text{ \AA}$ , Figure 3.6). Such a weak interaction may survive in the gas phase, but most probably not in a coordinating solvent. Although surprisingly many steps are required to regenerate the initial  $Pd(PMe_3)_2$  species **12**, due to energetically low-lying intermediates, the entire sequence should be facile as it does not require much activation (Figure 3.6).

The structural parameters of all intermediates and transition states of the neutral pathway of the reductive elimination/ligand exchange sequence are summarized in Table 3.7. Selected NPA charges and dipole moments are given in Table 3.8 and more detailed structural data is available in the Supporting Information.

**Table 3.7. Optimized geometric parameters for complexes involved during reductive elimination. Bond distances are given in Ångström and bond angles in degrees.**

No.	Pd–P(1)	Pd–P(2)	Pd–C(2)	Pd–O(4)	Pd–O(3)	P–Pd–P	P(2)–Pd–O(4)
<b>9</b>	–	2.395	2.086	2.232	3.578	–	96.5
<b>[9-10]<sup>‡</sup></b>	–	2.298	2.185	2.258	3.549	–	102.7
<b>10</b>	–	2.313	2.226	2.231	3.398	–	107.5
<b>15</b>	–	2.323	2.231	2.323	3.369	–	112.4
<b>[15-16]<sup>‡</sup></b>	–	2.291	2.302	3.095	3.596	–	113.8
<b>16</b>	–	2.277	2.215	4.761	4.437	–	112.8
<b>17</b>	2.337	2.367	2.309	–	–	117.8	–
<b>[17-18]<sup>‡</sup></b>	2.294	2.335	3.116	–	–	144.9	–
<b>18</b>	2.289	2.317	4.975	–	–	169.6	–

**Table 3.8. NPA charges (*e*) for key atoms and dipole moments (in Debye) for species 9 to 18.**

No.	Pd(1)	P(1)Me <sub>3</sub>	P(2)Me <sub>3</sub>	C(1)	O(4)	O(3)	B(1)	C(2)	μ (D) <sup>a</sup>
<b>9</b>	0.329	–	0.153	0.362	-0.719	-0.714	–	-0.251	–
<b>[9-10]<sup>‡</sup></b>	0.299	–	0.107	0.349	-0.736	-0.724	–	-0.241	–
<b>10</b>	0.318	–	0.066	0.492	-0.732	-0.708	–	-0.243	–
<b>15</b>	0.252	–	0.075	0.514	-0.663	-0.659	-0.228	-0.228	–
<b>[15-16]<sup>‡</sup></b>	0.068	–	0.104	0.536	-0.667	-0.673	-0.196	-0.196	–
<b>16</b>	0.002	–	0.123	0.539	-0.654	-0.679	-0.239	-0.239	–
<b>17</b>	0.116	0.109	0.116	0.519	–	–	-0.234	-0.234	4.872
<b>[17-18]<sup>‡</sup></b>	-0.145	0.101	0.113	0.551	–	–	-0.149	-0.149	3.524
<b>18</b>	-0.298	0.173	0.171	0.549	–	–	-0.143	-0.143	2.739

<sup>a</sup> The (origin-dependent) dipole moment is not reported for the anions.

### 3.3.3.2 Anionic cycle

We also calculated an alternative route for the reductive elimination leading to the anionic species [Pd(PMe<sub>3</sub>)<sub>2</sub>OAc]<sup>–</sup> (**1**) to resume the second catalytic cycle. When approaching an additional phosphine to **10**, a simple exchange with the other phosphine is observed. In contrast, the removal of the phenyl group from **10** by gradually increasing the Pd(1)–C(2) bond length results in the formation of the adduct **11** *via* the low-energy transition state [**10-11**]<sup>‡</sup> (ΔE<sub>e</sub> = 4.9 kcal/mol, ΔG<sub>298</sub> = 5.0 kcal/mol). In intermediate **11**, the acetophenone remains loosely bound to the palladium by an interaction between the electron-poor C(1) and the nucleophilic, electron-rich palladium center (Figure 3.7).

In **11**, the charge on C(1) is reduced to 0.419 *e*, as a consequence of the interaction with the palladium. The imaginary frequency (69 *icm*<sup>–1</sup>) of the transition state [**10-11**]<sup>‡</sup> reflects the concomitant elongation of the Pd(1)–C(2) bond and the formation of the Pd(1)–C(1) bond. In [**10-11**]<sup>‡</sup>, the acetate is coordinated to the metal center in a bidentate manner (Pd(1)–O(4) = 2.422 Å, Pd(1)–O(3) = 2.559 Å). This bidentate character diminishes in intermediate **11**, which has one strong palladium-oxygen bond (Pd(1)–O(4) = 2.174 Å, Pd(1)–O(3) = 3.088 Å).

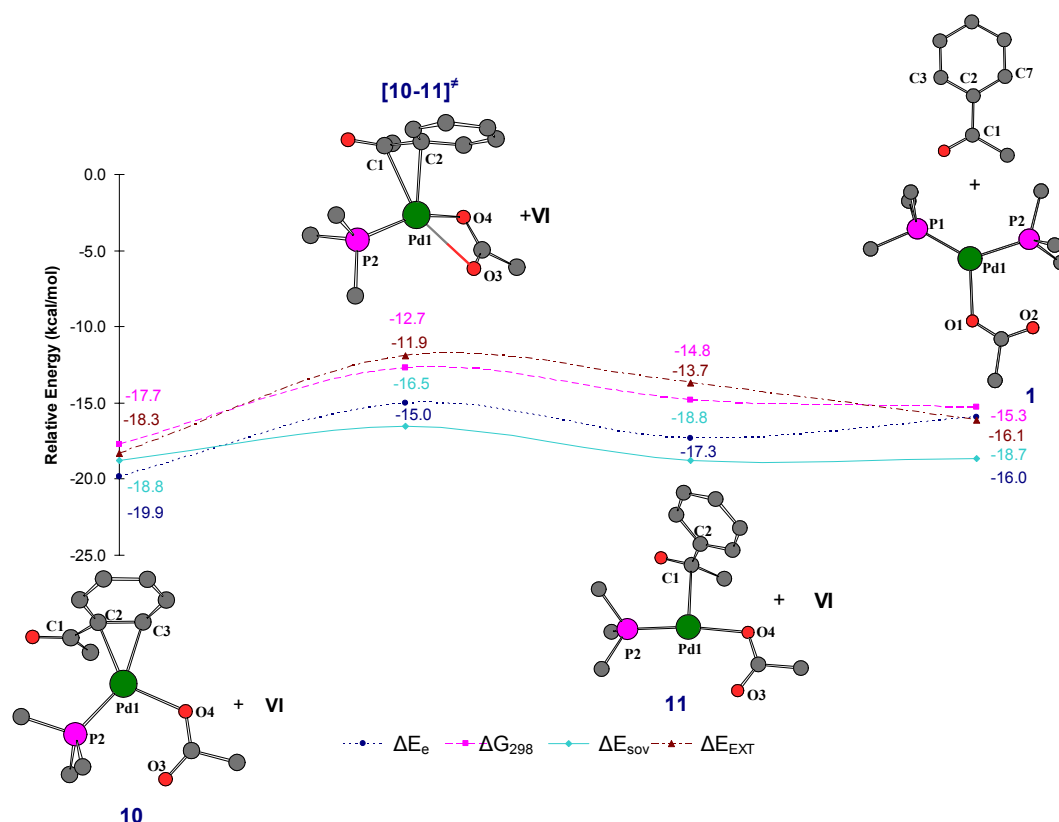


**Figure 3.7.** Energy profile for reductive elimination reaction involving the liberation of acetophenone and the regeneration of the anionic complex **1**. Conventions see Figure 3.1.

Bringing a phosphine molecule close to **11** results in the direct formation of the anionic species  $[\text{Pd}(\text{PMe}_3)_2\text{OAc}]^-$  (**1**), and the product acetophenone is liberated through a barrierless reaction step. Overall, this anionic path requires fewer steps but is energetically similar to the neutral pathway **15**  $\rightarrow$  **12**.

The structural parameters of the transition state  $[10-11]^{\ddagger}$  and intermediate **11** are summarized in Table 3.9. Selected NPA charges and dipole moments are given in Table 3.10, and more detailed structural data is available in the Supporting Information.

**Tables 3.9. Optimized geometric parameters for complexes  $[10-11]^{\ddagger}$  and **11**. Bond distances are given in Ångström and bond angles in degrees.**

No.	Pd–P(2)	Pd–C(2)	Pd–O(4)	Pd–O(3)	P(2)–Pd–O(4)
$[10-11]^{\ddagger}$	2.238	2.448	2.422	2.559	145.6
<b>11</b>	2.214	3.018	2.174	3.088	172.7

**Table 3.10. NPA charges for key atoms in [10-11]\* and 11.**

No.	Pd(1)	P(2)Me <sub>3</sub>	C(1)	O(4)	O(3)	C(2)
[10-11]*	0.275	0.043	0.419	-0.750	-0.689	-0.113
11	0.066	0.097	0.426	-0.776	-0.660	-0.113

### 3.4 Discussion and Conclusion

In summary, two mechanistically and energetically plausible catalytic cycles for the cross-coupling of phenylboronic acid with acetic anhydride have been identified, using either the neutral  $\text{Pd}(\text{PMe}_3)_2$  or the anionic  $[\text{Pd}(\text{PMe}_3)_2\text{OAc}]^-$  complex as the starting point. According to our calculations, both the neutral and the anionic pathway give rise to *cis*-configured palladium(II) diphosphine intermediates (**13** and **4**) in the oxidative addition step. In the neutral case, this is not unexpected as an increasing amount of evidence supports initial formation of the *cis*-configured intermediates in oxidative addition reactions of palladium(0) complexes, before they slowly isomerize to the isolable but significantly less reactive *trans*-configured palladium(II)diphosphine complexes.

For the anionic pathway, our calculated catalytic cycle is dramatically different from the mechanism proposed by Amatore and Jutand for cross-coupling reactions of aryl halides, except for the presence of the initial three-coordinate intermediate  $[\text{Pd}(\text{PMe}_3)_2\text{OAc}]^-$ . Despite careful searches, we could not find any evidence for the existence of stable five-coordinate palladium(II) intermediates. Instead, our calculations suggest that the higher catalytic activity of anionic complexes such as  $[\text{Pd}(\text{PMe}_3)_2\text{OAc}]^-$  arises from their stronger ability to coordinate to carbon electrophiles. This results in an exothermic pre-coordination of the substrate, which pulls it into close proximity of the palladium-center, thereby significantly lowering the activation barrier for the actual oxidative addition step.

For the transmetalation of boronic acids, the only identifiable pathway involves dissociation of one phosphine ligand from the palladium, while all attempts failed to initiate a transmetalation reaction starting from palladium(II)diphosphine intermediates. This is consistent with the experimental findings by Espinet *et al.*, which indicate that the transfer of an organyl residue from stannates to palladium is retarded by the presence of excess phosphine.[23] This might be an additional reason why the most active catalysts known for Suzuki couplings involve sterically extremely crowded phosphine ligands that preclude the formation of palladium diphosphine complexes.[33]

In view of the long-standing controversy over the role of the base in Suzuki couplings, it is worth mentioning that our calculations predict the base to coordinate both to boron and palladium in the decisive transition state of the transmetalation.

For the reductive elimination, two possible pathways were again found, regenerating either a neutral (**12**) or an anionic species (**1**). Both pathways are energetically equally favorable, thus demonstrating how easily a cross-over between the anionic and the neutral pathway could occur.

Figure 3.8 shows the energy profiles for both pathways relative to the reactants which are defined to have zero energy in each case. As discussed in preceding section (*vide supra*), a correction of 10 kcal/mol per internal hydrogen bond has been applied for **6** and **8** to avoid differential stabilizing effects that will operate only in the gas phase and not in solution. The top part of Figure 3.8 specifies the three phases of the catalytic cycle as well as the steps where the reactants are introduced (+**I**, +**II**) and where the products are liberated (–**III**, –**IV**).

At first sight, the largest barrier seems to be associated with the transformation **8** → **10** which, however, consists of two distinct steps: removal of borate **III** (**8** → **9**) followed by a rearrangement (**9** → **10**) that initiates the reductive elimination. In solution, intermediate **9** will equilibrate with the environment, and therefore the two steps **8** → **9** and **9** → **10** will be kinetically distinct, each of them having a rather small barrier. Hence, in an overall view, all individual steps on the two pathways exhibit reasonably small barriers (< 15 kcal/mol).

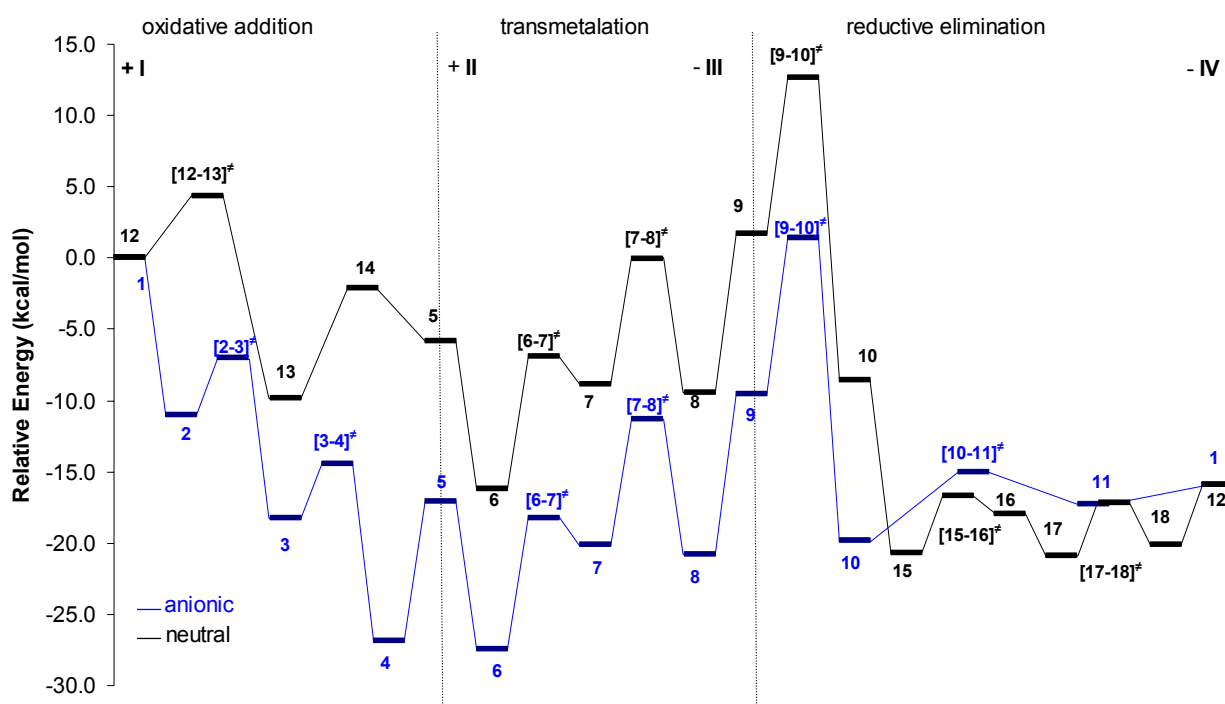




**Figure 3.8.** Relative energies ( $\Delta E_e$  in kcal/mol) for the intermediates and transition states involved in the neutral (black) and anionic (blue) cycle. A reference value of 0 has been assigned to the reactants in both cases, and the values for **6** and **8** have been corrected by 10 kcal/mol per internal hydrogen bond (see text).

The transformation **5**  $\rightarrow$  **10** is common to both pathways, and the two reaction profiles are therefore parallel in this region. The black curve for the neutral pathway is shifted by 11.3 kcal/mol relative to the blue one for the anionic pathway, because the reactants have been chosen to be **I** + **II** + Pd(PMe<sub>3</sub>)<sub>2</sub> (**12**) + [PhB(OH)<sub>2</sub>OAc]<sup>−</sup> (**V**) in the former case, and **I** + **II** + [Pd(PMe<sub>3</sub>)<sub>2</sub>OAc]<sup>−</sup> (**1**) in the latter case; the difference of 11.3 kcal/mol is simply the calculated energy for the formal reaction **12** + **V**  $\rightarrow$  **1** + **II** that connects the reactants. It is obvious that the relative position of the two curves depends on the choice of the model systems, *i.e.* on the source of acetate (*vide supra*): the formation of **1** is endothermic by 11.3 kcal/mol from **12** and **V**, but exothermic by 18.4 kcal/mol from **12** and free acetate. This implies that the relative preference for the neutral and anionic pathways will depend on the experimental conditions, *i.e.*, on the accessibility of acetate.

Figure 3.9 shows the free energy profiles for both pathways using the same conventions as in Figure 3.8. The overall appearance of the curves in Figure 3.8 and 3.9 is rather similar, but there are also some notable differences. Association reactions (adding reactants in steps **1**  $\rightarrow$  **3**, **12**  $\rightarrow$  **13** and **5**  $\rightarrow$  **6**) suffer from an entropic penalty because of the loss of translational and rotational degrees of freedom (typically around 10 kcal/mol at 298 K in the gas phase), while dissociation reactions (liberating products in steps **8**  $\rightarrow$  **9**, **11**  $\rightarrow$  **1** and **18**  $\rightarrow$  **12**) are entropically favored in an analogous manner. In solution, these entropic effects will be less pronounced than in the gas phase due to solvation and desolvation, but they will still be present to some extent.

The two free energy profiles in Figure 3.9 are of course again parallel in the central region (**5**  $\rightarrow$  **10**, see above). The final stages of the reductive elimination (beyond **10**) are predicted to be facile on both pathways. The main mechanistic distinction will therefore concern the initial oxidative addition, where the anionic pathway is clearly favored over the neutral pathway, with  $\Delta G^\ddagger_{298}$  barriers of 7.7 and 19.7 kcal/mol, respectively. This is consistent with the experimental finding that a catalyst generated *in situ* from palladium(II)acetate is more active than preformed neutral palladium-phosphine complexes, since under these conditions the formation of three-coordinate anionic complexes is to be expected.[5,6]

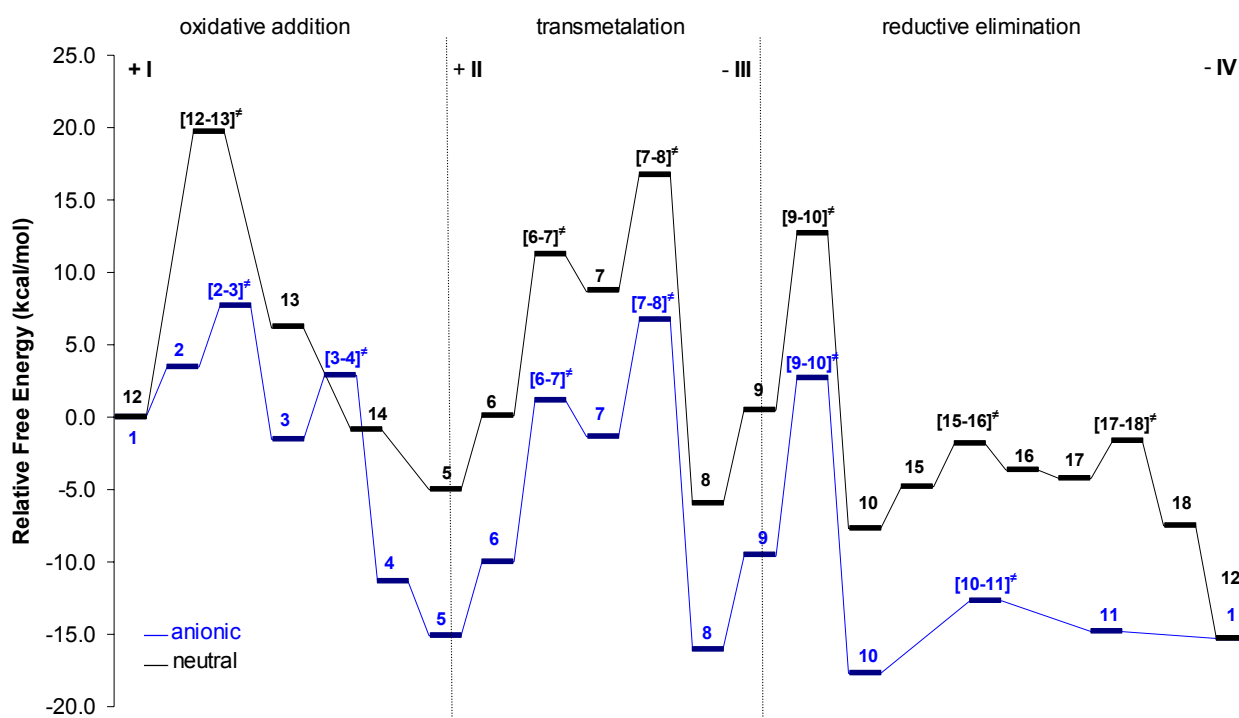


**Figure 3.9.** Relative free energies ( $\Delta G_{298}$  in kcal/mol) for the intermediates and transition states involved in the neutral (black) and anionic (blue) cycle. Conventions see Figure 3.8.

Looking at the overall free energy profiles in Figure 3.9, it is obvious that there is not a single step that would require excessive activation, and the computed barriers are in a reasonable range for a reaction that occurs experimentally at 60°C. Within the anionic pathway, the barriers for the initial oxidative addition stage are calculated to be lower than those for later stages, while they are of similar magnitude for the neutral pathway even after accounting for some overestimate for the entropic penalty in  $[12-13]^{\ddagger}$ . When replacing the  $\text{PMe}_3$  ligand by bulkier and less electron-rich phosphine ligands as commonly used in experimental work, the barriers for oxidative addition are generally expected to increase, while those for reductive elimination should decrease. Extrapolating from our current results on the basis of this qualitative expectation, the initial oxidative addition should become mechanistically more important implying a more pronounced overall preference for the anionic pathway with such ligands.

In conclusion, valuable insights on the mechanism of Pd-catalyzed cross-coupling reactions have been obtained by calculations that provide complete catalytic cycles for a suitable model system. In view of the extreme complexity of the experimentally employed catalytic systems, further studies especially on triarylphosphine-palladium catalysts are needed for a more complete understanding of this important transformation.

### 3.5 Supporting Information

#### Contents:

**Table 3.S1.** Absolute energies (hartree) from BP86/6-31G\* calculations.

**Figure 3.S1.** DFT optimized geometries of species involved in the catalytic cycles.  
Bond distances in Å and angles in degrees.

**Scheme 3.S1.** Energetics for the model reaction.

**Table 3.S1.** Absolute energies (hartree) from BP86/6-31G\* calculations.

No.	E <sub>c</sub>	E <sub>0</sub>	H <sub>298</sub>	G <sub>298</sub>	E <sub>sov</sub>
I	-381.723958	-381.628233	-381.619007	-381.66192	-381.728739
II	-408.238473	-408.117037	-408.107995	-408.150722	-408.243905
III	-405.1084707	-405.025221	-405.016081	-405.059156	-405.119714
IV	-384.879391	-384.745052	-384.736108	-384.777828	-384.882702
V	-636.783104	-636.613373	-636.599085	-636.653597	-636.844144
VI	-461.10031	-460.990062	-460.982266	-461.019548	-461.101837
VII	-228.497311	-228.455615	-228.450147	-228.483177	-228.585122
1	-1277.622937	-1277.352362	-1277.328357	-1277.407933	-1277.680236
2	-1659.364418	-1658.995643	-1658.962516	-1659.064268	-1659.418014
[2-3] <sup>‡</sup>	-1659.358138	-1658.989983	-1658.957304	-1659.057589	-1659.412501
3	-1659.376026	-1659.006568	-1658.974038	-1659.072284	-1659.429189
[3-4] <sup>‡</sup>	-1659.369886	-1659.000911	-1658.968878	-1659.065303	-1659.422368
4	-1659.389754	-1659.02094	-1658.987782	-1659.0879	-1659.443298
4a	-1659.384512	-1659.016133	-1658.982762	-1659.082221	-1659.436762
5	-1198.273826	-1198.017473	-1197.992248	-1198.074303	-1198.332859
5a	-1198.274903	-1198.018359	-1197.99322	-1198.074908	-1198.335823
6	-1606.544764	-1606.164508	-1606.130273	-1606.232883	-1606.597843
[6-7] <sup>‡</sup>	-1606.514101	-1606.134858	-1606.101515	-1606.19916	-1606.568807
7	-1606.517185	-1606.13774	-1606.103725	-1606.203129	-1606.570751
[7-8] <sup>‡</sup>	-1606.50313	-1606.124769	-1606.091138	-1606.190348	-1606.555289
8	-1606.550058	-1606.171671	-1606.136935	-1606.24251	-1606.600069
9	-1201.391876	-1201.09869	-1201.073109	-1201.157094	-1201.446218
[9-10] <sup>‡</sup>	-1201.374385	-1201.082017	-1201.057199	-1201.137633	-1201.431472
10	-1201.408251	-1201.114255	-1201.089165	-1201.170136	-1201.461289
[10-11] <sup>‡</sup>	-1201.400485	-1201.106671	-1201.082114	-1201.162089	-1201.457681
11	-1201.404193	-1201.108966	-1201.084058	-1201.16545	-1201.461269
12	-1049.096314	-1048.872977	-1048.854764	-1048.921076	-1049.098611
[12-13] <sup>‡</sup>	-1430.813299	-1430.493959	-1430.466966	-1430.551576	-1430.816661
13	-1430.835911	-1430.515591	-1430.488019	-1430.573042	-1430.842639
14	-969.723395	-969.515572	-969.495968	-969.564859	-969.728404
15	-1609.666109	-1609.249185	-1609.215004	-1609.31622	-1609.712814
[15-16] <sup>‡</sup>	-1609.659732	-1609.24294	-1609.209191	-1609.311447	-1609.705677
16	-1609.661645	-1609.244243	-1609.20976	-1609.314484	-1609.708979
17	-1433.983507	-1433.625077	-1433.59774	-1433.681237	-1433.986986

<b>[17-18]<sup>‡</sup></b>	-1433.977651	-1433.619284	-1433.592319	-1433.677225	-1433.980381
<b>18</b>	-1433.982276	-1433.62378	-1433.595891	-1433.68648	-1433.98559
<b>[4a-4b]<sup>‡</sup></b>	-1659.370904	-1659.003382	-1658.970383	-1659.070284	-1659.425239
<b>4b</b>	-1659.380041	-1659.011965	-1658.978316	-1659.081447	-1659.432319
<b>4c</b>	-1198.270238	-1198.014112	-1197.988987	-1198.071723	-1198.329631

---

$E_e$       Electronic energy

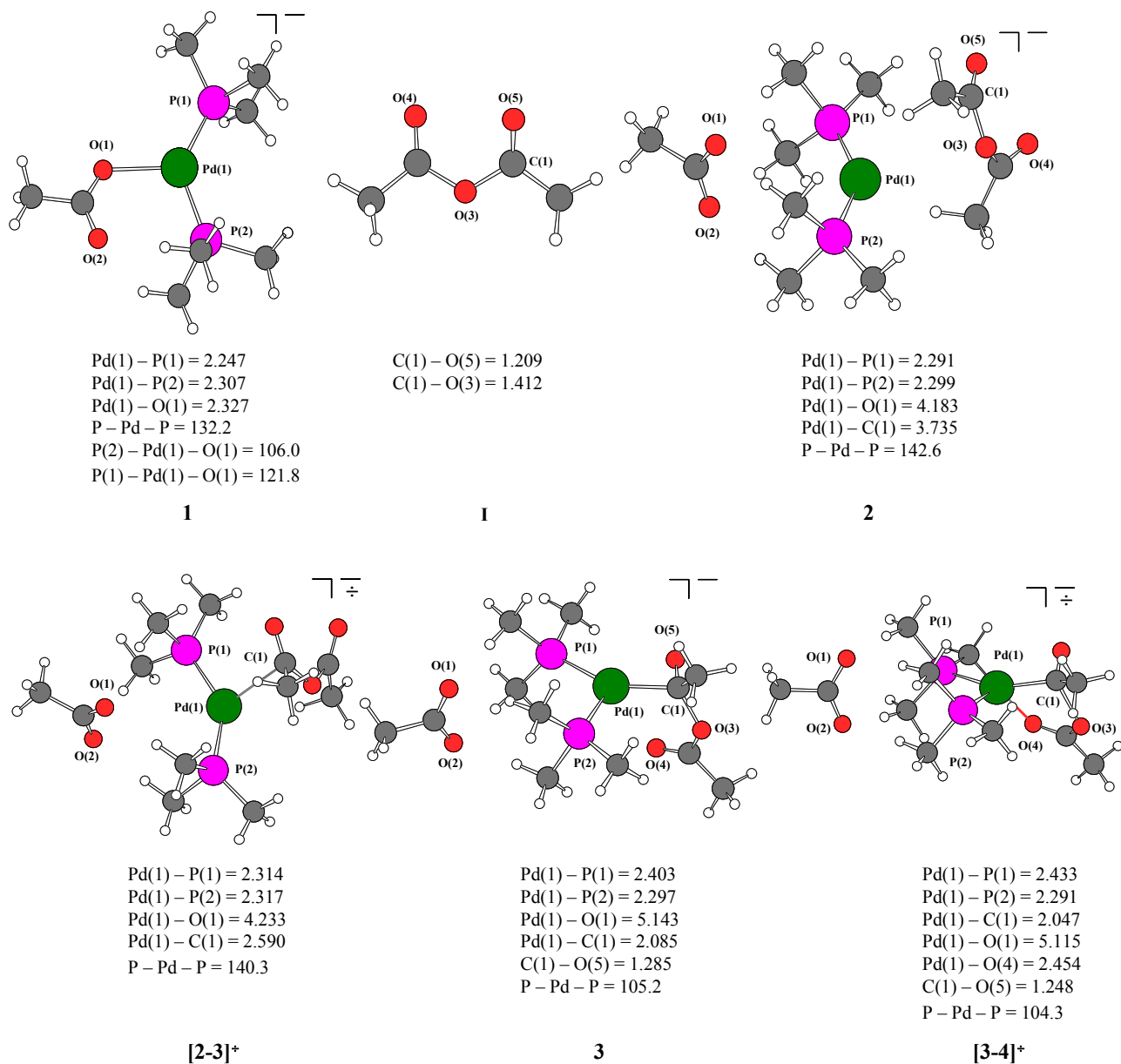
$E_0$       Total energy plus zero-point vibrational energy

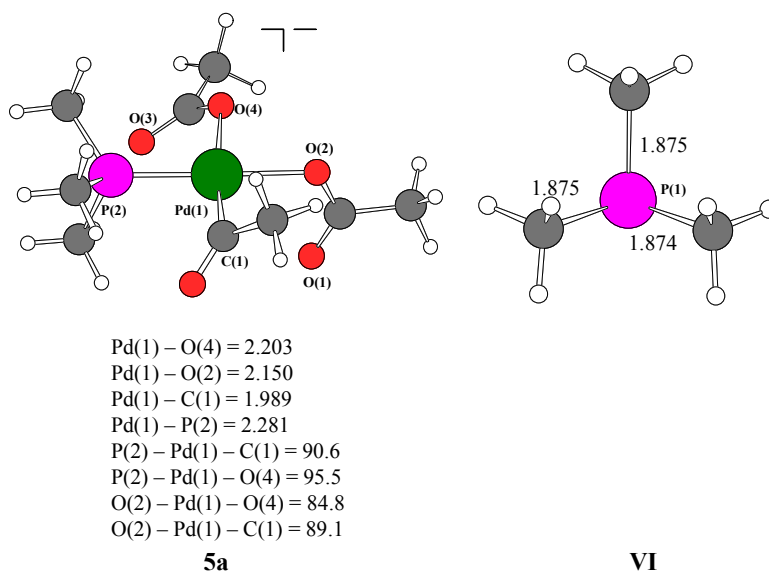
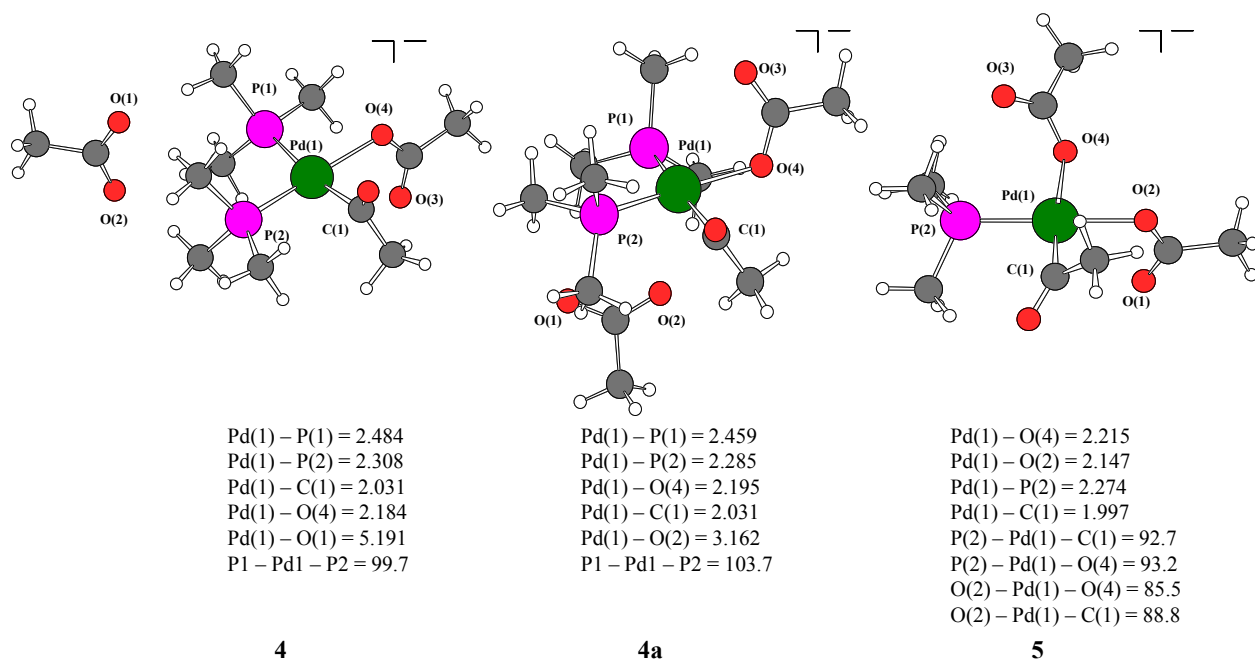
$H_{298}$     Enthalpy at 298 K

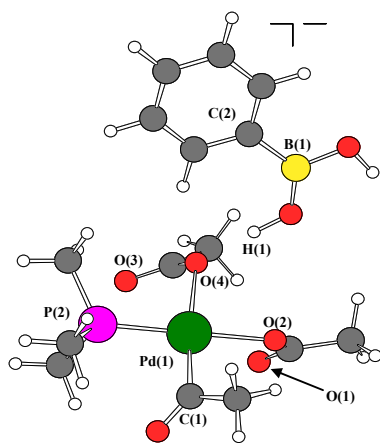
$G_{298}$     Gibbs free enthalpy at 298 K

$E_{\text{sov}}$     Total energy plus CPCM solvation energy (THF)

**Figure 3.S1.** DFT optimized geometries of species involved in the catalytic cycles. Bond distances in Å and angles in degrees.

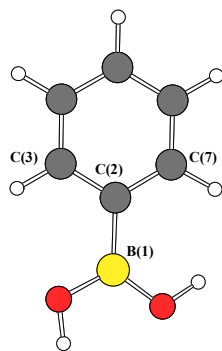






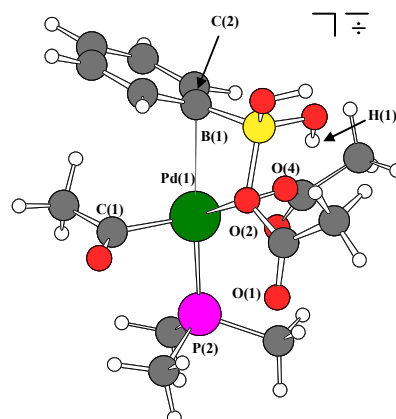
Pd(1) – O(4) = 2.267  
 Pd(1) – P(2) = 2.285  
 Pd(1) – O(2) = 2.129  
 Pd(1) – C(1) = 1.981  
 P(2) – Pd(1) – O(4) = 94.6  
 P(2) – Pd(1) – C(1) = 90.7  
 O(2) – Pd(1) – O(4) = 85.7  
 O(2) – Pd(1) – C(1) = 89.0

6



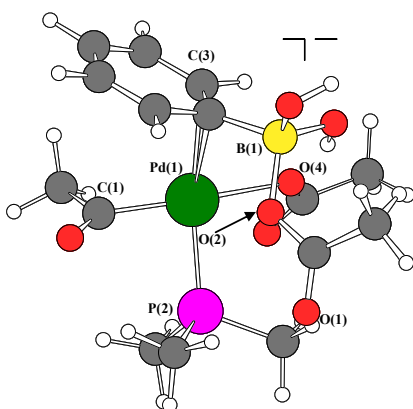
B(1) – C(2) = 1.573  
 C(2) – C(3) = 1.416  
 C(2) – C(7) = 1.415

II



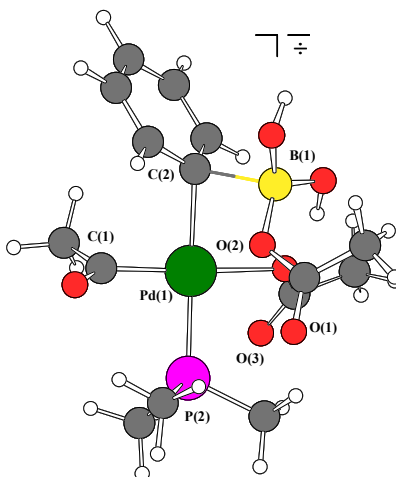
Pd(1) – C(2) = 2.817  
 Pd(1) – C(1) = 1.979  
 Pd(1) – P(2) = 2.293  
 C(2) – B(1) = 1.654  
 B(1) – O(2) = 1.637  
 Pd(1) – O(2) = 2.486  
 C(1) – Pd(1) – P(2) = 89.6  
 O(4) – Pd(1) – P(2) = 95.2  
 B(1) – Pd(1) – Pd(1) = 100.4

[6-7]<sup>+</sup>



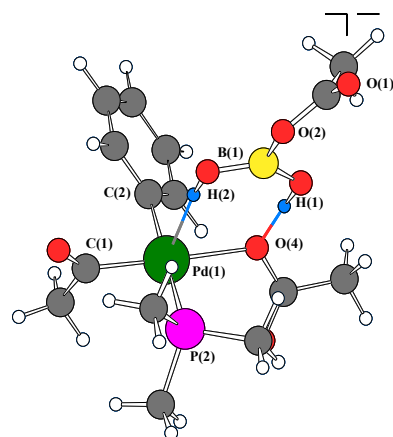
Pd(1) – C(2) = 2.549  
 Pd(1) – C(1) = 1.987  
 Pd(1) – P(2) = 2.315  
 C(2) – B(1) = 1.663  
 Pd(1) – O(4) = 2.231  
 Pd(1) – C(3) = 2.448  
 Pd(1) – O(2) = 3.066  
 C(1) – Pd(1) – P(2) = 86.8  
 O(4) – Pd(1) – P(2) = 94.2  
 B(1) – O(2) – Pd(1) = 83.1

7



Pd(1) – C(2) = 2.245  
 Pd(1) – C(1) = 1.983  
 Pd(1) – P(2) = 2.317  
 Pd(1) – O(4) = 2.259  
 C(2) – B(1) = 2.122  
 C(1) – Pd(1) – C(2) = 89.6  
 C(1) – Pd(1) – P(2) = 88.3  
 O(4) – Pd(1) – P(2) = 93.7

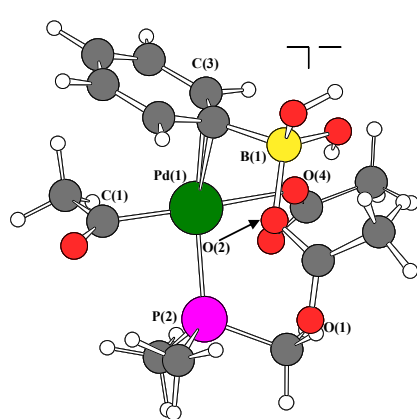
[7-8]<sup>+</sup>



Pd(1) – C(2) = 2.076  
 Pd(1) – C(1) = 1.989  
 Pd(1) – H(2) = 2.288  
 Pd(1) – P(2) = 2.383  
 Pd(1) – O(4) = 2.253  
 C(1) – Pd(1) – C(2) = 87.0  
 C(1) – Pd(1) – P(2) = 91.8  
 C(2) – Pd(1) – O(4) = 89.9

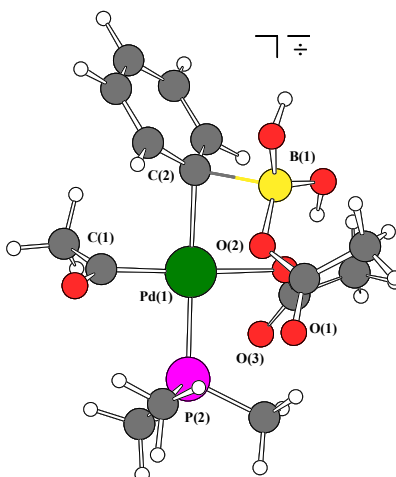
8





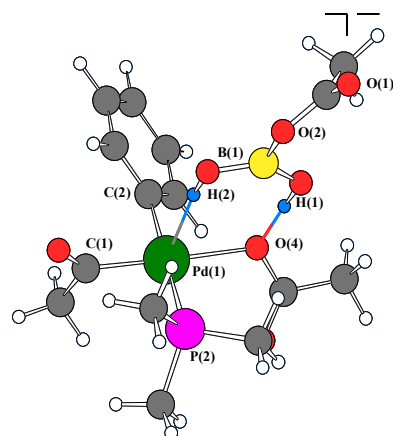
Pd(1) – C(2) = 2.549  
 Pd(1) – C(1) = 1.987  
 Pd(1) – P(2) = 2.315  
 C(2) – B(1) = 1.663  
 Pd(1) – O(4) = 2.231  
 Pd(1) – C(3) = 2.448  
 Pd(1) – O(2) = 3.066  
 C(1) – Pd(1) – P(2) = 86.8  
 O(4) – Pd(1) – P(2) = 94.2  
 B(1) – O(2) – Pd(1) = 83.1

7



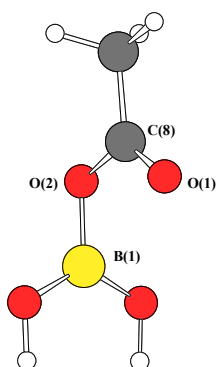
Pd(1) – C(2) = 2.245  
 Pd(1) – C(1) = 1.983  
 Pd(1) – P(2) = 2.317  
 Pd(1) – O(4) = 2.259  
 C(2) – B(1) = 2.122  
 C(1) – Pd(1) – C(2) = 89.6  
 C(1) – Pd(1) – P(2) = 88.3  
 O(4) – Pd(1) – P(2) = 93.7

[7-8]\*



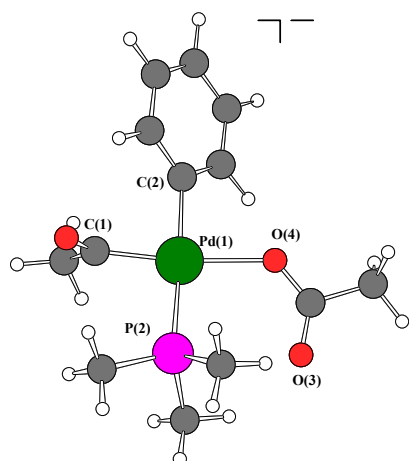
Pd(1) – C(2) = 2.076  
 Pd(1) – C(1) = 1.989  
 Pd(1) – H(2) = 2.288  
 Pd(1) – P(2) = 2.383  
 Pd(1) – O(4) = 2.253  
 C(1) – Pd(1) – C(2) = 87.0  
 C(1) – Pd(1) – P(2) = 91.8  
 C(2) – Pd(1) – O(4) = 89.9

8



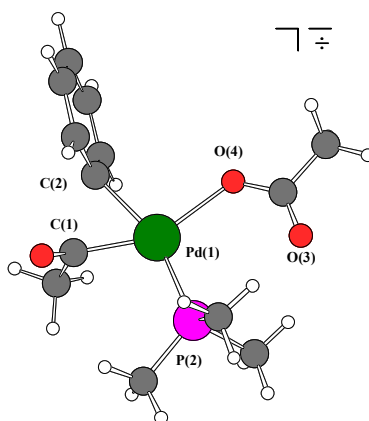
B(1) – O(2) = 1.418  
 O(2) – C(8) = 1.368  
 C(8) – O(1) = 1.223

IV



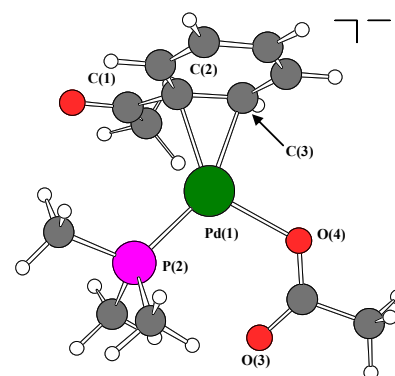
Pd(1) – C(1) = 1.987  
 Pd(1) – C(2) = 2.086  
 Pd(1) – P(2) = 2.395  
 Pd(1) – O(4) = 2.232  
 C(1) – Pd(1) – P(2) = 91.5  
 C(1) – Pd(1) – C(2) = 86.1  
 O(4) – Pd(1) – C(2) = 86.0

9



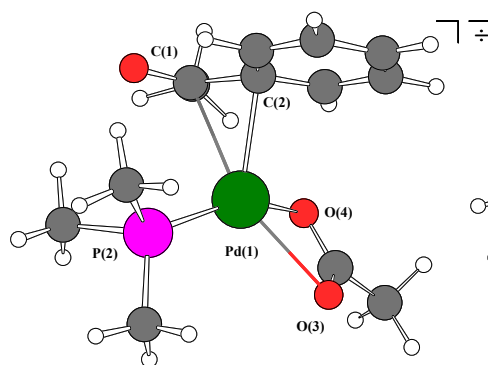
Pd(1) – C(1) = 2.032  
 Pd(1) – C(2) = 2.185  
 Pd(1) – O(4) = 2.258  
 Pd(1) – P(2) = 2.298  
 C(1) – C(2) = 1.965  
 C(1) – Pd(1) – P(2) = 104.5  
 C(1) – Pd(1) – C(2) = 55.4  
 C(2) – Pd(1) – O(4) = 97.4

[9-10]<sup>+</sup>



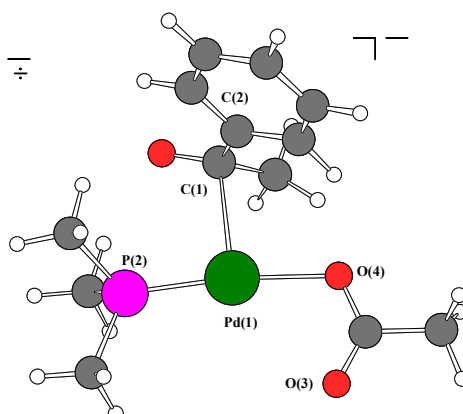
Pd(1) – C(2) = 2.226  
 Pd(1) – C(3) = 2.205  
 Pd(1) – P(2) = 2.313  
 Pd(1) – O(4) = 2.231  
 C(2) – C(1) = 1.488  
 P(2) – Pd(1) – O(4) = 107.5

10



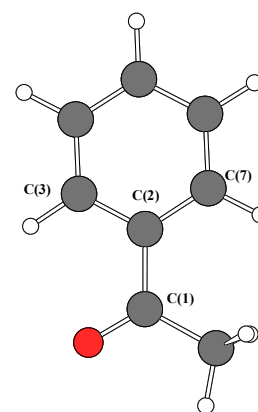
Pd(1) – C(1) = 2.479  
 Pd(1) – C(2) = 2.448  
 Pd(1) – P(2) = 2.238  
 Pd(1) – O(4) = 2.422  
 Pd(1) – O(3) = 2.559  
 P(2) – Pd(1) – O(3) = 115.5  
 C(2) – Pd(1) – P(2) = 107.6

[10-11]<sup>+</sup>



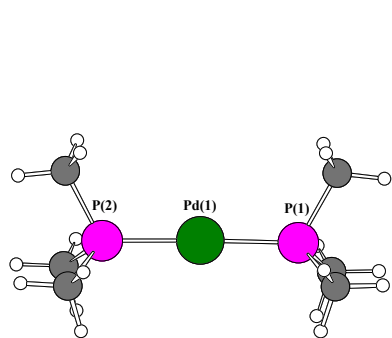
Pd(1) – C(1) = 2.560  
 Pd(1) – P(2) = 2.214  
 Pd(1) – O(4) = 2.174  
 Pd(1) – O(3) = 3.088  
 Pd(1) – C(2) = 3.018  
 P(2) – Pd(1) – C(1) = 90.8  
 P(2) – Pd(1) – O(4) = 172.7

11



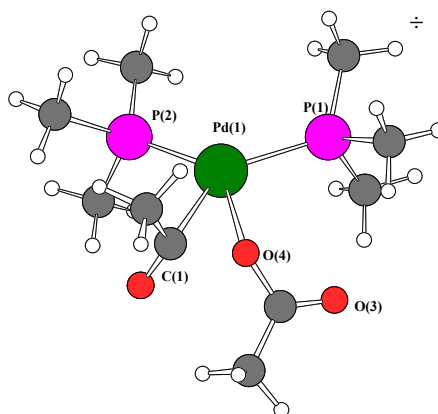
C(1) – C(2) = 1.505  
 C(2) – C(3) = 1.412  
 C(2) – C(7) = 1.413  
 C(1) – O(5) = 1.234

III



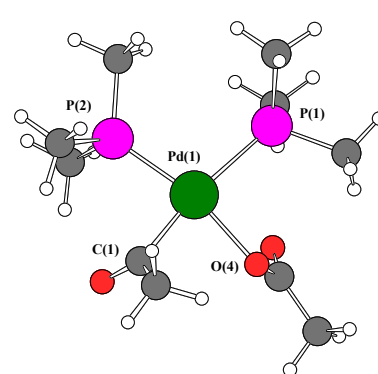
Pd(1) – P(1) = 2.922  
Pd(1) – P(2) = 2.991  
P2 – Pd1 – P1 = 178.6

12



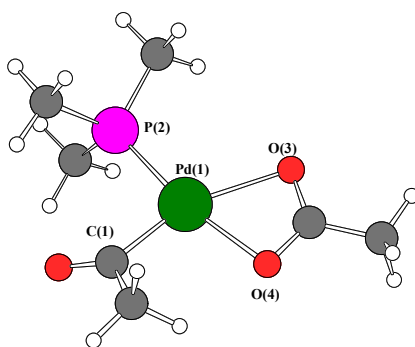
Pd(1) – P(1) = 2.441  
Pd(1) – P(2) = 2.280  
Pd(1) – C(1) = 2.215  
Pd(1) – O(4) = 2.344  
C(1) – O(4) = 1.604  
P2 – Pd1 – P1 = 122.9  
C(1) – Pd(1) – O(4) = 41.1

[12-13]<sup>+</sup>



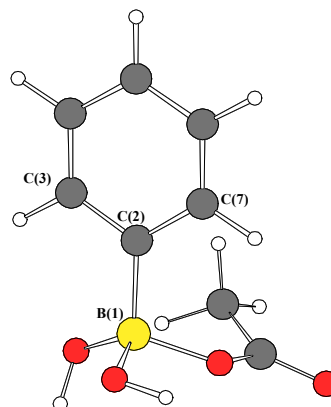
Pd(1) – P(1) = 2.483  
Pd(1) – P(2) = 2.292  
Pd(1) – C(1) = 2.048  
Pd(1) – O(4) = 2.164  
P(2) – Pd(1) – P(1) = 102.3  
C(1) – Pd(1) – O(4) = 80.5

13



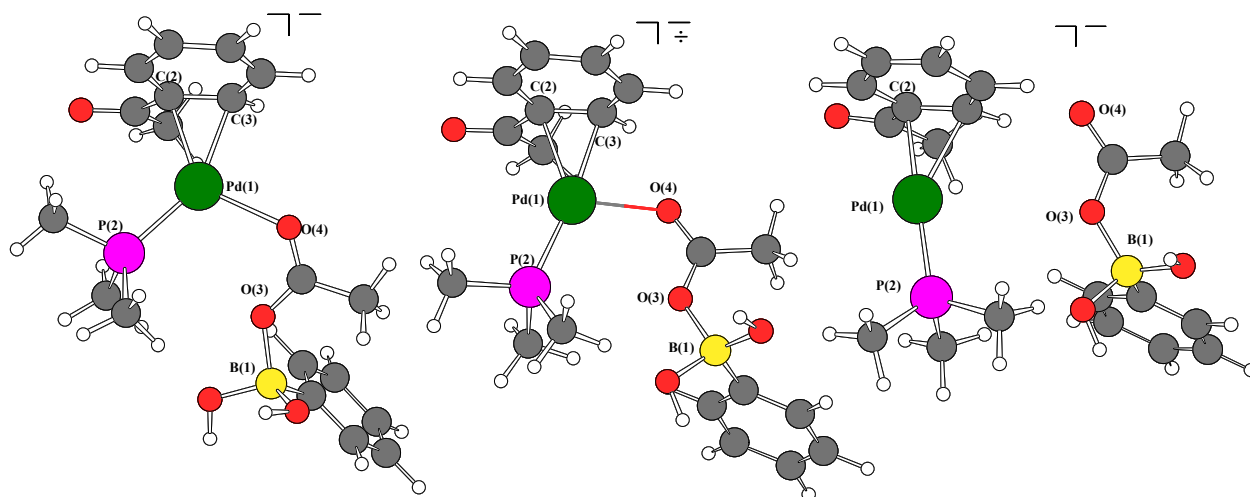
Pd(1) – P(2) = 2.272  
Pd(1) – C(1) = 1.988  
Pd(1) – O(4) = 2.179  
Pd(1) – O(3) = 2.310  
P(2) – Pd(1) – C(1) = 91.7  
O(3) – Pd(1) – P(2) = 108.8  
C(1) – Pd(1) – O(4) = 99.7

14



C(2) – B(1) = 1.641  
C(2) – C(3) = 1.415  
C(2) – C(7) = 1.416

V



Pd(1) – P(2) = 2.323  
Pd(1) – O(4) = 2.323  
Pd(1) – C(2) = 2.231  
Pd(1) – C(3) = 2.212  
B(1) – O(3) = 1.571  
O(4) – Pd(1) – P(2) = 112.4

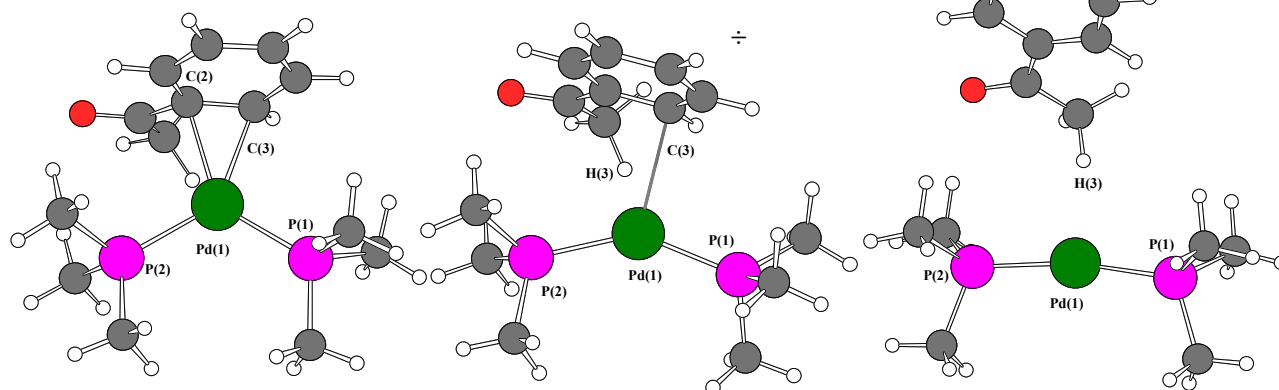
15

Pd(1) – C(2) = 2.302  
Pd(1) – C(3) = 2.208  
Pd(1) – O(4) = 3.095  
Pd(1) – P(2) = 2.291  
O(3) – B(1) = 1.555  
O(4) – Pd(1) – P(2) = 113.8

[15-16]<sup>+</sup>

Pd(1) – C(2) = 2.215  
Pd(1) – P(2) = 2.277  
Pd(1) – O(3) = 4.437  
Pd(1) – O(4) = 4.761  
B(1) – O(3) = 1.546  
O(4) – Pd(1) – P(2) = 112.8

16



Pd(1) – C(2) = 2.309  
Pd(1) – C(3) = 2.300  
Pd(1) – P(1) = 2.337  
Pd(1) – P(2) = 2.367  
P – Pd – P = 117.8

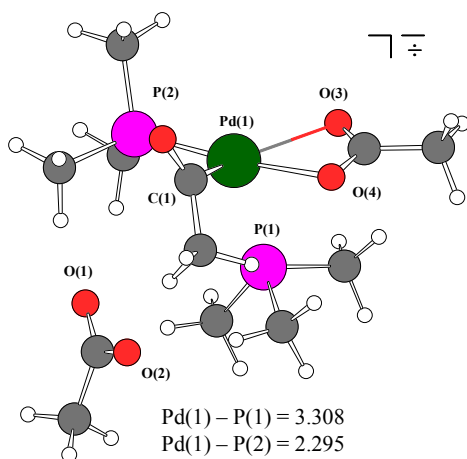
17

Pd(1) – P(1) = 2.294  
Pd(1) – P(2) = 2.335  
Pd(1) – C(3) = 2.758  
P – Pd – P = 144.9  
C(3) – Pd(1) – P(2) = 116.5

[17-18]<sup>+</sup>

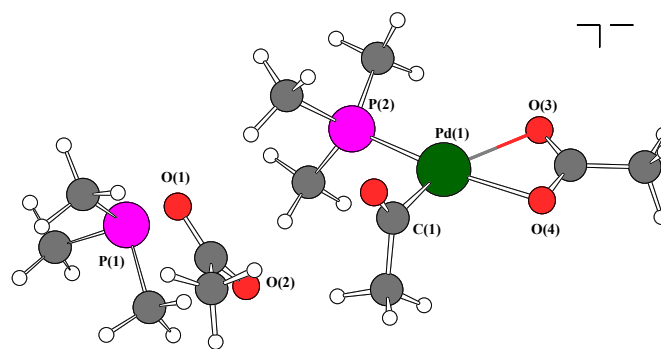
Pd(1) – P(1) = 2.289  
Pd(1) – P(2) = 2.317  
Pd(1) – H(3) = 2.353  
P – Pd – P = 169.6

18



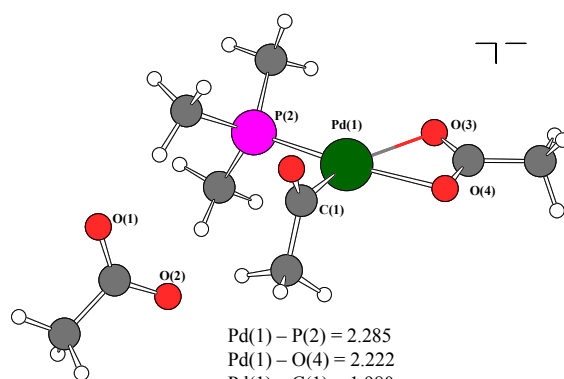
Pd(1) – P(1) = 3.308  
Pd(1) – P(2) = 2.295  
Pd(1) – O(4) = 2.196  
Pd(1) – C(1) = 1.977  
Pd(1) – O(2) = 4.527  
P1 – Pd1 – P2 = 92.1

**[4a-4b]\***



Pd(1) – P(1) = 7.498  
Pd(1) – P(2) = 2.289  
Pd(1) – O(4) = 2.217  
Pd(1) – C(1) = 1.975  
Pd(1) – O(2) = 4.721  
P1 – Pd1 – P2 = 30.4

**4b**

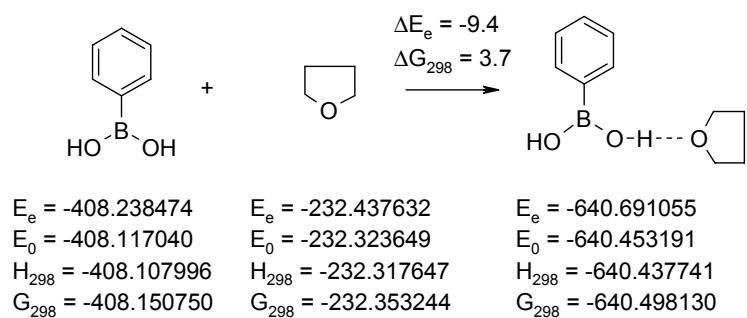
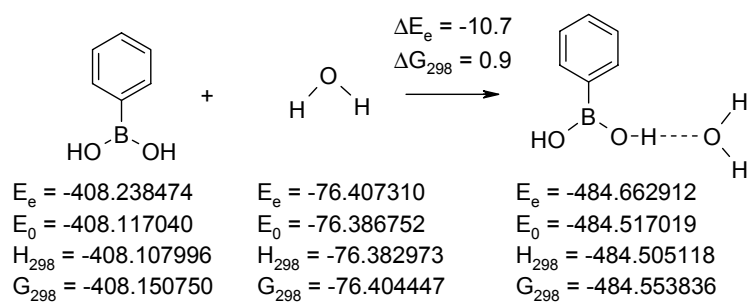


Pd(1) – P(2) = 2.285  
Pd(1) – O(4) = 2.222  
Pd(1) – C(1) = 1.980  
Pd(1) – O(3) = 2.379  
Pd(1) – O(2) = 4.717  
Pd(1) – O(1) = 5.464  
P1 – Pd1 – C1 = 91.2

**4c**

## Scheme 3.S1. Energetics for the model reaction

(Total energies in hartree, reaction energies in kcal/mol)



## Bibliography

- [1] (a) N. Miyaura, A. Suzuki, "Palladium-Catalyzed Cross-Coupling Reactions of Organoboron Compounds." *Chem Rev.* **1995**, 95, 2457-2483. (b) A. Suzuki, "Recent advances in the cross-coupling reactions of organoboron derivatives with organic electrophiles, 1995-1998." *J. Organomet. Chem.* **1999**, 576, 147-168. (c) T. Ishiyama, N. Miyaura, "Chemistry of Group 13 element-transition metal linkage — the platinum- and palladium-catalyzed reactions of (alkoxo)diborons." *J. Organomet. Chem.* **2000**, 611, 392-402. (d) A. Suzuki, "Metal-Catalyzed Cross-Coupling Reactions." F. Diederich, P. J. Stang, Eds., Wiley-VCH, Weinheim, **1998**, page 49.
- [2] (a) N. Miyaura, K. Yamada, A. Suzuki, "A new stereospecific cross-coupling by the palladium-catalyzed reaction of 1-alkenylboranes with 1-alkenyl or 1-alkynyl halides." *Tetrahedron Lett.* **1979**, 20, 3437-3440. (b) N. Miyaura, K. Yamada, H. Suginome, A. Suzuki, "Novel and Convenient Method for the Stereo- and Regiospecific Synthesis of Conjugated Alkadienes and Alkynes via the Palladium-Catalyzed Cross-Coupling Reaction of 1-Alkenylboranes with Bromoalkenes and Bromoalkynes." *J. Am. Chem. Soc.* **1985**, 107, 972-980. (c) N. Miyaura, A. Suzuki, "Palladium-catalyzed reaction of 1-alkenylboronates with vinylic halides-(1Z,3E)-1-phenyl-1,3-octadiene-(benzene, 1,3-octadienyl, (Z,E))." *Org. Synth.* **1990**, 68, 130-137. (d) M. Satoh, N. Miyaura, A. Suzuki, "Stereo- and Regiospecific Synthesis of Trisubstituted Alkenes via the Palladium-catalyzed Cross-coupling Reaction of Diisopropyl (E)-(1-Alkyl-1-alkenyl)boronates with Organic Halides" *Chem. Lett.* **1986**, 1329-1332. (e) N. Miyaura, M. Satoh, A. Suzuki, "A stereospecific synthesis of conjugated (E, Z)- and (Z, Z)-alkadienes by a palladium-catalyzed cross-coupling reaction of 1-alkenylboranes with 1-alkenyl bromides." *Tetrahedron Lett.* **1981**, 22, 127-130.
- [3] L. J. Gooßen, "Pd-catalyzed synthesis of arylacetic acid derivatives from boronic acids." *Chem. Commun.* **2001**, 7, 669-670.
- [4] (a) L. J. Gooßen, K. Ghosh, "Palladium-Catalyzed Synthesis of Aryl Ketones from Boronic Acids and Carboxylic Acids Activated in situ by Pivalic Anhydride." *Eur. J. Org. Chem.* **2002**, 19, 3254-3267. (b) K. Nagayama, I. Shimizu, A. Yamamoto, "Direct Hydrogenation of Carboxylic Acids to Corresponding Aldehydes Catalyzed by Palladium Complexes in the Presence of Pivalic Anhydride." *Chem. Lett.* **1998**, 1143-1144. (c) R.

Kakino, S. Kamusi, I. Shimizu, A. Yamamoto, "Synthesis of Unsymmetrical Ketones by Palladium-Catalyzed Cross-Coupling Reaction of Carboxylic Anhydrides with Organoboron Compounds." *Bull. Chem. Soc. Jpn.* **2002**, 75, 137-148.

[5] (a) C. Amatore, A. Jutand, "Anionic Pd(0) and Pd(II) Intermediates in Palladium-Catalyzed Heck and Cross-Coupling Reactions." *Acc. Chem. Res.* **2000**, 33, 314-321. (b) C. Amatore, M. Azzabi, A. Jutand, "Rates and mechanism of the reversible oxidative of (Z)- and (E)-1,2-dichloroethylene to low-ligated zerovalent palladium." *J. Am. Chem. Soc.* **1991**, 113, 1670-1677. (c) C. Amatore, A. Jutand, A. Suarez, "Intimate mechanism of oxidative addition to zerovalent palladium complexes in the presence of halide ions and its relevance to the mechanism of palladium-catalyzed nucleophilic substitutions." *J. Am. Chem. Soc.* **1993**, 115, 9531-9541.

[6] (a) L. J. Gooßen, D. Koley, H. Hermann, W. Thiel, "The mechanism of the oxidative addition of aryl halides to Pd-catalysts: a DFT investigation." *Chem. Commun.* **2004**, 2141-2143. (b) L. J. Gooßen, D. Koley, H. Hermann, W. Thiel, "Mechanistic pathways for oxidative addition of aryl halides to palladium(0) complexes: A DFT study." *Organometallics* **2005**, 24, 2398-2410.

[7] S. Kozuch, S. Shaik, A. Jutand, C. Amatore, "Active Anionic Zero-Valent Palladium Catalysts: Characterization by Density Functional Calculations." *Chem. Eur. J.* **2004**, 10, 3072-3080.

[8] A. Sundermann, O. Uzan, J. M. L. Martin, "Computational Study of a New Heck Reaction Mechanism Catalyzed by Palladium(ii/iv) Species." *Chem. Eur. J.* **2001**, 7, 1703-1711.

[9] (a) I. D. Hills, M. R. Netherton, G. C. Fu, "Toward an Improved Understanding of the Unusual Reactivity of Pd<sup>0</sup>/Trialkylphosphane Catalysts in Cross-Couplings of Alkyl Electrophiles: Quantifying the Factors That Determine the Rate of Oxidative Addition." *Angew. Chem., Int. Ed.* **2003**, 42, 5749-5752. (b) J. K. Eberhardt, R. Fröhlich, E-U. Würthwein, "N-Acylamidine Palladium(II) Complexes. Synthesis, Structures, and Catalytic Activity for Suzuki-Miyaura Cross-Coupling Reactions: Experiments and DFT Calculations" *J. Org. Chem.* **2003**, 68, 6690-6694.

[10] (a) Q. Cui, D. G. Musaev, K. Morokuma, "Density Functional Study on the Mechanism of Palladium(0)-Catalyzed Thioboration Reaction of Alkynes. Differences between



Pd(0) and Pt(0) Catalysts and between Thioboration and Diboration.” *Organometallics* **1998**, *17*, 1383-1392 and references therein. (b) A. E. Dorigo, P. v. R. Schleyer, “An Ab Initio Investigation of the RhI-Catalyzed Hydroboration of C=C Bonds: Evidence for Hydrogen Migration in the Key Step.” *Angew. Chem., Int. Ed. Engl.* **1995**, *34*, 115-118.

[11] (a) K. Albert, P. Gisdakis, N. Rösch, “On C—C Coupling by Carbene-Stabilized Palladium Catalysts: A Density Functional Study of the Heck Reaction.” *Organometallics* **1998**, *17*, 1608-1616. (b) R. J. Deeth, A. Smith, J. M. Brown, “Electronic Control of the Regiochemistry in Palladium–Phosphine Catalyzed Intermolecular Heck Reactions.” *J. Am. Chem. Soc.* **2004**, *126*, 7144-7151. (c) D. Balcells, F. Maseras, B. A. Keay, T. Ziegler, “Polyene Cyclization by a Double Intramolecular Heck Reaction. A DFT Study.” *Organometallics* **2004**, *23*, 2784-2796. (d) R. J. Deeth, A. Smith, K. K. Hii, J. M. Brown, “The Heck olefination reaction; A DFT study of the elimination pathway.” *Tetrahedron Lett.* **1998**, *39*, 3229-3232. (e) K. K. Hii, T. D. W. Claridge, J. M. Brown, A. Smith, R. J. Deeth, “The Intermolecular Asymmetric Heck Reaction: Mechanistic and Computational Studies.” *Helv. Chim. Acta* **2001**, *84*, 3043-3056. (f) H. von Schenck, B. Akermark, M. Svensson, “Electronic Control of the Regiochemistry in the Heck Reaction.” *J. Am. Chem. Soc.* **2003**, *125*, 3503-3508. (g) M. Ludwig, S. Stromberg, M. Svensson, B. Akermark, “An Exploratory Study of Regiocontrol in the Heck Type Reaction. Influence of Solvent Polarity and Bisphosphine Ligands.” *Organometallics* **1999**, *18*, 970-975.

[12] (a) K. Nagayama, F. Kawataka, M. Sakamoto, I. Shimizu, A. Yamamoto, “Preparation and Reactivities of Acyl(carboxylato)palladium Complexes.” *Chem. Lett.* **1995**, 367-368. (b) R. Kakino, H. Narahashi, I. Shimizu, A. Yamamoto, “Palladium-Catalyzed Direct Conversion of Carboxylic Acids into Ketones with Organoboronic Acids Promoted by Anhydride Activators.” *Bull. Chem. Soc. Jpn.* **2002**, *75*, 1333-1345.

[13] Gaussian 03, Revision B.01, M. J. Frisch, G. W. Trucks, H. B. Schlegel, G. E. Scuseria, M. A. Robb, J. R. Cheeseman, J. A. Montgomery, Jr., T. Vreven, K. N. Kudin, J. C. Burant, J. M. Millam, S. S. Iyengar, J. Tomasi, V. Barone, B. Mennucci, M. Cossi, G. Scalmani, N. Rega, G. A. Petersson, H. Nakatsuji, M. Hada, M. Ehara, K. Toyota, R. Fukuda, J. Hasegawa, M. Ishida, T. Nakajima, Y. Honda, O. Kitao, H. Nakai, M. Klene, X. Li, J. E. Knox, H. P. Hratchian, J. B. Cross, C. Adamo, J. Jaramillo, R. Gomperts, R. E. Stratmann, O. Yazyev, A. J. Austin, R. Cammi, C. Pomelli, J. W. Ochterski, P. Y. Ayala, K. Morokuma, G. A. Voth, P. Salvador, J. J. Dannenberg, V. G. Zakrzewski, S. Dapprich, A. D. Daniels, M. C.

Strain, O. Farkas, D. K. Malick, A. D. Rabuck, K. Raghavachari, J. B. Foresman, J. V. Ortiz, Q. Cui, A. G. Baboul, S. Clifford, J. Cioslowski, B. B. Stefanov, G. Liu, A. Liashenko, P. Piskorz, I. Komaromi, R. L. Martin, D. J. Fox, T. Keith, M. A. Al-Laham, C. Y. Peng, A. Nanayakkara, M. Challacombe, P. M. W. Gill, B. Johnson, W. Chen, M. W. Wong, C. Gonzalez, and J. A. Pople, Gaussian, Inc., Pittsburgh PA, **2003**.

[14] A. D. Becke, "Density-functional exchange-energy approximation with correct asymptotic behaviour." *Phys. Rev. A* **1988**, 33, 3098-3100.

[15] J. P. Perdew, "Density-functional approximation for the correlation energy of the inhomogeneous electron gas." *Phys. Rev. B* **1986**, 33, 8822-8824.

[16] W. J. Hehre, L. Radom, P. v. R. Schleyer, J. A. Pople, "Ab Initio Molecular Orbital Theory." Wiley, New York, **1986**.

[17] P. J. Hay, W. R. Wadt, "Ab initio effective core potentials for molecular calculations. Potentials for K to Au including the outermost core orbitals." *J. Chem. Phys.* **1985**, 82, 299-310.

[18] D. Andrae, U. Häußermann, M. Dolg, H. Stoll, H. Preuß, "Energy-adjusted *ab initio* pseudopotentials for the second and third row transition elements." *Theor. Chim. Acta* **1990**, 77, 123-141.

[19] (a) V. Barone. M. Cossi, "Quantum Calculations of Molecular Energies and Gradients in Solutions by a Conductor Solvent Model." *J. Phys. Chem. A* **1998**, 102, 1995-2001. (b) M. Cossi, N. Rega, G. Scalmani, V. Barone, "Energies, Structures, and Electronic Properties of Molecules in Solution with the C-PCM Solvation Model." *J. Comput. Chem.* **2003**, 24, 669-681.

[20] A. Klamt. G. Schüürmann, "COSMO: A New Approach to Dielectric Screening in Solvents with Explicit Expressions for the Screening Energy and its Gradient." *J. Chem. Soc., Perkin Trans 2.* **1993**, 799-805; (b) A. Schäfer, A. Klamt, D. Sattel, J. C. W. Lohrenz, F. Eckert, "COSMO Implementation in TURBOMOLE: Extension of an efficient quantum chemical code towards liquid systems." *Phys. Chem. Chem. Phys.* **2000**, 2, 2187-2193.

[21] (a) A. E. Reed, L. A. Curtiss, F. Weinhold, "Intermolecular Interactions from a Natural Bond Orbital, Donor-Acceptor Viewpoint." *Chem. Rev.* **1998**, 88, 899-926. (b) E. D. Glendening, A. E. Reed, J. E. Carpenter, F. Weinhold, F. *NBO Version 3.1*.

- [22] (a) F. Basolo, G. Pearson, "Mechanism of Inorganic Reactions." 2<sup>nd</sup> Edition, Wiley, New York, **1967**. (b) J. E. Huheey, E. A. Keiter, R. L. Keiter, "Inorganic Chemistry: Principles of Structures and Reactivity." 4<sup>th</sup> Edition, HarperCollins College Publishers, New York, **1993**.
- [23] (a) A. L. Casado, P. Espinet, "Mechanism of the Stille Reaction. 1. The Transmetalation Step. Coupling of R<sup>1</sup>I and R<sup>2</sup>SnBu<sub>3</sub> Catalyzed by *trans*-[PdR<sup>1</sup>IL<sub>2</sub>] (R<sup>1</sup> = C<sub>6</sub>Cl<sub>2</sub>F<sub>3</sub>; R<sup>2</sup> = Vinyl, 4-Methoxyphenyl; L = AsPh<sub>3</sub>)." *J. Am. Chem. Soc.* **1998**, *120*, 8978-8985. (b) A. L. Casado, P. Espinet, "On the Configuration Resulting from Oxidative Addition of RX to Pd(PPh<sub>3</sub>)<sub>4</sub> and the Mechanism of the *cis*-to-*trans* Isomerization of [PdRX(PPh<sub>3</sub>)<sub>2</sub>] Complexes (R = Aryl, X = Halide)." *Organometallics* **1998**, *17*, 954-959. (c) P. Espinet, A. M. Echavarren, "The Mechanisms of the Stille Reactions." *Angew. Chem., Int. Ed.* **2004**, *43*, 4704-4734. (d) J. A. Casares, P. Espinet, G. Salas, "14-Electron T-Shaped [PdRXL] Complexes: Evidence or Illusion? Mechanistic Consequences for the Stille Reaction and Related Processes." *Chem. Eur. J.* **2002**, *8*, 4843-4853.
- [24] N. Miyaura, "Cross-coupling reaction of organoboron compounds via base-assisted transmetalation to palladium(II) complexes." *J. Organomet. Chem.* **2002**, *653*, 54-57 and references therein.
- [25] E. Napolitano, V. Farina, M. Persico, "The Stille Reaction: A Density Functional Theory Analysis of the Transmetalation and the Importance of Coordination Expansion at Tin." *Organometallics* **2003**, *22*, 4030-4037 and references therein.
- [26] J. Louie, J. F. Hartwig, "Transmetalation Involving Organotin Aryl, Thiolate, and Amide Compounds. An Unusual Type of Dissociative Ligand Substitution Reaction." *J. Am. Chem. Soc.* **1995**, *117*, 11598-11599.
- [27] (a) T. Moriya, N. Miyaura, A. Suzuki, "Synthesis of Allenes by Palladium-Catalyzed Cross-Coupling Reaction of Organoboron Compounds with Propargylic Carbonates: Transmetalation of Organoboron Compounds with (Alkoxo)palladium Complexes Under Neutral Conditions." *Synlett* **1994**, 149-151.
- [28] The reaction channel from **4a** to **5** involves a transition state [**4a-4b**]<sup>‡</sup> leading to a van der Waals-adduct **4b** with loosely bound PMe<sub>3</sub> and acetate ligands, followed by complete removal of PMe<sub>3</sub> to yield another van der Waals-adduct **4c** and subsequent coordination of acetate to generate **5**. The corresponding data are included in the Supporting Information.

- [29] L. J. Gooßen, D. Koley, H. Hermann, W. Thiel, Manuscript in preparation.
- [30]  $\Delta E_e$  values for BOH—THF and BOH—OH<sub>2</sub> hydrogen bonds were calculated to be −9.4 and −10.7 kcal/mol, respectively. See the Supporting Information for details.
- [31] K. Matos, J. A. Sonderquist, “Alkylboranes in the Suzuki-Miyaura Coupling: Stereochemical and Mechanistic Studies.” *J. Org. Chem.* **1998**, 63, 461-470.
- [32] H. M. Senn, T. Ziegler, “Oxidative Addition of Aryl Halides to Palladium(0) Complexes: A Density-Functional Study Including Solvation.” *Organometallics* **2004**, 23, 2980-2988.
- [33] (a) D. W. Old, J. P. Wolfe, S. L. Buchwald, “A Highly Active Catalyst for Palladium-Catalyzed Cross-Coupling Reactions: Room-Temperature Suzuki Couplings and Aminations of Unactivated Aryl Chlorides.” *J. Am. Chem. Soc.* **1998**, 120, 9722-9723. (b) J. P. Wolfe, S. L. Buchwald, “A Highly Active Catalyst for the Room-Temperature Amination and Suzuki Coupling of Aryl Chlorides.” *Angew. Chem., Int. Ed.* **1999**, 38, 2413-2416.





## Palladium Monophosphine Intermediates in Catalytic Cross-Coupling Reactions: A DFT Study.

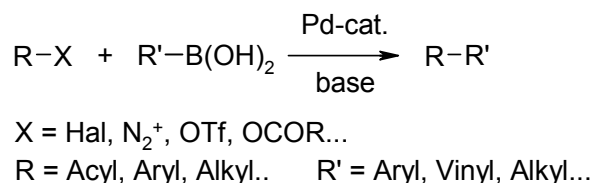
*Yet it is equally clear that knowledge of what is, does not open the door directly to what should be.*

(Albert Einstein, Out of My Later Years, Science and Religion, Section I, page 22)

### 4.1 Introduction

Palladium-catalyzed cross-couplings of boronic acids are powerful transformations, widely applied in organic synthesis.[1] A particularly prominent example is the Suzuki coupling of aryl halides with arylboronic acids, arguably the most general method for the construction of a biaryl moiety (Scheme 4.1; R, R' = Aryl), and there is a wealth of mechanistically related reactions, including the synthesis of dienes,[2] arylacetic acids[3] and arylketones (Scheme 4.1).[4,5]

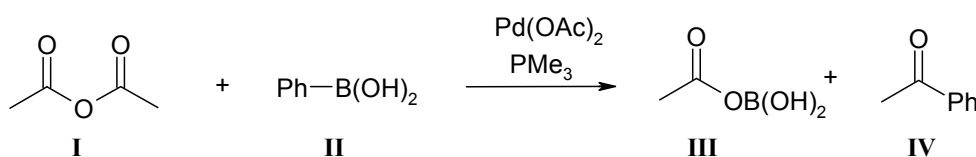
#### Scheme 4.1. Suzuki-type cross-coupling reactions of boronic acids.



The main components of the catalytic cycles for all these couplings are believed to be an oxidative addition of the carbon electrophile to a coordinatively unsaturated palladium(0) species, followed by a transmetalation step in which the carbon electrophile is transferred from boron to palladium, and finally a reductive elimination to release the product.[1] In order to rationally design and optimize such cross-coupling reactions a much more thorough understanding of this mechanism is indispensable. However, in-depth mechanistic studies as well as theoretical calculations on the Suzuki biaryl synthesis are hampered by the extreme complexity of the experimentally employed reaction systems, which in addition to the palladium phosphine catalysts and the substrates (arylboronic acids and aryl halides) also contain bases, coordinating solvents, and further additives such as halide salts.[1] Thus, an incredible variety of palladium species can potentially be formed, which must all be considered as possible intermediates in the catalytic process.

We have previously introduced the mechanistically closely related cross-coupling of acetic anhydride with phenylboronic acid (Scheme 4.2) as the most basic and still realistic model for a catalytic reaction of this type.[6] The similarity between the oxidative addition step of aryl halides and carboxylic anhydrides is well documented,[7] and the synthesis of aryl ketones from boronic acids is itself of high synthetic interest.[4] In this model reaction, the acetate ion plays a triple role, as the leaving group, the base, and the counter-ion in the palladium(II) precursor, so that the overall number of possible intermediates is greatly reduced. The choice of such a simple model reaction enables us to evaluate multiple intertwined reaction pathways in a comprehensive manner.

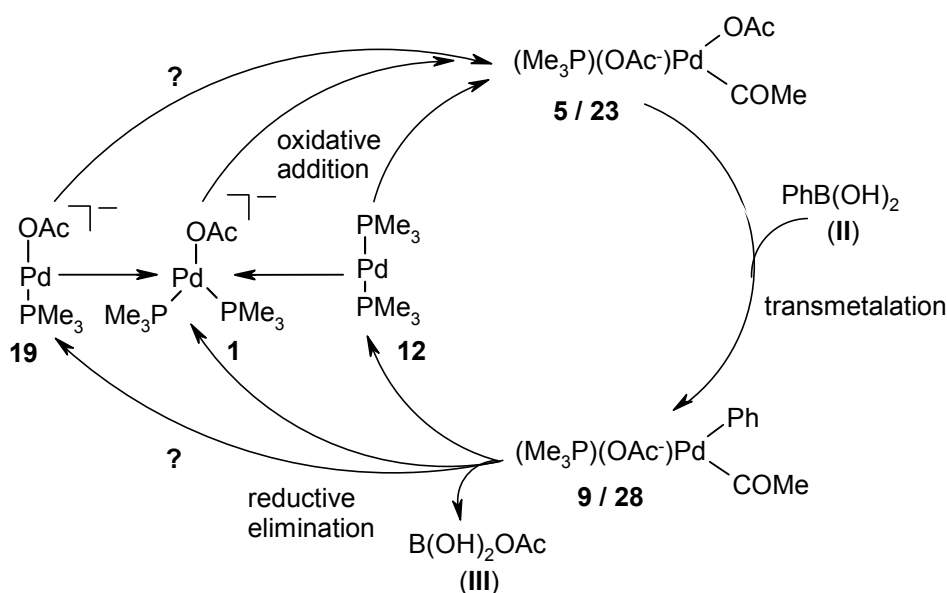
**Scheme 4.2. Cross-coupling of acetic anhydride with phenylboronic acid.**



In chapter 3, we presented two viable catalytic cycles for this model reaction, one starting from a neutral  $\text{Pd}(0)\text{L}_2$  complex (**12**), the other from a three-coordinate, anionic  $[\text{Pd}(0)\text{L}_2\text{X}]^-$  species (**1**) (Scheme 4.3).[6] According to calculations at the BP86/6-31G\* level of theory, both the neutral and the anionic palladium(0) species lead to similar cycles, dominated by *cis*-configured four-coordinate intermediates. This was remarkable but not unexpected for the neutral pathway as an increasing amount of evidence supports an initial formation of such *cis*-rather than *trans*-configured intermediates in cross-coupling reactions.[8] For the anionic pathway, our calculations support the intermediacy of three-coordinate intermediates  $[\text{Pd}(\text{PMe}_3)_2\text{OAc}]^-$  as proposed by Amatore and Jutand.[9,10] However, despite careful investigations, we could not find in our model systems any evidence for the existence of stable five-coordinate palladium(II) intermediates, which are currently believed to cause the profound effects of counter-ions on the performance of palladium catalysts. Instead, our calculations suggest that the higher catalytic activity of anionic complexes such as  $[\text{Pd}(\text{PMe}_3)_2\text{OAc}]^-$  arises from their propensity to draw carbon electrophiles into their coordination sphere. This is in good accordance with calculations performed on the oxidative addition of aryl halides.[11]



## Scheme 4.3. Neutral and anionic pathways for cross-coupling reactions



Another important finding from our calculations[6] was that the transfer of an aryl group from the boronic acid to palladium appears to be feasible only if just one phosphine ligand is bound to palladium. While being compatible with earlier experimental results,[12] it remains to be seen whether this is a general feature of such transmetalation reactions.[13] If so, there are obvious implications for practical strategies in catalytic cross-coupling work.

These previous studies raise the question whether a third catalytic cycle, consisting solely of monophosphine complexes, would not altogether be more favorable, as one of the phosphine ligands must be liberated in any case for the transmetalation to occur (Scheme 4.3, outer cycle). Moreover, an isomer **23** of the initial oxidative addition product **5**, in which both acetate ligands are positioned *trans* to each other, has not been considered before[6] although it might well lead to an advantageous transmetalation pathway. These issues are addressed in the present chapter: Starting from the coordinatively unsaturated anionic monophosphine complex **19**, new reaction pathways have been computed and cross-linked with the previously reported catalytic cycles, thus for the first time allowing a comprehensive comparison of neutral and anionic mono- and diphosphine palladium catalysts in a cross-coupling reaction.

Apart from our work,[6,11] there are several other recent computational studies that are relevant in the present context. Kozuch *et al.* have characterized active anionic zero-valent palladium catalysts by DFT calculations,[10] covering monodentate  $[\text{Pd}(\text{PR}_3)_2\text{X}]^-$  and bidentate  $[\text{Pd}\{\text{R}_2\text{P}(\text{CH}_2)_n\text{PR}_2\}\text{X}]^-$  species, and have explored the role of such anionic complexes (mostly with  $\text{R} = \text{H}$ ,  $\text{X} = \text{Cl}$ ) in the cross-coupling reaction  $\text{Ph}-\text{Cl} + \text{HS}^- \rightarrow \text{Ph}-\text{SH} + \text{Cl}^-$ , attributing the superiority of the anionic catalysts over the corresponding neutral species

to the “flattening” of the energy landscape of the catalytic cycle.[14] One of the recent studies on palladium-catalyzed oxidative addition reactions[11,14,15,16] analyzes the mechanism of anion assistance (Pd vs.  $\text{PdCl}^-$  catalyst) in H—H, C—H, C—C and C—Cl bond activation in terms of transition state interactions which are more stabilizing in the case of the anion.[15d] Finally, the role of the base in the transmetalation step of the Suzuki-Miyaura cross-coupling reactions has been investigated recently by DFT calculations on a model system containing  $\text{Pd}(\text{CH}=\text{CH}_2)(\text{PH}_3)_2\text{Br}$  as the starting catalyst complex,  $\text{CH}_2=\text{CHB}(\text{OH})_2$  as the organoboronic acid, and  $\text{OH}^-$  as the base.[17] Our present work differs from these studies[14,15,16,17] by addressing a different and more complex model system and by covering several complete and competing catalytic cycles.

## 4.2 Computational Details

All calculations were performed with the Gaussian98 and Gaussian03 suites of programs.[18] The DFT calculations employed the BP86 functional[19,20] using the standard 6-31G\* basis[21] for all atoms, except for palladium which was described by the LANL2DZ valence basis set in combination with the corresponding effective core potential.[22] Geometries were fully optimized, normally without symmetry constraints. Harmonic force constants were computed at the optimized geometries to characterize the stationary points as minima or saddle points. Zero-point vibrational corrections were determined from the harmonic vibrational frequencies to convert the total energies  $E_e$  to ground-state energies  $E_0$ . The rigid-rotor harmonic-oscillator approximation was applied for evaluating the thermal and entropic contributions that are needed to derive the enthalpies  $H_{298}$  and Gibbs free enthalpies  $G_{298}$  at 298 K. Transition states were located from a linear transit scan in which the reaction coordinate was kept fixed at different distances while all other degrees of freedom were optimized. After the linear transit search the transition states were optimized using the default Berny algorithm implemented in the Gaussian code.[18] In critical cases, the nature of a given transition state was analyzed by IRC (Intrinsic Reaction Coordinate) computations.

For further validation, single-point BP86 calculations were performed at the optimized BP86/6-31G\* geometries employing larger basis sets (EXT): Palladium was described by a Stuttgart-Dresden quasirelativistic pseudopotentials and the associate (8s7p5d)/[6s5p3d] valence basis set;[23] the 6-31+G\* basis was employed for O, P, B and C, and the 6-31G\*\* basis for all H atoms[21] (which will be abbreviated as BP86/EXT). Single-point solvent calculations were performed at the optimized gas-phase geometries for all the intermediates and transition states, using the CPCM[24] approach, which is an implementation of the conductor-like screening solvation model (COSMO)[25] in Gaussian03; THF was used as solvent (dielectric constant  $\epsilon = 7.58$ ) with UAHF (United Atom Hartree-Fock) radii for the respective atoms (Pd, H, B, C, O, P). The charge distribution around the metal center was analyzed using Weinhold's NPA (Natural Population Analysis) approach.[26]

### 4.3 Results

**4.3.1 Outline of the catalytic cycles.** The general features of the calculated anionic cycles are summarized in Scheme 4.4. For convenience, the numbering of the intermediates has been chosen to be consistent with Chapter 3.[6] The previously discussed cycle **1** → **5** → **9** → **1** and the presently computed cycle **19** → **23** → **28** → **19** are represented by blue and green arrows, respectively, while the interconnections are indicated by red arrows in Scheme 4.4. Due to these interconnections, oxidative addition of acetic anhydride to **1** or **19** can lead in each case to the formation of either **5** or **23**, which are starting points of transmetalation sequences where the acyl and phosphine ligands remain *cis* (**5** → **9**) or *trans* (**23** → **28**) to each other. In the final reductive elimination, both **9** and **28** can be converted into either **1** or **19**.

**Scheme 4.4. Anionic catalytic cycles**

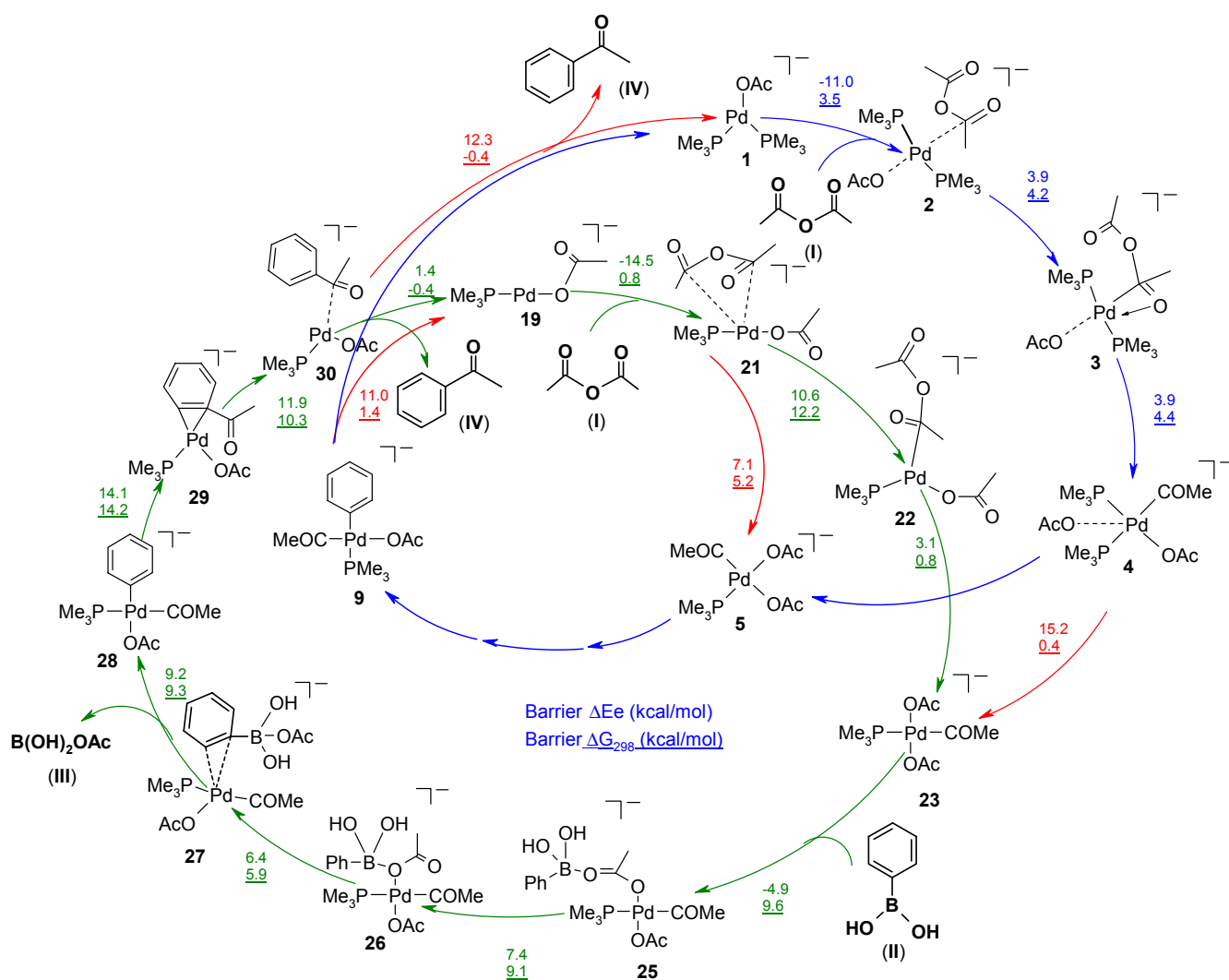


**Figure 4.1.** shows the anionic monophosphine complex **19**, the anionic “Amatore-Jutand-type” diphosphine complex **1**, and the neutral  $\text{Pd}(\text{PMe}_3)_2$  molecule **12**, which all serve as starting

points for the catalytic cycles considered here and previously.[6] The computed relative free energies are similar (Figure 4.1) confirming that each of these species can be involved in catalysis.[27] The geometries of **1** and **12** have already been reported.[6] In both anionic complexes, the acetate is coordinated in a monodentate fashion with the Pd–O bond in **1** being much longer than in **19** (2.327 Å vs. 2.131 Å). Compound **19** has a linear geometry; the Pd–P bond distance is shorter than in the other complexes (2.161 Å in **19** vs. 2.247 Å in **1** and 2.292 Å in **12**).

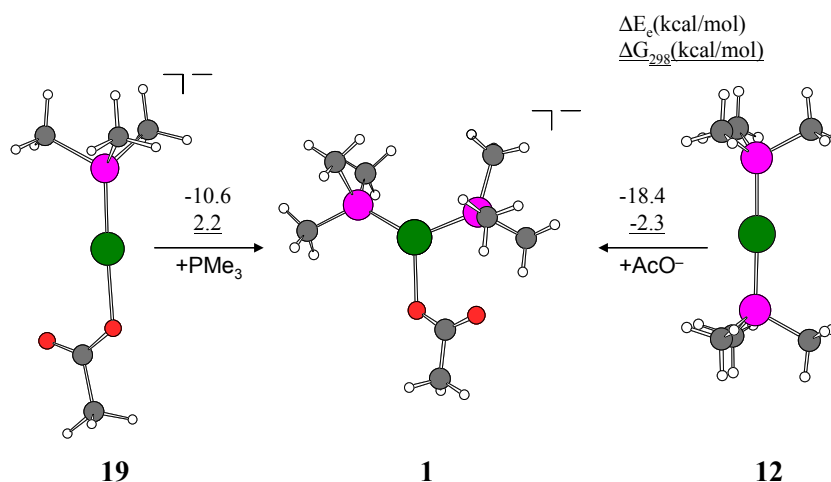


**Figure 4.1.** Energetics for interconversion between the palladium(0) catalysts considered presently.

The geometries and energies of all starting materials and products, namely acetic anhydride **I**, phenylboronic acid **II**, boric acid adduct **III**, acetophenone **IV**, trimethylphosphine **VI** and acetate **VII** (Figure 4.2) have also been reported previously.[6]

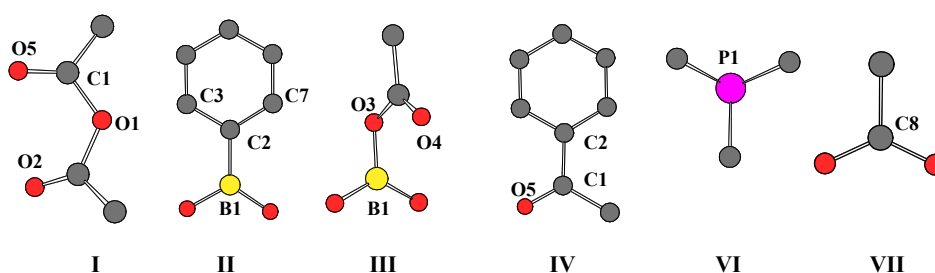


**Figure 4.2.** Starting materials and products. BP86/6-31G\* optimized structures are shown, with hydrogens removed for clarity. Color code: C gray, O red, B yellow, P violet.

In the calculation of the catalytic cycles, we have evaluated for each segment, *i.e.* oxidative addition, transmetalation and reductive elimination, the changes in electronic energy ( $\Delta E_e$ ) and Gibbs free energy ( $\Delta G_{298}$ ) at the optimized gas-phase geometries. The BP86/6-31G\* results were validated by calculating single-point energies of the resulting intermediates and transition

states with a larger basis set ( $\Delta E_{\text{EXT}}$ ). Finally, a solvent field was applied to account for solvent effects ( $\Delta E_{\text{sov}}$ ). The figures that display energy profiles for reaction steps will show these four quantities.

**4.3.2 Oxidative addition and ligand exchange starting from the anionic monosphosphine complex 19.** According to our calculations, the approach of a molecule of acetic anhydride (**1**) to the monophosphine complex  $[\text{Pd}(\text{PMe}_3)\text{OAc}]^-$  (**19**) directly leads to the adduct **20** in an exothermic reaction ( $\Delta E_e = -14.5$  kcal/mol,  $\Delta G_{298} = 0.8$  kcal/mol). In this intermediate, the acetic anhydride is located about 3.5 Å from the palladium center ( $\text{Pd}(1)\text{—C}(1) = 3.640$  Å,  $\text{Pd}(1)\text{—C}(8) = 3.608$  Å) and is oriented perpendicular to the P—Pd—O(4) plane (Figure 4.3). The stability of this adduct results from gas-phase interactions of C—H groups of the acetic anhydride with the two oxygen atoms (O(4) and O(3)) of the catalyst fragment (Figure 4.3). A certain charge transfer from the acetic anhydride to the metal center ( $\text{Pd}(1) = -0.236$  *e* in **20** vs.  $-0.195$  *e* in **19**) can be observed. In **20**, the C(8) atom is slightly closer to the palladium center than C(1) ( $\text{Pd}(1)\text{—C}(8) = 3.608$  Å,  $\text{Pd}(1)\text{—C}(1) = 3.640$  Å). Further shortening of the Pd(1)—C(8) bond initiates the strongly exothermic ( $\Delta E_e = -12.0$  kcal/mol,  $\Delta G_{298} = -12.8$  kcal/mol) oxidative addition of acetic anhydride to the palladium center under formation of the square planar palladium(II) complex **5b** in which the two acetyl groups are located *cis* to each other (Figure 4.3). The reaction requires only moderate activation ( $\Delta E_e = 7.1$  kcal/mol,  $\Delta G_{298} = 5.2$  kcal/mol). In the transition state  $[\mathbf{20-5b}]^\ddagger$  the P—Pd—O(4) angle is decreased by 22.5° in comparison to **20**, the Pd(1)—C(8) bond is shortened to 2.027 Å, and the C(8)—O(1) bond is elongated to 2.087 Å. The transition vector (72  $\text{icm}^{-1}$ ) reflects a further shortening of the Pd(1)—C(8) bond with a concomitant elongation of the C(8)—O(1) bond.

In the oxidative addition product **5b**, the C(8)—O(1) bond is completely cleaved, the Pd(1)—C(8) bond is further shortened to 1.988 Å, and the Pd(1)—O(1) distance amounts to 3.546 Å. A slight rearrangement of this intermediate leads to the formation of the energetically almost degenerate isomer **5** ( $\Delta E_e = -1.1$  kcal/mol,  $\Delta G_{298} = -0.9$  kcal/mol). As discussed before,[6] **5** is accessible also from the three-coordinate palladium(0) species **1**, and is a good starting point for a transmetalation reaction leading to the aryl-Pd-species **9**.

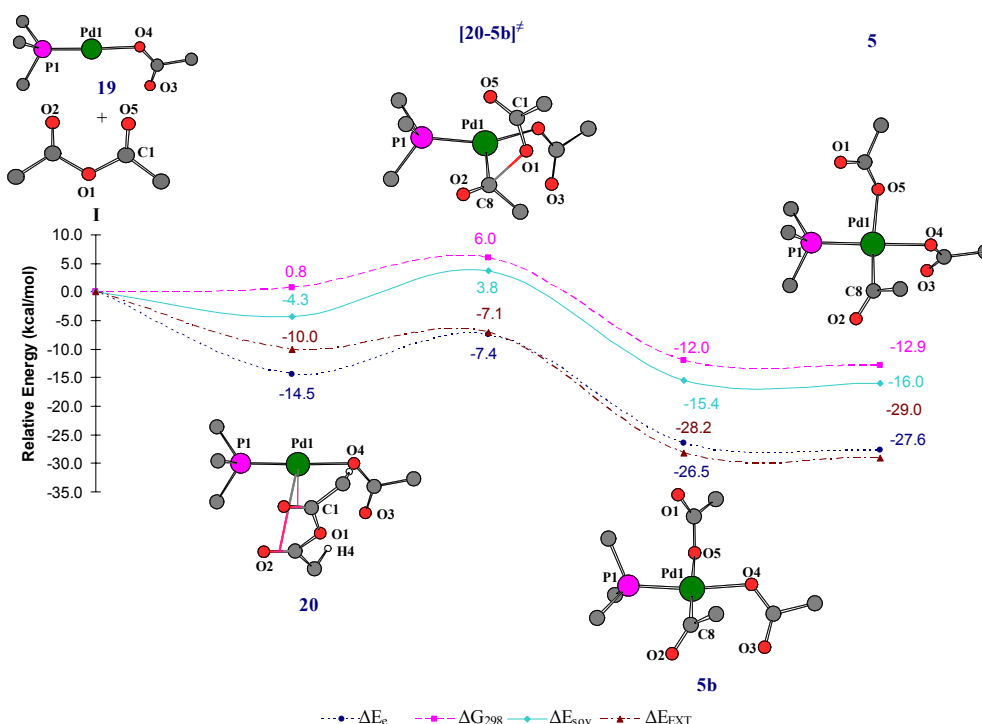


**Figure 4.3.** Energy profile for the conversion from **19** → **5**. Conventions see Figure 4.2.

The overall reaction profile obtained after basis set extension (see computational details) is almost identical to that calculated with the 6-31G\* basis set ( $\Delta E_{\text{EXT}}$  vs.  $\Delta E_e$ , Figure 4.3). This confirms the suitability of the chosen basis set for these reactions.[15c] Gratifyingly, the calculated energies within a THF solvent field (see computational details) also show a similar trend to the gas-phase electronic energies. We have performed such additional calculations for all subsequent reaction steps (see Figures 4.4-4.9) but we will not discuss them unless they differ significantly from the standard gas-phase BP86/6-31G\* results.

The structural parameters of all intermediates and transition states involved in the oxidative addition/ligand exchange sequence displayed in Figure 4.3 are summarized in Table 1. Selected NPA charges are given in Table 4.2 and more detailed structural data are available in the Supporting Information.

**Table 4.1. Optimized geometric parameters for complexes involved in the oxidative addition process 19 → 5. Bond distances are provided in Ångström and bond angles in degrees.**

No.	Pd–P1	Pd–C1	Pd–O1	Pd–O2	Pd–O3	Pd–O4	Pd–O5	P–Pd–O4
<b>19</b>	2.161	–	–	–	3.307	2.131	–	176.8
<b>20</b>	2.178	3.640	3.550	3.951	3.329	2.141	4.173	174.4
<b>[20-5b]<sup>‡</sup></b>	2.255	3.227/2.027*	2.850	2.899	3.411	2.164	3.019	151.9
<b>5b</b>	2.274	3.182/1.988*	3.546	2.877	3.323	2.120	2.254	171.5

\* Pd(1)–C(1)/Pd(1)–C(8)

**Table 4.2. NPA charges (*e*) for key atoms of various intermediates and transition states involved in the oxidative addition process 19 → 5.**

No.	Pd(1)	P(1)Me3	O(1)	O(2)	O(3)	O(4)	O(5)	C(1)	C(8)
<b>19</b>	-0.195	-0.020	–	–	-0.675	-0.759	–	–	–
<b>I</b>	–	–	-0.585	-0.509	–	–	-0.509	0.799	0.799
<b>[20-5b]<sup>‡</sup></b>	0.311	0.182	-0.652	-0.554	-0.679	-0.763	-0.693	0.777	0.497
<b>5b</b>	0.412	0.274	-0.694	-0.561	-0.666	-0.723	-0.749	0.776	0.400

Alternatively, the oxidative addition reaction might also proceed such that instead of **5** its isomer **23** is formed in which the acetyl groups are not located *cis* but *trans* to each other. As can be seen from Figure 4.4, such a pathway can indeed be found, but it requires several additional intermediates and appears to be energetically not quite as favorable.

The branching from the preceding pathway takes place after the formation of the initial adduct **20**, which can be converted into an almost degenerate isomer **21** ( $\Delta E_e = -0.4$  kcal/mol,  $\Delta G_{298} = -2.4$  kcal/mol) by a slight rotation of the acetic anhydride fragment. An important structural feature of **21** is the presence of two C–H interactions from the acetic anhydride fragment to the metal center and O(4) (C–H(4) = 1.129 Å and C–H(5) = 1.123 Å). These gas-phase interactions are also manifested by elongated Pd(1)–C(1) and Pd(1)–C(8) distances (Pd(1)–C(1) = 4.402 Å and Pd(1)–C(8) = 4.470 Å).



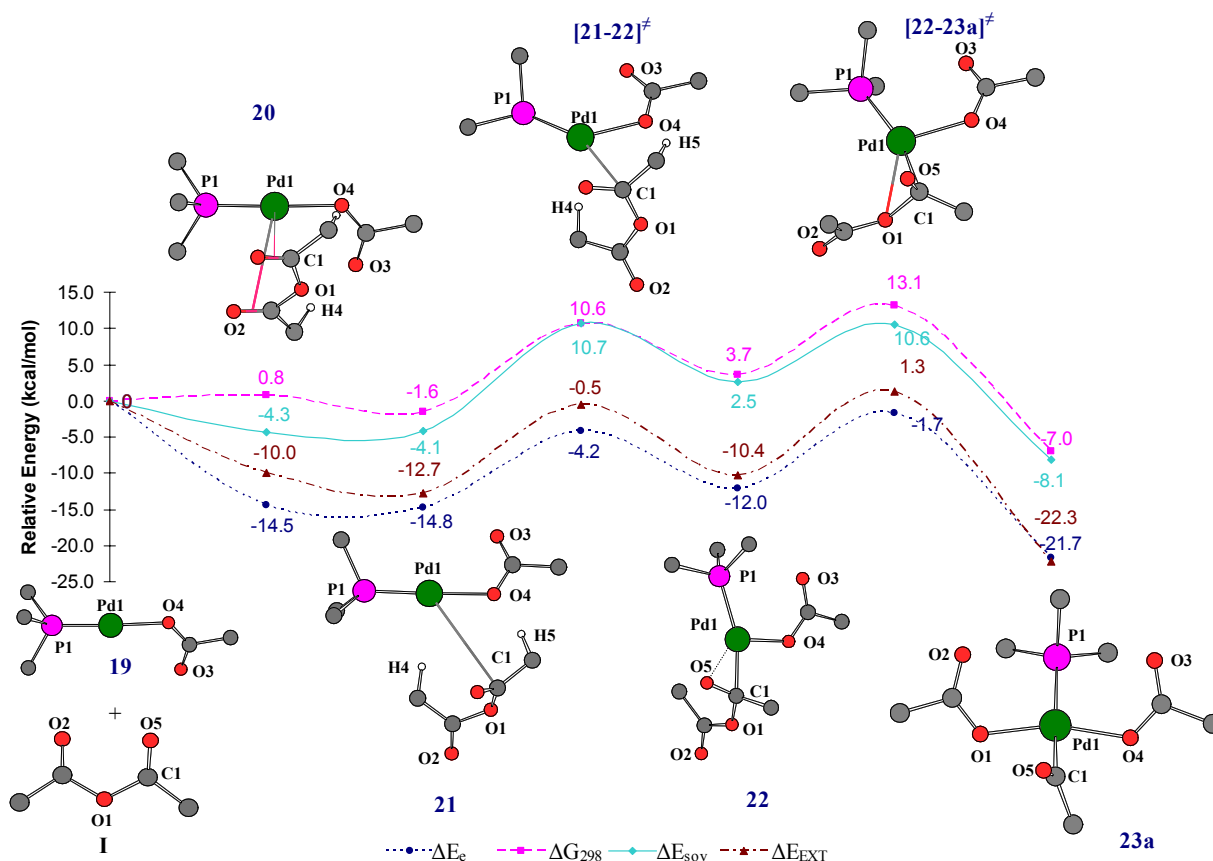


**Figure 4.4.** Energy profile for the conversion from **19** → **23a**. Conventions see Figure 4.2.

Gradual approach of the less distant C(1) towards the palladium center leads to the formation of another adduct **22**. In comparison to the previous route (Figure 4.3), the activation barrier of this additional rearrangement is rather high ( $\Delta E_e = 10.6$  kcal/mol,  $\Delta G_{298} = 12.2$  kcal/mol). In the transition state **[21-22]<sup>‡</sup>**, which was validated by an IRC calculation, the Pd(1)–C(1) distance is significantly shortened (Pd(1)–C(1) = 2.853 Å), the P–Pd–O(4) angle has decreased to 130.4°, and the C(1)–O(5) distance is slightly elongated (C(1)–O(5) = 1.231 Å vs. 1.209 Å in **I**). The transition vector of **[21-22]<sup>‡</sup>** (80  $\text{icm}^{-1}$ ) represents the approach of C(1) towards Pd(1).

The product **22** can be seen as a  $\pi$ -complex of the acetic anhydride, as the C(1)–O(5) bond coordinates to palladium in  $\eta^2$  fashion (Pd(1)–C(1) = 2.089 Å, Pd(1)–O(5) = 2.214 Å). The C(1)–O(5) of 1.290 Å is much longer than in free acetic anhydride (1.209 Å). NBO analysis suggests a bonding interaction between the occupied  $\pi_b$  C(1)–O(5) orbital and an unoccupied palladium orbital, and a strong back-donation from the occupied d-orbital of palladium to the unoccupied  $\pi^*$  C(1)–O(5) orbital. Overall, the conversion **21** → **22** is accompanied by a net electron transfer of *ca.* 0.4 *e* from palladium to the C(1)–O(5) moiety (see NPA charges in Table S4).

Decreasing the Pd(1)—O(1) distance in **22** initiates the actual oxidative addition of the acetic anhydride that leads to the formation of complex **23a**. This process is again strongly exothermic ( $\Delta E_e = -9.7$  kcal/mol,  $\Delta G_{298} = -10.7$  kcal/mol) but has a significant activation energy ( $\Delta E_e = 10.3$  kcal/mol,  $\Delta G_{298} = 9.4$  kcal/mol). In the corresponding transition state [**22-23a**]<sup>‡</sup>, the Pd(1)—O(1) distance of 2.486 Å and the C(1)—O(5) distance of 1.245 Å are shorter while the C(1)—O(1) of 1.620 Å is slightly longer than in **22**. The imaginary frequency (37  $\text{icm}^{-1}$ ) shows the formation of the Pd(1)—O(1) bond with simultaneous elongation of the C(1)—O(1) bond.

The product of the oxidative addition **23a** is again a square planar palladium(II) complex (Figure 4.4) but in contrast to **5**, the two acetates are now located *trans* to each other. The oxidative nature of this reaction sequence is reflected in an increase of the NPA charge on palladium from  $-0.195 e$  in **19** to  $0.466 e$  in **23a** (Table 4.4), and a decrease of the NPA charges on the new ligand atoms, in particular on C(1) (from  $0.799 e$  to  $0.395 e$ ). **23a** is easily converted into its rotamer **23** which is a good starting point for a transmetalation sequence (see below).

The structural parameters of all intermediates and transition states involved in the oxidative addition/ligand exchange sequence displayed in Figure 4.4 are summarized in Table 4.3. Selected NPA charges are given in Table 4.4 and more detailed structural data are available in the Supporting Information.

**Table 4.3. Optimized geometric parameters for complexes involved in the oxidative addition process  $19 \rightarrow 23$ . Bond distances are provided in Ångström and bond angles in degrees.**

No.	Pd—P1	Pd—C1	Pd—O1	Pd—O2	Pd—O3	Pd—O4	Pd—O5	P—Pd—O:
<b>21</b>	2.175	4.402	4.493	5.425	3.164	2.159	4.779	177.6
[ <b>21-22</b> ] <sup>‡</sup>	2.209	2.853	3.552	5.125	3.249	2.223	2.652	130.4
<b>22</b>	2.351	2.089	3.093	4.787	3.405	2.179	2.214	105.7
[ <b>22-23a</b> ] <sup>‡</sup>	2.352	2.086	2.486	4.122	3.407	2.214	2.672	108.8
<b>23a</b>	2.481	1.997	2.124	3.286	3.342	2.133	2.864	96.2

**Table 4.4. NPA charges (*e*) for key atoms of various intermediates and transition states involved in the oxidative addition process 19 → 23.**

No.	Pd(1)	P(1)Me <sub>3</sub>	O(1)	O(2)	O(3)	O(4)	O(5)	C(1)	C(8)
<b>21</b>	-0.152	0.026	-0.563	-0.553	-0.662	-0.772	-0.572	0.803	0.807
[21-22] <sup>‡</sup>	0.019	-0.049	-0.558	-0.564	-0.681	-0.784	-0.570	0.748	0.804
<b>22</b>	0.331	0.009	-0.550	-0.559	-0.707	-0.728	-0.656	0.490	0.802
[22-23a] <sup>‡</sup>	0.289	-0.002	-0.597	-0.597	-0.708	-0.752	-0.592	0.553	0.793
<b>23a</b>	0.466	0.095	-0.694	-0.682	-0.675	-0.708	-0.519	0.395	0.778

**4.3.3 Oxidative addition starting from the anionic disphosphine complex 1.** We have previously reported that a feasible pathway for the oxidative addition of acetic anhydride to complex **1** leads to the formation of the intermediate **5**, in which both acetyl ligands are positioned *cis* to each other (see Scheme 4.4, blue arrows).[6] Although this reaction sequence is energetically favorable, one must also consider an alternative route, in which the acetic anhydride adds in a different manner to yield isomer **23**, in which the two acetyl ligands are located *trans* to each other.

This alternative pathway is entered from the previously discussed[6] intermediate **4a** if P(2)Me<sub>3</sub> (rather than the less strongly bound P(1)Me<sub>3</sub> ligand) is moved away from the palladium-center. Thereby intermediate **24** is formed in an endothermic reaction ( $\Delta E_e = 9.5$  kcal/mol,  $\Delta G_{298} = 5.9$  kcal/mol) that requires only moderate activation ( $\Delta E_e = 12.8$  kcal/mol,  $\Delta G_{298} = 11.5$  kcal/mol).

The transition state [4a-24]<sup>‡</sup> has a trigonal bipyramidal geometry with the acyl group and the phosphines in equatorial positions (Pd–P(1)–P(2)–C(1) = 178.9°), and the oxygen atoms O4 and O2 of the acetyl ligands occupying the axial positions. The Pd(1)–P(2) distance is significantly increased (2.808 Å in [4a-24]<sup>‡</sup> vs. 2.285 Å in **4a**) while Pd(1)–O(2) distance is much reduced (2.199 Å in [4a-24]<sup>‡</sup> vs. 3.162 Å in **4a**). The transition vector (33 *icm*<sup>-1</sup>) reflects the removal of P(2)Me<sub>3</sub> fragment from the metal center (Figure 4.5).

In the product **24**, the phosphine has almost left the coordination sphere of the palladium (Pd–P(2) = 4.926 Å) while the acetyl group is now strongly bound (Pd–O(2) = 2.144 Å). A complete removal of the weakly bound phosphine from **24** is easily achieved affording the oxidative addition product **23b** ( $\Delta E_e = 3.0$  kcal/mol,  $\Delta G_{298} = -7.2$  kcal/mol). Only a minor conformational rearrangement of **23b** is needed to yield the isomeric complex **23** ( $\Delta E_e = -0.5$

kcal/mol,  $\Delta G_{298} = -1.8$  kcal/mol) which is a suitable starting point for the transmetalation process (see below).

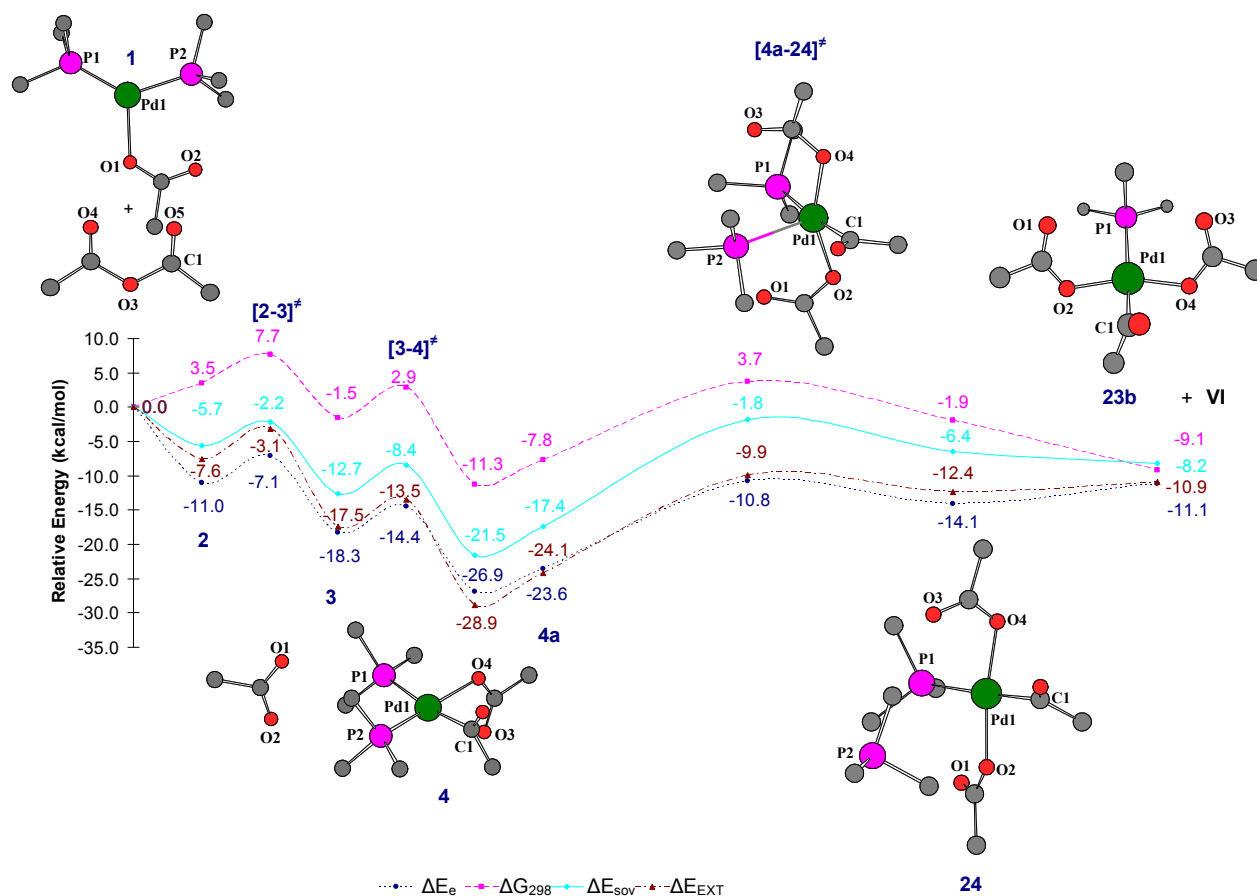


**Figure 4.5.** Energy profile for the oxidative addition starting from  $[\text{Pd}(\text{PMe}_3)_2\text{OAc}]^-$  (1) to 23. Conventions see Figure 4.2. Steps  $1 \rightarrow 4a$  have been discussed elsewhere.[6]

The structural parameters of all intermediates and transition states involved in the oxidative addition/ligand exchange sequence displayed in Figure 4.5 are summarized in Table 4.5. Selected NPA charges are given in Table 4.6 and more detailed structural data are available in the Supporting Information.

**Table 4.5. Optimized geometric parameters for complexes involved in the oxidative addition process 1 → 23. Bond distances are provided in Ångström and bond angles in degrees.**

No.	Pd—P1	Pd—P2	Pd—C1	Pd—O1	Pd—O2	Pd—O3	Pd—O4	Pd—O5	P1—Pd—O4
<b>4a</b>	2.459	2.285	2.031	4.226	3.162	3.195	2.195	2.967	87.5
<b>[4a-24]<sup>‡</sup></b>	2.467	2.808	1.992	3.335	2.199	3.333	2.191	2.895	96.0
<b>24</b>	2.478	4.926	2.000	3.376	2.144	3.141	2.129	2.877	91.9
<b>23b</b>	2.481	—	1.997	3.342	2.137	3.286	2.125	2.864	97.1

**Table 4.6. The NPA charges (*e*) for key atoms of various intermediates and transition states involved in the oxidative addition process 1 → 23.**

No.	Pd(1)	P(1)Me <sub>3</sub>	P(2)Me <sub>3</sub>	O(1)	O(2)	O(3)	O(4)	O(5)	C(1)
<b>4a</b>	0.345	0.145	0.307	-0.757	-0.743	-0.669	-0.734	-0.557	0.375
<b>[4a-24]<sup>‡</sup></b>	0.529	0.102	0.020	-0.687	-0.731	-0.696	-0.715	-0.553	0.418
<b>24</b>	0.465	0.106	0.026	-0.676	-0.717	-0.674	-0.691	-0.522	0.400
<b>23b</b>	0.466	0.095	—	-0.675	-0.708	-0.682	-0.694	-0.520	0.395

**4.3.4 An alternative transmetalation pathway.** The finding that the oxidative addition of acetic anhydride to palladium(0) species can also lead to complexes with the acyl and the phosphine ligand oriented *trans* to each other (**23a**, **23b**) raises the possibility that the latter might also serve as suitable starting points for transmetalation reactions, like the isomeric *cis*-complex **5**. We have indeed found a viable reaction pathway for the transfer of an aryl group from boronic acid starting from compound **23**, which is accessible from compounds **23a** and **23b** (Figure 4.4 and 4.5) just *via* slight rotation of one of the acetate ligands.

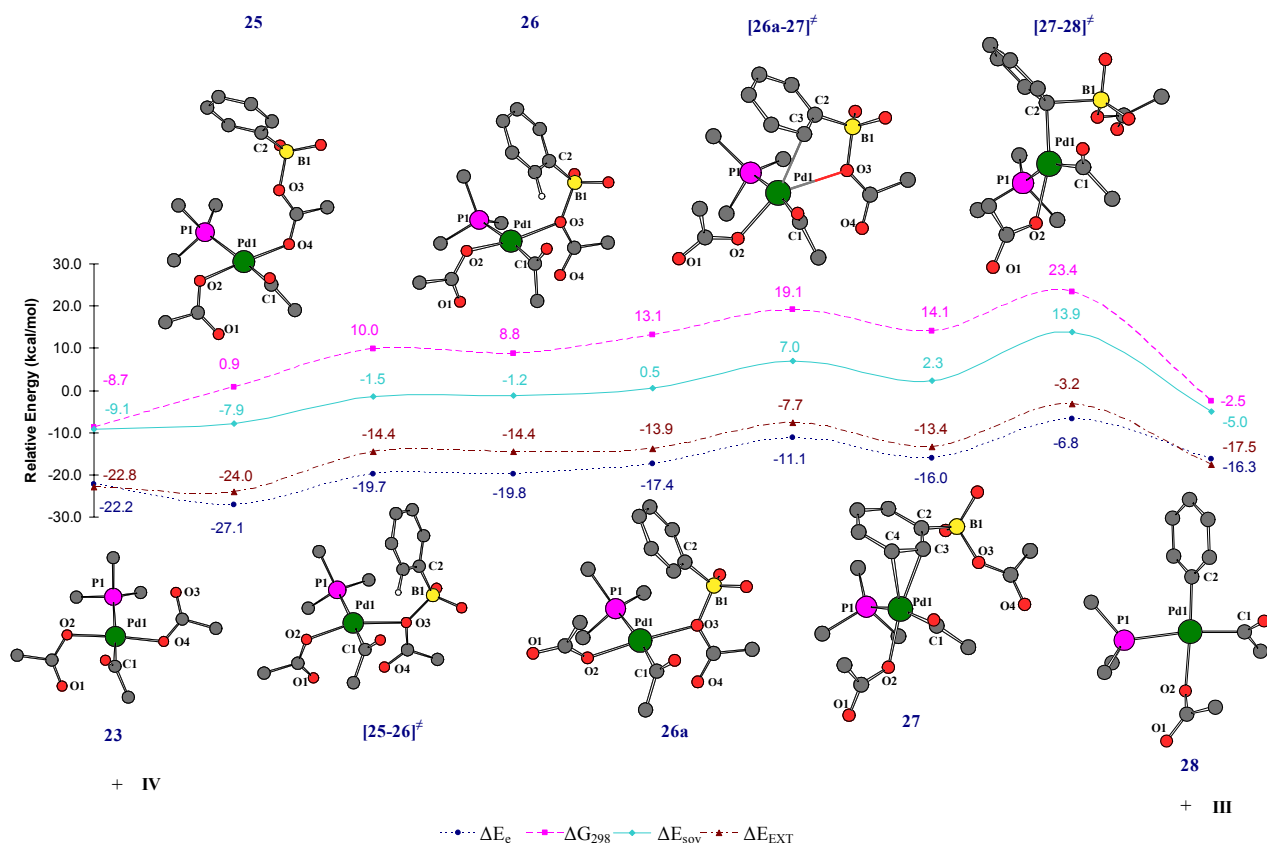


**Figure 4.6.** Energy profile for the transmetalation process **23** → **28**. Conventions see Figure 4.2. The energy scale refers to Figure 4.4.

The approach of a molecule of phenylboronic acid **II** leads to an exothermic coordination of the Lewis acidic boron center to the  $sp^2$  hybridized O(3) atom giving rise to intermediate **25** ( $\Delta E_e = -4.9$  kcal/mol,  $\Delta G_{298} = 9.6$  kcal/mol). The Pd(1)—O(3) and Pd(1)—O(4) distances in this adduct amount to 3.281 Å and 2.159 Å, respectively. Gradual decrease of the Pd(1)—O(3) distance then affords the intermediate **26**, in which the boron and the palladium both coordinate to O(3). Reaching the corresponding transition state **[25-26]**<sup>‡</sup> requires only moderate activation ( $\Delta E_e = 7.4$  kcal/mol,  $\Delta G_{298} = 9.1$  kcal/mol). Its geometry is already closely related to that of the product **26**, and the transition vector (49  $icm^{-1}$ ) represents the incoming of O(3) to Pd(1) and concomitant lengthening of Pd(1)—O(4)  $\sigma$  bond. This reaction pathway was validated by an IRC calculation.

During the rearrangement from **25** to **26**, the phenyl moiety moves closer to the palladium center, so that the Pd(1)—C(2) distance decreases from 5.282 Å to 3.590 Å. A slightly endothermic rotation of one of the acetate ligands under formation of intermediate **26a** sets the stage for the following coordination of the phenyl group ( $\Delta E_e = 2.3$  kcal/mol,  $\Delta G_{298} = 4.4$  kcal/mol). In structure **26a**, the  $sp^2$  O(1) atom is positioned further away from palladium and the O(1)—O(2)—Pd angle is significantly increased (153.7° vs. 91.9° in **26**). Decreasing the

Pd(1)—C(2) distance in **26a** then leads to the formation of intermediate **27**, in which the C(3)—C(4) phenyl double bond is coordinated to the palladium in an  $\eta^2$  fashion (Pd(1)—C(3) = 2.328 Å, Pd(1)—C(4) = 2.425 Å). The formation of such  $\pi$ -complexes is common in palladium chemistry, as such intermediates are also found in oxidative addition reactions of aryl halides with palladium(0) complexes.[16] The corresponding transition state **[26a-27]**<sup>‡</sup>, which was validated by an IRC calculation, has a small activation barrier ( $\Delta E_e = 6.4$  kcal/mol,  $\Delta G_{298} = 5.9$  kcal/mol). Its imaginary mode (55  $\text{icm}^{-1}$ ) involves the coordination of the phenyl moiety to palladium and a simultaneous elongation of the Pd(1)—O(3) bond. In **[26a-27]**<sup>‡</sup>, the C(3) atom of the phenyl group is already very close to the palladium center (C(3)—Pd(1) = 2.547 Å) while the Pd(1)—O(3) bond is almost cleaved (Pd(1)—O(3) = 2.793 Å, Table 4.7).

Simultaneous shortening of the Pd(1)—C(2) distance and lengthening of the C(2)—B(1) distance in **27** initiates the actual transfer of the phenyl group leading to intermediate **28** via the transition state **[27-28]**<sup>‡</sup>. This reaction step, which leads to a complete removal of the B(OH)<sub>2</sub>OAc (**III**) fragment, requires only a moderate activation energy ( $\Delta E_e = 9.2$  kcal/mol,  $\Delta G_{298} = 9.3$  kcal/mol). In the transition state **[27-28]**<sup>‡</sup>, the C(2)—B(1) bond is already stretched to 2.016 Å (Table 4.7) and the C(2) atom is within bonding distance to the palladium (Pd(1)—C(2) = 2.159 Å). The main component of the transition vector (320  $\text{icm}^{-1}$ ) represents the elongation of the C(2)—B(1) bond. The transmetalated product **28** has an almost square planar geometry with the aryl and the acyl group located *cis* to each other. It is ideally suited for the reductive elimination sequence outlined in the following section.

The structural parameters of all intermediates and transition states involved in the transmetalation/ligand exchange sequence are summarized in Table 4.7. Selected NPA charges are given in Table 4.8 and more detailed structural data are available in the Supporting Information.

**Table 4.7. Optimized geometric parameters for complexes involved in the transmetalation sequence 23 → 28. Bond distances are provided in Ångström and bond angles in degrees.**

No.	Pd–P1	Pd–C1	Pd–C2	Pd–O1	Pd–O2	Pd–O3	Pd–O4	C2–B1	P–Pd–O2
<b>23</b>	2.483	1.993	–	3.221	2.124	3.329	2.139	–	86.8
<b>25</b>	2.484	1.992	5.282	3.212	2.119	3.281	2.159	1.631	83.2
<b>[25-26]<sup>‡</sup></b>	2.455	1.983	5.282	3.167	2.167	2.425	2.732	1.631	93.2
<b>26</b>	2.459	1.991	3.590	3.197	2.155	2.322	2.876	1.624	92.7
<b>26a</b>	2.475	1.995	3.432	4.244	2.117	2.277	2.931	1.624	84.3
<b>[26a-27]<sup>‡</sup></b>	2.501	1.989	3.082	4.255	2.175	2.793	3.696	1.630	86.8
<b>27</b>	2.543	2.007	3.122	4.238	2.154	3.630	4.677	1.642	80.0
<b>[27-28]<sup>‡</sup></b>	2.541	2.016	2.159	4.248	2.172	3-127	4.919	2.016	77.8
<b>28</b>	2.465	2.014	2.033	4.244	2.209	–	–	–	77.9

**Table 4.8. NPA charges (*e*) for key atoms for all the intermediates of the transmetalation sequence 23 → 28.**

No.	Pd(1)	P(1)Me <sub>3</sub>	O(1)	O(2)	O(3)	O(4)	C(1)	C(2)	B(1)
<b>23</b>	0.463	0.073	-0.668	-0.706	-0.689	-0.713	0.429	–	–
<b>II</b>	–	–	–	–	–	–	–	-0.424	1.107
<b>25</b>	0.473	0.103	-0.659	-0.700	-0.637	-0.644	0.418	-0.330	1.079
<b>[25-26]<sup>‡</sup></b>	0.502	0.084	-0.678	-0.694	-0.681	-0.629	0.441	-0.345	1.093
<b>26</b>	0.498	0.084	-0.680	-0.701	-0.687	-0.627	0.447	-0.351	1.097
<b>26a</b>	0.525	0.115	-0.645	-0.729	-0.676	-0.616	0.393	-0.344	1.092
<b>[26a-27]<sup>‡</sup></b>	0.511	0.097	-0.624	-0.710	-0.693	-0.631	0.426	-0.304	1.079
<b>27</b>	0.529	0.092	-0.646	-0.738	-0.693	-0.632	0.431	-0.275	1.076
<b>[27-28]<sup>‡</sup></b>	0.478	0.108	-0.648	-0.737	-0.721	-0.615	0.393	-0.394	1.160
<b>III</b>	–	–	-0.565	-0.730	–	–	–	–	1.281
<b>28</b>	0.329	0.126	-0.674	-0.762	–	–	0.364	-0.205	–

**4.3.5 Reductive elimination under formation of the anionic monophosphine complex 19.** In order to close the alternative catalytic cycle, a reductive elimination pathway has to be identified that allows the conversion of compound **9** back to the anionic two-coordinate species **19**. In our preceding work we have shown that the reductive elimination of acetophenone from intermediate **9** may result in the formation of the anionic three-coordinate species **1** and the neutral Pd(0)L<sub>2</sub> species **12**. We now found that the anionic two-coordinate species **19** is also



accessible *via* this established route (for details see Chapter 3 and Tables 3.7-3.8): A two-step rearrangement of **9** leads to the formation of compound **11**, in which the acetophenone is only loosely bound by an interaction of the electrophilic carbonyl carbon with the electron-rich palladium center (Figure 4.7).

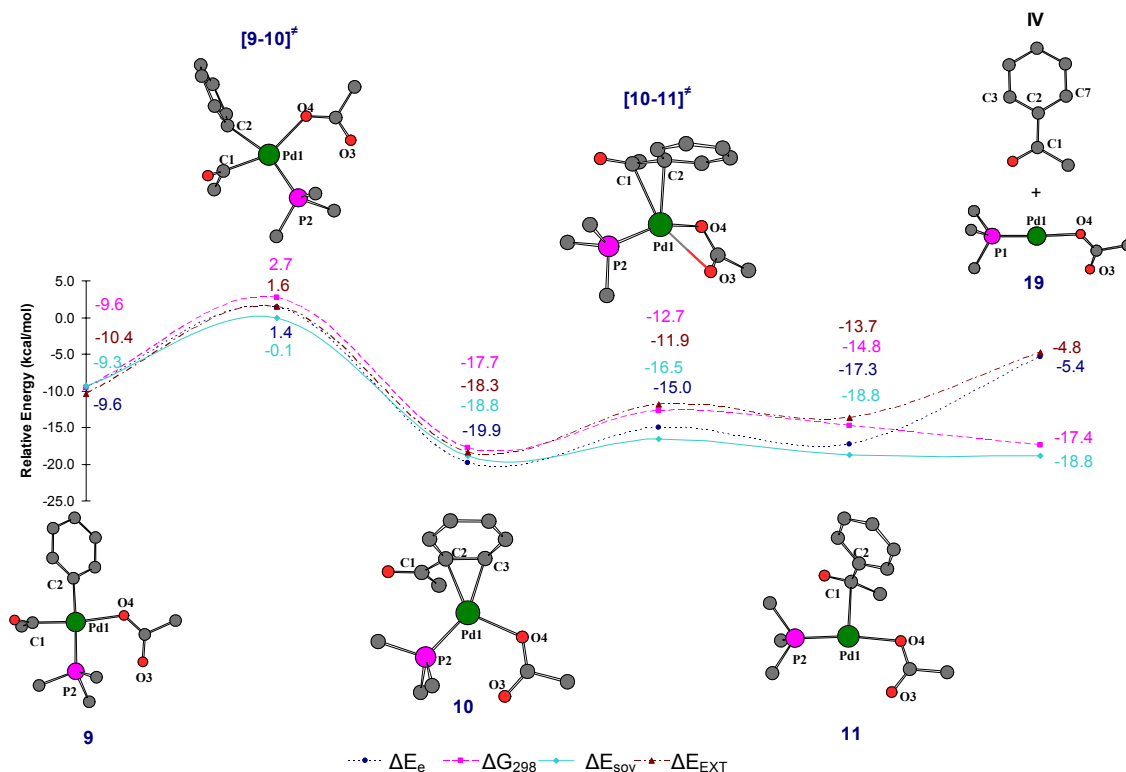


**Figure 4.7.** Energy profile for the reductive elimination from intermediate **9** to **19**. Conventions see Figure 4.2. See reference 6 for a discussion of the first two steps.

Starting from this intermediate **11**, substitution of acetophenone by phosphine yields **1**, as shown previously.[6] However, if no phosphine is provided, the two-coordinate anionic complex **19** can be formed directly by dissociation of acetophenone. This final reaction step is quite facile ( $\Delta E_e = 11.9$  kcal/mol,  $\Delta G_{298} = -2.6$  kcal/mol). One can thus imagine that it will depend on the reaction conditions, *i.e.* the concentration of phosphine in solution, which of the coordinatively unsaturated palladium(0) species **1** and **19** is regenerated after completion of the catalytic cycle. At this point a cross-over between the different pathways can easily occur.

A viable route for the reductive elimination of acetophenone was also found when starting from intermediate **28**, the end point of the alternative transmetalation sequence (Figure 4.8). This reaction pathway also starts with the formation of a C—C bond between C(2) and C(1), which can be initiated by a gradual decrease of the C(2)—C(1) distance in **28**. In this first step, intermediate **29**, a  $\pi$ -complex of acetophenone, is formed in an exergonic reaction ( $\Delta E_e = -14.5$  kcal/mol,  $\Delta G_{298} = -13.0$  kcal/mol) which requires considerable activation ( $\Delta E_e = 14.1$

kcal/mol,  $\Delta G_{298} = 14.2$  kcal/mol). In the transition state  $[28-29]^\ddagger$  the C(2)—C(1) distance is already as short as 1.911 Å and the C(2)—Pd—C(1) angle has decreased to 54.5°. The transition vector (327  $\text{icm}^{-1}$ ) represents a narrowing of the C(2)—Pd—C(1) angle, with the acyl group and the aryl ring further approaching each other.

In the  $\eta^2$ -type  $\pi$ -complex **29** (Figure 4.8), the C(2)—C(3) double bond of the phenyl ring is coordinated to the metal center (Pd(1)—C(2) = 2.203 Å and Pd(1)—C(3) = 2.199 Å). The NPA analysis indicates some electron transfer from the bonding  $\pi$  C(2)—C(3) orbital to an unoccupied orbital of the palladium along with back-donation from the  $d_\pi$  orbital of the metal to the  $\pi^*$  C(2)—C(3) orbital.

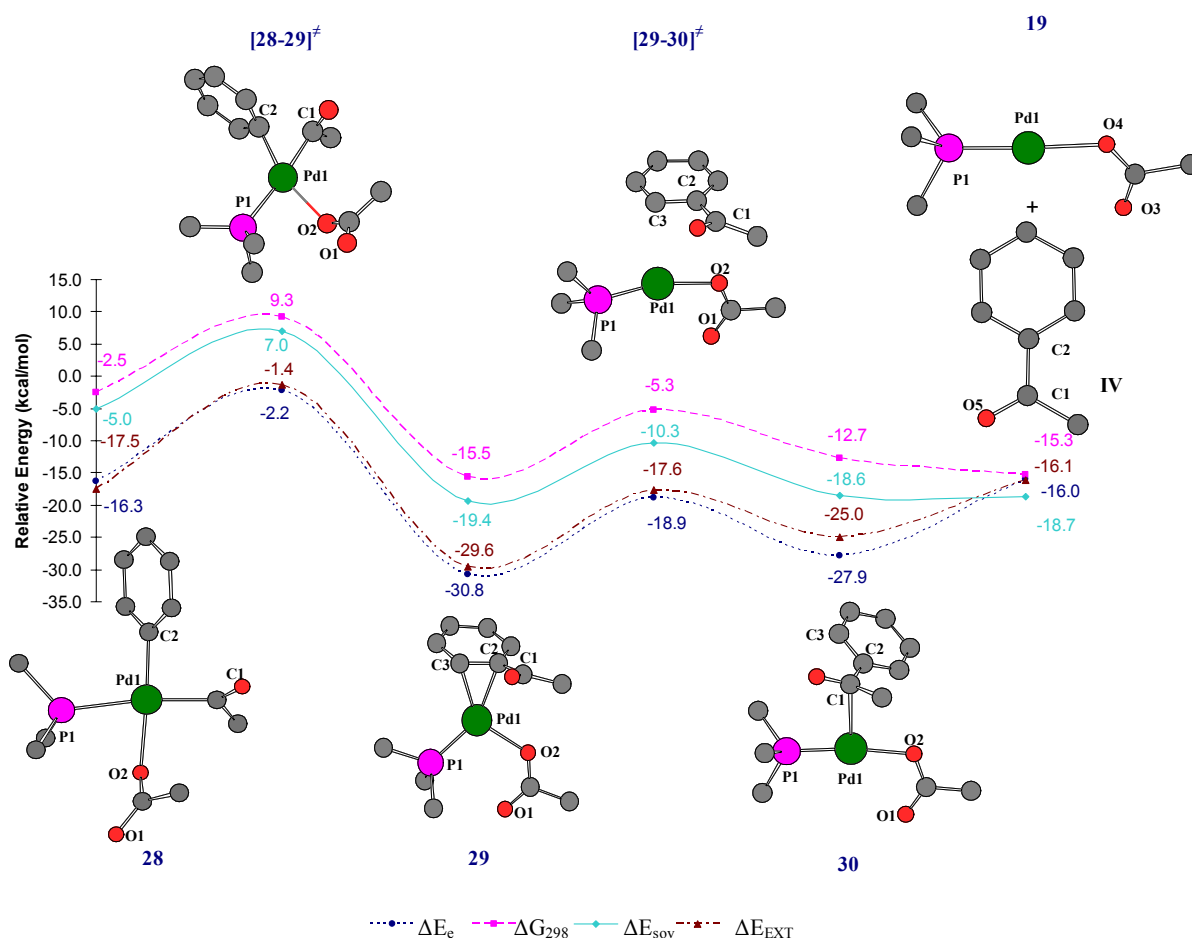


**Figure 4.8.** Energy profile for the reductive elimination process from **28** to **19**. Conventions see Figure 4.2.

Further elongation of the Pd(1)—C(2) bond in **29** leads to the formation of intermediate **30**, in which the acetophenone remains loosely connected to the palladium *via* an interaction between its electrophilic carbonyl carbon and the electron-rich palladium center (Pd(1)—C(1) = 2.554 Å). Reaching the corresponding transition state  $[29-30]^\ddagger$  requires less energy than the preceding step ( $\Delta E_e = 11.9$  kcal/mol,  $\Delta G_{298} = 10.3$  kcal/mol). In  $[29-30]^\ddagger$  the Pd(1)—C(2)

distance becomes much larger ( $\text{Pd(1)}-\text{C(2)} = 3.248 \text{ \AA}$  in **[29-30]**<sup>‡</sup> vs.  $2.203 \text{ \AA}$  in **29**) and the transition mode ( $39 \text{ icm}^{-1}$ ) represents a motion of the phenyl fragment further away from the metal center. The resulting van der Waals complex **30** features a weak coordination of O(5), C(1) and C(2) to the metal center ( $\text{Pd(1)}-\text{O(5)} = 3.236 \text{ \AA}$ ,  $\text{Pd(1)}-\text{C(1)} = 2.554 \text{ \AA}$  and  $\text{Pd(1)}-\text{C(2)} = 3.012 \text{ \AA}$ ).

At this point, two pathways are conceivable for the complete decooordination of acetophenone (**IV**) from **30**. If no additional phosphine is present, dissociation of acetophenone directly leads to the two-coordinate complex **19** in an exergonic reaction ( $\Delta E_e = 11.9 \text{ kcal/mol}$ ,  $\Delta G_{298} = -2.6 \text{ kcal/mol}$ ). Acetophenone is also liberated when approaching a phosphine ( $\text{PMe}_3$ ) molecule to the intermediate **30** which yields the three-coordinate palladium(0) species **1** in a substitution reaction ( $\Delta E_e = 1.3 \text{ kcal/mol}$ ,  $\Delta G_{298} = -0.4 \text{ kcal/mol}$ ) (Figure 4.9). Both these pathways are computed to be very facile (see  $\Delta G_{298}$  values), and therefore the exact reaction conditions will determine which catalytic species is regenerated.

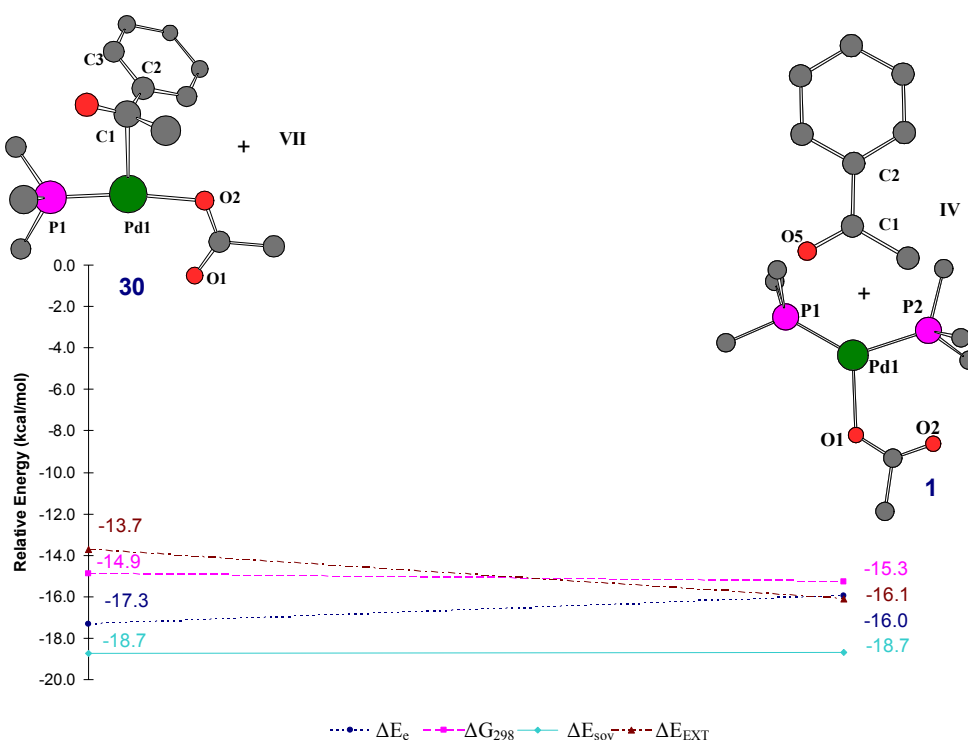


**Figure 4.9.** The pathway for the regeneration of tri-coordinate catalyst **1**. Conventions see Figure 4.2.

The structural parameters of all intermediates and transition states involved in the reductive elimination/ligand exchange sequence are summarized in Table 4.9. Selected NPA charges are given in Table 4.10 and more detailed structural data are available in the Supporting Information.

**Table 4.9. Optimized geometric parameters for complexes [28-29]<sup>‡</sup>-30. Bond distances are provided in Ångström and bond angles in degrees.**

No.	Pd—P1	Pd—C1	Pd—C2	Pd—O1	Pd—O2	C2—C1	P—Pd—O2
[28-29] <sup>‡</sup>	2.398	2.112	2.059	4.048	2.275	1.911	79.7
<b>29</b>	2.299	2.798	2.203	3.517	2.666	1.493	106.0
[29-30] <sup>‡</sup>	2.183	3.571	3.248	3.226	2.182	1.497	165.8
<b>30</b>	2.215	2.554	3.012	3.086	2.174	1.521	172.5

**Table 4.10. NPA charges (*e*) for key atoms for all the intermediates involved during the reductive elimination/ligand exchange process [28-29]<sup>‡</sup> → 30.**

No.	Pd(1)	P(1)Me <sub>3</sub>	O(1)	O(2)	C(1)	C(2)
[28-29] <sup>‡</sup>	0.269	0.061	-0.691	-0.791	0.381	-0.223
<b>29</b>	0.288	0.056	-0.712	-0.758	0.509	-0.263
[29-30] <sup>‡</sup>	-0.079	-0.002	-0.669	-0.779	0.554	-0.142
<b>30</b>	0.035	0.089	-0.663	-0.785	0.438	-0.118
<b>IV</b>	—	—	—	—	0.545	-0.156

#### 4.4 Discussion and Conclusions

In summary, mechanistically and energetically plausible catalytic cycles for the cross-coupling of phenylboronic acid with acetic anhydride have been identified, using either the three-coordinate anionic  $[\text{Pd}(\text{PMe}_3)_2\text{OAc}]^-$  complex (**1**) or the two-coordinate anionic  $[\text{Pd}(\text{PMe}_3)\text{OAc}]^-$  complex (**19**) as starting points. The oxidative addition of a molecule of acetic anhydride to either of the two species leads to the formation of anionic palladium(II) monophosphine complexes with two acetyl ligands located either *cis* (**5**) or *trans* (**23**) to each other. Starting from complex **23**, an alternative pathway for the transmetalation reaction with phenylboronic acid has been found that is dominated by *trans* configured intermediates, in contrast to the previously described mechanism[6] starting from compound **5**. The product of this reaction sequence, intermediate **28**, is a suitable starting point for the reductive elimination of the product acetone. If a second phosphine molecule is provided, this step gives rise to the anionic bisphosphine complex **1**, otherwise the monophosphine complex **19** is regenerated.

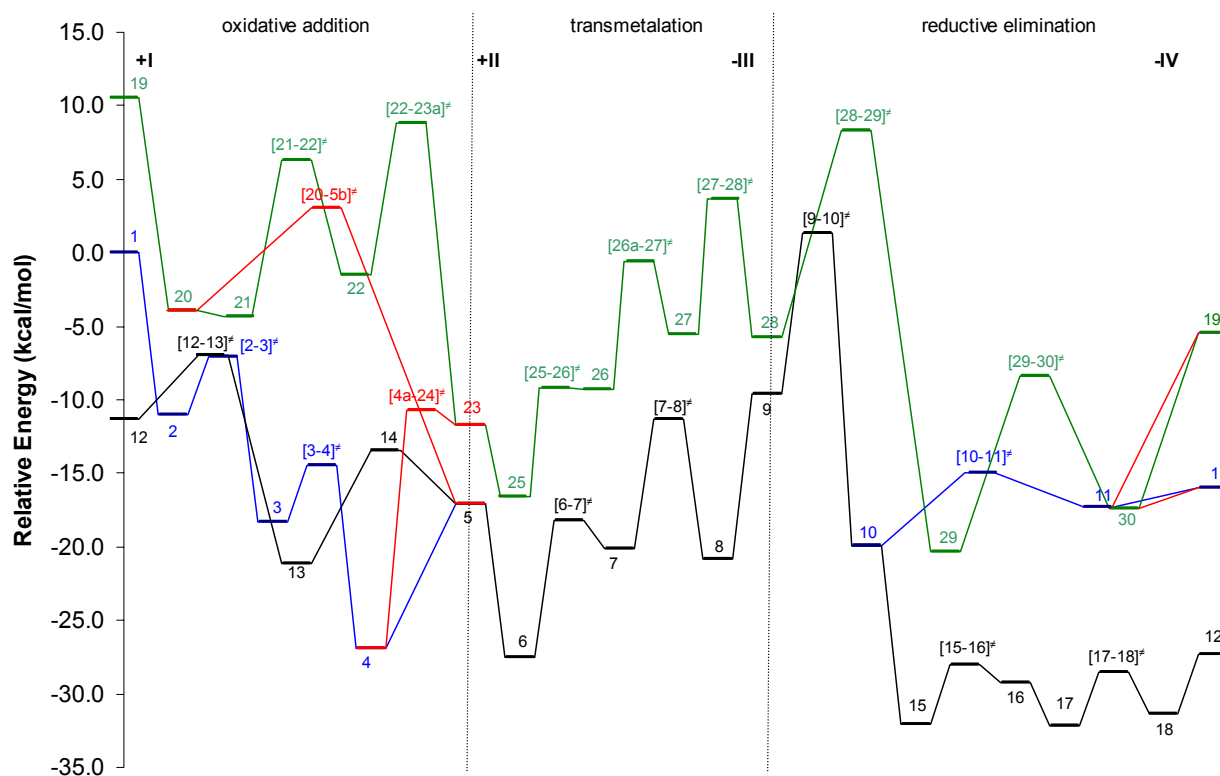


**Figure 4.10.** Relative energies ( $\Delta E_e$  in kcal/mol) of the most significant intermediates and transition states involved in the catalytic cycles calculated here and in our previous work.[6]

Figure 4.10 shows the energy profiles of all calculated reaction pathways for the catalytic cross-coupling of phenylboronic acid with acetic anhydride. The top part of the figure specifies the three phases of the catalytic cycle as well as the steps where the reactants are introduced (+I, +II) and where the products are liberated (-III, -IV). The data for the neutral cycle  $12 \rightarrow 5 \rightarrow 9 \rightarrow 12$  (black) and the anionic cycle  $1 \rightarrow 5 \rightarrow 9 \rightarrow 1$  (blue/black/blue) have been taken from our previous Chapter[6] where a correction of 10 kcal/mol per internal hydrogen bond has been applied for **6** and **8** to avoid differential stabilizing effects that will operate only in the gas phase and not in solution. Our present work provides data for the alternative anionic cycle  $19 \rightarrow 23 \rightarrow 28 \rightarrow 19$  (green) and for the interconnections between different cycles (red) during oxidative addition ( $1 \rightarrow 23$ ,  $19 \rightarrow 5$ ) and reductive elimination ( $9 \rightarrow 19$ ,  $28 \rightarrow 1$ ).

Concerning the starting points of the three cycles in Figure 4.10, the reactants have been chosen to be  $12 + \text{I} + \text{II} + [\text{PhB}(\text{OH})_2\text{OAc}]^-$  (**V**) for the neutral pathway,  $1 + \text{I} + \text{II}$  for the previously studied anionic pathway, and  $19 + \text{I} + \text{II} + \text{PMe}_3$  (**VI**) for the new anionic pathway. The relative energy of the latter two reactants is thus determined by the dissociation reaction  $1 \rightarrow 19 + \text{PMe}_3$  (see Figure 4.1) which seems a natural choice. The relative energy of the starting point for the neutral cycle depends on the chosen source of acetate: we have argued previously[6] that it would seem realistic in view of the usual experimental conditions to

provide acetate in the form of the Lewis adduct  $[\text{PhB}(\text{OH})_2\text{OAc}]^-$  (**V**), and we have adopted the same convention here. It should be stressed, however, that the relative position of the black curve in Figure 4.10 depends on this assumption, *i.e.*, on the accessibility of acetate.

It is obvious from Figure 4.10 that the catalytic cycles even of this model reaction are quite complex and consist of many elementary steps. None of these steps requires excessive activation since the individual barriers in Figure 4.10 are typically around 10 kcal/mol or even less. The largest barrier of 16.1 kcal/mol is found for the reaction **4**  $\rightarrow$  **23** that interconnects the two anionic pathways during oxidative addition. The other interconnections **20**  $\rightarrow$  **5**, **11**  $\rightarrow$  **19** and **30**  $\rightarrow$  **1** require energies of only 7.1, 11.9, and 1.3 kcal/mol, respectively. Judging from the energy profiles, all computed pathways appear to be feasible and should therefore be included in mechanistic considerations.

We now focus on a comparison of the two anionic pathways and refer to our previous Chapter[6] for a discussion of the neutral pathway. The green profile in Figure 4.10 starting from the monophosphine anion  $[\text{Pd}(\text{PMe}_3)\text{OAc}]^-$  (**19**) remains above the blue/black/blue profile starting from the diphosphine anion  $[\text{Pd}(\text{PMe}_3)_2\text{OAc}]^-$  (**1**) throughout the cycle, the energy differences being 10.6 kcal/mol at the beginning and end of the cycle (**19** *vs.* **1**), 5.5 kcal/mol after oxidative addition (**23** *vs.* **5**), and 4.2 kcal/mol after transmetalation (**28** *vs.* **9**). On both anionic pathways, the oxidative addition is computed to be exothermic (by 17-22 kcal/mol), the transmetalation is slightly endothermic (by 6-8 kcal/mol), and the reductive elimination is slightly exothermic for **9**  $\rightarrow$  **1** (by 6 kcal/mol) and essentially thermoneutral for **28**  $\rightarrow$  **19**.

In both cases, the oxidative addition begins with the exothermic formation of an adduct (**2**, **21**) with acetic anhydride which rearranges to a covalently bound complex (**3**, **22**) before undergoing the actual oxidative addition to a four-coordinate intermediate (**5**, **23**); the latter conversion is a two-step process in the case of **3**  $\rightarrow$  **5** due to the need to split off one phosphine ligand, and a simple one-step process **22**  $\rightarrow$  **23** in the case of the three-coordinate complex **22** (see Scheme 4.4). The transmetalation involves in both cases a crucial intermediate (**7**, **27**) with an  $\eta^2$ -bound phenyl ligand  $\text{PhB}(\text{OH})_2\text{OAc}$ , while the other intermediates are different (hydrogen-bonded adducts **6** and **8**, Lewis adducts **25** and **26**); since both these paths have been confirmed by IRC calculations, it seems that the detailed course of transmetalation can be system-dependent. Finally, in both cases, the reductive elimination starts with the formation of an  $\eta^2$   $\pi$ -complex with the  $\text{PhCOMe}$  ligand (**10**, **29**) which requires some activation whereas the subsequent steps are facile. The maximum individual energy barriers in Figure 4.10 for

oxidative addition, transmetalation, and reductive elimination are 9.8, 11.2, and 11.0 kcal/mol in the diphosphine anionic cycle  $\mathbf{1} \rightarrow \mathbf{5} \rightarrow \mathbf{9} \rightarrow \mathbf{1}$ , and 10.6, 9.2, and 14.1 kcal/mol in the monophosphine anionic cycle  $\mathbf{19} \rightarrow \mathbf{23} \rightarrow \mathbf{28} \rightarrow \mathbf{19}$ . These data, and inspection of Figure 4.10, indicate that these two anionic cycles are quite similar in many respects.

Figure 4.11 shows the free energy profiles for all pathways considered using the same conventions as in Figure 4.10. Both figures share a number of common features, but there are also notable differences. The relative position of the starting points  $\mathbf{1}$  and  $\mathbf{12}$  is almost the same in both figures, while that of  $\mathbf{19}$  is now much lower ( $-2.2$  kcal/mol in Figure 4.11 vs. 10.6 kcal/mol in Figure 4.10) due to the entropic contribution to the free energy of the reaction  $\mathbf{1} \rightarrow \mathbf{19} + \text{PMe}_3$  (see Figure 4.1). Generally speaking, dissociation reactions are entropically favored, while association reactions suffer from an entropic penalty because of the loss of translational and rotational degrees of freedom (typically around 10 kcal/mol at 298 K in the gas phase). The major differences between Figures 4.10 and 4.11 are caused by such entropic effects and occur in steps where reactants are added or products are liberated. One should keep in mind, of course, that these entropic effects will be less pronounced in solution due to solvation and desolvation, but they will still be present.

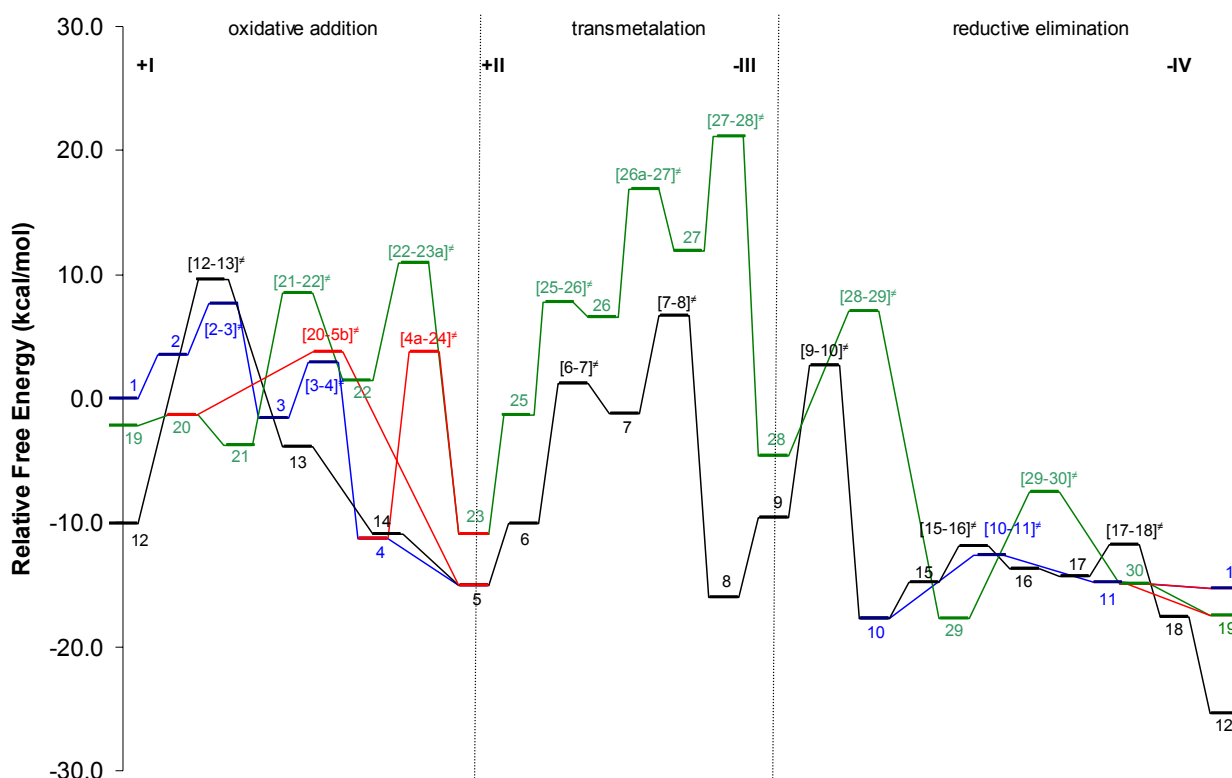


**Figure 4.11.** Relative free energies ( $\Delta G_{298}$  in kcal/mol) of the most significant intermediates and transition states involved in the catalytic cycles calculated here and in our previous work.[6]

Closer inspection of Figure 4.11 confirms that the individual barriers remain moderate also on the free energy scale. The maximum such barriers for oxidative addition, transmetalation, and reductive elimination are 7.7, 11.2, and 12.3 kcal/mol in the diphosphine anionic cycle ( $\mathbf{1} \rightarrow \mathbf{5} \rightarrow \mathbf{9} \rightarrow \mathbf{1}$ ); 12.2, 10.3, and 11.8 kcal/mol in the monophosphine anionic cycle ( $\mathbf{19} \rightarrow \mathbf{23} \rightarrow \mathbf{28} \rightarrow \mathbf{19}$ ); and 19.7, 11.2, and 12.3 kcal/mol in the neutral cycle ( $\mathbf{12} \rightarrow \mathbf{5} \rightarrow \mathbf{9} \rightarrow \mathbf{12}$ ). The largest free energy barrier of 19.7 kcal/mol thus occurs during the oxidative addition on the neutral pathway. It is also obvious from Figure 4.11 that the interconnections between the pathways remain accessible in terms of free energy since the most demanding such case  $\mathbf{4} \rightarrow \mathbf{23}$  is associated with a free energy barrier of 15.0 kcal/mol.

Which of the catalytic cycles is the most favorable one? In a proper treatment of this problem, one would set up the kinetic equations for the intertwined catalytic cycles (Schemes 4.3 and 4.4) and solve them on the basis of the computed free energies (Figure 4.11). It is clear that this is extremely complex in the present case and that the results will depend on the actual reaction conditions, in particular on the concentrations; even in much simpler composite reactions, the results from such kinetic analysis can normally be interpreted in a useful manner only for certain limiting cases.[28] Given the need to resort to an approximate treatment, a common approach is to invoke a kinetic steady-state hypothesis and to assume that the concentration of the intermediates remains constant in an efficient catalytic cycle.[28] One can then deduce that the maximum rate of the cycle is proportional to  $\exp(-\Delta G_{\text{max}}/RT)$  where  $\Delta G_{\text{max}}$  is the free energy span of the cycle, *i.e.*, the free energy difference between the highest and lowest point.[29] The largest possible rate (highest turnover number) of the catalytic cycle is obtained for the lowest free energy span.[29]

Following recent precedent[14] we apply this concept to the cycles in Figure 4.11. In addition to the three cycles discussed up to now, two further anionic cycles are present in Figure 4.11 when considering interconnections, namely  $\mathbf{1} \rightarrow \mathbf{23} \rightarrow \mathbf{28} \rightarrow \mathbf{1}$  and  $\mathbf{19} \rightarrow \mathbf{5} \rightarrow \mathbf{9} \rightarrow \mathbf{19}$ . Table 4.11 lists the free energy spans for all five cycles, as well as the overall and the largest individual free energy barriers. In terms of the free energy span, the diphosphine anionic cycle ( $\mathbf{1} \rightarrow \mathbf{5} \rightarrow \mathbf{9} \rightarrow \mathbf{1}$ ) and the interconnected monophosphine anionic cycle ( $\mathbf{19} \rightarrow \mathbf{5} \rightarrow \mathbf{9} \rightarrow \mathbf{19}$ ) are most favorable, with a slight edge for the latter. These two cycles are also associated with the lowest overall and individual free energy barriers (Table 4.11). The alternative anionic cycles proceed *via* less stable intermediates, and hence a less advantageous transmetalation route ( $\mathbf{23} \rightarrow \mathbf{28}$  rather than  $\mathbf{5} \rightarrow \mathbf{9}$ , see Figure 4.11), and they are therefore not competitive. The neutral cycle suffers from the large free energy barrier for oxidative addition.



In summary, our calculations favor the two anionic cycles specified above. Experimentally, the fastest turnover is observed for this coupling reaction if anionic palladium species are present, and just enough phosphine is added to keep the palladium in solution while excess phosphine retards the reaction.[4,12,13] These experimental findings are consistent with an interconnected monophosphine anionic cycle (**19** → **5** → **9** → **19**).

Given the limitations of our computational approach which have been discussed here and in our preceding paper,[6] one should emphasize the qualitative conclusions that emerge from our calculations. While we have attempted to identify the “best” catalytic cycle for the reaction studied presently, we have actually found several catalytic pathways that are interconnected and may contribute to catalytic turnover. In the present case, anionic pathways seem to be preferred, but the balance between the competing pathways can clearly be affected by the reaction conditions. Likewise, when going from the current simplified model system to other Suzuki-type palladium-catalyzed cross-coupling reactions, this balance can shift again. In view of this mechanistic complexity, further studies are needed to better understand the course of Suzuki-type reactions with catalysts that are commonly used in real-life experiments (*e.g.*, triarylphosphine-palladium complexes).

**Table 4.11. Free energy data (kcal/mol) for catalytic cycles in Figure 4.11.**

Cycle	Type <sup>a</sup>	$\Delta G_{\max}^b$	$\Delta G_{\max}^{\ddagger c}$	$\Delta G_{\text{f} \max}^{\ddagger d}$
<b>1</b> → <b>5</b> → <b>9</b> → <b>1</b>	a2	27.6	7.7	12.3
<b>19</b> → <b>23</b> → <b>28</b> → <b>19</b>	a1	38.9	23.4	12.2
<b>12</b> → <b>5</b> → <b>9</b> → <b>12</b>	n2	35.7	19.7	19.7
<b>1</b> → <b>23</b> → <b>28</b> → <b>1</b>	a2	38.9	21.2	12.2
<b>19</b> → <b>5</b> → <b>9</b> → <b>19</b>	a1	24.4	8.9	12.3

- (a) a2 anionic diphosphine, a1 anionic monophosphine, n2 neutral diphosphine.
- (b) Free energy span, difference between the highest and lowest point of the catalytic cycle
- (c) Overall free energy barrier, difference between the highest and the starting point.
- (d) Largest free energy barrier for any individual step.

## 4.5 Supporting Information

### Contents:

**Table 4.S1.** Absolute energies (hartree) from BP86/6-31G\* calculations.

**Figure 4.S1.** DFT optimized geometries of species involved in the catalytic cycles.  
Bond distances in Å and angles in degrees.

**Table 4.S1.** Absolute energies (hartree) from BP86/6-31G\* calculations.

No.	E <sub>c</sub>	E <sub>0</sub>	H <sub>298</sub>	G <sub>298</sub>	E <sub>sov</sub>
<b>I</b>	-381.723958	-381.628233	-381.619007	-381.66192	-381.728739
<b>II</b>	-408.238473	-408.117037	-408.107995	-408.150722	-408.243905
<b>III</b>	-405.1084707	-405.025221	-405.016081	-405.059156	-405.119714
<b>IV</b>	-384.879391	-384.745052	-384.736108	-384.777828	-384.882702
<b>VI</b>	-461.10031	-460.990062	-460.982266	-461.019548	-461.101837
<b>VII</b>	-228.497311	-228.455615	-228.450147	-228.483177	-228.585122
<b>1</b>	-1277.622937	-1277.352362	-1277.328357	-1277.407933	-1277.680236
<b>2</b>	-1659.364418	-1658.995643	-1658.962516	-1659.064268	-1659.418014
<b>[2-3]<sup>‡</sup></b>	-1659.358138	-1658.989983	-1658.957304	-1659.057589	-1659.412501
<b>3</b>	-1659.376026	-1659.006568	-1658.974038	-1659.072284	-1659.429189
<b>[3-4]<sup>‡</sup></b>	-1659.369886	-1659.000911	-1658.968878	-1659.065303	-1659.422368
<b>4</b>	-1659.389754	-1659.02094	-1658.987782	-1659.0879	-1659.443298
<b>4a</b>	-1659.384512	-1659.016133	-1658.982762	-1659.082221	-1659.436762
<b>19</b>	-816.50582	-816.346151	-816.330545	-816.391851	-816.57864
<b>20</b>	-1198.252814	-1197.995395	-1197.970455	-1198.052484	-1198.314189
<b>21</b>	-1198.253404	-1197.996729	-1197.971688	-1198.056284	-1198.313899
<b>[21-22]<sup>‡</sup></b>	-1198.236492	-1197.980589	-1197.956431	-1198.036802	-1198.290309
<b>22</b>	-1198.248962	-1197.992066	-1197.967534	-1198.047931	-1198.30335
<b>[22-23a]<sup>‡</sup></b>	-1198.232516	-1197.976652	-1197.952166	-1198.032826	-1198.290461
<b>23a</b>	-1198.264334	-1198.00825	-1197.982818	-1198.06487	-1198.320272
<b>23</b>	-1198.265149	-1198.009556	-1197.983851	-1198.067666	-1198.321896
<b>25</b>	-1606.511444	-1606.133207	-1606.098323	-1606.203104	-1606.563906
<b>[25-26]<sup>‡</sup></b>	-1606.499692	-1606.121872	-1606.08771	-1606.188626	-1606.553599
<b>26</b>	-1606.499769	-1606.121824	-1606.086828	-1606.190529	-1606.553248
<b>26a</b>	-1606.496058	-1606.117316	-1606.082954	-1606.183571	-1606.550437
<b>[26a-27]<sup>‡</sup></b>	-1606.485902	-1606.107927	-1606.074114	-1606.17409	-1606.540109
<b>27</b>	-1606.493815	-1606.114965	-1606.080865	-1606.18207	-1606.547546
<b>[27-28]</b>	-1606.479107	-1606.101637	-1606.06767	-1606.167227	-1606.529161
<b>28</b>	-1201.385712	-1201.092672	-1201.067213	-1201.149262	-1201.439555
<b>[28-29]<sup>‡</sup></b>	-1201.363258	-1201.071407	-1201.046054	-1201.13052	-1201.420457
<b>29</b>	-1201.408876	-1201.114573	-1201.089666	-1201.170105	-1201.462499
<b>[29-30]<sup>‡</sup></b>	-1201.389931	-1201.095926	-1201.071174	-1201.15376	-1201.447989
<b>30</b>	-1201.404201	-1201.109007	-1201.084081	-1201.165579	-1201.461182
<b>9</b>	-1201.391876	-1201.09869	-1201.073109	-1201.157094	-1201.446218

<b>[9-10]<sup>‡</sup></b>	-1201.374385	-1201.082017	-1201.057199	-1201.137633	-1201.431472
<b>10</b>	-1201.408251	-1201.114255	-1201.089165	-1201.170136	-1201.461289
<b>[10-11]<sup>‡</sup></b>	-1201.400485	-1201.106671	-1201.082114	-1201.162089	-1201.457681
<b>11</b>	-1201.404193	-1201.108966	-1201.084058	-1201.16545	-1201.461269
<b>9</b>	-1201.391876	-1201.09869	-1201.073109	-1201.157094	-1201.446218
<b>[4a-24]<sup>‡</sup></b>	-1659.36403	-1658.997459	-1658.964049	-1659.063937	-1659.411859
<b>24</b>	-1659.369287	-1659.002084	-1658.967742	-1659.072928	-1659.419245
<b>23b</b>	-1198.264333	-1198.00825	-1197.982818	-1198.064869	-1198.320235

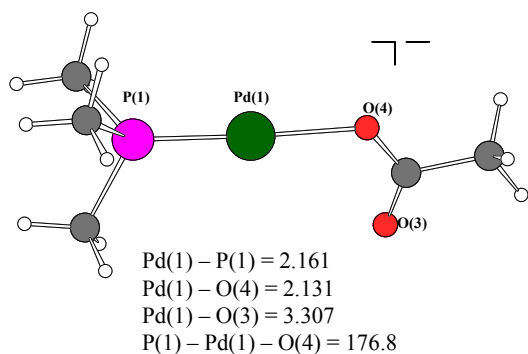
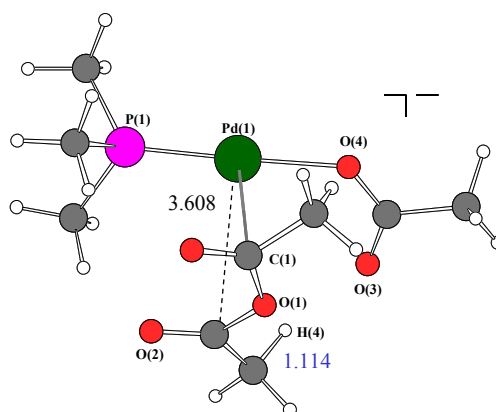
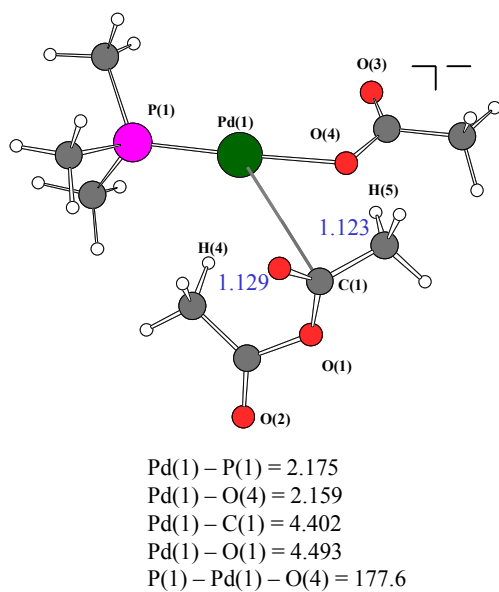
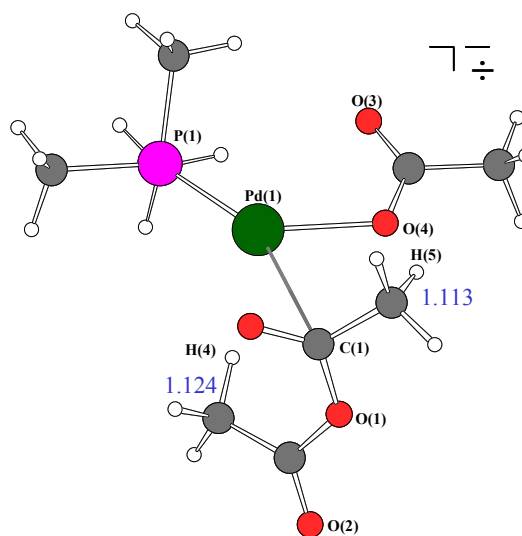
$E_e$  Electronic energy

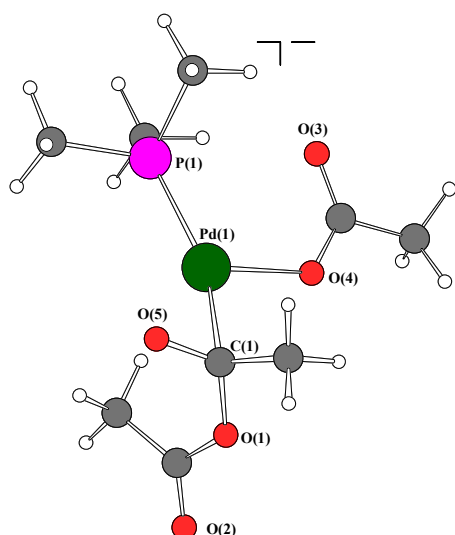
$E_0$  Total energy plus zero-point vibrational energy

$H_{298}$  Enthalpy at 298 K

$G_{298}$  Gibbs free enthalpy at 298 K

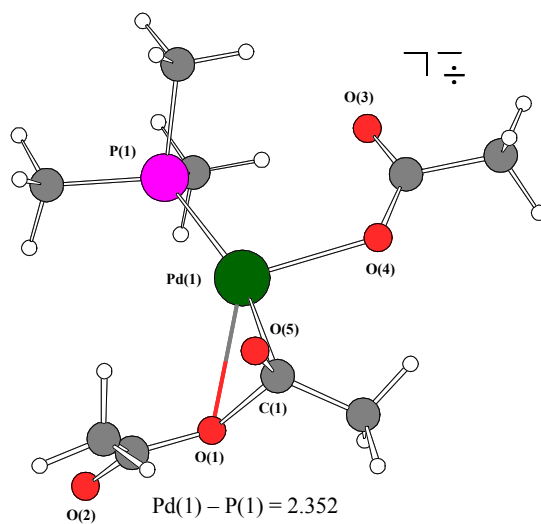
$E_{sov}$  Total energy plus CPCM solvation energy (THF)

**Figure 4.S1.** DFT optimized geometries of species involved in the catalytic cycles. Bond distances in Å and angles in degrees.**19****20****21****[21-22]#**



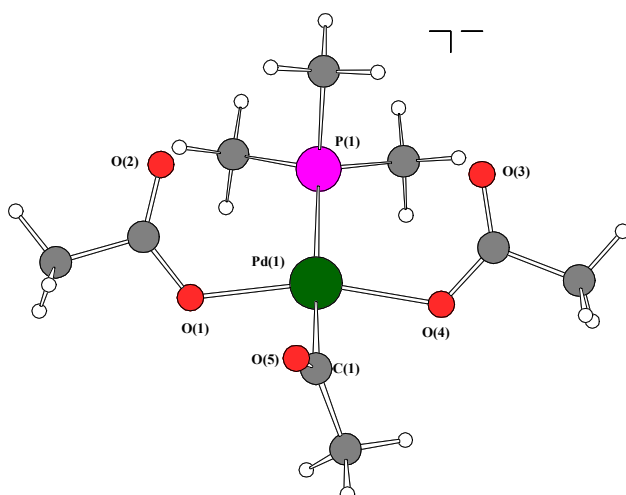
Pd(1) – P(1) = 2.351  
 Pd(1) – O(4) = 2.179  
 Pd(1) – C(1) = 2.089  
 Pd(1) – O(5) = 2.214  
 C(1) – O(5) = 1.290  
 P(1) – Pd(1) – O(4) = 105.7

**22**



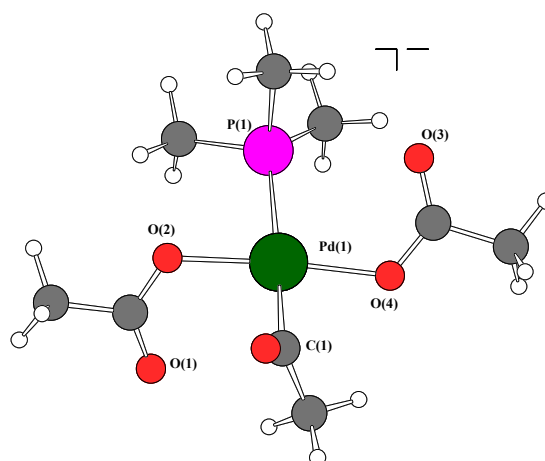
Pd(1) – P(1) = 2.352  
 Pd(1) – O(4) = 2.243  
 Pd(1) – C(1) = 2.086  
 Pd(1) – O(1) = 2.486  
 C(1) – O(5) = 1.245  
 Pd(1) – O(5) = 2.672  
 O(1) – C(1) = 1.620  
 P(1) – Pd(1) – O(4) = 108.8

**[22-23a]‡**



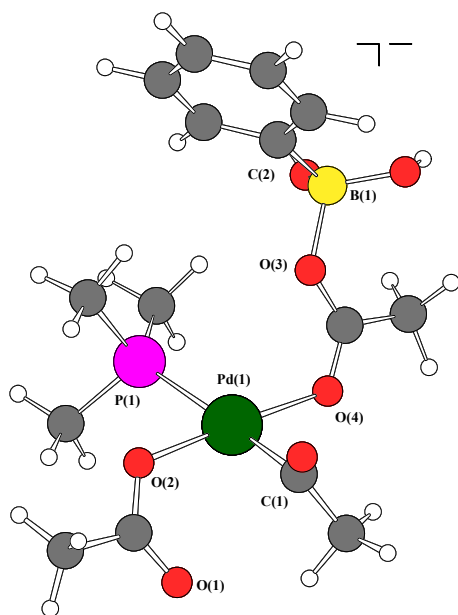
Pd(1) – P(1) = 2.481  
 Pd(1) – O(4) = 2.136  
 Pd(1) – C(1) = 1.997  
 Pd(1) – O(1) = 2.124  
 C(1) – O(5) = 1.222  
 Pd(1) – O(5) = 2.864  
 O(1) – C(1) = 2.768  
 P(1) – Pd(1) – O(4) = 96.2  
 O(1) – Pd(1) – C(1) = 84.3

**23a**



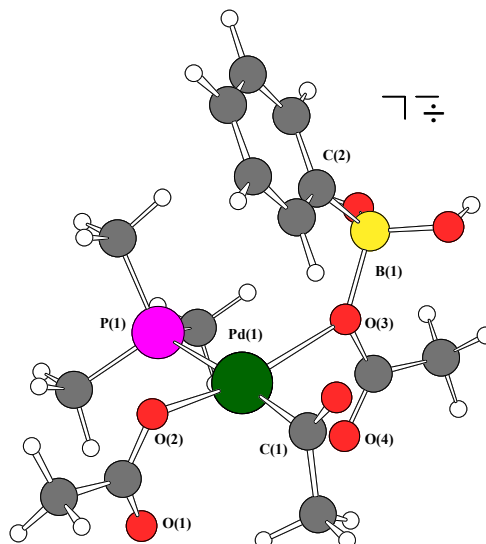
Pd(1) – C(1) = 1.993  
 Pd(1) – O(2) = 2.124  
 Pd(1) – O(4) = 2.139  
 Pd(1) – P(1) = 2.483  
 O(2) – Pd(1) – C(1) = 90.4  
 P(1) – Pd(1) – O(2) = 86.8  
 O(4) – Pd(1) – C(1) = 84.4

**23**



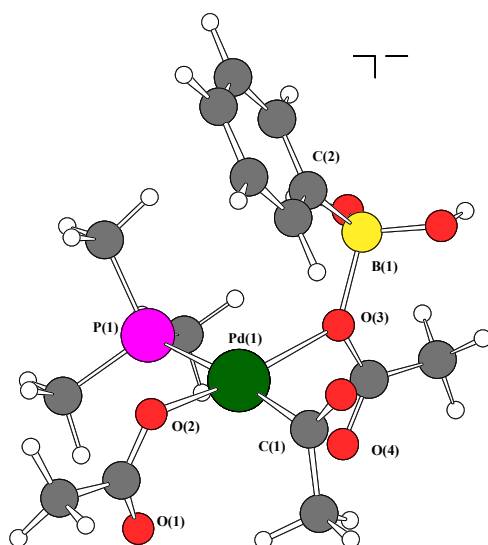
Pd(1) – C(1) = 1.992  
 Pd(1) – O(2) = 2.119  
 Pd(1) – P(1) = 2.484  
 Pd(1) – O(4) = 2.159  
 Pd(1) – O(3) = 3.281  
 B(1) – O(3) = 1.609  
 O(2) – Pd(1) – C(1) = 91.7  
 P(1) – Pd(1) – O(2) = 83.2  
 O(4) – Pd(1) – C(1) = 87.6

25



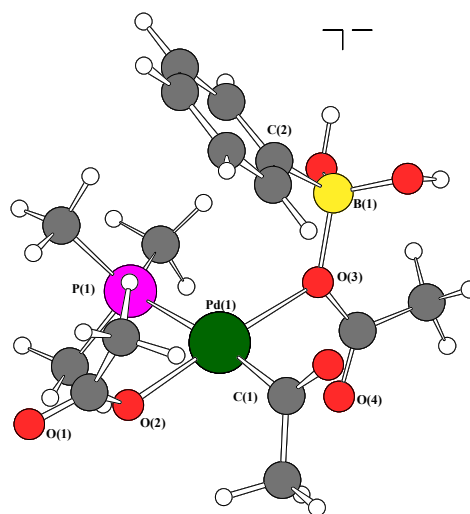
Pd(1) – C(1) = 1.983  
 Pd(1) – O(2) = 2.167  
 Pd(1) – P(1) = 2.455  
 Pd(1) – O(3) = 2.425  
 B(1) – O(3) = 1.656  
 Pd(1) – O(4) = 2.732  
 O(3) – Pd(1) – C(1) = 85.5  
 P(1) – Pd(1) – O(2) = 93.2  
 O(3) – Pd(1) – C(1) = 92.2

[25-26]<sup>‡</sup>



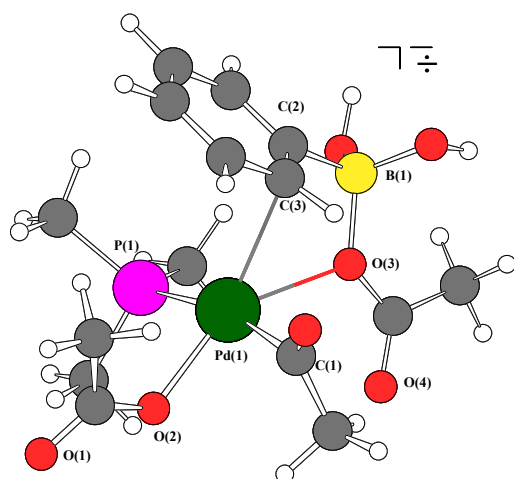
Pd(1) – C(1) = 1.991  
 Pd(1) – O(3) = 2.322  
 Pd(1) – P(1) = 2.459  
 Pd(1) – O(2) = 2.155  
 B(1) – O(3) = 1.705  
 P(1) – Pd(1) – O(2) = 92.7  
 C(1) – Pd(1) – O(2) = 85.5

26



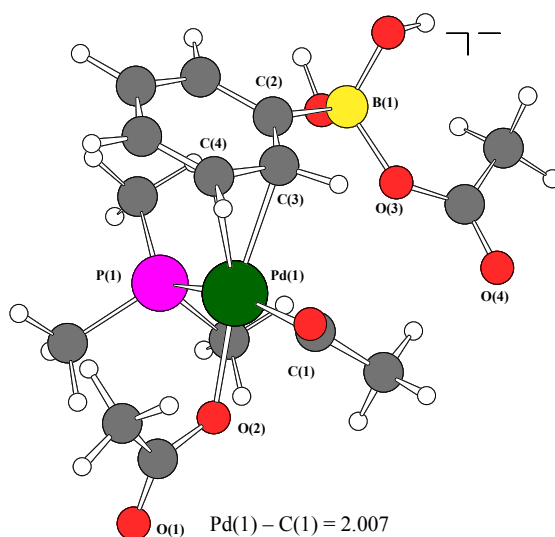
Pd(1) – C(1) = 1.995  
 Pd(1) – O(2) = 2.117  
 Pd(1) – P(1) = 2.475  
 Pd(1) – O(3) = 2.277  
 B(1) – O(3) = 1.635  
 P(1) – Pd(1) – O(2) = 84.3  
 C(1) – Pd(1) – O(2) = 90.3

26a



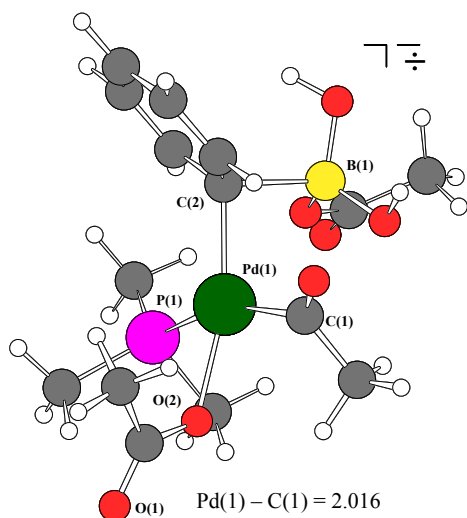
Pd(1) – C(1) = 1.989  
 Pd(1) – P(1) = 2.501  
 Pd(1) – O(2) = 2.175  
 Pd(1) – C(3) = 2.547  
 B(1) – O(3) = 1.577  
 Pd(1) – O(3) = 2.793  
 Pd(1) – C(2) = 3.082  
 P(1) – Pd(1) – O(2) = 86.8  
 C(2) – Pd(1) – O(2) = 163.6  
 O(3) – Pd(1) – C(1) = 96.7  
 O(3) – Pd(1) – P(1) = 85.9

[26a-27]<sup>‡</sup>



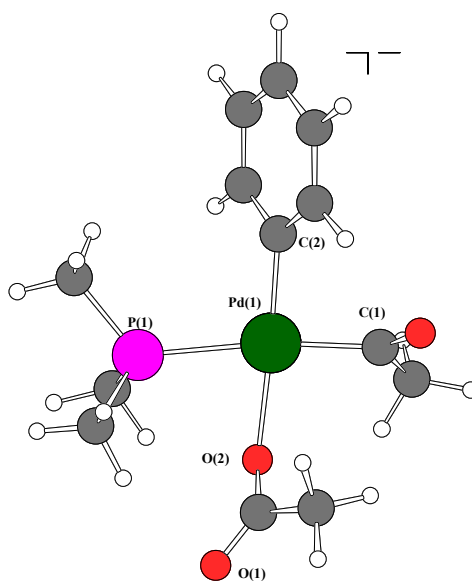
Pd(1) – C(1) = 2.007  
 Pd(1) – P(1) = 2.543  
 Pd(1) – O(2) = 2.154  
 B(1) – O(3) = 1.542  
 Pd(1) – O(3) = 3.630  
 Pd(1) – C(3) = 2.328  
 Pd(1) – C(4) = 2.425  
 P(1) – Pd(1) – O(2) = 80.0  
 C(2) – Pd(1) – O(2) = 156.6  
 O(3) – Pd(1) – C(1) = 86.0  
 O(3) – Pd(1) – P(1) = 88.9

27



Pd(1) – C(1) = 2.016  
 Pd(1) – C(2) = 2.159  
 Pd(1) – P(1) = 2.541  
 Pd(1) – O(2) = 2.172  
 C(2) – B(1) = 2.016  
 P(1) – Pd(1) – O(2) = 77.8  
 C(2) – Pd(1) – O(2) = 164.1  
 C(2) – Pd(1) – C(1) = 96.6

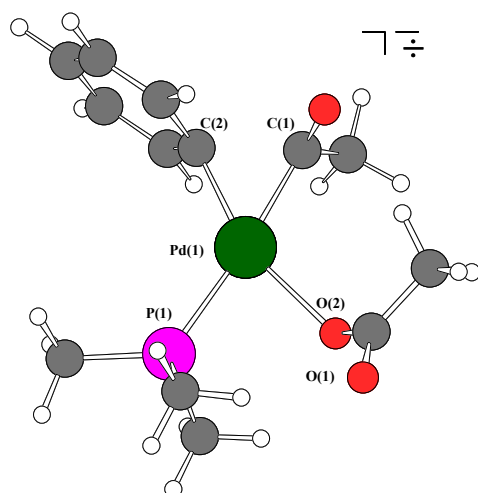
[27-28]<sup>‡</sup>



Pd(1) – P(1) = 2.465  
 Pd(1) – C(1) = 2.014  
 Pd(1) – O(2) = 2.209  
 Pd(1) – C(2) = 2.033  
 C(2) – Pd(1) – P(1) = 99.1  
 C(2) – Pd(1) – C(1) = 88.5  
 O(2) – Pd(1) – P(1) = 77.9  
 O(2) – Pd(1) – C(1) = 94.3

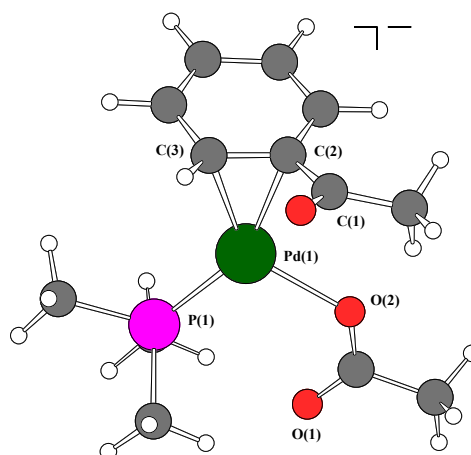
28





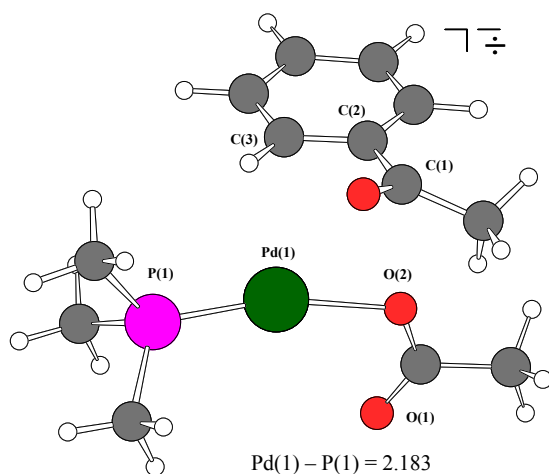
C(2) – C(1) = 1.911  
 Pd(1) – C(2) = 2.059  
 Pd(1) – C(1) = 2.112  
 Pd(1) – O(2) = 2.275  
 Pd(1) – P(1) = 2.398  
 C(2) – Pd(1) – C(1) = 54.5  
 P(1) – Pd(1) – O(2) = 79.7

[28-29]<sup>‡</sup>



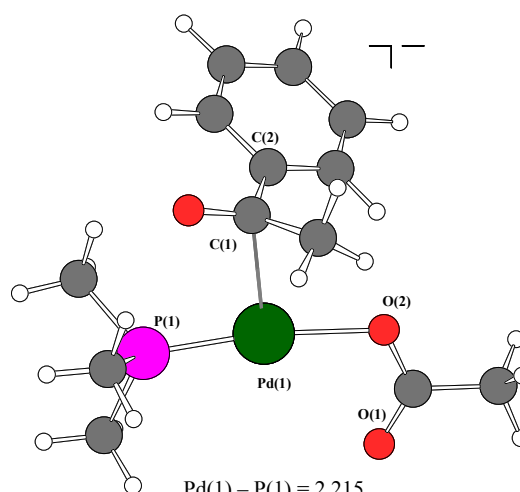
Pd(1) – C(2) = 2.203  
 Pd(1) – C(3) = 2.199  
 Pd(1) – P(1) = 2.299  
 Pd(1) – O(3) = 2.266  
 P(1) – Pd(1) – O(2) = 105.9

29



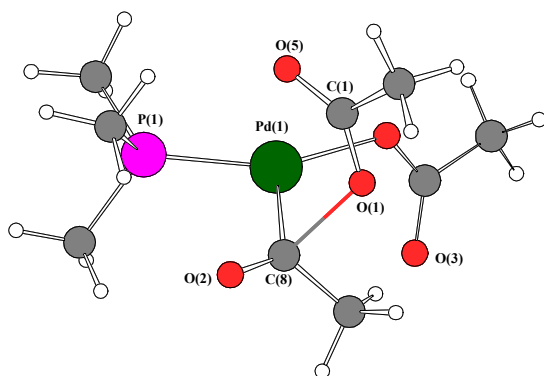
Pd(1) – P(1) = 2.183  
 Pd(1) – O(2) = 2.182  
 Pd(1) – C(2) = 3.248  
 Pd(1) – C(1) = 3.571  
 Pd(1) – C(3) = 2.884  
 P(1) – Pd(1) – O(2) = 165.8  
 C(1) – Pd(1) – O(2) = 67.0

[29-30]<sup>‡</sup>



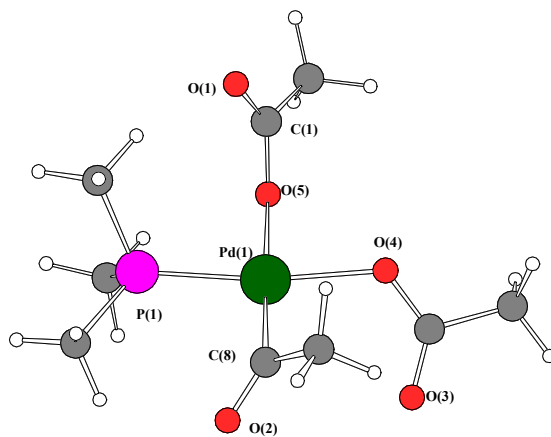
Pd(1) – P(1) = 2.215  
 Pd(1) – O(2) = 2.174  
 Pd(1) – C(1) = 2.554  
 Pd(1) – C(2) = 3.012  
 P(1) – Pd(1) – O(2) = 172.5  
 C(1) – Pd(1) – P(1) = 90.9

30



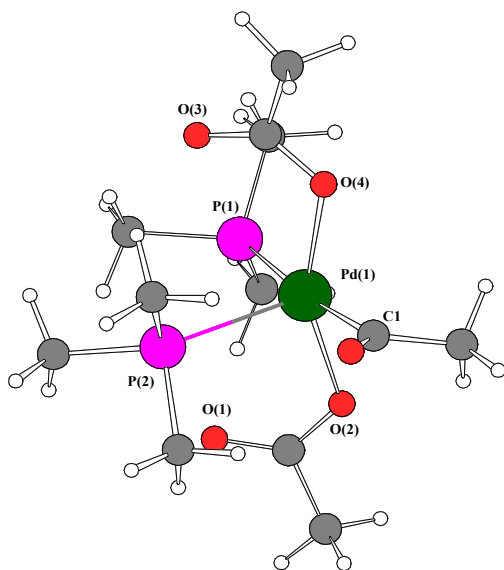
Pd(1) – P(1) = 2.255  
 Pd(1) – O(4) = 2.164  
 Pd(1) – C(8) = 2.027  
 Pd(1) – O(1) = 2.850  
 Pd(1) – O(2) = 2.899  
 Pd(1) – O(3) = 3.411  
 Pd(1) – O(5) = 3.019  
 Pd(1) – C(1) = 3.227  
 C(8) – O(1) = 2.087  
 P(1) – Pd(1) – O(4) = 151.9

**[20-5b]‡**



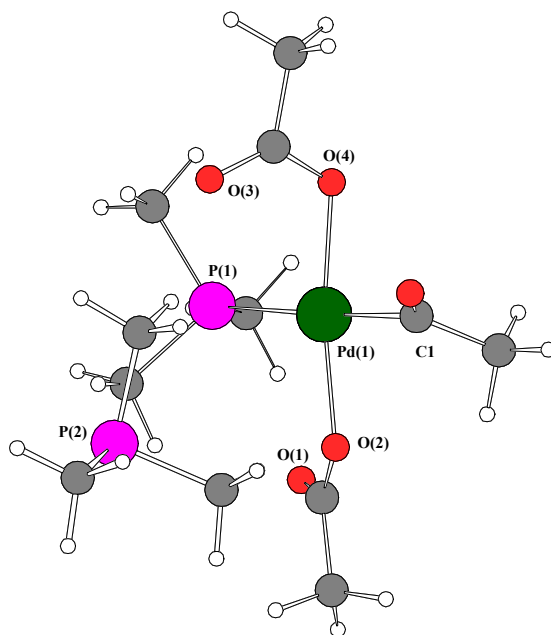
Pd(1) – P(1) = 2.274  
 Pd(1) – O(4) = 2.120  
 Pd(1) – C(8) = 1.988  
 Pd(1) – O(1) = 3.546  
 Pd(1) – O(2) = 2.877  
 Pd(1) – O(3) = 3.323  
 Pd(1) – O(5) = 2.254  
 Pd(1) – C(1) = 3.182  
 P(1) – Pd(1) – O(4) = 171.5

**5b**



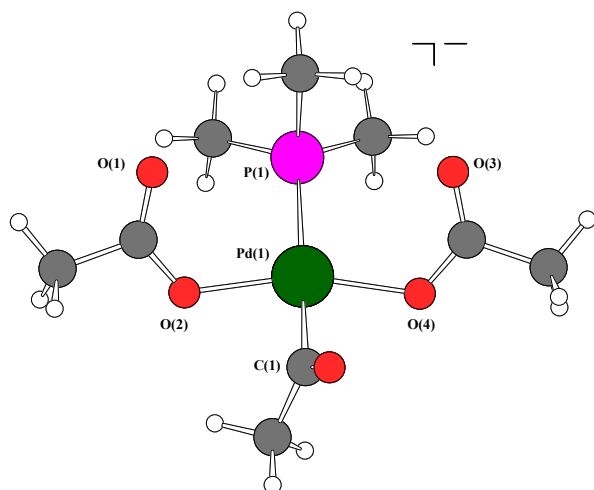
Pd(1) – P(1) = 2.467  
 Pd(1) – P(2) = 2.808  
 Pd(1) – O(4) = 2.191  
 Pd(1) – C(1) = 1.992  
 Pd(1) – O(2) = 2.199  
 Pd(1) – O(3) = 3.333  
 Pd(1) – O(1) = 3.335  
 Pd(1) – O(5) = 2.895  
 P(1) – Pd(1) – P(2) = 96.2  
 P(1) – Pd(1) – O(4) = 96.0

**[4a-24]‡**



Pd(1) – P(1) = 2.478  
 Pd(1) – P(2) = 4.926  
 Pd(1) – O(4) = 2.129  
 Pd(1) – C(1) = 2.000  
 Pd(1) – O(2) = 2.144  
 Pd(1) – O(3) = 3.141  
 Pd(1) – O(1) = 3.376  
 Pd(1) – O(5) = 2.877  
 P(1) – Pd(1) – P(2) = 86.8  
 P(1) – Pd(1) – O(4) = 91.9

**24**



$\text{Pd(1)} - \text{C(1)} = 1.997$   
 $\text{Pd(1)} - \text{O(2)} = 2.137$   
 $\text{Pd(1)} - \text{O(4)} = 2.125$   
 $\text{Pd(1)} - \text{P(1)} = 2.481$   
 $\text{O(2)} - \text{Pd(1)} - \text{C(1)} = 83.2$   
 $\text{P(1)} - \text{Pd(1)} - \text{O(2)} = 96.2$   
 $\text{O(4)} - \text{Pd(1)} - \text{C(1)} = 84.3$

**23b**

## Bibliography:

- [1] (a) N. Miyaura, A. Suzuki, "Palladium-Catalyzed Cross-Coupling Reactions of Organoboron Compounds." *Chem Rev.* **1995**, 95, 2457-2483. (b) A. Suzuki, "Recent advances in the cross-coupling reactions of organoboron derivatives with organic electrophiles, 1995-1998." *J. Organomet. Chem.* **1999**, 576, 147-168. (c) T. Ishiyama, N. Miyaura, "Chemistry of Group 13 element-transition metal linkage — the platinum- and palladium-catalyzed reactions of (alkoxo)diborons." *J. Organomet. Chem.* **2000**, 611, 392-402. (d) A. Suzuki "Metal-Catalyzed Cross-Coupling Reactions." F. Diederich, P. J. Stang, Eds., Wiley-VCH, Weinheim, **1998**, page 49.
- [2] (a) N. Miyaura, K. Yamada, A. Suzuki, "A new stereospecific cross-coupling by the palladium-catalyzed reaction of 1-alkenylboranes with 1-alkenyl or 1-alkynyl halides." *Tetrahedron Lett.* **1979**, 20, 3437-3440. (b) N. Miyaura, K. Yamada, H. Suginome, A. Suzuki, "Novel and Convenient Method for the Stereo- and Regiospecific Synthesis of Conjugated Alkadienes and Alkynes via the Palladium-Catalyzed Cross-Coupling Reaction of 1-Alkenylboranes with Bromoalkenes and Bromoalkynes." *J. Am. Chem. Soc.* **1985**, 107, 972-980. (c) M. Satoh, N. Miyaura, A. Suzuki, "Stereo- and Regiospecific Synthesis of Trisubstituted Alkenes via the Palladium-catalyzed Cross-coupling Reaction of Diisopropyl (E)-(1-Alkyl-1-alkenyl)boronates with Organic Halides" *Chem. Lett.* **1986**, 1329-1332. (d) N. Miyaura, M. Satoh, A. Suzuki, "A stereospecific synthesis of conjugated (E, Z)- and (Z, Z)-aliquadienes by a palladium-catalyzed cross-coupling reaction of 1-alkenylboranes with 1-alkenyl bromides." *Tetrahedron Lett.* **1981**, 22, 127-130.
- [3] L. J. Gooßen, "Pd-catalyzed synthesis of arylacetic acid derivatives from boronic acids." *Chem. Commun.* **2001**, 7, 669-670.
- [4] (a) L. J. Gooßen, K. Ghosh, "Palladium-Catalyzed Synthesis of Aryl Ketones from Boronic Acids and Carboxylic Acids or Anhydrides." *Angew. Chem., Int. Ed.* **2001**, 40, 3458-3460. (b) L. J. Gooßen, K. Ghosh, "Palladium-Catalyzed Synthesis of Aryl Ketones from Boronic Acids and Carboxylic Acids Activated in situ by Pivalic Anhydride." *Eur. J. Org. Chem.* **2002**, 19, 3254-3267. (c) L. J. Gooßen, L. Winkel, A. Döhring, K. Ghosh, J. Paetzold, "Pd-Catalyzed Synthesis of Functionalized Arylketones from Boronic Acids and Carboxylic

Acids Activated in situ with Dimethyl Dicarbonate.” *Synlett* **2002**, 8, 1237-1240. (d) L. J. Gooßen, K. Ghosh, “A New Practical Ketone Synthesis Directly from Carboxylic Acids: First Application of Coupling Reagents in Palladium Catalysis.” *Chem. Commun.* **2001**, 20, 2084-2085.

[5] R. Kakino, S. Kamusi, I. Shimizu, A. Yamamoto, “Synthesis of Unsymmetrical Ketones by Palladium-Catalyzed Cross-Coupling Reaction of Carboxylic Anhydrides with Organoboron Compounds.” *Bull. Chem. Soc. Jpn.* **2002**, 75, 137-148.

[6] L. J. Gooßen, D. Koley, H. Hermann, W. Thiel, submitted for publication; Chapter 3.

[7] (a) K. Nagayama, F. Kawataka, M. Sakamoto, I. Shimizu, A. Yamamoto, “Preparation and Reactivities of Acyl(carboxylato)palladium Complexes.” *Chem. Lett.* **1995**, 367-368. (b) R. Kakino, H. Narahashi, I. Shimizu, A. Yamamoto, “Palladium-Catalyzed Direct Conversion of Carboxylic Acids into Ketones with Organoboronic Acids Promoted by Anhydride Activators.” *Bull. Chem. Soc. Jpn.* **2002**, 75, 1333-1345. (c) R. Kakino, H. Narahashi, I. Shimizu, A. Yamamoto, “Direct Hydrogenation of Carboxylic Acids to Corresponding Aldehydes Catalyzed by Palladium Complexes in the Presence of Pivalic Anhydride.” *Chem. Lett.* **1998**, 1143-1144.

[8] (a) A. L. Casado, P. Espinet, “Mechanism of the Stille Reaction. 1. The Transmetalation Step. Coupling of  $R^1I$  and  $R^2SnBu_3$  Catalyzed by *trans*-[PdR<sup>1</sup>IL<sub>2</sub>] ( $R^1$  = C<sub>6</sub>Cl<sub>2</sub>F<sub>3</sub>;  $R^2$  = Vinyl, 4-Methoxyphenyl; L = AsPh<sub>3</sub>).” *J. Am. Chem. Soc.* **1998**, 120, 8978-8985. (b) A. L. Casado, P. Espinet, “On the Configuration Resulting from Oxidative Addition of RX to Pd(PPh<sub>3</sub>)<sub>4</sub> and the Mechanism of the *cis*-to-*trans* Isomerization of [PdRX(PPh<sub>3</sub>)<sub>2</sub>] Complexes (R = Aryl, X = Halide).” *Organometallics* **1998**, 17, 954-959. (c) P. Espinet, A. M. Echavarren, “The Mechanisms of the Stille Reactions.” *Angew. Chem., Int. Ed.* **2004**, 43, 4704-4734. (d) J. A. Casares, P. Espinet, G. Salas, “14-Electron T-Shaped [PdRXL] Complexes: Evidence or Illusion? Mechanistic Consequences for the Stille Reaction and Related Processes.” *Chem. Eur. J.* **2002**, 8, 4843-4853.

[9] (a) C. Amatore, A. Jutand, “Anionic Pd(0) and Pd(II) Intermediates in Palladium-Catalyzed Heck and Cross-Coupling Reactions.” *Acc. Chem. Res.* **2000**, 33, 314-321. (b) C. Amatore, M. Azzabi, A. Jutand, “Rates and mechanism of the reversible oxidative of (Z)- and (E)-1,2-dichloroethylene to low-ligated zerovalent palladium.” *J. Am. Chem. Soc.* **1991**, 113, 1670-1677. (c) C. Amatore, A. Jutand, A. Suarez, “Intimate mechanism of oxidative addition

to zerovalent palladium complexes in the presence of halide ions and its relevance to the mechanism of palladium-catalyzed nucleophilic substitutions.” *J. Am. Chem. Soc.* **1993**, *115*, 9531-9541. d) C. Amatore, A. Jutand, M. A. M'Barki, “Evidence of the Formation of Zerovalent Palladium from Pd(OAc)<sub>2</sub> and Triphenylphosphine.” *Organometallics* **1992**, *11*, 3009-3012. (e) C. Amatore, E. Carré, A. Jutand, M. A. M'Barki, G. Meyer, “Evidence for the Ligation of Palladium(0) Complexes by Acetate Ions: Consequences on the Mechanism of Their Oxidative Addition with Phenyl Iodide and Pd(OAc)(PPh<sub>3</sub>)<sub>2</sub> as Intermediate in the Heck Reaction.” *Organometallics* **1995**, *14*, 5605-5614.

[10] S. Kozuch, S. Shaik, A. Jutand, C. Amatore, “Active Anionic Zero-Valent Palladium Catalysts: Characterization by Density Functional Calculations.” *Chem. Eur. J.* **2004**, *10*, 3072-3080.

[11] (a) L. J. Gooßen, D. Koley, H. Hermann, W. Thiel, “The mechanism of the oxidative addition of aryl halides to Pd-catalysts: a DFT investigation.” *Chem. Commun.* **2004**, 2141-2143. (b) L. J. Gooßen, D. Koley, H. Hermann, W. Thiel, “Mechanistic Pathways for Oxidative Addition of Aryl Halides to Palladium(0) Complexes: A DFT Study.” *Organometallics* **2005**, *24*, 2398-2410.

[12] J. Louie, J. F. Hartwig, “Transmetalation Involving Organotin Aryl, Thiolate, and Amide Compounds. An Unusual Type of Dissociative Ligand Substitution Reaction.” *J. Am. Chem. Soc.* **1995**, *117*, 11598-11599.

[13] (a) V. Farina, B. Krisnan, “Large Rate Accelerations in the Stille Reaction with Tri-2-furylphosphine and Triphenylarsine as Palladium Ligands: Mechanistic and Synthetic Implications.” *J. Am. Chem. Soc.* **1991**, *113*, 9585-9595. (b) V. Farina, G. P. Roth, “Recent Advances In The Stille Reaction.” L. S. Liebeskind, Ed., *Adv. Metalorg. Chem.* **1996**, *5*, Jai Press Ltd., England, page 1-53. (c) C. Amatore, A. Bahsoun, A. Jutand, G. Meyer, A. NdediNtepe, L. Ricard, “Mechanism of the Stille Reaction Catalyzed by Palladium Ligated to Arsine Ligand: PhPdI(AsPh<sub>3</sub>)(DMF) Is the Species Reacting with Vinylstannane in DMF.” *J. Am. Chem. Soc.* **2003**, *125*, 4212-4222.

[14] S. Kozuch, C. Amatore, A. Jutand, S. Shaik, “What Makes for a Good Catalytic Cycle? A Theoretical Study of the Role of an Anionic Palladium(0) Complex in the Cross-Coupling of an Aryl Halide with an Anionic Nucleophile.” *Organometallics* **2005**, *24*, 2319-2330.

- [15] (a) F. M. Bickelhaupt, T. Ziegler, P. v. R. Schleyer, "Oxidative Insertion as Frontside  $\text{S}_{\text{N}}2$  Substitution: A Theoretical Study of the Model Reaction System  $\text{Pd} + \text{CH}_3\text{Cl}$ ." *Organometallics* **1995**, *14*, 2288-2296. (b) A. Diefenbach, F. M. Bickelhaupt, "Oxidative addition of Pd to C—H, C—C and C—Cl bonds: Importance of relativistic effects in DFT calculations." *J. Chem. Phys.* **2001**, *115*, 4030-4040. (c) G. T. de Jong, M. Sola, L. Visscher, F. M. Bickelhaupt, "Ab initio benchmark study for the oxidative addition of  $\text{CH}_4$  to Pd: Importance of basis-set flexibility and polarization." *J. Chem. Phys.* **2004**, *121*, 9982-9992. (d) A. Diefenbach, G. T. de Jong, F. M. Bickelhaupt, "Activation of H—H, C—H, C—C and C—Cl Bonds by Pd and  $\text{PdCl}^-$ . Understanding Anion Assistance in C-X Bond Activation." *J. Chem. Theory Comp.* **2005**, *1*, 286-298.
- [16] (a) H. M. Senn, T. Ziegler, "Oxidative Addition of Aryl Halides to Palladium(0) Complexes: A Density-Functional Study Including Solvation." *Organometallics* **2004**, *23*, 2980-2988. (b) A. Sundermann, O. Uzan, J. M. L. Martin, "Computational Study of a New Heck Reaction Mechanism Catalyzed by Palladium(ii/iv) Species." *Chem. Eur. J.* **2001**, *7*, 1703-1711. (c) K. Albert, P. Gisdakis, N. Rösch, "On C—C Coupling by Carbene-Stabilized Palladium Catalysts: A Density Functional Study of the Heck Reaction." *Organometallics* **1998**, *17*, 1608-1616. (d) M. Reinhold, J. E. McGrady, R. N. Perutz, "A Comparison of C—F and C—H Bond Activation by Zerovalent Ni and Pt: A Density Functional Study." *J. Am. Chem. Soc.* **2004**, *126*, 5268-5276.
- [17] A. A. C. Braga, N. H. Morgon, G. Ujaque, F. Maseras, "Computational Characterization of the Role of the Base in the Suzuki-Miyaura Cross-Coupling Reaction." *J. Am. Chem. Soc.* **2005**, *127*, 9298-9307.
- [18] Gaussian 03, Revision B.01, M. J. Frisch, G. W. Trucks, H. B. Schlegel, G. E. Scuseria, M. A. Robb, J. R. Cheeseman, J. A. Montgomery, Jr., T. Vreven, K. N. Kudin, J. C. Burant, J. M. Millam, S. S. Iyengar, J. Tomasi, V. Barone, B. Mennucci, M. Cossi, G. Scalmani, N. Rega, G. A. Petersson, H. Nakatsuji, M. Hada, M. Ehara, K. Toyota, R. Fukuda, J. Hasegawa, M. Ishida, T. Nakajima, Y. Honda, O. Kitao, H. Nakai, M. Klene, X. Li, J. E. Knox, H. P. Hratchian, J. B. Cross, C. Adamo, J. Jaramillo, R. Gomperts, R. E. Stratmann, O. Yazyev, A. J. Austin, R. Cammi, C. Pomelli, J. W. Ochterski, P. Y. Ayala, K. Morokuma, G. A. Voth, P. Salvador, J. J. Dannenberg, V. G. Zakrzewski, S. Dapprich, A. D. Daniels, M. C. Strain, O. Farkas, D. K. Malick, A. D. Rabuck, K. Raghavachari, J. B. Foresman, J. V. Ortiz, Q. Cui, A. G. Baboul, S. Clifford, J. Cioslowski, B. B. Stefanov, G. Liu, A. Liashenko, P.

Piskorz, I. Komaromi, R. L. Martin, D. J. Fox, T. Keith, M. A. Al-Laham, C. Y. Peng, A. Nanayakkara, M. Challacombe, P. M. W. Gill, B. Johnson, W. Chen, M. W. Wong, C. Gonzalez, and J. A. Pople, Gaussian, Inc., Pittsburgh PA, **2003**.

[19] A. D. Becke, "Density-functional exchange-energy approximation with correct asymptotic behaviour." *Phys. Rev. A* **1988**, 38, 3098-3100.

[20] J. P. Perdew, "Density-functional approximation for the correlation energy of the inhomogeneous electron gas." *Phys. Rev. B* **1986**, 33, 8822-8824.

[21] W. J. Hehre, L. Radom, P. v. R. Schleyer, J. A. Pople, "Ab Initio Molecular Orbital Theory.", Wiley, New York, **1986**.

[22] P. J. Hay, W. R. Wadt, "*Ab initio* effective core potentials for molecular calculations. Potentials for K to Au including the outermost core orbitals." *J. Chem. Phys.* **1985**, 82, 299-310.

[23] D. Andrae, U. Häußermann, M. Dolg, H. Stoll, H. Preuß, "Energy-adjusted ab initio pseudopotentials for the second and third row transition elements." *Theor. Chim. Acta* **1990**, 77, 123-141.

[24] (a) V. Barone, M. Cossi, "Quantum Calculations of Molecular Energies and Gradients in Solutions by a Conductor Solvent Model." *J. Phys. Chem. A* **1998**, 102, 1995-2001. (b) M. Cossi, N. Rega, G. Scalmani, V. Barone, "Energies, Structures, and Electronic Properties of Molecules in Solution with the C-PCM Solvation Model." *J. Comput. Chem.* **2003**, 24, 669-681.

[25] (a) A Klamt, G. Schüürmann, "COSMO: A New Approach to Dielectric Screening in Solvents with Explicit Expressions for the Screening Energy and its Gradient." *J. Chem. Soc. Perkin Trans 2*. **1993**, 799-805. (b) A. Schäfer, A. Klamt, D. Sattel, J. C. W. Lohrenz, F. Eckert, "COSMO Implementation in TURBOMOLE: Extension of an efficient quantum chemical code towards liquid systems." *Phys. Chem. Chem. Phys.* **2000**, 2, 2187-2193.

[26] (a) A. E. Reed, L. A. Curtiss, F. Weinhold, "Intermolecular Interactions from a Natural Bond Orbital, Donor-Acceptor Viewpoint." *Chem. Rev.* **1998**, 88, 899-926. (b) E. D. Glendening, A. E. Reed, J. E. Carpenter, Weinhold, F. *NBO Version 3.1*.

[27] Adding a bare metal counterion ( $K^+$ ) in the calculation of the anion **1** leads to dissociation into the corresponding neutral palladium species and the metal acetate. Such a gas-



phase description is however not realistic because the ions will be solvated under the experimental conditions, and counterions are therefore not included in this work.

[28] K. J. Laidler, "Chemical Kinetics.", 3<sup>rd</sup> Ed., Harper and Row Publishers, New York, NY, 1987.

[29] C. Amatore, A. Jutand, "Mechanistic and kinetic studies of palladium catalytic systems." *J. Organomet. Chem.* **1999**, 576, 254-278.







## Density Functional Study of Proton Sponges: Proton Affinity, Structural Behavior and Palladium Complexes.

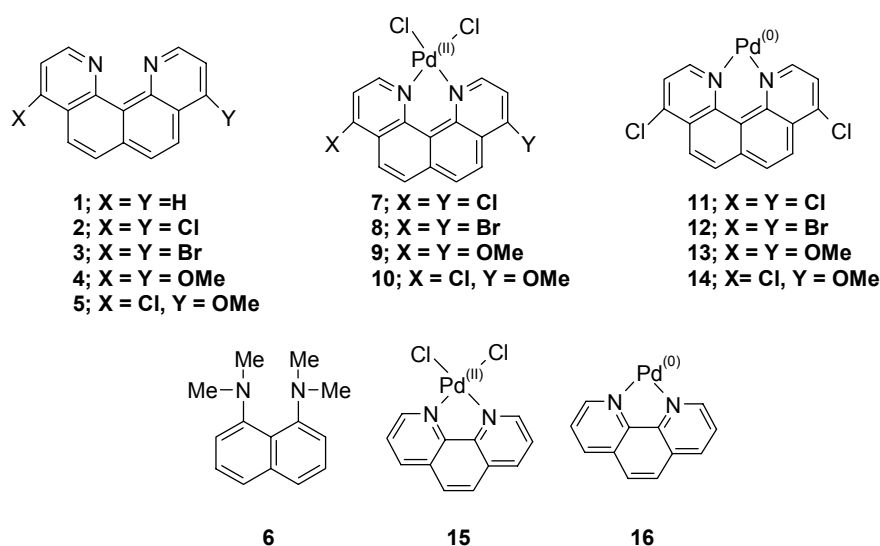
*The rapid progress true Science now makes occasions my regretting sometimes that I was born so soon. It is impossible to imagine the heights to which may be carried, in a thousand years, the power of man over matter. O that moral science were in as fair a way of improvement, that men would cease to be wolves to one another, and that human beings would at length learn what they now improperly call humanity.*

(Benjamin Franklin, Letters to Joseph Priestley, 8<sup>th</sup> Feb 1780, In Linus Pauling, College Chemistry, Chapter 1, page 3)

### 5.1 Introduction

Proton sponges are organic diamines with exceptionally enhanced basicity. According to literature data sources, around 200 papers have been published on proton sponges and their complexes.[1] The parent proton sponge 1,8-*bis*(dimethylamino)naphthalene **6** has been known since the early 1940s.[2] However, its high basicity ( $pK_a \sim 12$ ) was realized by Alder *et al.*[3] only in the late 1960s. With mineral or organic acids proton sponges form very stable ionic complexes containing strong, charge-induced intramolecular H-bonds. Recent research in the field of proton sponges has followed several routes: (a) synthesis of novel proton sponges and their complexes;[4,5,6] (b) computational investigations of factors responsible for enhanced basicity, such as cationic H-bond energies,[7,8] strain energies[8,9,10,11,12] and aromatic stabilization energies;[13,14] (c) experimental studies of structural and spectroscopic properties;[15,16] and (d) applications in catalysis.[17]

## Scheme 5.1



The original proton sponges were *bis*(dialkylamino)arenes in which the basic centers, and thus the N...H...N hydrogen bridges of the conjugate acids are hydrophobically shielded by alkyl substituents. In 1987 Zirnstein and Staab synthesized a new type of proton sponge, 4,9-dichloroquino[7,8-*h*]quinoline **2**, in which such hydrophobic shielding is absent while the two nitrogen atoms are arranged in a manner similar to **6** (Scheme 5.1).[18,19] Recently Wüstefeld *et al.* reported transition metal complexes of the proton sponge ligand **2** and briefly discussed the bonding situation in these complexes.[20] The X-ray structure of the platinum complex reveals a strongly bowed aromatic system with an extreme “out-of-plane” position of the metal atom[20] which should make it readily accessible and catalytically active.

This chapter describes the results from a DFT study that addresses the structural and electronic properties of the proton sponges displayed in Scheme 5.1, and the stability and reactivity of their palladium complexes.

## 5.2 Computational Details

All calculations were performed with the Gaussian98 and Gaussian03 suites of programs.[21] Unless noted otherwise, the DFT calculations employed the BP86 functional[22,23] using the standard 6-31G\* basis[24] for all atoms except palladium which is described by the LANL2DZ(Los Alamos) small-core pseudopotential[25] with the associated basis set.[25,21]

Geometries were fully optimized, normally without symmetry constraints (exceptions see below). Harmonic force constants were computed at the optimized geometries to characterize the stationary points as minima or saddle points. Zero-point vibrational corrections were determined from the harmonic vibrational frequencies to convert the total energies  $E_e$  to ground-state energies  $E_0$ . The rigid-rotor harmonic-oscillator approximation was applied for evaluating the thermal and entropic contributions that are needed to derive the enthalpies  $H_{298}$  and Gibbs free enthalpies  $G_{298}$  at 298K. Transition states were located from a linear transit scan in which the reaction coordinate was kept fixed at different distances while all other degrees of freedom were optimized. After the linear transit search the transition states were optimized using the default Berny algorithm implemented in the Gaussian code. The proton transfer reactions for the proton sponges were studied using the B3LYP functional[22,26,27] with the standard 6-31G\* basis.[24]

The ligands (**1-5**) and their corresponding conjugate acids (**1H<sup>+</sup>-5H<sup>+</sup>**) were fully optimized in the solvent dichloromethane which was described by a polarized continuum model[28] (dielectric constant  $\epsilon = 8.93$ ). Specifically, we employed the SCI-PCM method which involves an SCRF (Self Consistent Reaction Field) calculation using a cavity determined self-consistently from an isodensity surface.[29] Numerical second derivatives were computed for all the structures thus optimized, in order to evaluate the thermochemistry in solution. To study the weak interactions and characterize the H-bonds, we have used Bader's AIM (atoms-in-molecule) theory as implemented in the MORPHY program.[30]

In the study of the Heck olefination process, single-point solvent calculations were done at the optimized gas-phase geometries for all relevant intermediates. The polarized continuum model (PCM) of Tomasi *et al.*[28] was employed using N-methyl-2-pyrrolidone (NMP) as solvent (dielectric constant  $\epsilon = 32.2$ ) with Pauling radii for the respective atoms (Pd, H, C, Cl, Br, N). Weinhold's natural population analysis (NPA) was applied to address the charge distribution around the metal center for all complexes.[31] Wiberg bond indices (WBIs) were also calculated to quantify covalent interactions.[32]

### 5.3 Results and discussion

#### 5.3.1 Ligands

##### 5.3.1.1 Structural features

The ligands **1-5** were first computed without symmetry constraints ( $C_1$ ). Compounds **2-4** were also optimized under the constraint of planarity ( $C_s$ , xy plane = molecular plane). In the case of the dichloro compound **2**, additional optimizations were done in the following point groups:

- $C_2$  :  $C_2$  axis = C12—C15 central bond, nonplanar structure possible.
- $C_s$  :  $C_s$  plane containing C12—C15 central bond = yz plane perpendicular to the aromatic rings, nonplanar structure possible.
- $C_{2v}$  :  $C_2$  axis = C12—C15 central bond, planar structure imposed.

These calculations show that the minimum structures are slightly nonplanar and have  $C_2$  symmetry (explicitly proven only for **2**). The planar structures are about 0.1-0.2 kcal/mol less stable and have one negative eigenvalue of the force constant matrix (transition state for inversion, very low imaginary frequency, effectively  $C_{2v}$  symmetry as shown explicitly for **2**). In the dichloro compound **2**, the  $C_1$  and  $C_2$  runs yield the same nonplanar structure.

Table 5.1 presents optimized structural parameters for the ligands in the gas phase (**1-5**) and in dichloromethane solution (**1s-5s**) as well as the corresponding data for their conjugated acids (**1H<sup>+</sup>-5H<sup>+</sup>**, **1sH<sup>+</sup>-5sH<sup>+</sup>**). The first line of Table 5.1 lists some experimental X-ray data[19] for the parent compound **1**: the distances obviously agree well with the calculated values, but the measured out-of-plane twist in the crystal is smaller than the computed gas-phase value (see further discussion below).

Table 5.2 collects the energies of the planar structures relative to the nonplanar minimum. It also includes the computed imaginary frequencies for these planar structures.

Experimentally, the ligands (**1**, **2**, **4**) are essentially planar;[19,33] in the case of the bromo compound **3** experimental data are not yet available.[33] Given the tiny energy differences computed between the nonplanar and planar structures (Table 5.2) it is conceivable that intermolecular interactions and packing effects in the crystals can overcome the predicted geometric preference and lead to planar structures. On the other hand, slight  $C_2$  distortions in the free ligands **1-4** seem plausible because they relieve the steric interactions between the two nitrogen atoms (lone pairs).



The published[19] experimental X-ray structure for the parent compound **1** shows some C<sub>2</sub>-type distortion since the two nitrogen atoms lie 0.07 Å above and 0.06 Å below the best plane through the ten “naphthalene” carbon atoms, respectively. The corresponding computed values are 0.24 Å. It should be stressed again, however, that the predicted deviations from planarity in the ligands **1-4** are rather small (dihedral angles of 8-11°, Table 5.1) and energetically of little consequence (energy differences of 0.1-0.3 kcal/mol, Table 5.2).

The optimization of the ligands in dichloromethane (**1s-5s**) leads to slight changes in the geometrical parameters (Table 5.2). The distances between the N atoms increase upon solvation for all the proton sponges by about 0.02 Å while the other changes are less pronounced. The dipole moments become significantly larger upon solvation (Table 5.1).

**Table 5.1. Structural parameters and dipole moments for the substituted quino[7,8-*h*]quinolines and their conjugated acids (BP86/6-31G\* results)**

No.	Substituents	Point group	N1-N2 (Å)	N2-H11 (Å)	N1-H11-N2 (°)	C16-C14 (Å)	C5-C6 (Å)	Φ <sup>a</sup> (°)	θ <sup>a</sup> (°)	Φ+θ (°)	A (D) <sup>b</sup>
1 <sup>c</sup>	H	C <sub>1</sub>	2.728	—	—	2.584	2.450	1.40	—	—	—
<b>1</b>	H	C <sub>1</sub>	2.739	—	—	2.586	2.464	9.68	9.68	19.36	1.847
<b>2</b>	Cl	C <sub>1</sub> /C <sub>2</sub>	2.709	—	—	2.579	2.467	11.52	11.52	23.04	0.732
<b>3</b>	Br	C <sub>1</sub>	2.708	—	—	2.579	2.467	11.48	11.48	22.96	0.813
<b>4</b>	OCH <sub>3</sub>	C <sub>1</sub>	2.723	—	—	2.585	2.462	9.83	9.83	19.66	0.597
<b>1</b>	H	C <sub>s</sub>	2.733	—	—	2.599	2.455	0.00	0.00	0.00	1.912
<b>2</b>	Cl	C <sub>s</sub> /C <sub>2v</sub>	2.701	—	—	2.598	2.453	0.00	0.00	0.00	0.757
<b>3</b>	Br	C <sub>s</sub>	2.699	—	—	2.598	2.453	0.00	0.00	0.00	0.842
<b>4</b>	OCH <sub>3</sub>	C <sub>s</sub>	2.716	—	—	2.598	2.453	0.00	0.00	0.00	0.692
<b>5</b>	Cl & OCH <sub>3</sub>	C <sub>1</sub>	2.715	—	—	2.582	2.465	10.92	10.49	20.98	3.775
<b>1s</b>	H	C <sub>1</sub>	2.760	—	—	2.593	2.461	9.35	9.35	18.70	2.753
<b>2s</b>	Cl	C <sub>1</sub>	2.725	—	—	2.583	2.464	11.53	11.53	23.06	1.225
<b>3s</b>	Br	C <sub>1</sub>	2.724	—	—	2.582	2.464	11.62	11.62	23.24	1.337
<b>4s</b>	OCH <sub>3</sub>	C <sub>1</sub>	2.743	—	—	2.595	2.457	8.72	8.72	17.44	1.094
<b>5s</b>	Cl & OCH <sub>3</sub>	C <sub>1</sub>	2.733	—	—	2.588	2.462	10.89	10.31	20.62	4.720
<b>1H<sup>+</sup></b>	H	C <sub>1</sub>	2.611	1.078	142.09	2.546	2.487	0.00	0.00	0.00	—
<b>2H<sup>+</sup></b>	Cl	C <sub>1</sub>	2.592	1.080	142.62	2.550	2.484	0.00	0.00	0.00	—
<b>3H<sup>+</sup></b>	Br	C <sub>1</sub>	2.592	1.080	142.65	2.550	2.484	0.00	0.00	0.00	—
<b>4H<sup>+</sup></b>	OCH <sub>3</sub>	C <sub>1</sub>	2.594	1.078	142.29	2.546	2.484	0.00	0.00	0.00	—
<b>5H<sup>+</sup></b>	Cl & OCH <sub>3</sub>	C <sub>s</sub>	2.604	1.070	141.47	2.551	2.482	0.00	0.00	0.00	—
<b>5H<sup>+</sup>a</b>	Cl & OCH <sub>3</sub>	C <sub>s</sub>	2.578	1.089	143.58	2.544	2.485	0.00	0.00	0.00	—
<b>1sH<sup>+</sup></b>	H	C <sub>1</sub>	2.618	1.071	140.90	2.548	2.487	0.00	0.00	0.00	—
<b>2sH<sup>+</sup></b>	Cl	C <sub>1</sub>	2.597	1.073	141.39	2.550	2.483	0.00	0.00	0.00	—
<b>3sH<sup>+</sup></b>	Br	C <sub>1</sub>	2.598	1.073	141.34	2.551	2.482	0.01	0.00	0.01	—
<b>4sH<sup>+</sup></b>	OCH <sub>3</sub>	C <sub>1</sub>	2.603	1.070	141.15	2.549	2.483	0.01	0.00	0.01	—
<b>5sH<sup>+</sup>a</b>	Cl & OCH <sub>3</sub>	C <sub>1</sub>	2.616	1.063	139.91	2.554	2.481	0.00	0.00	0.00	—

<sup>a</sup>Dihedral angles: Φ = N1-C16-C15-C14; θ = C16-C15-C14-N2, <sup>b</sup>The (origin-dependent) dipole moment is not reported for the cations. <sup>c</sup>X-ray data from ref. 19; all other entries are computational results.

**Table 5.2.** Energies (kcal/mol) of planar relative to twisted ligands and imaginary frequencies  $\omega$  ( $i$  cm<sup>-1</sup>) for the inversion mode in the planar structures (BP86/6-31G\* results)

No.	Substituent	Point group	$\Delta E_c$	$\Delta E_0$	$\Delta H_{298}$	$\Delta G_{298}$	$\omega$
1	H	C <sub>s</sub>	0.1	0.1	-0.4	1.0	38
2	Cl	C <sub>s</sub> /C <sub>2v</sub>	0.3	0.2	-0.3	1.1	38
3	Br	C <sub>s</sub>	0.3	0.3	-0.2	1.3	37
4	OCH <sub>3</sub>	C <sub>s</sub>	0.1	0.2	-0.4	1.3	32

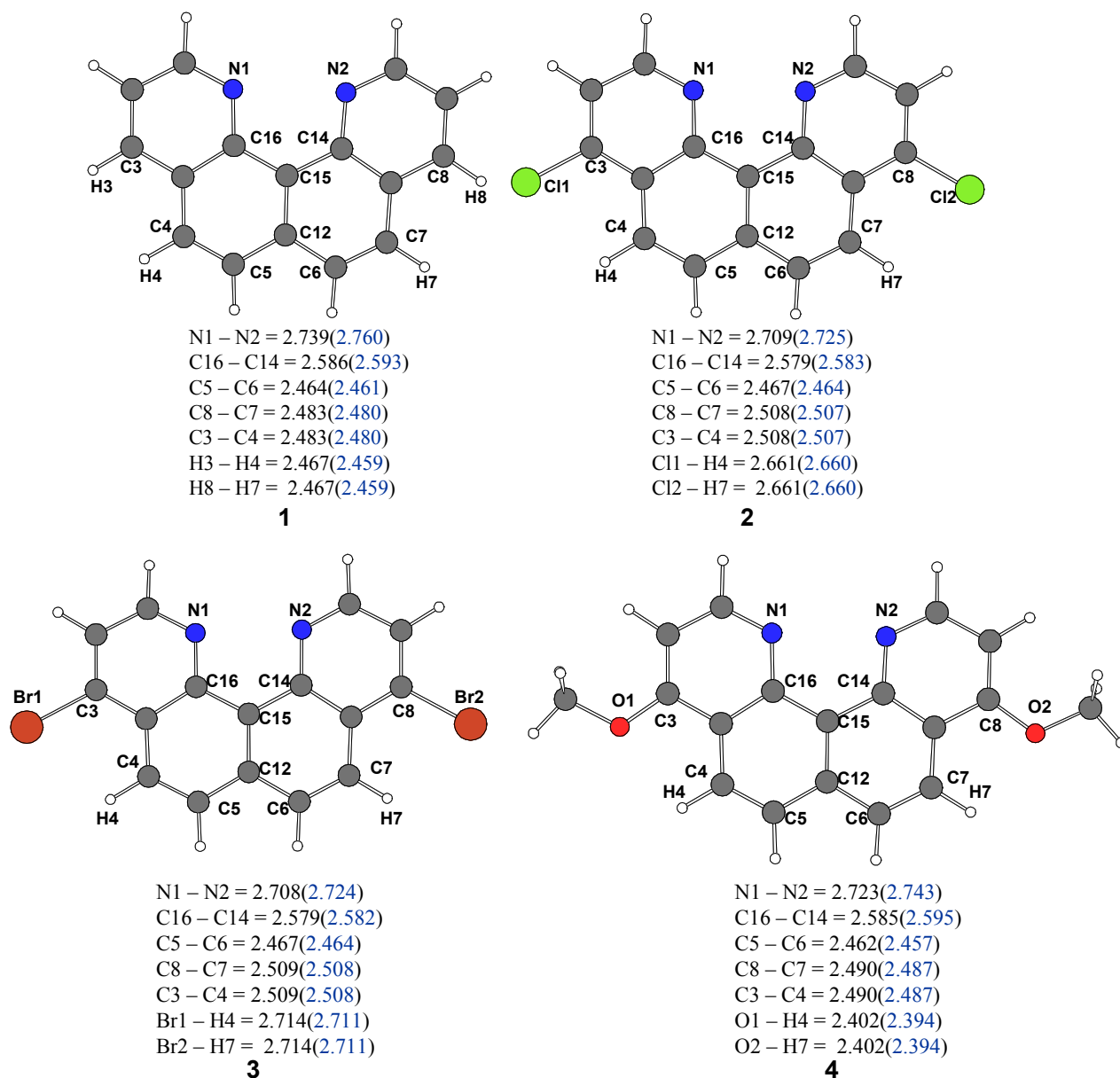


**Figure 5.1.** Optimized structures of the proton sponges (1-4) in the gas phase including selected bond lengths in Å. The values in parentheses represent the optimized parameters in dichloromethane.

### 5.3.1.2 Conjugate acids and proton affinity

Over the past decade, there have been numerous computational studies of Alder-type proton sponges such as **6** and their conjugate acids.[8,9,10,12,13,34] One of the central goals of these investigations was to understand the high basicities of proton sponges. There is general consensus that the conjugate acids such as **6H**<sup>+</sup> are stabilized by a strong intramolecular hydrogen bond [N—H···N]<sup>+</sup> which is asymmetric and contains one covalent N—H bond, with a relatively small barrier to intramolecular proton transfer.[11,35] An analysis of solution NMR spectra with isotopic perturbation confirms that the proton in **6H**<sup>+</sup> resides in a double-well potential,[36] in analogy to the situation in dicarboxylic acids.[37] The enhanced proton affinity of Alder-type proton sponges relative to amines is mainly attributed to the formation of a strong intramolecular hydrogen bond (see above) but other factors may also contribute:[8,13] (a) the relief of strain caused by loss of destabilizing lone-pair repulsion between the two nitrogen atoms upon protonation **6** → **6H**<sup>+</sup>;<sup>[35]</sup> (b) the more pronounced electron delocalization in the conjugate acid **6H**<sup>+</sup>;<sup>[8,13]</sup> (c) the higher solvation energy of the protonated cation **6H**<sup>+</sup> in polar solvents.[8,13] The cited theoretical studies have analyzed and quantified these effects in Alder-type proton sponges such as **6**[8,9,10,11,13,35] and have also attempted to establish relationships between basicity, hydrogen-bond strengths, and structural parameters.

In the present work we have studied the basicities of proton sponges (**1-5**) both in the gas phase and in dichloromethane (solvent). Table 5.1 and Figure 5.2 report some key details of the optimized structures of the conjugate acids, including the N···N distances, N—H distances and N—H···N hydrogen-bonding angles.

As pointed out before, the aromatic systems in **1-5** are distorted (nonplanar), to reduce the repulsive interaction between the nitrogen lone-pairs. In the respective conjugate acids, one of these lone-pairs becomes an N—H bonding electron pair upon protonation, and the repulsive lone-pair interaction is replaced by a cationic hydrogen bond. Therefore, these conjugate acids have completely planar structures with substantially reduced N—N distances (cf. Figure 5.1 and 5.2). For example, the N—N distance in **1H**<sup>+</sup> is 2.611 Å, which is 0.128 Å less than in **1**.

To study the basicities of these proton sponges, we have calculated the proton affinities both in the gas phase and in dichloromethane using the general formula,[38]

$$\text{Proton affinity (PA)} = H_{298}(\text{base, B}) - H_{298}(\text{conjugate acid, BH}^+).$$

where  $H_{298}$  denotes the absolute enthalpy at 298 K.

The results are documented in Table 5.3. The computed values are higher in solution than in the gas phase, by 31-36 kcal/mol, which reflects the higher electrostatic stabilization of the conjugate acid cation by solvation.

The computed (BP86) gas-phase proton affinity for **6** is 248.5 kcal/mol which is in good accordance with the (MP2/6-31G\*\*/HF/6-31G\*) value obtained by Peräkylä (248.9 kcal/mol).[11] Moreover, the proton affinity of **6** is lower than that of the Staab-type proton sponges (**1-4**)[18,19] that we have investigated in this work, by 3-18 kcal/mol (Table 5.3). Proton sponge **4** shows the highest proton affinity (266.1 kcal/mol), which may indicate a particularly strong stabilization of the protonated cation by enhanced electron delocalization due to the *trans*-oriented methoxy substituents.

**Table 5.3. Proton affinities in kcal/mol (BP86/6-31G\* results)**

	Gas phase		Solution <sup>a</sup>
<b>1</b>	256.3	<b>1s</b>	291.3
<b>2</b>	251.2	<b>2s</b>	287.7
<b>3</b>	251.9	<b>3s</b>	287.8
<b>4</b>	266.1	<b>4s</b>	297.0
<b>5</b>	259.5	<b>5s</b>	293.5
<b>5a</b>	258.1		
<b>6</b>	248.5		

<sup>a</sup>Solvent dichloromethane.

Figure 5.3 illustrates the proton transfer in the conjugate acids of symmetrically (**6**, **2**) and asymmetrically (**5**) substituted proton sponges. In the former case, reactant and product are identical ( $6\text{H}^+ \rightarrow 6\text{H}^+$ ,  $2\text{H}^+ \rightarrow 2\text{H}^+$ ), and the corresponding transition states are symmetrical ( $C_{2v}$ ). In the latter case ( $5\text{H}^+ \rightarrow 5\text{H}^+\text{a}$ ), the reactant is more stable by 2.3 kcal/mol ( $\Delta E_c$ ) indicating that the positive charge at the protonated nitrogen atom is better stabilized by the electron-donating p-methoxy substituent in  $5\text{H}^+$  than by the p-chloro substituent in  $5\text{H}^+\text{a}$ .

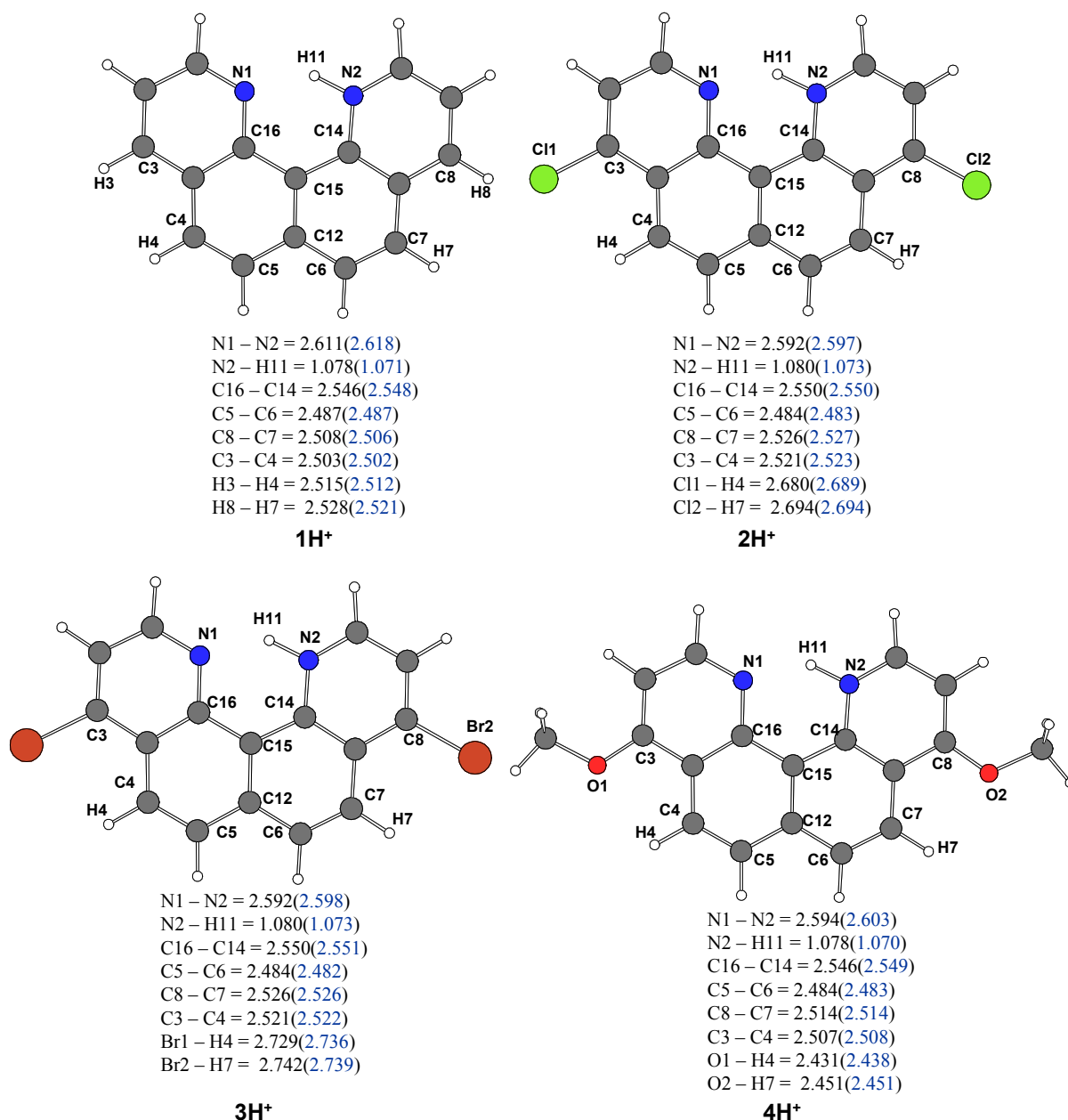


**Figure 5.2.** Optimized structures of the protonated proton sponges (**1H<sup>+</sup>**–**4H<sup>+</sup>**) in the gas phase including selected bond lengths in Å. The values in parentheses represent the optimized parameters in dichloromethane.

In order to provide a potential curve for proton transfer, we have performed B3LYP/6-31G\* optimizations where we constrained the difference between the two different N–H distances ( $r_1$ – $r_2$ ) and relaxed the other degrees of freedom. The resulting potential curves are shown in Figure 5.4. In each case, we find a double-well potential in agreement with the experimental evidence for **6H<sup>+</sup>**.<sup>[36]</sup> The actual transition states were located by eigenvector following starting from the highest point of these curves. Each of these transition states has one mode with an imaginary frequency (Figure 5.3) representing the motion of the proton between the

two nitrogen atoms. The barriers for  $6\text{H}^+$ ,  $2\text{H}^+$  and  $5\text{H}^+$  are computed to be 1.2, 3.6 and 4.9 kcal/mol ( $\Delta E_e$ ), respectively, at the B3LYP/6-31G\* level.

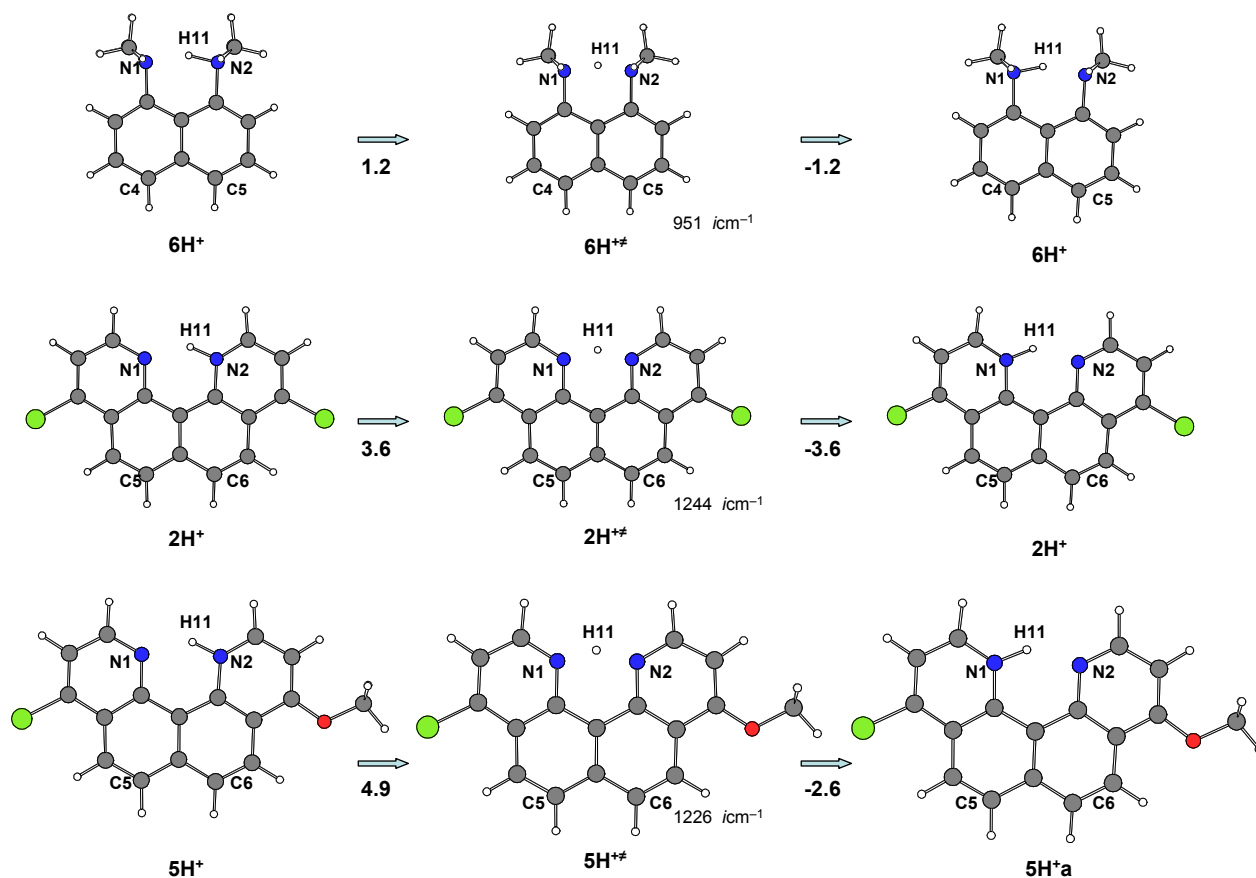


**Figure 5.3.** Reaction scheme for proton transfer. Energies ( $\Delta E_e$ ) are given in kcal/mol (B3LYP/6-31G\*).

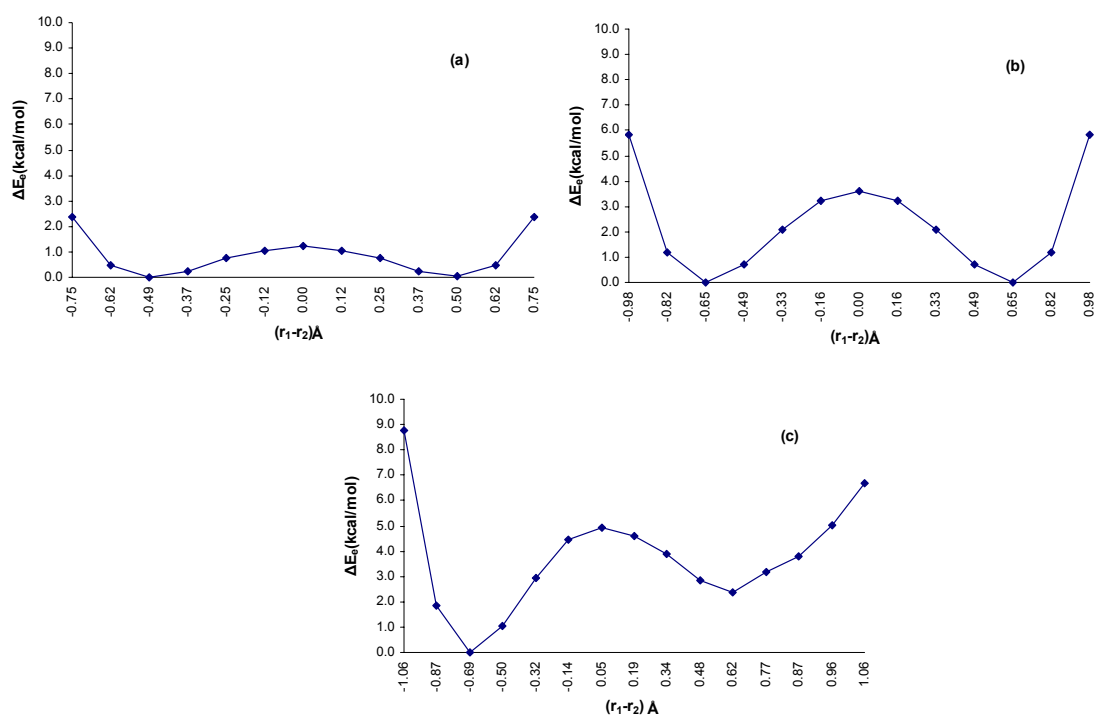


**Figure 5.4.** Potential energy curves for N...H...N proton transfer (a)  $6\text{H}^+$ , (b)  $1\text{H}^+$ , (c)  $5\text{H}^+$  (B3LYP/6-31G\*, see text).

Table 5.4 lists selected geometrical parameters, HOMO-LUMO gaps, and NPA charges on the migrating proton for the species shown in Figure 5.3. The N—N distances in the transition states ( $6\text{H}^{+\ddagger}$ ,  $2\text{H}^{+\ddagger}$  and  $5\text{H}^{+\ddagger}$ ) are smaller than those in the respective conjugate acids ( $6\text{H}^+$ ,  $2\text{H}^+$ ,  $5\text{H}^+$ ,  $5\text{H}^+\text{a}$ ). There is also an increase in the N—H—N bond angle in  $6\text{H}^{+\ddagger}$ ,  $2\text{H}^{+\ddagger}$  and  $5\text{H}^{+\ddagger}$  which is larger and closer to linearity in  $6\text{H}^{+\ddagger}$  than in  $2\text{H}^{+\ddagger}$  or  $5\text{H}^{+\ddagger}$  (by  $12^\circ$ ). It has been suggested[39] that a larger N—H—N angle leads to a smaller proton-transfer barrier which is consistent with our results because the lowest barrier is found for  $6\text{H}^+$  (see Figure 5.4).

We have also performed a natural bond orbital analysis[31] for the proton transfer reactions in Figure 5.3, with focus on the N(1)—H(11)—N(2) fragment, where one may expect some charge transfer. The NPA charge on H(11) generally becomes slightly smaller in the transition state (by 0.005-0.009  $e$ ). N(1) and N(2) change their roles as H-bond acceptors and donors during proton transfer which is accompanied by a charge transfer of 0.045  $e$  between N(1) and N(2).

**Table 5.4. Structural parameters, HOMO-LUMO gaps and NPA charge of the bridging H(11) for the conjugated acids and their respective proton transfer transition states (B3LYP/6-31G\*).**

No.	N(1)—H(11) (Å)	N(2)—H(11) (Å)	N(1)—N(2) (Å)	N(1)—H(11)—N(2) (°)	HOMO-LUMO gap (eV)	Charge on H <sup>+</sup> ( $e$ )
$6^*\text{H}^+$	1.593	1.099	2.642	157.39	4.68	0.494
$6^*\text{H}^{+\ddagger}$	1.293	1.293	2.550	160.96	4.69	0.489
$6^*\text{H}^+$	1.099	1.593	2.642	157.39	4.68	0.494
$2^*\text{H}^+$	1.706	1.054	2.609	140.89	3.75	0.484
$2^*\text{H}^{+\ddagger}$	1.283	1.283	2.472	148.90	3.98	0.476
$2^*\text{H}^+$	1.054	1.706	2.609	140.89	3.75	0.484
$5^*\text{H}^+$	1.735	1.047	2.622	139.69	3.99	0.482
$5^*\text{H}^{+\ddagger}$	1.259	1.308	2.472	148.76	3.97	0.475
$5^*\text{H}^+\text{a}$	1.060	1.682	2.599	141.76	3.58	0.484

### 5.3.1.3 Strain energy

Perrin proposed that the unusually strong low-barrier hydrogen bond in proton sponges is mainly attributed to the relief of strain on protonation[36,37] and several attempts were made to evaluate the strain energies.[8,9,11,13]

Peräkylä[11] estimated the strain energy of the prototypical Alder proton sponge **6** from the isodesmic reaction [40] displayed in Scheme 5.2(a):

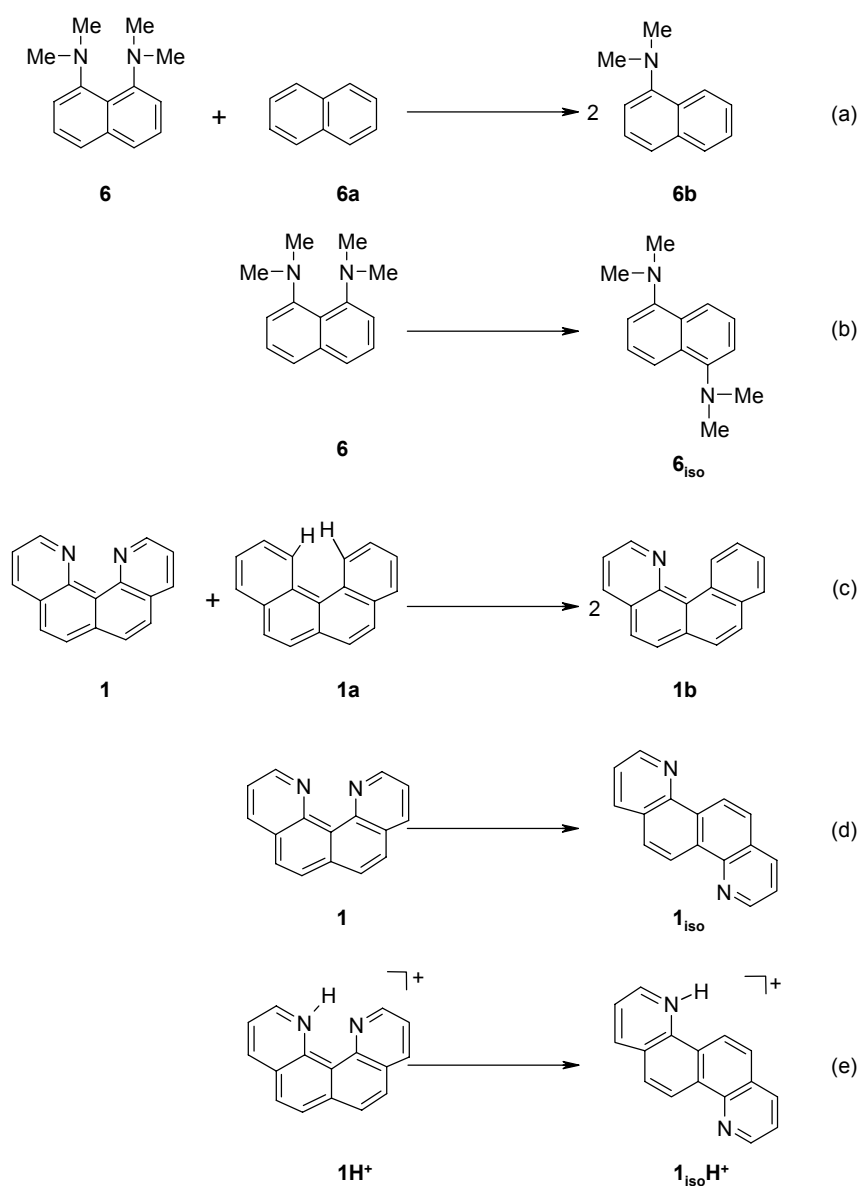
$$\text{Strain energy (SE)}(\mathbf{6}) = H_{298}(\mathbf{6}) + H_{298}(\mathbf{6a}) - 2H_{298}(\mathbf{6b}) \quad (5.1)$$

where the term  $H_{298}$  in eqn. 5.1 represents the absolute enthalpy at 298 K.

The strain energy obtained for **6** is 5.7 kcal/mol ( $\Delta E_e = 5.7$  kcal/mol), which is in excellent agreement with Peräkylä's result (5.4 kcal/mol at MP2/6-31G\*//HF/6-31G\* + ZPE).[11] An alternative estimate of the strain energy in **6** is provided by the isomerization reaction **6**  $\rightarrow$  **6<sub>iso</sub>** in Scheme 2(b) which yields a slightly lower value of 5.0 kcal/mol.

In the case of the Staab-type proton sponge **1**, the isodesmic reaction in Scheme 5.2(c) cannot be used for estimating the strain energy in **1** because the reference compound **1a** is severely strained itself due to the steric hindrance between the two nearly overlapping hydrogen atoms (see drawing of **1a**).

**Scheme 5.2. Reactions for calculating strain energies and H-bond energies**



We have therefore evaluated the strain energy in **1** from the isomerization reaction in Scheme 5.2(d) and obtain a value of 10.7 kcal/mol ( $\Delta E_e = 11.1$  kcal/mol). Since the difference between



the strain energies obtained from isodesmic and isomerization reactions is only 0.7 kcal/mol (*vide supra*) for the Alder-type proton sponge **6**, we expect the calculated value for **1** (10.7 kcal/mol) to be realistic. Comparing **1** and **6**, the strain energy from isomerization is thus higher in **1** by 5.7 kcal/mol which accounts for the major part of the difference in the computed gas-phase proton affinities (7.8 kcal/mol, see Table 5.3).

The isomerization reactions in Scheme 5.2(b,d) may also involve some change in the resonance energy of the  $\pi$  system. To confirm that this effect is negligible compared with the change in the strain energy, we have calculated the Hückel energies[21,41,42] of the respective isomers (*i.e.* **1** and **1<sub>iso</sub>**). These Hückel energies differ by only 0.4 kcal/mol which indicates that  $\pi$ -electron delocalization is indeed similar in both isomers.

In the conjugate acid **1H<sup>+</sup>**, the isomerization reaction in Scheme 5.2(e) is endothermic by 13.7 kcal/mol ( $\Delta E_e = 13.2$  kcal/mol). The stabilization by the intramolecular hydrogen bond (favoring **1H<sup>+</sup>**) thus overcomes the destabilization due to strain (favoring **1<sub>iso</sub>H<sup>+</sup>**). Assuming identical changes of the strain energies during the isomerizations 5.2(d,e) the strength of the intramolecular hydrogen bond in **1H<sup>+</sup>** can be estimated as  $13.7 + 10.7 = 24.4$  kcal/mol ( $\Delta E_e = 24.3$  kcal/mol).

#### 5.3.1.4 Bader analysis

In 1994, Wozniak, Howard and coworkers applied Bader's AIM concept[30] to characterize the electron distribution in the proton sponge **6** and its conjugate acid **6H<sup>+</sup>**. [10] We have performed an analogous topological analysis of the total electron densities for **6**, **2**, **5** and their respective proton transfer transition states (see Figure 5.3).

Any bonded pair of atoms has a bond path, *i.e.*, a connecting line with maximum electron density. The bond critical point (BCP) is a point on this line where the gradient  $\nabla\rho_b$  of the density is equal to zero. The magnitude of the electron density ( $\rho_b$ ) and its Laplacian ( $\nabla^2\rho_b$ ) at the BCP provide information about the strength and type of bond. The Laplacian indicates whether the density is locally concentrated ( $\nabla^2\rho_b < 0$ ) or depleted ( $\nabla^2\rho_b > 0$ ). Ellipticities at BCP represent the deviations of the bonding density from cylindrical symmetry. It is quantitatively expressed as  $\epsilon = \lambda_2/\lambda_1 - 1$ , where  $\lambda_1$  and  $\lambda_2$  are eigenvalues of the Hessian of  $\rho$  at BCP.[30]

The total charge density at (3,-1) BCPs,  $\rho_b$ , the Laplacian of the charge density at this point  $\nabla^2\rho_b$ , and the respective ellipticities,  $\epsilon_b$  are reported in Table 5.5. The  $\epsilon_b$  values reflect the extent of the  $\pi$ -bonding character in a given aromatic frame work.[43]

The large values of  $\rho_b$  and  $\nabla^2\rho_b$  in C(1)—N(1) for **6** indicate that the nitrogen lone pair density has become partially delocalized over the  $\pi$ -system of the molecule. Similar observations are also reported by Platts *et al.*[10] In fact, even higher  $\rho_b$  values (in the C(16)—N(1) bond) for **2** and **5** support a significant delocalization of the nitrogen lone pair over the aromatic system (Table 5.5). After protonation, the largest charge depletion occurs in the C—N bond and also the C—C bond ellipticities change (Table 5.5).

In the proton sponges **6**, **2** and **5**, the  $\nabla^2\rho_b$  values for the fused C—C bond (*i.e.* C(9)—C(10) for **6** and C(15)—C(12) for **2** and **5**) are relatively low (Table 5.5). The N(1)—H(11) bond shows a moderate amount of electron density in **2H<sup>+</sup>** and **5H<sup>+</sup>a** (–1.403 au and –1.360 au). The low negative values of  $\nabla^2\rho_b$  for the N—H bond are uncommon for hydrogen bonds but they have also been found in calculations of other strong H-bonded systems.[10]

The aromaticity has decreased in the aromatic framework after protonation of the proton sponges.[10] There is an increase of the charge density at the fused C—C bond which is reflected in its higher negative value  $\nabla^2\rho_b$  (Table 5.5).

We have found a (3,+1) ring critical point with a single negative curvature of  $\rho_b$  (RCP), directed along the axis perpendicular to the ring surface, for **6**, **2** and **5**.

**Table 5.5. Electron density  $\rho_b$ , Laplacian of the electron density  $\nabla^2\rho_b$  and ellipticities  $\epsilon_b$  at BCPs in **6**, **2**, **5**, the respective conjugate acids (**6H<sup>+</sup>**, **2H<sup>+</sup>**, **5H<sup>+</sup>a**) and the proton transfer transition states (**6H<sup>+</sup>‡**, **2H<sup>+</sup>‡**, **5H<sup>+</sup>‡**)**

<b>6</b>				<b>6H<sup>+</sup></b>			<b>6H<sup>+</sup>‡</b>		
Bonds	$\rho_b$	$\nabla^2\rho_b$	$\epsilon_b$	$\rho_b$	$\nabla^2\rho_b$	$\epsilon_b$	$\rho_b$	$\nabla^2\rho_b$	$\epsilon_b$
N(1)—H(11)	—	—	—	0.266	-1.168	0.001	0.160	-0.223	0.001
N(2)—H(11)	—	—	—	0.077	0.140	0.006	0.160	-0.223	0.001
C(9)—C(10)	0.288	-0.723	0.169	0.289	-0.734	0.151	0.290	-0.743	0.150
C(1)—N(1)	0.293	-0.917	0.104	0.252	-0.679	0.034	0.261	-0.726	0.010
C(8)—N(2)	0.293	-0.917	0.104	0.270	-0.759	0.009	0.261	-0.726	0.010
<b>2</b>				<b>2H<sup>+</sup></b>			<b>2H<sup>+</sup>‡</b>		
Bonds	$\rho_b$	$\nabla^2\rho_b$	$\epsilon_b$	$\rho_b$	$\nabla^2\rho_b$	$\epsilon_b$	$\rho_b$	$\nabla^2\rho_b$	$\epsilon_b$
N(1)—H(11)	—	—	—	0.291	-1.403	0.020	0.155	-0.220	0.022
N(2)—H(11)	—	—	—	0.054	0.145	0.010	0.155	-0.220	0.022
C(15)—C(12)	0.302	-0.793	0.189	0.302	-0.797	0.180	0.306	-0.816	0.182
C(16)—N(1)	0.336	-1.132	0.109	0.315	-0.810	0.112	0.324	-0.962	0.116
C(14)—N(2)	0.336	-1.132	0.109	0.331	-1.079	0.121	0.324	-0.962	0.116
<b>5</b>				<b>5H<sup>+</sup>a</b>			<b>5H<sup>+</sup>‡</b>		
Bonds	$\rho_b$	$\nabla^2\rho_b$	$\epsilon_b$	$\rho_b$	$\nabla^2\rho_b$	$\epsilon_b$	$\rho_b$	$\nabla^2\rho_b$	$\epsilon_b$
N(1)—H(11)	—	—	—	0.286	-1.360	0.019	0.165	-0.307	0.022
N(2)—H(11)	—	—	—	0.057	0.148	0.018	0.145	-0.140	0.024
C(15)—C(12)	0.301	-0.786	0.188	0.301	-0.792	0.179	0.305	-0.810	0.181
C(16)—N(1)	0.336	-1.129	0.109	0.315	-0.813	0.110	0.323	-0.946	0.114
C(14)—N(2)	0.334	-1.138	0.103	0.329	-1.091	0.116	0.323	-1.001	0.110

### 5.3.2 Complexes

#### 5.3.2.1 Palladium(II) complexes

As mentioned earlier Wüstefeld *et al.* synthesized and characterized the platinum complex of the proton sponge ligand **2** and briefly discussed the bonding situation.[20] Using DFT methodologies we have explored the palladium(II) and palladium(0) complexes with ligands (**2-5**). Figures 5.5 and 5.6 display the key geometrical parameters of these complexes (**7-14**). Table 5.6 documents important distances and dihedral angles. NPA charges and Wiberg bond indices are given in Table 5.7. The energies for the formation of palladium(II) complexes are listed in Table 5.8.

**Table 5.6. Bond lengths (Å) and angles (deg); numbering according to Figures 5.5 and 5.6**

Pd(II)										
No.	Pd1—N1 (Å)	Pd1—N2 (Å)	Pd1—Cl3 (Å)	Pd1—Cl4 (Å)	N1—N2 (Å)	C16—C14 (Å)	C6—C5 (Å)	Φ <sup>a</sup> (°)	Ψ <sup>b</sup> (°)	(Φ+Ψ) (°)
<b>7</b>	2.055	2.055	2.332	2.332	2.845	2.599	2.443	-12.0	12.0	24.0
<b>8</b>	2.055	2.055	2.332	2.332	2.843	2.599	2.443	-12.2	12.2	24.4
<b>9</b>	2.057	2.057	2.340	2.340	2.842	2.595	2.444	-10.8	10.8	21.6
<b>10</b>	2.055	2.057	2.337	2.335	2.843	2.597	2.444	-12.0	10.8	22.8
Pd(0)										
No.	Pd1—N1 (Å)	Pd1—N2 (Å)	Pd1—C1 (Å)	Pd1—C10 (Å)	N1—N2 (Å)	C16—C14 (Å)	C6—C5 (Å)	Φ <sup>a</sup> (°)	Ψ <sup>b</sup> (°)	(Φ+Ψ) (°)
<b>11</b>	2.046	2.168	2.525	3.063	2.955	2.579	2.476	24.5	21.5	46.0
<b>12</b>	2.046	2.169	2.519	3.063	2.951	2.578	2.477	24.6	21.6	46.2
<b>13</b>	2.053	2.177	2.547	3.084	2.975	2.585	2.474	24.4	20.8	45.2
<b>14</b>	2.042	2.189	2.469	3.104	2.942	2.577	2.477	25.1	19.8	44.9

<sup>a</sup>Φ = N(1)—C(16)—C(15)—C(14); <sup>b</sup>Ψ = C(16)—C(15)—C(14)—N(2)

**Table 5.7. NPA charges (*e*) and Wiberg bond indices for palladium(II) and palladium(0) complexes (**7-14**)**

Pd(II)										
No.	Pd1 ( <i>e</i> )	N1 ( <i>e</i> )	N2 ( <i>e</i> )	Cl3 ( <i>e</i> )	Cl4 ( <i>e</i> )	Pd1—N1	Pd1—N2	Pd1—Cl3	Pd1—Cl4	μ(D)
<b>7</b>	0.622	-0.446	-0.446	-0.481	-0.481	0.321	0.321	0.491	0.491	11.895
<b>8</b>	0.622	-0.445	-0.445	-0.481	-0.481	0.322	0.322	0.491	0.491	12.013
<b>9</b>	0.614	-0.459	-0.459	-0.502	-0.502	0.324	0.324	0.482	0.482	13.268
<b>10</b>	0.618	-0.444	-0.462	-0.492	-0.491	0.324	0.321	0.486	0.488	13.193
Pd(0)										
No.	Pd1 ( <i>e</i> )	N1 ( <i>e</i> )	N2 ( <i>e</i> )	C1 ( <i>e</i> )	C10 ( <i>e</i> )	Pd1—N1	Pd1—N2	Pd1—C1	Pd1—C10	μ(D)
<b>11</b>	0.356	-0.505	-0.517	-0.121	0.026	0.342	0.228	0.224	0.052	1.679
<b>12</b>	0.359	-0.503	-0.516	-0.123	0.026	0.343	0.228	0.224	0.052	1.739
<b>13</b>	0.307	-0.517	-0.531	-0.112	0.033	0.326	0.219	0.234	0.052	1.970
<b>14</b>	0.344	-0.500	-0.529	-0.137	0.038	0.353	0.209	0.242	0.043	5.795

The geometries of these complexes are strongly bowed. The deformation of the ligand from planarity is different in the isolated molecule and in the complex.[20] In the latter case, it is much more pronounced, of course, but the direction is also different: the two nitrogen (N1 and N2) atoms lie on different sides of the aromatic plane in the isolated molecule (C<sub>2</sub> distortion, C<sub>2</sub> axis passing through C15—C12), but on the same side in the complex (C<sub>s</sub> distortion, C<sub>s</sub> plane containing the central C15—C12 bond and the Pd1 atom). The DFT calculations show a

similar bend in all palladium(II) complexes (**7-10**) resembling the X-ray crystal structure for the platinum analogue of **7**.<sup>[20]</sup> The coordination geometry around the metal is calculated to be essentially planar in **7-10**, and the angles with the adjacent atoms are close to 90° (to within 1°).

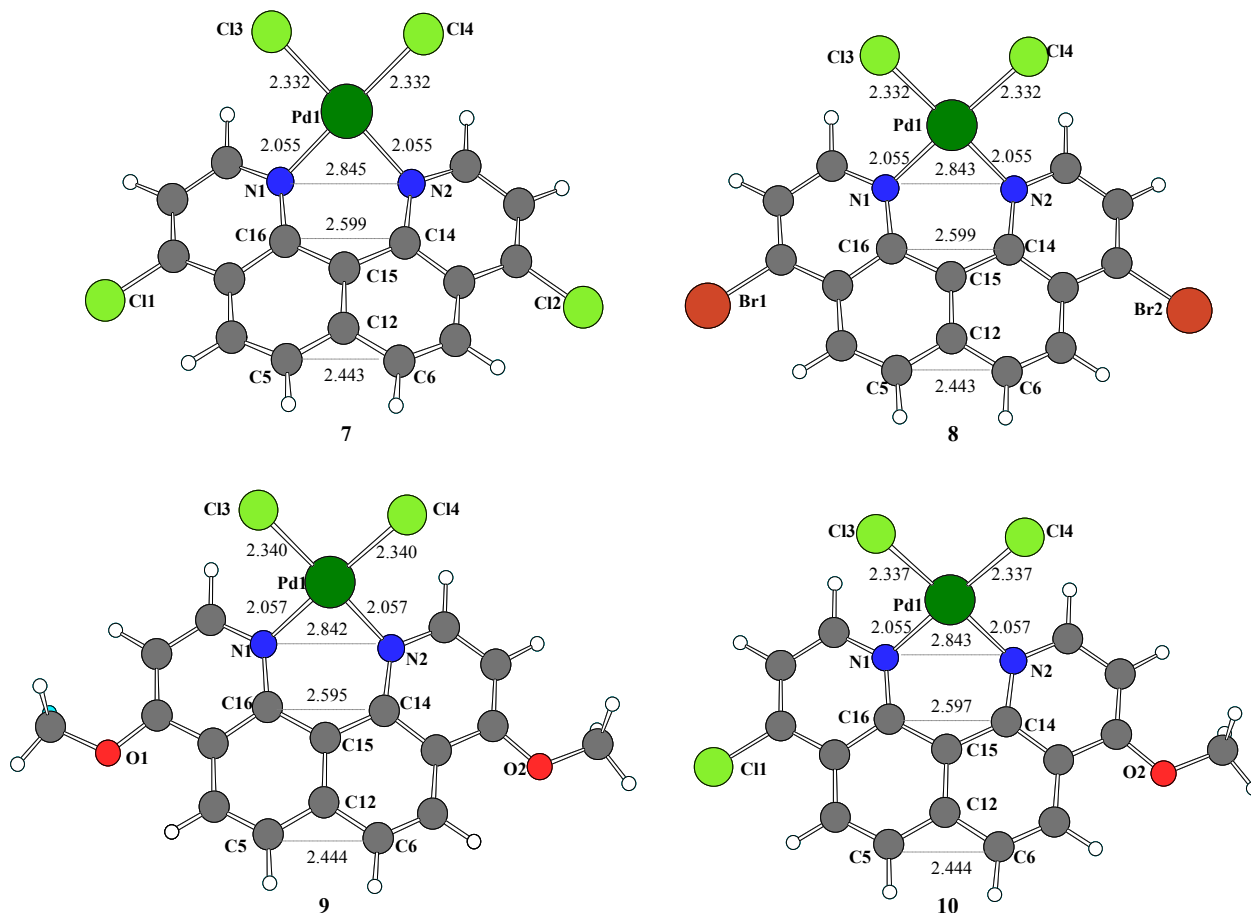


**Figure 5.5.** Optimized structures of palladium(II) complexes **7-10**, distances are provided in Å.

**Table 5.8.** Reaction energies (kcal/mol) for palladium(II) complex formation with ligands **2-5** and phenanthroline

No.	Reaction	$\Delta E_e$	$\Delta E_0$	$\Delta H_{298}$	$\Delta G_{298}$
<b>7</b>	<b>2</b> + PdCl <sub>2</sub> → <b>7</b>	-70.4	-68.1	-68.2	-53.9
<b>8</b>	<b>3</b> + PdCl <sub>2</sub> → <b>8</b>	-70.4	-68.1	-68.2	-54.0
<b>9</b>	<b>4</b> + PdCl <sub>2</sub> → <b>9</b>	-76.6	-74.1	-74.3	-60.0
<b>10</b>	<b>5</b> + PdCl <sub>2</sub> → <b>10</b>	-73.5	-71.1	-71.2	-56.9
<b>15<sup>a</sup></b>	Phen + PdCl <sub>2</sub> → <b>15</b>	-78.3	-75.9	-76.1	-62.1

<sup>a</sup>Phen = phenanthroline, see Scheme 5.1.

The formation of the palladium(II) complexes **7-10** from PdCl<sub>2</sub> and the proton sponges **2-5** is strongly exothermic, by 70-77 kcal/mol (Table 5.8). The phenanthroline ligand is bound even more strongly in **15**. A comparison of **7** and **15** shows that the phenanthroline complex is more stable by 7.9 kcal/mol, has somewhat stronger covalent Pd—Cl bonds (WBI of 0.501, see Table

5.7), and more electron density on the chlorine atoms (NPA charge of  $-0.499 e$ ) due to charge transfer from the lone-pair orbitals of the phenanthroline nitrogen atoms to the antibonding  $\sigma^*(\text{Pd}-\text{Cl})$  orbital in *trans* position.

The overall complexation energy ( $E_{\text{comp}}$ ) is often partitioned into two terms: intrinsic interaction energy ( $E_{\text{int}}$ ) at the optimized geometry of the complex, and distortion energy ( $E_{\text{dis}}$ ) needed to distort the two fragments from their own optimum geometry to the geometry adopted in the complex. Such an energy partitioning for the palladium(II) complex **7** yields:

$$E_{\text{comp}} = -70.4 \text{ kcal/mol}; E_{\text{dis}} = 8.2 \text{ kcal/mol}; E_{\text{int}} = -78.6 \text{ kcal/mol}$$

### 5.3.2.2 Palladium(0) complexes

Palladium(0) complexes act as excellent catalysts for Heck olefination.[44] We shall first discuss the energetic and structural features of the palladium(0) complexes of proton sponges **2-5**. Their formation energies can be obtained from the general equation:



These complexation reactions are computed to be exothermic by 36-38 kcal/mol (Table 5.9), slightly more so than in the case of the phenanthroline ligand **16**. The palladium(0) complexes are thus significantly less stable than the corresponding palladium(II) complexes (Table 5.8).

**Table 5.9. Reaction energies (kcal/mol) for palladium(0) complex formation for ligands 2-5 and phenanthroline**

No.	Reaction	$\Delta E_e$	$\Delta E_0$	$\Delta H_{298}$	$\Delta G_{298}$
<b>11</b>	Pd + <b>2</b> → <b>11</b>	-37.5	-37.6	-37.8	-29.2
<b>12</b>	Pd + <b>3</b> → <b>12</b>	-37.7	-37.7	-37.9	-29.4
<b>13</b>	Pd + <b>4</b> → <b>13</b>	-35.9	-36.0	-36.2	-27.6
<b>14</b>	Pd + <b>5</b> → <b>14</b>	-37.9	-37.9	-38.2	-29.4
<b>16<sup>a</sup></b>	Pd + Phen→ <b>16</b>	-34.6	-34.6	-34.7	-26.9

<sup>a</sup>Phen = phenanthroline ligand, see Scheme 5.1.

Figure 5.6 shows key geometrical parameters of the palladium(0) complexes (**11-14**). It is obvious that the palladium is placed asymmetrically between the nitrogen atoms, contrary to the situation in the palladium(II) complexes (Figure 5.5): the two Pd–N bond lengths differ by 0.12-0.15 Å in **11-14**. To estimate the energy gain due to the conformational distortion of the complex, we have performed two constrained optimizations of **11** under  $C_s$  and  $C_{2v}$  symmetry: the resulting structures are 14.8 and 15.2 kcal/mol ( $\Delta G_{298}$ ) less stable than **11**. There are two modes with imaginary frequencies ( $246 \text{ i cm}^{-1}$  and  $10 \text{ i cm}^{-1}$ ) in the  $C_{2v}$  optimized structure of **11**, which correspond to different bending motions of the ligand framework. To confirm the

structural integrity of palladium(0) complexes, we have re-optimized **11** at the BP86/EXT level[45,46] and obtained a qualitatively similar minimum structure.

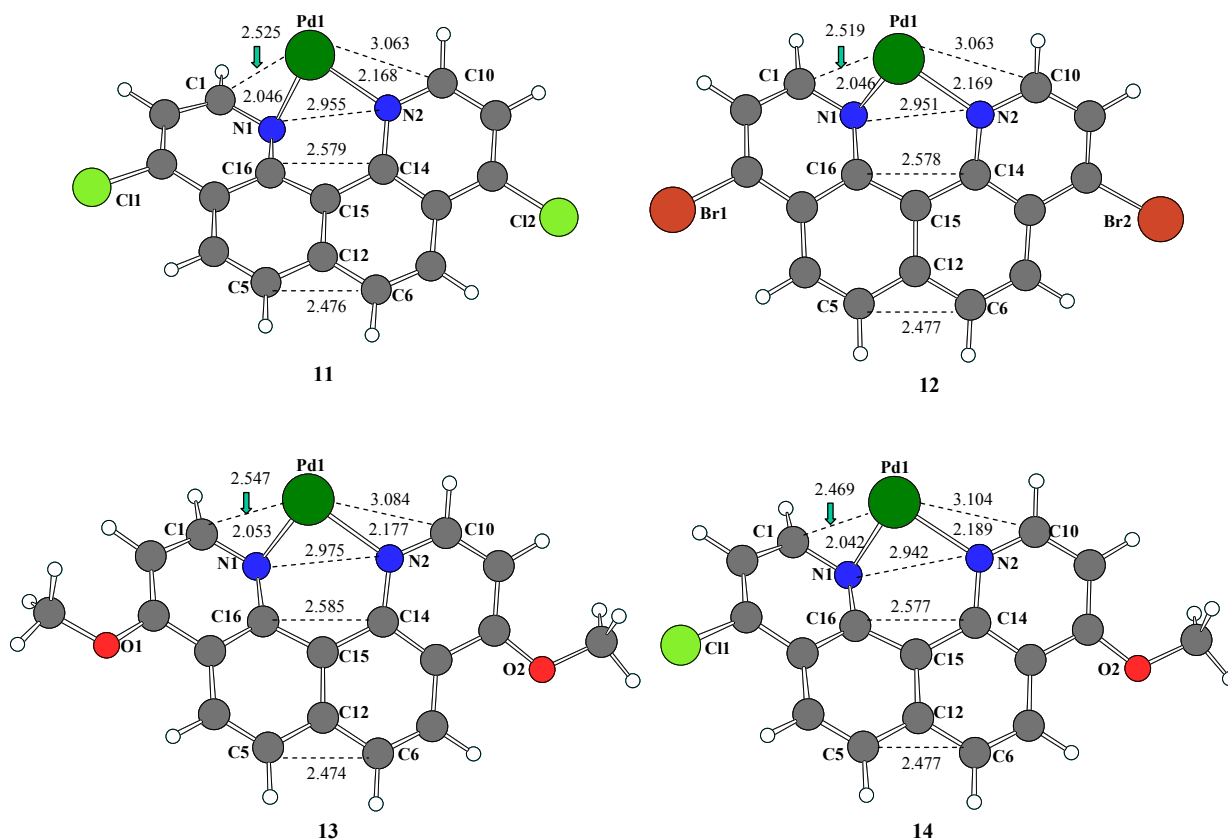


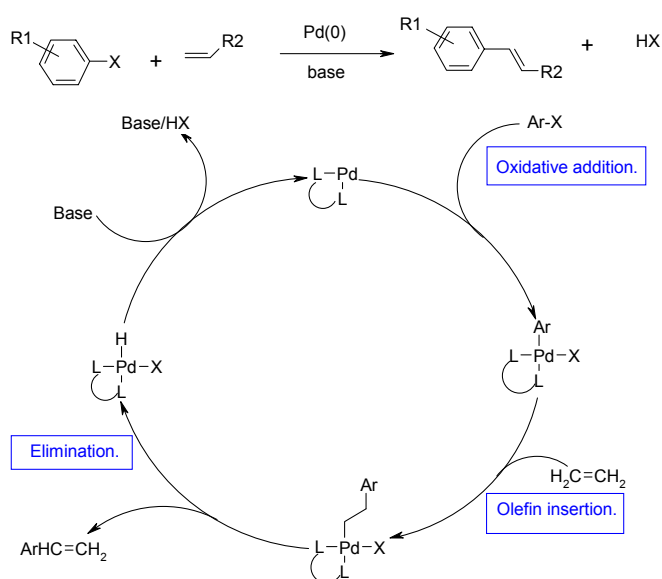
**Figure 5.6.** Optimized structures of palladium(0) complexes **11-14**, distances are provided in Å. Further comments on the prototypical complex **11**: The distance Pd(1)—N(1) is 0.122 Å shorter than Pd(1)—N(2), and Pd(1)—C(1) is even 0.538 Å shorter than Pd(1)—C(10) (Figure 5.6). Both relevant dihedral angles [N(2)—C(14)—C(15)—C(16) and N(1)—C(16)—C(15)—C(14)] are greater in **11** than in the free ligand **2** (see Tables 5.1 and 5.6) indicating more twisting and deformation in **11**. Compared with the corresponding palladium(II) complex **7**, the Pd—N(1) bond length is similar in **11**, but the Pd—N(2) and N(1)—N(2) distances are larger by about 0.1 Å, and the ligand is not bowed much in **11**.

According to the NPA analysis for **11**, the N(1)—C(1) bonding  $\pi$  orbital (occupied) donates electron density to an unoccupied orbital of palladium (predominantly s), with concomitant back-donation from a bonding d-orbital of palladium to the unoccupied  $\pi^*$  orbital of N(1)—C(1). These orbital interactions are large missing in the  $C_{2v}$  and  $C_s$  optimized structures of **11** which may contribute to their lower stability (see above). It is noteworthy, however, that the palladium(0) phenanthroline complex **16** shows a symmetrical structure, with the palladium equidistant to the two nitrogen atoms.

### 5.3.3 Heck olefination by palladium(0) complexes

Heck olefination is an important tool for the formation of C—C bonds in organic synthesis.[44] Heck and other cross-coupling reactions use palladium(0) complexes as the active catalyst to trigger the reaction. Experimental results reveal[47] that the palladium(0) complexes **11-14** are excellent Heck catalysts with an average yield of 96%. Scheme 5.3 shows the standard Heck reaction and the corresponding catalytic cycle. We have calculated the key intermediates involved in the Heck reaction between phenylbromide and styrene using catalyst **11**. The DFT optimized structures are given in Figure 5.7 and Table 5.10.

**Scheme 5.3. Heck reaction and the catalytic cycle**



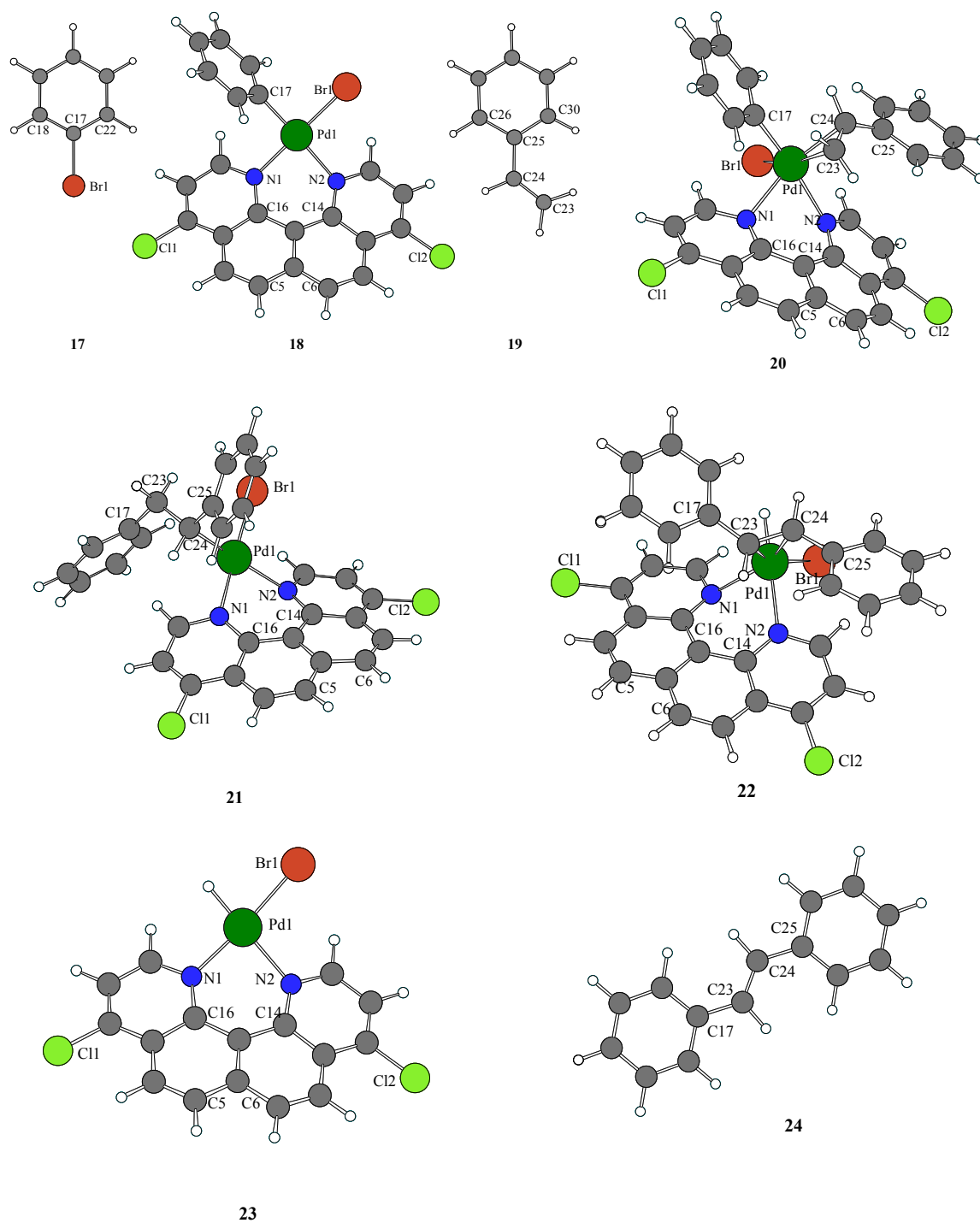


**Figure 5.7.** DFT optimized structures of species (17-24) involved in Heck cycle.



### 5.3.3.1 Oxidative addition

The oxidative addition of phenylbromide **17** to **11** yields the *cis* complex **18**. The chelating proton sponge ligand in **11** ensures the formation of *cis* product rather than *trans* product.[48] The reaction rate depends on the substituent of the phenyl group: electron-withdrawing groups and good leaving groups X (I > Br > Cl) facilitate the addition. The d<sup>8</sup> palladium(II) center in **18** has a perfect square planar environment with four bonding partners. The Pd(1)—N(2) bond (2.169 Å) is longer than the Pd(1)—N(1) bond (2.093 Å) which can be explained by the *trans*-effect: C<sub>6</sub>H<sub>5</sub><sup>−</sup> is known to exhibit a stronger *trans*-influence than Br<sup>−</sup>, hence leading to a longer Pd—N bond *trans* to it. The “out-of-plane” conformation of the ligand is maintained in **18**, and the N(1)—Pd(1)—N(2) bond angle is smaller in **18** than in **11**. The change in formal oxidation state is accompanied by an increase of the NPA charge at palladium by 0.148 *e*. The oxidative addition is highly exothermic; the computed energy for the reaction **11** + **17** → **18** is −50.9 kcal/mol (ΔE<sub>e</sub>) in the gas phase, and −55.4 kcal/mol (ΔE<sub>sov</sub>) in NMP, *i.e.*, the reaction is more exothermic in solution. We have not located the transition state for oxidative addition in our system. Early theoretical studies on the oxidative addition of C—H and C—C bonds to d<sup>10</sup> platinum(0) and palladium(0) complexes have reported essentially planar transition states (around palladium) which lead to the desired product in a least-motion approach[49], but there is also more recent work with a transition state that features a perpendicular orientation of the reactant.[50]

### 5.3.3.2 Coordination of styrene

The addition of styrene (**19**) to **18** would seem to require a vacant coordination site which can be generated by dissociation of one of the palladium-ligand bonds.[51] We have been able to find a five-coordinate π complex **20**, where styrene is only weakly bound, by 0.6 kcal/mol (ΔE<sub>e</sub>). Complex **20** shows η<sup>2</sup> coordination, with Pd—C distances around 2.9 Å and a coordinating C(23)—C(24) bond that is elongated by 0.071 Å relative to free styrene. Compared with **18**, the coordination of styrene causes a lengthening of the Pd—X bonds, by 0.143 Å for X = Br(1), by 0.221 Å for X = N(1), and by 0.069 Å for X = N(2).

The interactions in transition metal π-complexes can be explained in terms of σ donation and π back donation (Dewar–Chatt–Duncanson model).[52] Electrons are transferred from the filled olefin π orbital to an empty metal d-orbital, accompanied by back-donation from a filled metal d-orbital to the olefin π\* orbital. η<sup>2</sup>-π complexes of type **20** have also been found in other computational studies of palladium chemistry.[48,50,51] Rix *et al.* have characterized similar

$\eta^2$ -alkene complexes at low temperature during palladium-catalyzed alkene polymerizations.[53]

### 5.3.3.3 Insertion

In the insertion step the  $\eta^2$ - $\pi$  complex **20** is converted into the  $\sigma$  complex **21**. Formally this involves the breaking of the Pd(1)—C(17) bond and the formation of the Pd(1)—C(24) and C(17)—C(23) bonds. We have not located the corresponding transition state, but in other related systems, the insertion has been computed to proceed in a single concerted step through a four-membered transition state, and the calculated barriers of 9.1 and 11.5 kcal/mol[50,51] are low for the types of ligands studied (chelating bis-phosphine[50], and diaminocarbenes[51]). During the insertion **20**  $\rightarrow$  **21**, the Pd(1)—C(24) distance decreases from 2.203 Å in **20** to 2.098 Å in **21**, and there is a change of hybridization of the olefin carbons from  $sp^2$  to  $sp^3$ , which is accompanied by a further elongation of the C(23)—C(24) bond by 0.121 Å (see Table 5.10). After the insertion the NPA charge at the palladium atom has decreased by 0.199  $e$ . The insertion step is exothermic, by  $-21.2$  kcal/mol ( $\Delta E_e$ ) in the gas phase and  $-19.5$  kcal/mol ( $\Delta E_{\text{sov}}$ ) in NMP, in fact more so than in the other systems investigated.[50,51]

In the  $\pi$ -complex **20**, the Pd—N distances are elongated (see above) due to electron donation from the electron-rich styrene moiety. After insertion, the Pd—N distances become shorter again, by 0.226 and 0.043 Å, and assume similar values as in complex **19**; analogous changes are found for the N(1)—Pd(1)—N(2) bond angle (see Table 5.10). The typical “out-of-plane” conformation of the ligand still persists, and the metal center retains a square planar environment. The two phenyl groups are oriented *trans* to each other in **21** with a dihedral angle of nearly 170°.

**Table 5.10.** Calculated geometric parameters, dipole moments, and NPA charges for the species (17-24) involved in the Heck cycle. Bond distances in Angstrom (Å), angles in degrees (°), dipole moments  $\mu$  in Debye (D), and NPA charges in  $e$ .

	17	18	19	20	21	22	23	24
Pd1—N1	—	2.094	—	2.315	2.089	2.305	2.064	—
Pd1—N2	—	2.169	—	2.238	2.195	2.239	2.166	—
Pd1—C17	—	2.002	—	2.023	3.509	3.127	—	—
Pd1—Br1	—	2.455	—	2.598	2.495	2.565	2.437	—
C17—Br1	1.918	—	—	3.315	4.181	5.521	—	—
Pd1—C23	—	—	—	2.169	3.079	2.208	—	—
Pd1—C24	—	—	—	2.203	2.098	2.168	—	—
C23—C24	—	—	1.474	1.422	1.542	1.429	—	1.361
N1—N2	—	2.879	—	2.785	2.844	2.801	2.909	—
C14—C16	—	2.617	—	2.594	2.604	2.601	2.629	—
C5—C6	—	2.435	—	2.454	2.444	2.452	2.428	—
N1—Pd1—N2	—	84.9	—	75.4	83.1	76.1	86.9	—
$\mu$	1.776	8.705	0.197	7.183	7.997	7.134	9.134	0.000
<b>NPA charges</b>								
Pd1	—	0.504	—	0.719	0.520	0.565	0.342	—
N1	—	-0.463	—	-0.478	-0.463	-0.481	-0.461	—
N2	—	-0.484	—	-0.471	-0.483	-0.489	-0.494	—
Br1	0.062	-0.466	—	-0.599	-0.525	-0.559	-0.459	—
C17	-0.122	-0.147	—	-0.109	-0.036	-0.064	—	-0.078
C23	—	—	-0.419	-0.567	-0.509	-0.337	—	-0.209
C24	—	—	-0.239	-0.304	-0.340	-0.306	—	-0.209

### 5.3.3.4 $\beta$ -Hydride elimination

This product of the Heck olefination is generated through  $\beta$  hydride elimination from **21** and subsequent dissociation of styrene from **22**. A necessary condition for  $\beta$  hydride elimination is that the Pd(1)—C(24) and C(23)—H bonds are *cis* to each other. In the insertion product **21**, a  $C_\alpha$ — $C_\beta$  bond rotation around C(23)—C(24) is required to reach this conformation with favorable  $\beta$ -agostic interaction. We have not investigated this internal rotation which has been reported to require a considerable amount of activation (10 kcal/mol)[50] in a related system. After the formation of the  $\beta$ -agostic complex, the elimination will occur with simultaneous Pd—H $_\beta$  bond formation and Pd— $C_\alpha$  bond dissociation to yield the hydride **22**. The process of  $\beta$  hydride elimination is endothermic by 15.9 kcal/mol ( $\Delta E_e$ ) in the gas phase and by 13.3 kcal/mol ( $\Delta E_{\text{sov}}$ ) in NMP. The overall insertion/elimination reaction is exothermic by -5.3 kcal/mol; similar values of -9.8 and -8.9 kcal/mol have been reported for a chelating phosphine system[50] and a diaminocarbene stabilized system.[51] Complex **22** shows an axial orientation of bromide, with the two coordinating nitrogen atoms and the hydride ligand in a pseudo planar regime while the central C=C bond of the generated *trans*-stilbene forms an  $\eta^2$ - $\pi$  complex with palladium. The dissociation of *trans*-stilbene **24** from **22** affords the palladium—hydride complex **23**. The catalytic cycle is formally closed by removal of HBr from **23** which regenerates the palladium(0) catalyst **11**.

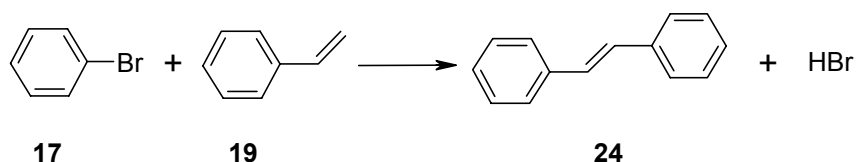
**Table 5.11. Energy changes for steps in the Heck cycle (kcal/mol)**

No.	Reaction	$\Delta E_c$	$\Delta E_0$	$\Delta H_{298}$	$\Delta G_{298}$	$\Delta E_{\text{sov}}^a$
1	<b>11</b> + <b>17</b> $\rightleftharpoons$ <b>18</b>	-50.9	-49.1	-48.8	-36.6	-55.4
2	<b>18</b> + <b>19</b> $\rightleftharpoons$ <b>20</b>	-0.6	0.4	0.5	14.0	2.5
3	<b>20</b> $\rightleftharpoons$ <b>21</b>	-21.2	-19.5	-19.9	-20.2	-19.5
4	<b>21</b> $\rightleftharpoons$ <b>22</b>	15.9	13.6	13.8	13.1	13.3
5	<b>22</b> $\rightleftharpoons$ <b>23</b> + <b>24</b>	-0.3	-0.9	-1.3	-14.3	-5.4
6	<b>23</b> $\rightleftharpoons$ <b>11</b> + HBr	49.8	46.3	33.0	36.2	55.6

<sup>a</sup>Solvent NMP.

### 5.3.3.5 Discussion

The energy changes for the individual steps in the catalytic cycle of the investigated Heck olefination reaction are summarized in Table 5.11, and the corresponding energy profile is shown in Figure 5.8. The overall reaction



is computed to be exothermic by  $\Delta H_{298} = -8.6$  kcal/mol. The tabulated experimental values for the standard enthalpies of formation  $\Delta_f H_{298}$  in the gas phase[54] are  $105.4 \pm 4.1$  kJ/mol for **17**,  $147.9 \pm 1.5$  kJ/mol for **19**,  $236.1 \pm 1.3$  kJ/mol for **24**, and  $-36.29 \pm 0.16$  kJ/mol for HBr. The standard reaction enthalpy derived from these experimental values amounts to  $\Delta H_{298} = -53.5 \pm 4.6$  kJ/mol =  $-12.8 \pm 1.1$  kcal/mol. The DFT calculations thus reproduce the experimental reaction enthalpy as well as expected (deviation of  $4.2 \pm 1.1$  kcal/mol).

The energy profile in Figure 5.8 exhibits a dramatic drop in the first step (oxidative addition, **11** + **17**  $\rightarrow$  **18**) and a similar dramatic rise in the last step (removal of HBr, **23**  $\rightarrow$  **11** + HBr). The associated energy changes of the order of 50 kcal/mol are too large for a valid catalytic cycle. This indicates that the chosen gas-phase model is inadequate for these two steps. In solution, under realistic experimental conditions with added base (acetate), catalyst **11** will not be present as two-coordinate species (Figure 5.6) but will have more directly coordinated partners, and the product HBr will not be an isolated molecule but interact strongly (*e.g.*, with acetate). Such specific interactions are not taken into account in the continuum solvation models used presently ( $E_{\text{sov}}$ ). Their inclusion would certainly stabilize the reactant (**11** + R) and product (**11** + P) side in Figure 5.8, but a detailed study of these effects is beyond the scope of the present work.

Focusing on the intermediates in the Heck cycle (Figure 5.8) the variations in the computed energies become less pronounced. The energy span of the five intermediates considered is computed to be 21.8, 22.4, and 19.5 kcal/mol for  $\Delta E_c$ ,  $\Delta G_{298}$ , and  $\Delta E_{\text{sov}}$ , respectively. Such

energy spans are not uncommon in catalytic cycles, and the corresponding steps in the Heck reaction thus seem feasible as far as the calculated relative energies of the intermediates are concerned.

Comparing with other published computational model studies on Heck olefination[50,51] we note that the initial oxidative addition is always calculated to be quite exothermic, by 33.9 kcal/mol for a bis-phosphine catalyst plus PhI[50] and 34.1 kcal/mol for a diaminocarbene catalyst plus PhBr,[51] but less so than in our case (50.2 kcal/mol). For the following insertion step, the published studies assume an initial dissociation of the halide anion so that the coordination and subsequent insertion of ethylene involve only four-coordinate complexes, the halide anion being present not at all[50,51] or only at a large distance as a spectator counterion.[51] By contrast, in our case, Br remains bound to Pd during the coordination and insertion of styrene which prevents a direct comparison with the literature data for this part of the cycle. However, the insertion product is found to be the most stable intermediate in all cases. Furthermore, the subsequent  $\beta$ -hydride elimination is slightly endothermic both in our and the published[50,51] model systems. Hence, in spite of some differences, the three computational studies share a number of common features.

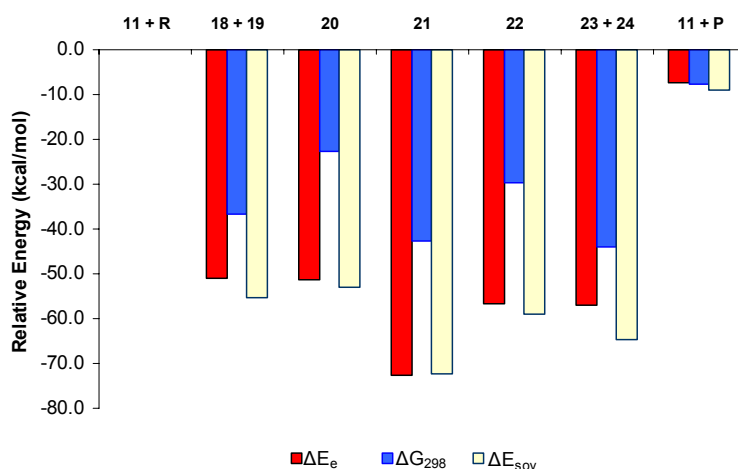
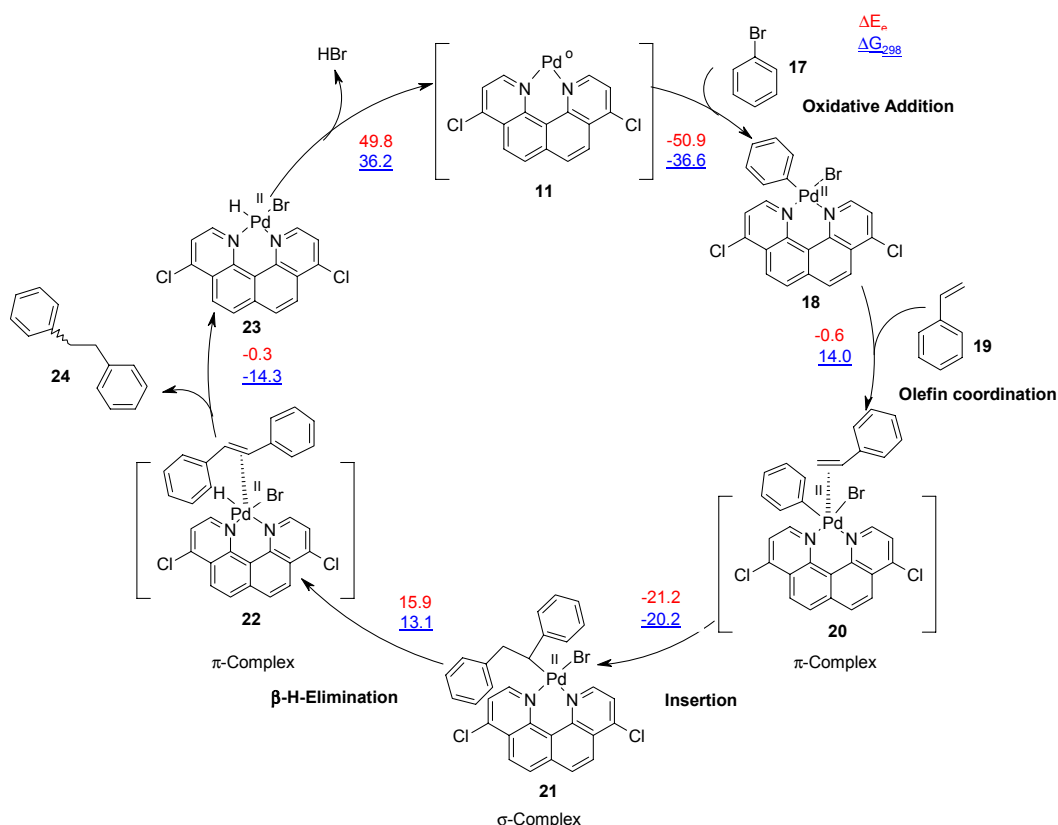


**Figure 5.8.** The energy profile for the catalytic cycle. Reactants R = **17** + **18**, products P = **24** + HBr. Energies are given relative to **11** + R.

Firm conclusions on the mechanism of the Heck reaction between phenylbromide and styrene in the presence of catalyst **11** cannot be drawn from the current DFT calculations because the transition states have not been located in the proposed catalytic cycle. The published papers on simpler model systems[50,51] have reported transition states for the relevant steps, and the calculated barriers are not excessive. We may expect by analogy that this should also be true for our larger model system. Confirming this expectation would require extensive calculations which are beyond the scope of this investigation.

**Scheme 5.4.** Energy changes (kcal/mol) in the steps of the Heck cycle. Structures in parentheses represent probable intermediates.



## 5.4 Conclusions

DFT calculations yield realistic geometries for the Staab-type proton sponges and their conjugate acids. The latter contain an asymmetric intramolecular N—H···N hydrogen bond in a double-well potential with a small barrier to proton transfer (Figures 5.3 and 5.4). In agreement with experiment, the Staab-type proton sponges are computed to have higher proton affinities than the Alder-type proton sponges. Their extremely high basicity is rationalized in terms of the calculated strain energies and hydrogen-bond energies (Scheme 5.2).

DFT calculations on palladium(II) and palladium(0) complexes of the Staab-type proton sponges show that the former are much more stable (binding energies of 70–77 vs. 36–38 kcal/mol, Tables 5.8 and 5.9). The observed unusual out-of-plane distortion of the proton sponge ligand[20] is well reproduced in the palladium(II) complex **7**. Unexpected asymmetrical geometries are predicted for palladium(0) complexes such as **11** where the metal is coordinated to two nitrogen atoms and one additional carbon atom (Figure 5.6). The involvement of such palladium(0) complexes in Heck olefination reactions has been studied by considering the intermediates in a plausible catalytic cycle. The computed relative energies of the central five intermediates (Figure 5.8) do not vary too much so that the proposed cycle

would seem feasible. A more definite assessment would require the location of the relevant transition states.

## 5.5 Supporting Information

### Contents:

**Figure 5.S1.** Isoelectron density surface (isodensity = 0.002 electron/bohr<sup>3</sup>) with an electrostatic potential map for compounds **6**, **1**, **5** and their respective conjugate acids.

**Table 5.S1.** Absolute energies (hartree) for all the ligands and their respective conjugate acids (BP86/6-31G\*).

**Table 5.S2.** Absolute energies (hartree) for the hydrogen transfer process.(B3LYP/6-31G\*).

**Table 5.S3.** Absolute energies (hartree) of palladium complexes and the ligands (BP86/6-31G\*).

**Table 5.S4.** Absolute energies (hartree) for the intermediates involved in Heck cycle (BP86/6-31G\*).

**Table 5.S5.** Absolute energies (hartree) for all the ligands and their respective conjugate acids (B3LYP/6-31G\*).

**Table 5.S6.** Structural parameters and dipole moments for the substituted quino[7,8-h]quinolines and their conjugated acids (B3LYP/6-31G\*).

**Table 5.S7.** Energies (kcal/mol) of planar relative to twisted ligands and imaginary frequencies  $\omega$  ( $i$  cm<sup>-1</sup>) for the inversion mode in the planar structures (B3LYP/6-31G\*).

**Table 5.S8.** Proton affinities in kcal/mol (B3LYP/6-31G\*).



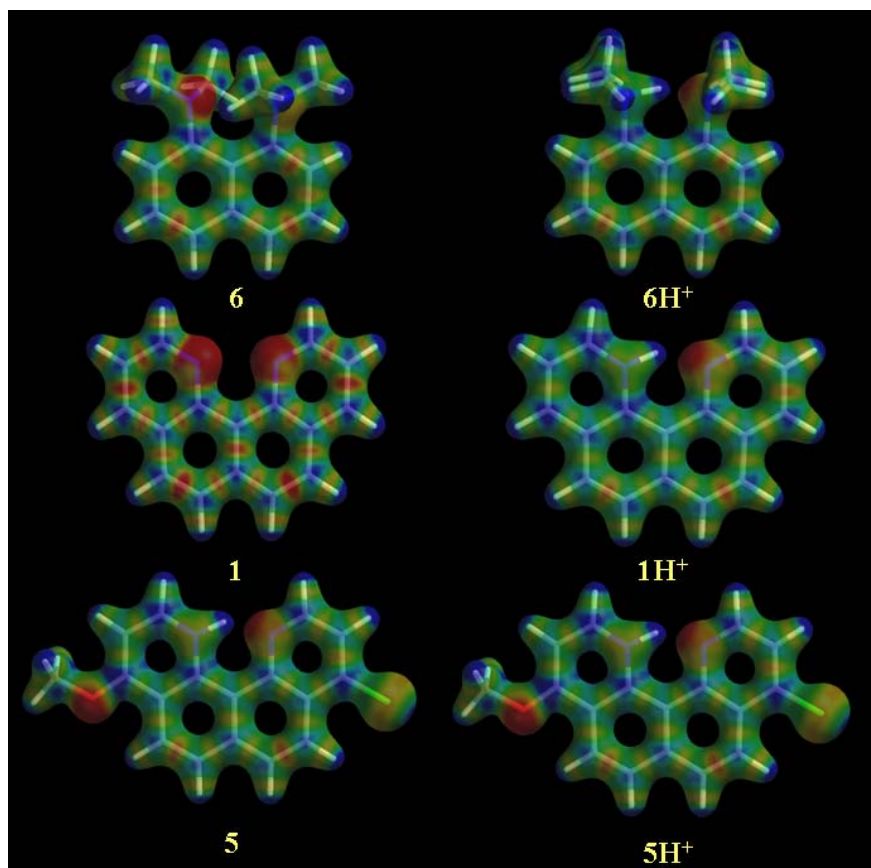


**Figure 5.S1.** Isoelectron density surface (isodensity = 0.002 electron/bohr<sup>3</sup>) with an electrostatic potential map for compounds **6**, **1**, **5** and their respective conjugate acids.

The potential is coded according to the visible spectrum (red<orange<yellow<green<blue) with red representing the most negative potential and blue the most positive potential. The most negative potentials on the neutral proton sponges are located at the nitrogen atoms. In the respective conjugate acids the potential on the nitrogen atom diminishes after protonation. In an overall assessment, the electrostatic potential maps appear to be more uniform in the conjugate acids which may be indicative of a more uniform electron distribution and an enhanced electron delocalization.

**Table 5.S1.** Absolute energies (hartree) for all the ligands and their respective conjugate acids (BP86/6-31G\*).

No.	Substituents	Point group	E <sub>e</sub>	E <sub>0</sub>	H <sub>298</sub>	G <sub>298</sub>
<b>6</b>		C <sub>1</sub>	-653.792966	-653.507101	-653.490872	-653.547963
<b>1</b>	H	C <sub>1</sub>	-725.244375	-725.033651	-725.020336	-725.072524
<b>2</b>	Cl	C <sub>1</sub>	-1644.500004	-1644.308041	-1644.292187	-1644.350970
		C <sub>2</sub>	-1644.499992	-1644.308024	-1644.292169	-1644.350304
<b>3</b>	Br	C <sub>1</sub>	-5867.965732	-5867.774710	-5867.758376	-5867.819638
<b>4</b>	OCH <sub>3</sub>	C <sub>1</sub>	-954.298710	-954.024095	-954.005432	-954.069633
<b>1</b>	H	C <sub>s</sub>	-725.244147	-725.033548	-725.021049	-725.070972
<b>2</b>	Cl	C <sub>s</sub>	-1644.499528	-1644.307706	-1644.292652	-1644.349178
		C <sub>2v</sub>	-1644.499528	-1644.307706	-1644.292652	-1644.348524
<b>3</b>	Br	C <sub>s</sub>	-5867.965219	-5867.774281	-5867.758759	-5867.817638
<b>4</b>	OCH <sub>3</sub>	C <sub>s</sub>	-954.298474	-954.023839	-954.006071	-954.067632
<b>5</b>	Cl & OCH <sub>3</sub>	C <sub>1</sub>	-1299.399763	-1299.166469	-1299.149204	-1299.210707
<b>1s</b>	H	C <sub>1</sub>	-725.251580	-725.040666	-725.027370	-725.079448
<b>2s</b>	Cl	C <sub>1</sub>	-1644.505757	-1644.313782	-1644.297905	-1644.356817
<b>3s</b>	Br	C <sub>1</sub>	-5867.971485	-5867.780422	-5867.764086	-5867.825302
<b>4s</b>	OCH <sub>3</sub>	C <sub>1</sub>	-954.308829	-954.034198	-954.015475	-954.080314
<b>5s</b>	Cl & OCH <sub>3</sub>	C <sub>1</sub>	-1299.407617	-1299.174332	-1299.157028	-1299.218779
<b>6H<sup>+</sup></b>		C <sub>1</sub>	-654.2014025	-653.903246	-653.886874	-653.944577
<b>1H<sup>+</sup></b>	H	C <sub>1</sub>	-725.666486	-725.441775	-725.428727	-725.479711
<b>2H<sup>+</sup></b>	Cl	C <sub>1</sub>	-1644.913617	-1644.708037	-1644.692452	-1644.750141
<b>3H<sup>+</sup></b>	Br	C <sub>1</sub>	-5868.380438	-5868.175801	-5868.159742	-5868.219895
<b>4H<sup>+</sup></b>	OCH <sub>3</sub>	C <sub>1</sub>	-954.736487	-954.447993	-954.429523	-954.492563
<b>5H<sup>+</sup></b>	Cl & OCH <sub>3</sub>	C <sub>s</sub>	-1299.827065	-1299.579902	-1299.562822	-1299.623349
<b>5H<sup>+</sup>a</b>	Cl & OCH <sub>3</sub>	C <sub>s</sub>	-1299.824152	-1299.577527	-1299.560463	-1299.620940
<b>1sH<sup>+</sup></b>	H	C <sub>1</sub>	-725.729186	-725.504620	-725.491517	-725.542642
<b>2sH<sup>+</sup></b>	Cl	C <sub>1</sub>	-1644.977507	-1644.771945	-1644.756322	-1644.814047
<b>3sH<sup>+</sup></b>	Br	C <sub>1</sub>	-5868.443561	-5868.238886	-5868.222791	-5868.282972
<b>4sH<sup>+</sup></b>	OCH <sub>3</sub>	C <sub>1</sub>	-954.795686	-954.507375	-954.488832	-954.552356
<b>5sH<sup>+</sup></b>	Cl & OCH <sub>3</sub>	C <sub>1</sub>	-1299.889083	-1299.641919	-1299.624801	-1299.685636

BP86/6-31G\* level of theory ("6D 7F")

**Table 5.S2.** Absolute energies (hartree) for the hydrogen transfer process.(B3LYP/6-31G\*).

No.	E <sub>e</sub> (au)	E <sub>0</sub> (au)	H <sub>298</sub> (au)	G <sub>298</sub> (au)
<b>6H<sup>+</sup></b>	-654.217800	-653.909469	-653.893530	-653.950465
<b>6H<sup>+</sup>‡</b>	-654.215931	-653.911102	-653.895406	-653.951601
<b>6H<sup>+</sup></b>	-654.217800	-653.909469	-653.893530	-653.950465
<b>2H<sup>+</sup></b>	-1644.850136	-1644.637655	-1644.622535	-1644.679360
<b>2H<sup>+</sup>‡</b>	-1644.844399	-1644.636269	-1644.621388	-1644.677604
<b>5H<sup>+</sup></b>	-1299.796062	-1299.540755	-1299.524171	-1299.583777
<b>5H<sup>+</sup>‡</b>	-1299.788220	-1299.537461	-1299.521148	-1299.580058
<b>5H<sup>+</sup>a</b>	-1299.792283	-1299.537370	-1299.520817	-1299.580338

B3LYP/6-31G\* level of theory ("6D 7F")

**Table 5.S3.** Absolute energies (hartree) of palladium complexes and the ligands (BP86/6-31G\*).

Entry	Point Group	E <sub>e</sub>	E <sub>0</sub>	H <sub>298</sub>	G <sub>298</sub>
<b>6</b>	C <sub>1</sub>	-653.780078	-653.494104	-653.477881	-653.534959
<b>2</b>	C <sub>1</sub>	-1644.477399	-1644.285287	-1644.269444	-1644.328219
	C <sub>2</sub>	-1644.477399	-1644.285287	-1644.269444	-1644.327564
<b>3</b>	C <sub>1</sub>	-5867.347613	-5867.156398	-5867.140084	-5867.201272
<b>4</b>	C <sub>1</sub>	-954.279986	-954.005139	-953.986501	-954.050664
<b>5</b>	C <sub>1</sub>	-1299.379105	-1299.145623	-1299.128375	-1299.189852
<b>Phenanthroline</b>	C <sub>1</sub>	-571.595786	-571.430034	-571.419576	-571.465002
<b>PdCl<sub>2</sub></b>	C <sub>2v</sub>	-1047.263696	-1047.261837	-1047.256620	-1047.291167
<b>Pd(0)</b>	-	-126.758904	-126.758904	-126.756544	-126.775496
<b>7</b>	C <sub>1</sub>	-2691.853283	-2691.655601	-2691.634819	-2691.705349
<b>8</b>	C <sub>1</sub>	-6914.723493	-6914.526736	-6914.505454	-6914.578473
<b>9</b>	C <sub>1</sub>	-2001.665761	-2001.385117	-2001.361469	-2001.437503
<b>10</b>	C <sub>1</sub>	-2346.759929	-2346.520745	-2346.498536	-2346.571775
<b>11</b>	C <sub>1</sub>	-1771.296116	-1771.104063	-1771.086231	-1771.150303
	C <sub>2v</sub>	-1771.274001	-1771.082194	-1771.065588	-1771.126056
	C <sub>s</sub>	-1771.274000	-1771.082196	-1771.065589	-1771.126718
<b>12</b>	C <sub>1</sub>	-5994.166532	-5993.975403	-5993.957087	-5994.023602
<b>13</b>	C <sub>1</sub>	-1081.096051	-1080.821339	-1080.800707	-1080.870123
<b>14</b>	C <sub>1</sub>	-1426.198394	-1425.964932	-1425.945717	-1426.012274
<b>15</b>	C <sub>1</sub>	-1618.984288	-1618.812773	-1618.797430	-1618.855056
<b>16</b>	C <sub>1</sub>	-698.409785	-698.244087	-698.231397	-698.283435

BP86/6-31G\* level of theory ("5D 7F")

**Table 5.S4.** Absolute energies (hartree) for the intermediates involved in Heck cycle (BP86/6-31G\*).

No.	E <sub>e</sub>	E <sub>0</sub>	H <sub>298</sub>	G <sub>298</sub>	E <sub>sov</sub>
<b>17</b>	-2803.293956	-2803.205777	-2803.198979	-2803.236112	-2803.300013
<b>18</b>	-4574.671111	-4574.388089	-4574.362936	-4574.444666	-4574.696616
<b>19</b>	-309.628325	-309.498592	-309.490679	-309.530113	-309.635465
<b>20</b>	-4884.300342	-4883.88605	-4883.852781	-4883.952541	-4884.328172
<b>21</b>	-4884.33407	-4883.917193	-4883.884478	-4883.984709	-4884.359189
<b>22</b>	-4884.308691	-4883.895598	-4883.862491	-4883.963901	-4884.338026
<b>23</b>	-4343.628917	-4343.425564	-4343.40579	-4343.475052	-4343.655247
<b>24</b>	-540.680286	-540.471412	-540.45879	-540.51161	-540.69146
<b>OAc<sup>-</sup></b>	-228.497312	-228.450684	-228.44521	-228.478314	-228.614602
<b>HBr/OAc<sup>-</sup></b>	-2800.830189	-2800.771233	-2800.763628	-2800.80454	-2800.930006

E<sub>e</sub> Electronic energyE<sub>0</sub> Total energy plus zero-point vibrational energyH<sub>298</sub> Enthalpy at 298 KG<sub>298</sub> Gibbs free enthalpy at 298 KE<sub>sov</sub> Total energy plus CPCM solvation energy (NMP)

**Table 5.S5.** Absolute energies (hartree) for all the ligands and their respective conjugate acids (B3LYP/6-31G\*).

No.	Point Group	E <sub>e</sub>	E <sub>0</sub>	H <sub>298</sub>	G <sub>298</sub>
6	C <sub>1</sub>	-653.807853	-653.513183	-653.497362	-653.553831
1	C <sub>1</sub>	-725.247753	-725.030268	-725.017398	-725.068297
1	C <sub>2v</sub>	-725.247670	-725.030241	-725.018211	-725.066627
1	C <sub>s</sub>	-725.247669	-725.030231	-725.018199	-725.067279
2	C <sub>1</sub>	-1644.436168	-1644.237920	-1644.222551	-1644.279838
2	C <sub>2</sub>	-1644.436168	-1644.237920	-1644.222551	-1644.279837
2	C <sub>s</sub>	-1644.435887	-1644.237719	-1644.223170	-1644.278718
2	C <sub>2v</sub>	-1644.435887	-1644.237719	-1644.223170	-1644.278064
3	C <sub>1</sub>	-5867.455677	-5867.258336	-5867.242489	-5867.302177
3	C <sub>s</sub>	-5867.455385	-5867.258123	-5867.243103	-5867.300995
4	C <sub>1</sub>	-954.298723	-954.015209	-953.997080	-954.060437
4	C <sub>s</sub>	-954.298615	-954.015084	-953.997838	-954.058489
5	C <sub>1</sub>	-1299.367833	-1299.126952	-1299.110198	-1299.170846
6s	C <sub>1</sub>	-653.814720	-653.520204	-653.504339	-653.560845
1s	C <sub>1</sub>	-725.254909	-725.037382	-725.024487	-725.075932
2s	C <sub>1</sub>	-1644.441907	-1644.243674	-1644.228272	-1644.286468
3s	C <sub>1</sub>	-5867.461434	-5867.264104	-5867.248228	-5867.308807
4s	C <sub>1</sub>	-954.308580	-954.025107	-954.006973	-954.070198
5s	C <sub>1</sub>	-1299.375547	-1299.134678	-1299.117897	-1299.178696
6H <sup>+</sup>	C <sub>1</sub>	-654.217800	-653.909469	-653.893530	-653.950465
1H <sup>+</sup>	C <sub>1</sub>	-725.671228	-725.439142	-725.426528	-725.476760
2H <sup>+</sup>	C <sub>1</sub>	-1644.850136	-1644.637655	-1644.622535	-1644.679359
3H <sup>+</sup>	C <sub>1</sub>	-5867.870892	-5867.659336	-5867.643736	-5867.703004
4H <sup>+</sup>	C <sub>1</sub>	-954.737162	-954.439155	-954.421226	-954.483258
5H <sup>+</sup>	C <sub>s</sub>	-1299.796062	-1299.540755	-1299.524171	-1299.583777
5H <sup>+</sup> a	C <sub>s</sub>	-1299.792283	-1299.537370	-1299.520817	-1299.580338
6sH <sup>+</sup>	C <sub>1</sub>	-654.285891	-653.976820	-653.960891	-654.017994
1sH <sup>+</sup>	C <sub>1</sub>	-725.734301	-725.502279	-725.489601	-725.540002
2sH <sup>+</sup>	C <sub>1</sub>	-1644.914915	-1644.702351	-1644.687225	-1644.743966
3sH <sup>+</sup>	C <sub>1</sub>	-5867.934856	-5867.723214	-5867.707597	-5867.766838
4sH <sup>+</sup>	C <sub>1</sub>	-954.796811	-954.498996	-954.481023	-954.543311
5sH <sup>+</sup> a	C <sub>1</sub>	-1299.858824	-1299.603567	-1299.586941	-1299.646916
6H <sup>+</sup> ‡	C <sub>1</sub>	-654.215932	-653.911102	-653.895406	-653.951601
2H <sup>+</sup> ‡	C <sub>1</sub>	-1644.844399	-1644.636269	-1644.621388	-1644.677604
5H <sup>+</sup> ‡	C <sub>1</sub>	-1299.788220	-1299.537461	-1299.521148	-1299.580058

E<sub>e</sub> Electronic energyE<sub>0</sub> Total energy plus zero-point vibrational energyH<sub>298</sub> Enthalpy at 298 KG<sub>298</sub> Gibbs free enthalpy at 298 K

**Table 5.S6.** Structural parameters and dipole moments for the substituted quino[7,8-h]quinolines and their conjugated acids (B3LYP/6-31G\*).

No.	Substituents	Point group	N1-N2 (Å)	N2-H11 (Å)	N1-H11-N2 (°)	C16-C14 (Å)	C5-C6 (Å)	$\Phi^a$ (°)	$\Theta^a$ (°)	$\Phi+\Theta$ (°)	A (D) <sup>b</sup>
1 <sup>c</sup>	H	C <sub>1</sub>	2.728	—	—	2.584	2.450	1.40	—	—	—
1	H	C <sub>1</sub>	2.739	—	—	2.583	2.453	7.72	7.72	15.44	1.895
2	Cl	C <sub>1</sub> /C <sub>2</sub>	2.711	—	—	2.577	2.455	10.28	10.28	20.56	0.699
3	Br	C <sub>1</sub>	2.709	—	—	2.577	2.456	10.40	10.40	20.80	0.797
4	OCH <sub>3</sub>	C <sub>1</sub>	2.724	—	—	2.582	2.451	8.28	8.28	16.56	0.552
1	H	C <sub>s</sub>	2.734	—	—	2.591	2.447	0.00	0.00	0.00	1.930
2	Cl	C <sub>s</sub> /C <sub>2v</sub>	2.702	—	—	2.591	2.445	0.00	0.00	0.00	0.712
3	Br	C <sub>s</sub>	2.701	—	—	2.592	2.445	0.00	0.00	0.00	0.814
4	OCH <sub>3</sub>	C <sub>s</sub>	2.717	—	—	2.590	2.445	0.00	0.00	0.00	0.611
5	Cl & OCH <sub>3</sub>	C <sub>1</sub>	2.717	—	—	2.579	2.453	9.55	9.13	18.67	3.677
1s	H	C <sub>1</sub>	2.761	—	—	2.589	2.450	8.01	8.01	16.02	2.778
2s	Cl	C <sub>1</sub>	2.726	—	—	2.582	2.452	9.86	9.86	19.72	1.164
3s	Br	C <sub>1</sub>	2.725	—	—	2.581	2.452	10.29	10.29	20.58	1.290
4s	OCH <sub>3</sub>	C <sub>1</sub>	2.745	—	—	2.590	2.447	7.81	7.81	15.62	1.003
5s	Cl & OCH <sub>3</sub>	C <sub>1</sub>	2.734	—	—	2.586	2.449	8.88	8.35	17.23	4.521
1H <sup>+</sup>	H	C <sub>1</sub>	2.629	1.052	140.37	2.542	2.475	0.00	0.00	0.00	—
2H <sup>+</sup>	Cl	C <sub>1</sub>	2.609	1.054	140.89	2.547	2.471	0.00	0.00	0.00	—
3H <sup>+</sup>	Br	C <sub>1</sub>	2.609	1.054	140.96	2.547	2.471	0.00	0.00	0.00	—
4H <sup>+</sup>	OCH <sub>3</sub>	C <sub>1</sub>	2.613	1.052	140.53	2.543	2.472	0.00	0.00	0.00	—
5H <sup>+</sup>	Cl & OCH <sub>3</sub>	C <sub>s</sub>	2.622	1.047	139.69	2.548	2.469	0.00	0.00	0.00	—
5H <sup>+</sup> a	Cl & OCH <sub>3</sub>	C <sub>s</sub>	2.599	1.059	141.76	2.541	2.473	0.00	0.00	0.00	—
1sH <sup>+</sup>	H	C <sub>1</sub>	2.654	1.043	138.36	2.548	2.470	0.00	0.00	0.00	—
2sH <sup>+</sup>	Cl	C <sub>1</sub>	2.617	1.049	139.57	2.548	2.470	0.00	0.00	0.00	—
3sH <sup>+</sup>	Br	C <sub>1</sub>	2.617	1.048	139.60	2.549	2.469	0.01	0.00	0.01	—
4sH <sup>+</sup>	OCH <sub>3</sub>	C <sub>1</sub>	2.640	1.041	138.45	2.551	2.468	0.00	0.00	0.00	—
5sH <sup>+</sup> a	Cl & OCH <sub>3</sub>	C <sub>1</sub>	2.623	1.041	138.11	2.550	2.469	0.00	0.00	0.00	—

<sup>a</sup>Dihedral angles:  $\Phi$  = N1—C16—C15—C14;  $\Theta$  = C16—C15—C14—N2, <sup>b</sup>The (origin-dependent) dipole moment is not reported for the cations.

X-ray data from ref.19; all other entries are computational results.

**Table 5.S7.** Energies (kcal/mol) of planar relative to twisted ligands and imaginary frequencies  $\omega$  ( $i$  cm<sup>-1</sup>) for the inversion mode in the planar structures (B3LYP/6-31G\*).

No.	Substituent	Point group	$\Delta E_c$	$\Delta E_0$	$\Delta H_{298}$	$\Delta G_{298}$	$\omega$
1	H	C <sub>s</sub>	0.1	0.0	-0.5	0.6	30
2	Cl	C <sub>s</sub> /C <sub>2v</sub>	0.2	0.1	-0.4	0.7	34
3	Br	C <sub>s</sub>	0.2	0.1	-0.4	0.7	32
4	OCH <sub>3</sub>	C <sub>s</sub>	0.1	0.1	-0.5	1.2	26

**Table 5.S8.** Proton affinities in kcal/mol (B3LYP/6-31G\*).

Gas Phase		Solution <sup>a</sup>	
1	256.7	1s	291.9
2	251.0	2s	288.0
3	251.8	3s	288.3
4	266.2	4s	297.5
5	242.2	5s	294.3
5a	257.7	6s	286.5 <sup>[55]</sup>
6	248.6 <sup>[55]</sup>		

<sup>a</sup>Solvent dichloromethane.

## Bibliography

- [1] ISI Web of Science; (<http://go5.isiknowledge.com>) keywords “proton” and “sponges”.
- [2] W. G. Brown, N. J. Letang, “Hydrogen Exchange Reactions of Aromatic Tertiary Amines.” *J. Am. Chem. Soc.* **1941**, 63, 358-361.
- [3] R. W. Alder, P. S. Bowman, W. R. S. Steele, D. R. Winterman, “The Remarkable Basicity of 1,8-Bis(dimethylamino)naphthalene.” *Chem. Commun.* **1968**, 723-724.
- [4] H. A. Staab, K. Elbl-Weier, C. Krieger, “New “Proton Sponges”, 13<sup>[≠]</sup> Syntheses, Structures and Basicities of 1,2,4,5-Tetrakis(dimethylamino)benzene and 2,3,6,7-Tetrakis(dimethylamino)naphthalene.” *Eur. J. Org. Chem.* **2000**, 327-333.
- [5] H. A. Staab, A. Kirsch, T. Barth, C. Krieger, F. A. Neugebauer, “New “Proton Sponges”, 14<sup>[≠]</sup> Isomeric Tetrakis(dimethylamino)naphthalenes: Syntheses, Structure Dependence of Basicities, Crystal Structures, and Physical Properties.” *Eur. J. Org. Chem.* **2000**, 1617-1622.
- [6] E. H. Wong, G. R. Weisman, D. C. Hill, D. P. Peed, M. E. Roger, J. S. Condon, M. A. Fagan, J. C. Calabrese, K-Ch. Lam, I. Guzei, A. L. Rheingold, “Synthesis and Characterization of Cross-Bridged Cyclams and Pendant-Armed Derivatives and Structural Studies of Their Copper(II) Complexes.” *J. Am. Chem. Soc.* **2000**, 122, 10561-10572.
- [7] S. J. Ikuta, “Electron correlation effect on the geometries and energetics: Proton-bound ammonia dimer, (H<sub>3</sub>N—N···NH<sub>3</sub>)<sup>+</sup>.” *J. Chem. Phys.* **1987**, 87, 1900-1901.
- [8] S. T. Howard, “Relationship between Basicity, Strain, and Intramolecular Hydrogen-Bond Energy in Proton Sponges.” *J. Am. Chem. Soc.* **2000**, 122, 8238-8244.
- [9] S. T. Howard, J. A. Platts, “Ab Initio Studies of Proton Sponges. 4. Calculating the Strain Energy.” *J. Org. Chem.* **1998**, 63, 3568-3571.
- [10] J. A. Platts, S. T. Howard, K. Wozniak “Ab Initio Studies of Proton Sponges: 1,8-Bis(dimethylamino)naphthalene.” *J. Org. Chem.* **1994**, 59, 4647-4651.
- [11] M. Peräkylä, “Ab Initio Quantum Mechanical Study on the Origin of the pK<sub>a</sub> Differences of the Proton Sponges 1,8-Bis(dimethylamino)-2,7-dimethoxynaphthalene, 1,6-Dimethyl-1,6-diazacyclodecane, and 1,6-Diazabicyclo[4.4.4]tetradecane.” *J. Org. Chem.* **1996**, 61, 7420-7425.

- [12] S. T. Howard, I. A. Fallis, "Ab Initio Studies of Proton Sponges (V): 1,4,7,10-Tetraaza-tricyclo[5,5,2,2<sup>4,10</sup>]hexadecane, a Tricyclic Proton Sponge." *J. Org. Chem.* **1998**, *63*, 7117-7119.
- [13] S. T. Howard, "Conformers, Energetics, and Basicity of 2,2'-Bipyridine." *J. Am. Chem. Soc.* **1996**, *118*, 10269-10274.
- [14] A. Gobbi, G. Frenking, "Y-Conjugated Compounds: The Equilibrium Geometries and Electronic Structures of Guanidine, Guanidinium Cation, Urea, and 1,1-Diaminoethylene." *J. Am. Soc. Chem.* **1993**, *115*, 2362-2372.
- [15] M. A. Fox, A. E. Goeta, J. A. K. Howard, A. K. Hughes, A. L. Johnson, D. A. Keen, K. Wade, C. C. Wilson, "The Molecular Structure of (PSH<sup>+</sup>)(*nido*-7,8-C<sub>2</sub>B<sub>9</sub>H<sub>12</sub><sup>-</sup>) Determined by Neutron Diffraction (PS = Proton Sponge, 1,8-Bis(dimethylamino)naphthalene)." *Inorg. Chem.* **2001**, *40*, 173-175.
- [16] E. Bartoszak, Z. Dega-Szafran, M. Grunwald-Wyspianska, M. Jaskolski, M. J. Szafran, "X-Ray, Fourier-transform Infrared, <sup>1</sup>H and <sup>13</sup>C Nuclear Magnetic Resonance, and PM3 Studies of (N—H···N)<sup>+</sup> and (O—H···O)<sup>-</sup> Intramolecular Hydrogen Bonds in a Complex of 1,8-Bis(dimethylamino)naphthalene with Maleic Acid." *J. Chem. Soc., Faraday Trans.* **1993**, *89*, 2085-2094.
- [17] (a) P. A. Frey, "Low-Barrier Hydrogen Bonds and Enzymic Catalysis." *Science* **1994**, *264*, 1887-1890, (b) W. W. Cleland, M. M. Kreevoy, *Response to "On Low-Barrier Hydrogen Bonds and Enzyme Catalysis by A. Warshel, A. Papazyan, P. A. Kollmann, Science, 1995, 269, 102-104."* *Science* **1995**, *269*, 104-104. (c) O. E. L. Ash, J. L. Sudmeier, E. C. D. Fabo, W. W. Bachovchin, "A Low-Barrier Hydrogen Bond in the Catalytic Triad of Serine Proteases? Theory Versus Experiment." *Science* **1997**, *278*, 1128-1132.
- [18] M. A. Zirnstein, H. A. Staab, "Quino[7,8-*h*]quinoline, a New Type of "Proton Sponge"." *Angew. Chem., Int. Ed. Engl.* **1987**, *26*, 460-461.
- [19] C. Krieger, I. Newsom, M. A. Zirnstein, H. A. Staab, "Structure of Quino[7,8-*h*]quinoline and Quino[8,7-*h*]quinoline." *Angew. Chem., Int. Ed. Engl.* **1989**, *28*, 84-86.
- [20] H. U. Wüstefeld, W. C. Kaska, F. Schüth, G. Stucky, X. Bu, B. Krebs, "Transition Metal Complexes with the Proton Sponge 4,9-Dichloroquino[7,8-*h*]quinoline: Highly Twisted Aromatic Systems and an Extreme "Out-of-Plane" Position of the Coordinated Transition Metal Atom." *Angew Chem., Int. Ed. Engl.* **2001**, *40*, 3182-3184.

- [21] Gaussian 03, Revision B.01, M. J. Frisch, G. W. Trucks, H. B. Schlegel, G. E. Scuseria, M. A. Robb, J. R. Cheeseman, J. A. Montgomery, Jr., T. Vreven, K. N. Kudin, J. C. Burant, J. M. Millam, S. S. Iyengar, J. Tomasi, V. Barone, B. Mennucci, M. Cossi, G. Scalmani, N. Rega, G. A. Petersson, H. Nakatsuji, M. Hada, M. Ehara, K. Toyota, R. Fukuda, J. Hasegawa, M. Ishida, T. Nakajima, Y. Honda, O. Kitao, H. Nakai, M. Klene, X. Li, J. E. Knox, H. P. Hratchian, J. B. Cross, C. Adamo, J. Jaramillo, R. Gomperts, R. E. Stratmann, O. Yazyev, A. J. Austin, R. Cammi, C. Pomelli, J. W. Ochterski, P. Y. Ayala, K. Morokuma, G. A. Voth, P. Salvador, J. J. Dannenberg, V. G. Zakrzewski, S. Dapprich, A. D. Daniels, M. C. Strain, O. Farkas, D. K. Malick, A. D. Rabuck, K. Raghavachari, J. B. Foresman, J. V. Ortiz, Q. Cui, A. G. Baboul, S. Clifford, J. Cioslowski, B. B. Stefanov, G. Liu, A. Liashenko, P. Piskorz, I. Komaromi, R. L. Martin, D. J. Fox, T. Keith, M. A. Al-Laham, C. Y. Peng, A. Nanayakkara, M. Challacombe, P. M. W. Gill, B. Johnson, W. Chen, M. W. Wong, C. Gonzalez, and J. A. Pople, Gaussian, Inc., Pittsburgh PA, **2003**.
- [22] A. D. Becke, "Density-functional exchange-energy approximation with correct asymptotic behaviour." *Phys. Rev. A* **1988**, 38, 3098-3100.
- [23] J. P. Perdew, "Density-functional approximation for the correlation energy of the inhomogeneous electron gas." *Phys. Rev. B* **1986**, 33, 8822-8824.
- [24] W. J. Hehre, L. Radom, P. v. R. Schleyer, J. A. Pople, "Ab Initio Molecular Orbital Theory", Wiley, New York, **1986**, page 65-68.
- [25] P. J. Hay, W. R. Wadt, "*Ab initio* effective core potentials for molecular calculations. Potentials for K to Au including the outermost core orbitals." *J. Chem. Phys.* **1985**, 82, 299-310.
- [26] A. D. Becke, "Density-functional thermochemistry. III. The role of exact exchange." *J. Chem. Phys.* **1993**, 98, 5648-5652.
- [27] C. Lee, W. Yang, R. G. Parr, "Development of the Colle-Salvetti correlation-energy formula into a functional of the electron density." *Phys. Rev. B* **1988**, 37, 785-789.
- [28] J. Tomasi, M. Persico, "Molecular Interactions in Solution: An Overview of Methods Based on Continuous Distributions of the Solvent." *Chem Rev.* **1994**, 94, 2027-2094.
- [29] A. R. Leach, "Molecular modelling: principles and applications", **2001**, 2<sup>nd</sup> ed., Pearson Education Limited.



- [30] (a) R. F. W. Bader, "A Quantum Theory of Molecular Structure and Its Application." *Chem. Rev.* **1991**, *91*, 893-928. (b) R. F. W. Bader, P. L. A. Popelier, T. A. Keith, "Theoretical Definition of a Functional Group and the Molecular Orbital Paradigm." *Angew. Chem. Int. Ed. Engl.* **1994**, *33*, 620-631. (c) R. F. W. Bader, "Atoms in Molecules: A Quantum Theory", Oxford University Press: Oxford, **1990**.
- [31] (a) A. E. Reed, L. A. Curtiss, F. Weinhold, "Intermolecular Interactions from a Natural Bond Orbital, Donor-Acceptor Viewpoint." *Chem. Rev.* **1998**, *88*, 899-926. (b) E. D. Glendening, A. E. Reed, J. E. Carpenter, Weinhold, F. *NBO Version 3.1*.
- [32] K. B. Wiberg, "Application of the Pople-Santry-Segal CNDO method to the cyclopropylcarbiny and cyclobutyl cation and to bicyclobutane." *Tetrahedron* **1968**, *24*, 1083-1096.
- [33] H. U. Wüstefeld, private communication (**2005**). The X-ray structure of **2** and **4** has been resolved, but has not yet been published.
- [34] J. A. Platts, S. T. Howard, "Ab Initio Studies of Proton Sponges. 3. 4,5-Bis(dimethylamino)fluorene and 4,5-Bis(dimethylamino)phenanthrene." *J. Org. Chem.* **1996**, *61*, 4480-4482.
- [35] E. Fujiwara, K. Omoto, H. Fujimoto, "Theoretical Study of Strong Basicity in Aromatic Diamines." *J. Org. Chem.* **1997**, *62*, 7234-7238.
- [36] C. L. Perrin, B. K. Ohta, "Symmetry of N-H-N Hydrogen Bonds in 1,8-Bis(dimethylamino)naphthalene·H<sup>+</sup> and 2,7-Dimethoxy-1,8-bis(dimethylamino)naphthalene·H<sup>+</sup>." *J. Am. Chem. Soc.* **2001**, *123*, 6520-6526.
- [37] C. L. Perrin, "Symmetries of Hydrogen Bonds in Solution." *Science*, **1994**, *266*, 1665-1668.
- [38] J. B. Foresman, Æ. Frisch, "Exploring Chemistry with Electronic Structures Methods." **1996**, 2<sup>nd</sup> ed., Gaussian, Inc., Pittsburgh, PA 15106 U.S.A.
- [39] X. Duan, S. Scheiner, "Energetics, Proton Transfer Rates, and Kinetic Isotope Effects in Bent Hydrogen Bonds." *J. Am. Chem. Soc.* **1992**, *114*, 5849-5856.
- [40] W. J. Hehre, J. A. Pople, "Molecular Orbital Theory of the Electronic Structure of Organic Compounds. III. *Ab Initio* Studies of Charge Distribution Using a Minimal Slater-Type Basis." *J. Am. Chem. Soc.* **1970**, *92*, 2191-2197.

- [41] Extended Hückel calculation using the default parameter set from the Hoffmann group, see ref 42.
- [42] R. Hoffmann, "An Extended Hückel Theory. I. Hydrocarbons." *J. Chem. Phys.* **1963**, *39*, 1397-1412.
- [43] R. F. W. Bader, T. S. Slee, D. Cremer, E. Kraka, "Description of Conjugation and Hyperconjugation in Terms of Electron Distributions." *J. Am. Chem. Soc.* **1983**, *105*, 5061-5068.
- [44] (a) A. De Meijere, F. E. Meyer, "Fine Feathers Make Fine Birds: The Heck Reaction in Modern Garb." *Angew. Chem., Int. Ed. Engl.* **1995**, *33*, 2379-2411. (b) W. Cabri, I. Candiani, "Recent Developments and New Perspectives in the Heck Reaction." *Acc. Chem. Res.* **1995**, *28*, 2-7. c) I. P. Beletskaya, A. V. Cheprakov, "The Heck Reaction as a Sharpening Stone of Palladium Catalysis." *Chem. Rev.* **2000**, *100*, 3009-3066.
- [45] BP86 functional with 6-31+G\*\* basis at carbon, hydrogen, nitrogen and chlorine. Palladium was described by the Stuttgart-Dresden quasirelativistic pseudopotential with the respective valence basis set in a (8s7p5d)/[6s5p3d] contraction, see ref. 46
- [46] D. Andrae, U. Häußermann, M. Dolg, H. Stoll, H. Preuß, "Energy-adjusted ab initio pseudopotentials for the second and third row transition elements." *Theor. Chim. Acta* **1990**, *77*, 123-141.
- [47] H. U. Wüstefeld, private communication (**2005**).
- [48] H. M. Senn, T. Ziegler, "Oxidative Addition of Aryl Halides to Palladium(0) Complexes: A Density-Functional Study Including Solvation." *Organometallics* **2004**, *23*, 2980-2988.
- [49] (a) J. J. Low, W. A. Goddard III, "Theoretical Studies of Oxidative Addition and Reductive Elimination:  $H_2 + Pt(PH_3)_2 \rightarrow Pt(H)_2(PH_3)_2$ ." *J. Am. Chem. Soc.* **1984**, *106*, 6928-6937. (b) S. Obara, K. Kituara, K. Morokuma, "Reaction Mechanisms of Oxidative Addition [ $H_2 + Pt^0(PH_3)_2 \rightarrow Pt^{II}(H)_2(PH_3)_2$ ] and Reductive Elimination [ $Pt^{II}(H)(CH_3)(PH_3)_2 \rightarrow CH_4 + Pt^0(PH_3)_2$ ]. Ab Initio MO Study." *J. Am. Chem. Soc.* **1984**, *106*, 7482-7492.
- [50] A. Sundermann, O. Uzan, J. M. L. Martin, "Computational Study of a New Heck Reaction Mechanism Catalyzed by Palladium(ii/iv) Species." *Chem. Eur. J.* **2001**, *7*, 1703-1711.

- [51] K. Albert, P. Gisdakis, N. Rösch, "On C–C Coupling by Carbene-Stabilized Palladium Catalysts: A Density Functional Study of the Heck Reaction." *Organometallics* **1998**, *17*, 1608-1616.
- [52] (a) M. J. S. Dewar, "A Review of the  $\pi$ -Complex Theory." *Bull. Soc. Chim. Fr.* **1951**, *18*, C71-C79. (b) J. Chatt, L. A. Duncanson, "Olefin co-ordination compounds. Part III. Infra-red spectra and structure: attempted preparation of acetylene complexes." *J. Chem. Soc.* **1953**, 2939-2947.
- [53] F. C. Rix, M. Brookhart, P. S. White, "Mechanistic Studies of the Palladium(II)-Catalyzed Copolymerization of Ethylene with Carbon Monoxide." *J. Am. Chem. Soc.* **1996**, *118*, 4746-4764.
- [54] J. B. Pedley, R. D. Naylor, S. P. Kirby, "Thermochemical Data of Organic Compounds." 2<sup>nd</sup> Ed., Chapman and Hall, London, **1986**.
- [55] Calculations performed using PCM model instead of SCIPCM, due to difficulties encountered during wave function convergence. Benchmark calculations show that the energies from these models differ by less than 0.1 kcal/mol.







## DFT Investigation of the Single-Center, Two-State Model for the Broken Rate Order of Transition Metal Catalyzed Olefin Polymerization.

*The triumph of a theory is to embrace the greatest number and the greatest variety of facts*

(Charles Adolphe Wurtz, A History of Chemical Theory from the Age of Lavoisier to the Present Time, Lavoisier, I, page 7)

### 6.1 Introduction

The introduction and availability of structurally well-defined homogeneous catalysts, in particular the metallocene-based class of catalysts, has formed the basis for an impressive level of mechanistic insight in the field of transition metal catalyzed olefin polymerization. The active species in metallocene-based polymerization has been identified as a transition metal alkyl cation of the general formula  $[L_2MR]^+$  ( $L = \text{Cp}$  or related ligands;  $M = \text{transition metal}$ ;  $R = \text{alkyl group}$ ).<sup>[1]</sup> It is clear that the determination and characterization of the active polymerizing complex has had tremendous impact on the subsequent mechanistic investigations and on the further developments in the field of olefin polymerization. The metal alkyl cation has often been the starting point for mechanistic discussions and investigations, exemplified by the numerous molecular-level computational studies that have relied on the alkyl metallocene cation as model for the active catalyst.<sup>[2-11]</sup> These investigations have added detail and resolution to the propagation mechanism developed by Cossée and Arlman<sup>[12]</sup> as well as to the mechanism of most of the other key elementary reactions of olefin polymerization. The computational efforts have produced a particularly detailed picture for the reaction pathway of olefin insertion into the metal—alkyl bond from the pre-insertion metal—olefin complex, and highlighted the role of agostic interactions at different stages of the reaction. Results from such calculations have often compared favorably to experimental observations when such comparisons have been possible. In polymerization of propene using *ansa*-zirconocenes, for example, structural considerations limited to the central reacting cation may explain the tacticity of the polypropene formed<sup>[13]</sup> and even suffice for predictions thereof with surprisingly high accuracy.<sup>[6]</sup>

The properties of the catalyst may, however, also be heavily influenced by the degree of cation—anion association, as determined by factors such as the exact nature of the solvent or the anion.<sup>[14]</sup> The role of the co-catalyst anion has been the subject of a series of theoretical

investigations, and has been studied particularly intensively in recent years.[2,4,15-18] These modeling efforts have been facilitated and stimulated by the development of the borate family of anions and structurally well-characterized catalysts such as  $[\text{Cp}_2\text{ZrPr}^+(\text{YB}(\text{C}_6\text{F}_5)_3)]^-$  ( $\text{Y} = \text{H}, \text{CH}_3$ ).[19] The detailed control of the molecular structure of the catalyst has also been extended to synthesis of single molecule catalysts with tethered co-catalyst anions and olefins.[20,21] Such systems have allowed for the observation of insertion events using advanced NMR techniques, and an unprecedented microscopic insight into the workings of the metallocene catalysts.

Despite these developments and advances, there are still mechanistic problems that remain to be solved. The perhaps most puzzling discrepancy between the existing, largely accepted, mechanism and experimental observation concerns the influence of monomer concentration on the propagation rate. The Cossée-Arman mechanism involves the coordination and insertion of only one monomer at the time, resulting in a propagation rate-law which is first-order in monomer concentration, *i.e.*,

$$R_p = k_p[\text{C}][\text{M}]^n \quad (n = 1) \quad (6.1)$$

where  $[\text{C}]$  is the concentration of active centers and  $[\text{M}]$  the concentration of monomer. However, the observed reaction order with respect to monomer concentration is not restricted to unity and rate orders higher than unity have been reported for a broad spectrum of catalysts and monomers.[22-24] For metallocene-based polymerizations in the homogeneous phase, all conceivable indirect effects such as mass- or heat-transfer limitations have been ruled out.[23,24] This led Mülhaupt *et al.*[24] to claim that the observed broken rate order must be caused by “equilibria involving the active species” and that the monomer “might be involved in an equilibrium between dormant and active catalyst sites” whereas Schaper *et al.*[25] pointed out that this must be due to the “intrinsic mechanisms of the polymerization catalysis”. One possible mechanistic explanation for a rate order higher than unity in monomer concentration would be the simultaneous participation of more than one monomer in the propagation cycle. Mechanisms that postulate the presence of two monomers at the transition metal center have been suggested[26] and these ideas have also been subjected to quantum chemical investigation.[2,27] However, as pointed out by Fait *et al.*,[28] a mechanism based on the involvement of more than one monomer is not necessary in order to obtain a rate law implying an effective order higher than one in monomer concentration. With the assumption that the active center of a catalyst exists in two states, one affording slow and the other fast propagation, it is possible to explain rate orders  $1 < n < 2$ .

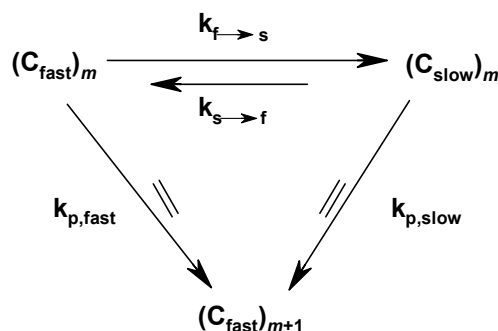


**6.1.1 The single-center, two-state model.** The model by Fait *et al.*[28] places certain requirements and limitations on the allowed relative energies and kinetic constants of the propagation:

1. The catalytic center has two active, monomer-free states,  $C_{\text{fast}}$  and  $C_{\text{slow}}$ , with different propagation rate constants,  $k_{p,\text{fast}}$  and  $k_{p,\text{slow}}$ .
2.  $C_{\text{slow}}$  has lower free energy than  $C_{\text{fast}}$ .
3. The rate of interconversion from the fast to the slow state ( $C_{\text{fast}} \rightarrow C_{\text{slow}}$ ) is intermediate between the rate of propagation for the fast and slow state, respectively, *i.e.*:  $k_{p,\text{fast}}[M] > k_{f \rightarrow s} > k_{p,\text{slow}}[M] > k_{s \rightarrow f}$ .
4. Monomer insertion transforms  $C_{\text{slow}}$  into  $C_{\text{fast}}$ .

A propagation cycle for polymerization of ethylene adhering to these requirements is illustrated in Scheme 6.1, where  $m$  and  $m + 1$  indicate the number of monomer units inserted into the polymer chain.

**Scheme 6.1.**



**6.1.2 The strategy.** The single-center, two-state model is attractive in its simplicity. For example, no major revision of the Cossée-Arlman mechanism, *e.g.*, through inclusion of a second monomer molecule, is required. The model is purely kinetic in nature but the authors suggest that the two states of the active center “could differ in the conformation of the growing polymer chain”, an explanation in agreement with the suggestions cited above,[24,25] *i.e.*, that the reasons for the broken rate order are more likely due to mechanistic details such as equilibria between different species, or states, of the active catalyst. In principle it should be possible to locate candidates for such species, for example by quantum chemical modeling. We are not aware of studies that have been specifically aimed at detecting such equilibria, but one computational study reported a stable zirconocene cation with a secondary alkyl chain to be a candidate for a slow propagating state.[5] Other computational studies have investigated possible active and dormant states arising from different adducts between  $[\text{Cp}_2\text{ZrMe}]^+$ ,

trimethyl aluminum (TMA) and models of methylated methyl aluminoxane, [MeMAO]<sup>+</sup>. [29,30]

An attractive strategy in order to search for candidate slow and fast states could involve computational comparison of catalysts with confirmed different rate orders in monomer concentration. These catalysts should be as similar as possible, and of course, computationally tractable. An excellent pair of catalysts for this task seem to be the simple zirconocenes L<sub>2</sub>ZrCl<sub>2</sub> (L = Cp, *i.e.*, cyclopentadienyl, and L = Cp\*, *i.e.*, pentamethyl cyclopentadienyl). These catalysts are structurally closely related, yet an analysis of kinetic data from two different laboratories shows that they have different rate orders, *n* = 0.99 for L = Cp and *n* = 1.4 for Cp\*, respectively, for polymerization of ethylene with methyl aluminoxane (MAO) as co-catalyst.[9,10] A difference of 0.4 between the two rate orders was confirmed by explicit comparison of the two catalysts in the laboratory of Gerhard Fink,[31] *albeit* with higher absolute values (*n* = 1.3 for L = Cp and *n* = 1.7 for Cp\*), and these two catalysts were thus selected for an explicit search for slow and fast states that could possibly match the single-center, two-state kinetic model. Thorshaug *et al.*[9,10] have reported a detailed combined experimental and computational study of these two catalysts. A pattern of energies matching a single-center, two-state model cannot be discerned among their computational results and a new comparative study of these two catalysts should focus on sections of the potential energy surface not covered by the investigation of Thorshaug *et al.*

To this end, we have performed a density functional theory investigation of different conformers and isomers of the alkyl cation models of the active centers, [L<sub>2</sub>Zr—Pr]<sup>+</sup> (L = Cp, Cp\*; Pr = *n*-propyl as the model of the growing polymer chain), of the two catalysts as well as their corresponding ethylene coordination and insertion reactions. In addition to our highly specific goal to search for potential explanations for the difference in rate order recorded for these two catalysts, the current study will focus especially on the entrance side of the potential energy surface of propagation and thereby complement earlier mechanistic studies of these metallocenes.[9,10]

## 6.2 Computational Details

We used gradient-corrected density functional theory (DFT) with the gradient corrections included self-consistently both during geometry optimization and energy evaluation. The local exchange-correlation potential developed by Vosko *et al.*[32] was augmented with Becke's[33] non-local exchange corrections and Perdew and Wang's[34] non-local correlation corrections. The resulting BPW91 functional was used in the spin-restricted formulation implemented in the Gaussian98[35] and 03[36] set of programs. Detailed studies show that the BPW91 functional is capable of providing accurate energy profiles for the monomer insertion step during metal-catalyzed olefin polymerization.[37] Some validation calculations (where indicated) were performed, using the Gaussian set of programs with the three-parameter hybrid density functional method of Becke (termed "B3LYP"),[38] and with the coupled-cluster approximation including single and double excitations and with contributions from connected triples added perturbatively (CCSD(T)).[39] All valence electrons were correlated in the CCSD(T) calculations.

In the geometry optimizations, effective core potentials (ECP)[40] for the small Ar core of zirconium and the small Ne core of titanium were used in combination with valence basis sets contracted to [3s,3p,2d].[40] For aluminum, an ECP[41] was used for the Ne core in combination with a [2s,2p] contracted valence basis[41] set extended with a polarization function ( $\alpha_d=0.325$ ). Oxygen, carbon and hydrogen atoms were described by standard Dunning-Hay[42] valence double- $\zeta$  basis sets, with a scale factor of 1.2 (1.15) applied for the inner (outer) exponents of H. Polarization functions were added to O ( $\alpha_d=0.961$ ) atoms, and to C ( $\alpha_d=0.75$ ) atoms of the ethylene or the polymer chain. The Gaussian98 defaults[35] were applied for convergence criteria whereas the "ultrafine" (99,590) grid was used in numerical integrations. Each stationary point was characterized by analytic calculation of the second derivative matrix. Zero-point and thermal corrections to the energies were computed from the harmonic frequencies using standard procedures. The T $\Delta$ S contributions calculated for ethylene coordination in the gas phase (10—12 kcal/mol) at 298.15 K do not reflect the actual entropic cost of binding the olefin to the catalyst complex in solution. The discrepancy can be reduced by taking into account the solvation entropy of ethylene since the solvation entropies of the catalyst complex with and without ethylene should be similar.[43] The ethylene solvation entropy amounts to 15.4 eu in toluene,[44] equivalent to 4.6 kcal/mol at 298.15 K, or *ca.* 40% of the calculated gas-phase value for T $\Delta$ S. Similar reasoning leads to the same percentage (40%) for the solvation entropy of H<sub>2</sub> in toluene. The entropic cost of olefin and dihydrogen coordination to or elimination from the transition metal complex in solution

(toluene) has thus been approximated by 60% of the corresponding gas-phase values. This correction strategy has been applied also to transition states of coordination/elimination, and is expected to be a good estimate of the true entropy contribution in condensed phase.[43]

All energies reported in the current work are based on single-point energy calculations using basis sets that were improved compared to those of the geometry optimizations described above: C and H atoms of the ethylene or the polymer chain were described by augmented Dunning triple- $\zeta$  sets denoted TZD2P[37] to account for known basis set sensitivities[37] and polarization functions were included for the C atoms of the Cp rings ( $\alpha_d=0.75$ ). The outermost primitive was split off from each of the contracted 5s, 5p and 5d functions in the Zr valence basis set described above to give a final [4s,4p,3d]-basis set involving 311, 111 and 211 contractions for the 5s, 5p and 5d functions, respectively. Titanium was described by Wachters (14s,11p,6d) primitive basis set extended by (6f)[45] and contracted to [8s,7p,4d,2f], whereas hydrogen atoms directly bound to Ti were described by Dunning basis sets contracted to [3s,1p].[37] The SCF convergence criterion used for these single-points calculations was  $10^{-5}$  (RMS density change) and the “ultrafine” (99,590) grid was used for the numerical integrations.

### 6.3 Results and Discussion

In the following we will present computational results for the various elementary reactions of the monomer-free alkyl cations,  $[L_2Zr-Pr]^+$  ( $L = Cp, Cp^*$ ;  $Pr = n\text{-propyl}$ ), as well as its coordination and insertion of ethylene. We will compare our results with published computational and experimental data and with the pattern required for the single-center, two-state model (*vide supra*), at first assuming that the slow center can be identified among the conformations formed by the *n*-propyl with the zirconocene fragment  $L_2Zr$ . Finally, we will also investigate the possibility of generating a slow state by isomerization of the *n*-propyl group. Structures involving  $L = Cp$  are labeled by a leading “**I**” and those of  $L = Cp^*$  by “**II**”. In the case of an agostic  $Zr-H-C$  structure, this is followed by a Greek letter identifying the carbon atom involved.

**6.3.1 Primary alkyl cations.** The calculated structures and relative energies of zirconium alkyl cations  $[Cp_2Zr-Pr]^+$  with primary alkyl groups in  $\alpha$ -,  $\beta$ - and  $\gamma$ -agostic conformations and their respective unimolecular interconversion reactions are shown in Figure 6.1, whereas the corresponding results for  $[Cp^*_2Zr-Pr]^+$  are given in Figure 6.2. The usual order with respect to relative stability of these three conformations for zirconocenes emerges from our calculations, with the  $\beta$ -agostic structure being the most, and the  $\alpha$ -agostic the least stable structure, respectively. The free energy difference between these two structures amounts to more than 8 kcal/mol for  $L = Cp$ , and more than 6 kcal/mol for  $L = Cp^*$ . The stability for the  $\beta$ -agostic structure is reflected in the structures, with the  $C\beta-H\beta$  bond being elongated by 6–9 pm due to the agostic interaction, see Figures 6.1 and 6.2. For the  $Cp^*$ -complex, however, the  $\gamma$ - and  $\alpha$ -agostic conformations are in fact of similar energies. The stabilization of the  $\alpha$ -agostic structure with respect to the other two conformations upon going from  $L = Cp$  to  $Cp^*$  is due to destabilization of pyramidal (bent) structures for the three-coordinate metal complex,  $[L_2Zr-Pr]^+$  for bulkier ligands,  $L$ . The  $\alpha$ -agostic structure, **II $\alpha$ 2** is planar,  $\Theta = 0.0^\circ$ ,<sup>[46]</sup> whereas the other agostic structures are more pyramidal, with deviations from planarity of  $\Theta = 3.0^\circ$  (**II $\beta$ 1**) and  $\Theta = 9.8^\circ$  (**II $\gamma$ 1**).

It should also be noted that the most stable (by 0.5 kcal/mol)  $\alpha$ -agostic conformation located for  $L = Cp$  (structure **I $\alpha$ 1**, Figure 6.1) is, in fact, not a minimum for  $L = Cp^*$ . The conformation of the propyl chain in **I $\alpha$ 2** (**II $\alpha$ 2**) is similar to that of **I $\gamma$ 1** (**II $\gamma$ 1**) (see below for the interconversion between **I $\alpha$ 2** and **I $\gamma$ 1**), whereas **I $\alpha$ 1** can be generated from **I $\alpha$ 2** by a facile  $\sim 180^\circ$  rotation ( $\Delta G^\ddagger_{298} = 2.5$  kcal/mol relative to **I $\alpha$ 2**) of the terminal ethyl group around the  $C\alpha-C\beta$  bond. This rotation places a  $\beta$ -agostic hydrogen in position for coordination to the

metal through the base of the  $L_2ZrPr$  pyramid. Because the  $L_2ZrPr$  fragment is planar in the case of  $L = Cp^*$  ( $\Theta = 0.0^\circ$  for **II $\alpha$ 2**), access to the metal atom from the base of the pyramid is easier than for  $L = Cp$  ( $\Theta = 11.5^\circ$  for **I $\alpha$ 2**). Relaxation to **II $\beta$ 1** is thus the reason for the lack of stability for this  $\alpha$ -agostic conformation of the chain for the bulkier  $Cp^*$  ligand.

We have located transition states for interconversion between pairs of agostic structures for both  $L = Cp$  and  $Cp^*$ . Interconversion between the primary product of ethylene insertion, **I $\gamma$ 1**, and the most stable conformation, **I $\beta$ 1**, is dominated by rotation around  $C\alpha-C\beta$  and proceeds with a free energy barrier of *ca.* 4 kcal/mol for  $L = Cp$ , or close to 10 kcal/mol for the reverse reaction. Slightly more energy (*ca.* 5 kcal/mol) is needed to overcome the barrier to give the  $\alpha$ -agostic reactant, **I $\alpha$ 1**, directly from the  $\gamma$ -agostic reactant through widening of the  $Zr-C\alpha-C\beta$  angle by more than  $50^\circ$ . In contrast, more than 10 kcal/mol is required to overcome the corresponding barrier from **I $\beta$ 1**. For  $L = Cp^*$ , the stabilization of the  $\alpha$ -agostic conformation for the sterically more demanding ligand results in a lowering of barriers to forming the  $\alpha$ -agostic conformation from both of the other two conformations, to below 2 kcal/mol in order to reach **II $\gamma$ 1—II $\alpha$ 2**<sup>‡</sup>. The corresponding barrier starting from **II $\beta$ 1** is higher than 8 kcal/mol. Our results for the  $\gamma$ - and  $\beta$ -agostic structures and their interconversion are comparable to those of Thorshaug *et al.*, [9] whereas the stabilization of the  $\alpha$ -agostic structure for the  $[Cp^*_2Zr-Pr]^+$  complex and the lowering of the barriers for its formation have apparently not been reported previously.

We now turn to the question of whether the pattern seen for these unimolecular rearrangements could be commensurate with the interconversions described by Fait *et al.* [28] for a single-center, two-state mechanism. For both catalysts, the only candidate so far for  $C_{slow}$  is the  $\beta$ -agostic structure. The primary, kinetic product of insertion, the  $\gamma$ -agostic conformation, **I $\gamma$ 1**, seems to be an interesting candidate for  $C_{fast}$ , provided that the subsequent coordination and insertion of ethylene proceed with lower barriers than the unimolecular conversion to the  $\beta$ -agostic conformation. In addition, for  $L = Cp$ , coordination of ethylene would have to take place for **I $\gamma$ 1**, and not for **I $\alpha$ 1**, because the barrier to formation of **I $\beta$ 1** (the assumed  $C_{slow}$ ) is lower than that for formation of **I $\alpha$ 1**. Thorshaug *et al.* reported virtually barrierless coordination of ethylene to  $\gamma$ -agostic alkyl cations  $[Cp_2Zr-R]^+$ , making this scenario seem possible. For  $L = Cp^*$ , the  $\alpha$ -agostic species may in principle be responsible for the “fast” reaction with ethylene since its formation from **II $\gamma$ 1** ( $C_{fast}$ ) is associated with the lowest of all the interconversion barriers calculated for the present primary propyl cations. Thus, our results

for the ethylene-free alkyl cations indicate that ethylene approach to the catalyst complex should be explicitly investigated for all three agostic conformations, and that the  $\alpha$ -agostic conformer in particular may turn out to be important for  $[\text{Cp}^*_2\text{Zr}-\text{Pr}]^+$ .

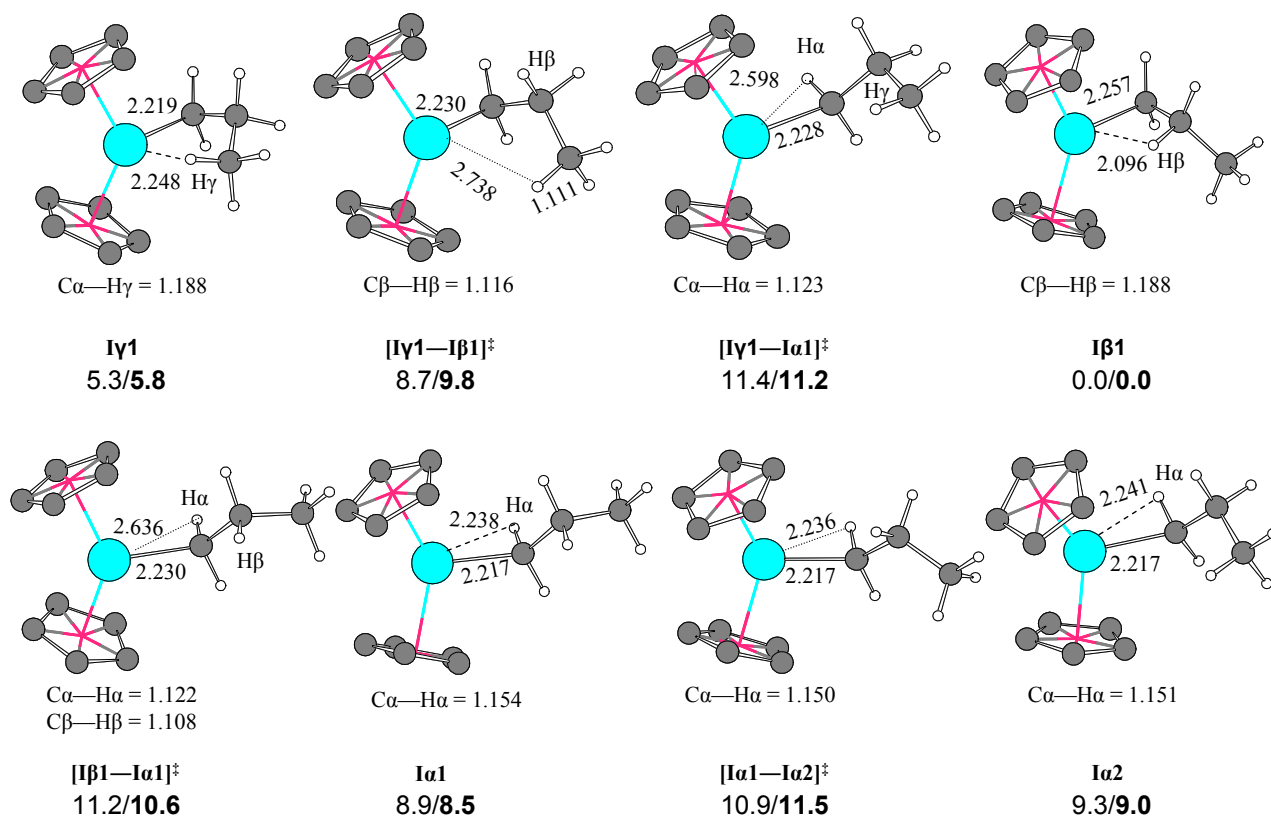


**Figure 6.1.** Different conformers of the primary alkyl cation,  $[\text{Cp}_2\text{Zr}-\text{Pr}]^+$ , and the corresponding transition states of their interconversion. Bond distances are given in angstroms, whereas energies are given in kcal/mol ( $\Delta H_{298}/\Delta G_{298}$ ) relative to **Iβ1** and free ethylene. Hydrogen atoms of the Cp ligands have been omitted for clarity.

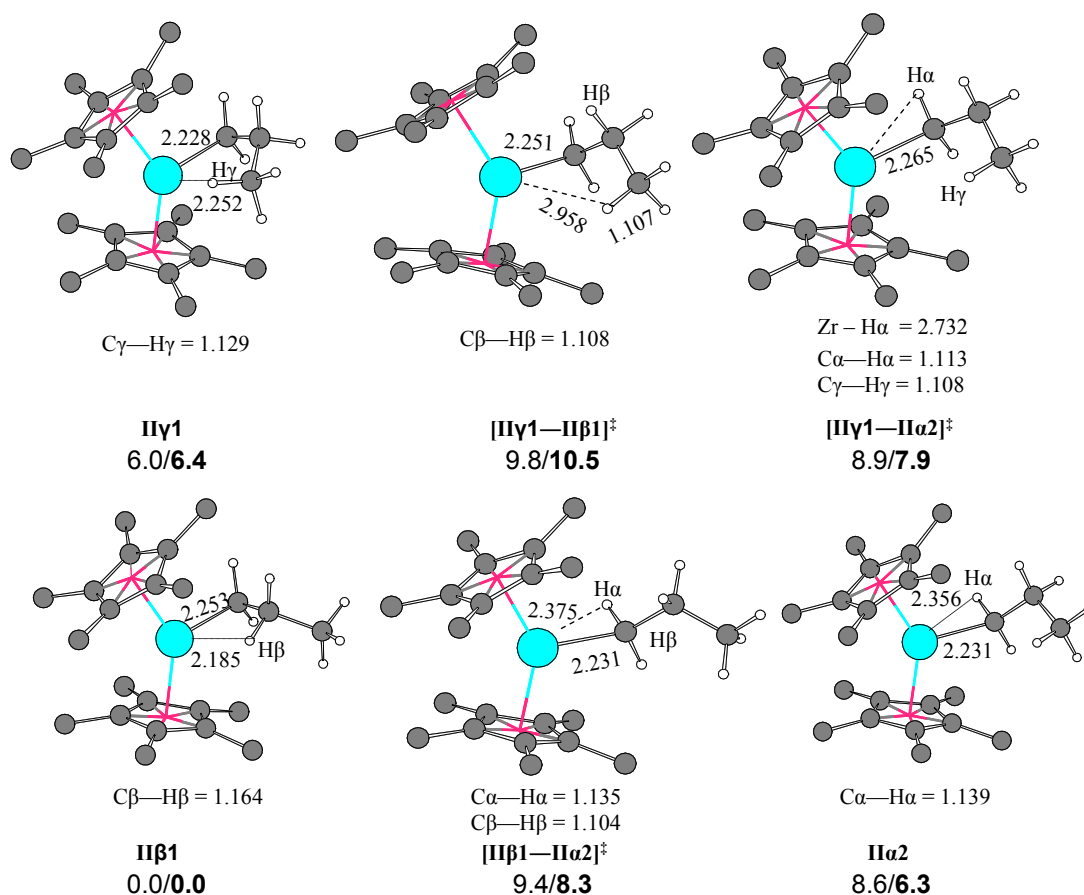


**Figure 6.2.** Different conformers of the primary alkyl cation,  $[\text{Cp}^*_2\text{Zr}-\text{Pr}]^+$ , and the corresponding transition states of their interconversion. Bond distances are given in angstroms. Energies are given in kcal/mol ( $\Delta\text{H}_{298}/\Delta\text{G}_{298}$ ) relative to **II $\beta$ 1** and free ethylene. Hydrogen atoms of the Cp\* ligands have been omitted for clarity.

### 6.3.2 Frontside olefin coordination and insertion.[47]

We start this section by considering coordination of ethylene to the candidate fast state discovered above, the  $\gamma$ -agostic conformation for  $\text{L} = \text{Cp}$ , **I $\gamma$ 1**. However, our calculations suggest that approach of ethylene to this conformer is less favored than other modes of monomer approach, and is associated with a free energy barrier of 7.2 kcal/mol relative to **I $\gamma$ 1** (12.9 kcal/mol relative to **I $\beta$ 1**, cf. Figure 6.3). The major part of this barrier arises from the entropic costs (5.5 kcal/mol) of approaching an ethylene molecule toward the apex of the  $\text{L}_2\text{ZrPr}$  pyramid which is essentially covered by the propyl chain, see Figure 6.3. The electronic contribution (1.7 kcal/mol) is very similar to the energy barriers of Thorshaug *et al.*[9] for  $[\text{Cp}_2\text{Zr}-\text{Pr}]^+$ . Taking into account their reported increase in the electronic barrier to coordination for Zr cations with longer (and more realistic) alkyl chains than propyl, we can safely assume that the true free energy barrier for ethylene coordination to realistic  $\gamma$ -agostic



complexes is higher than that reported here, and that coordination to this conformer is unimportant.

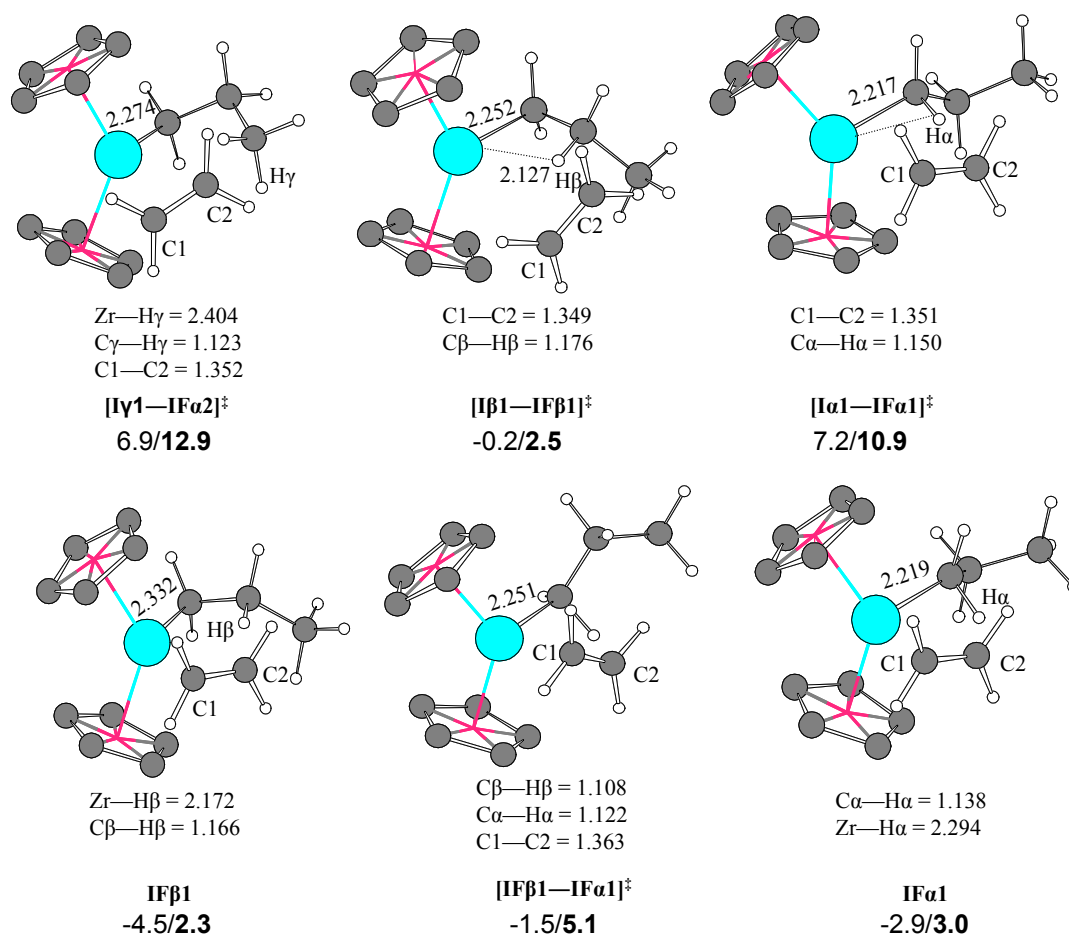
In contrast, ethylene coordination to the two other conformations of the growing polymer chain results in transition structures that are significantly less sterically crowded and thus more stable.[48] Coordination to the  $\beta$ -agostic reactant is even thermoneutral and barrierless relative to **I $\beta$ 1**. [49] For  $L = \text{Cp}$ , our gas-phase calculations predict that the  $\gamma$ -agostic kinetic product of ethylene insertion rearranges ( $\Delta G^\ddagger_{298} = 4.0$  kcal/mol) to the more stable  $\beta$ -agostic conformer and that ethylene coordinates to the latter species without a barrier.

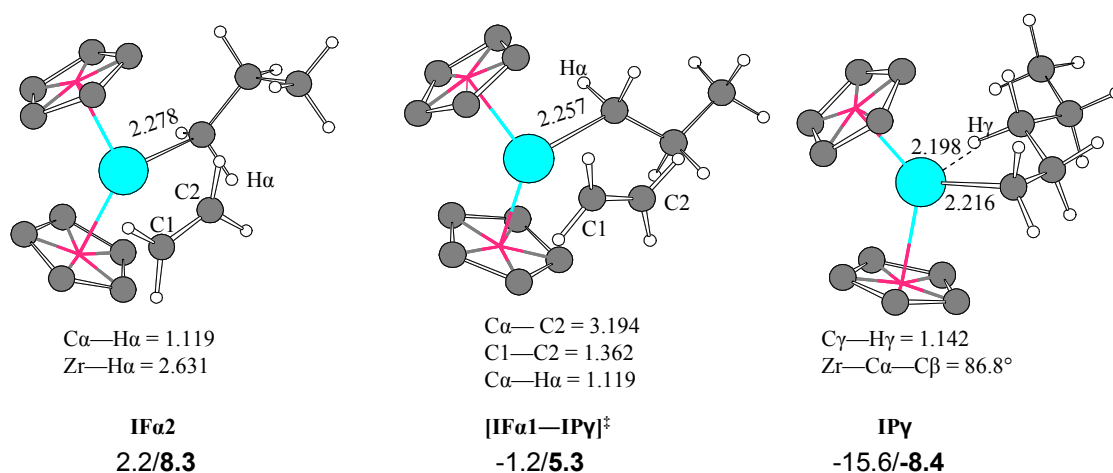
The unfavorable coordination to **I $\gamma$ 1** for  $L = \text{Cp}$  induced us not to investigate coordination of ethylene to **II $\gamma$ 1** since the crowding of the pentamethyl substituted analogue is expected to be even more pronounced. The results for coordination to the  $\beta$ - and  $\alpha$ -agostic species support this expectation, see Figure 6.4. Coordination to the sterically more demanding  $\text{Cp}^*$  analogue preferably takes place when the propyl group has the least possible association with the metal atom, namely the  $\alpha$ -agostic structure, **II $\alpha$ 2**. The free energy barrier for this complexation is 7.2 (13.5) kcal/mol relative to **II $\alpha$ 2** (**II $\beta$ 1**), lower than the corresponding barrier (14.2 kcal/mol) of coordination to **II $\beta$ 1**. Thus, for  $L = \text{Cp}^*$ , our gas-phase calculations predict that the  $\gamma$ -agostic kinetic product of ethylene insertion rearranges ( $\Delta G^\ddagger_{298} = 1.5$  kcal/mol) to the  $\alpha$ -agostic conformer and that ethylene coordinates to the latter species (*via* TS [**II $\alpha$ 2**—**IIF $\alpha$ 1**] $^\ddagger$ ) with a low barrier,[50] in contrast to the clear preference for coordination to the  $\beta$ -agostic reactant seen for  $L = \text{Cp}$ . A growing polymer chain in an  $\alpha$ -agostic conformation shields the metal against attack from an olefin to a lesser extent than a chain in a  $\beta$ - or  $\gamma$ -agostic conformation (Figures 6.3 and 6.4). The preferred type of ethylene coordination ( $\beta$  for  $L = \text{Cp}$  versus  $\alpha$  for  $L = \text{Cp}^*$ ) thus depends on the steric hindrance experienced by the approaching olefin. A similar preference for olefin coordination to the  $\alpha$ -agostic alkyl cation has been noted already for half-sandwich Cr(III)-based catalysts for ethylene oligomerization,[51] but has, to our knowledge, not previously been reported for zirconocenes.

For  $L = \text{Cp}$ , the  $\beta$ - and  $\alpha$ -agostic  $\pi$ -complexes are of similar stability, and the interconversion between them is facile, with a free energy barrier of 2.7 kcal/mol from **IF $\beta$ 1**. There exist several frontside  $\alpha$ -agostic  $\pi$ -complexes that are slightly less stable than **IF $\alpha$ 1**. They differ mainly in their relative ethylene—propyl conformations (structures not reported), and their interconversions are facile. The lowest-energy path of ethylene insertion starts from a frontside  $\alpha$ -agostic  $\pi$ -complex[52] and is triggered by a rotation ( $\Delta G^\ddagger_{298} = 2.3$  kcal/mol relative to **IF $\alpha$ 1**)

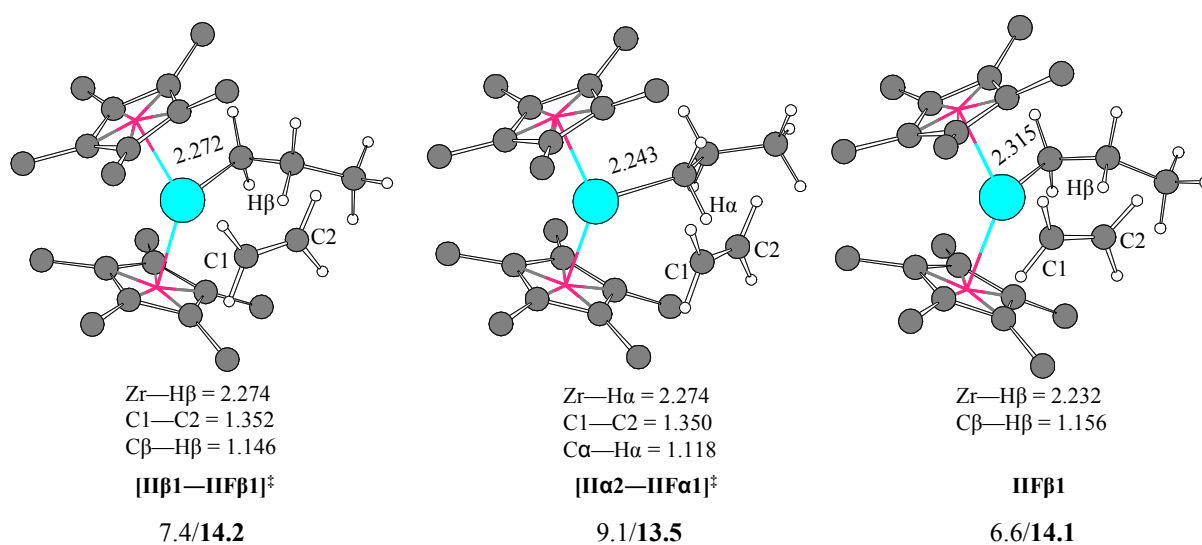
around the Zr—Pr bond to obtain an  $\alpha$ -agostic interaction opposite to ethylene. No minimum exists for this conformation, and insertion of ethylene proceeds without barrier after passing the TS of rotation around the Zr—Pr bond, **[IF $\alpha$ 1—I $\gamma$ P]**<sup>‡</sup>. A C $\alpha$ —H $\alpha$  bond distance of 1.119 Å indicates the beginning formation of a backside Zr—H $\alpha$  agostic interaction that assists insertion and later manifests itself as a  $\gamma$ -agostic bond in the Zr—pentyl insertion product (**I $\gamma$ P**, Figure 6.3).

For L = Cp\*, the most stable  $\pi$ -complex is in fact  $\alpha$ -agostic, see structure **IIF $\alpha$ 1**, Figure 6.4. A second  $\alpha$ -agostic  $\pi$ -complex, **IIF $\alpha$ 2** (Figure 6.4), has the propyl group in the same conformation as in **II $\alpha$ 2** and is 5.3 kcal/mol less stable than **IIF $\alpha$ 1**. The high energy of **IIF $\alpha$ 2** indicates that this  $\pi$ -complex is unimportant for propagation, and therefore ethylene coordination and insertion have not been investigated for this conformation of the propyl group. Ethylene insertion for **IIF $\alpha$ 1** is facile, with a barrier from the  $\pi$ -complex of 4.9 kcal/mol, or 17.6 kcal/mol relative to **II $\beta$ 1**.





**Figure 6.3.** Transition states and minima along the pathway of frontside ethylene coordination and insertion for  $[\text{Cp}_2\text{Zr—Pr}]^+$ . Bond distances are given in angstroms, whereas energies are given in kcal/mol ( $\Delta H_{298}/\Delta G_{298}$ ) relative to the **IPβ1** and free ethylene. Hydrogen atoms of the Cp ligand have been omitted for clarity.



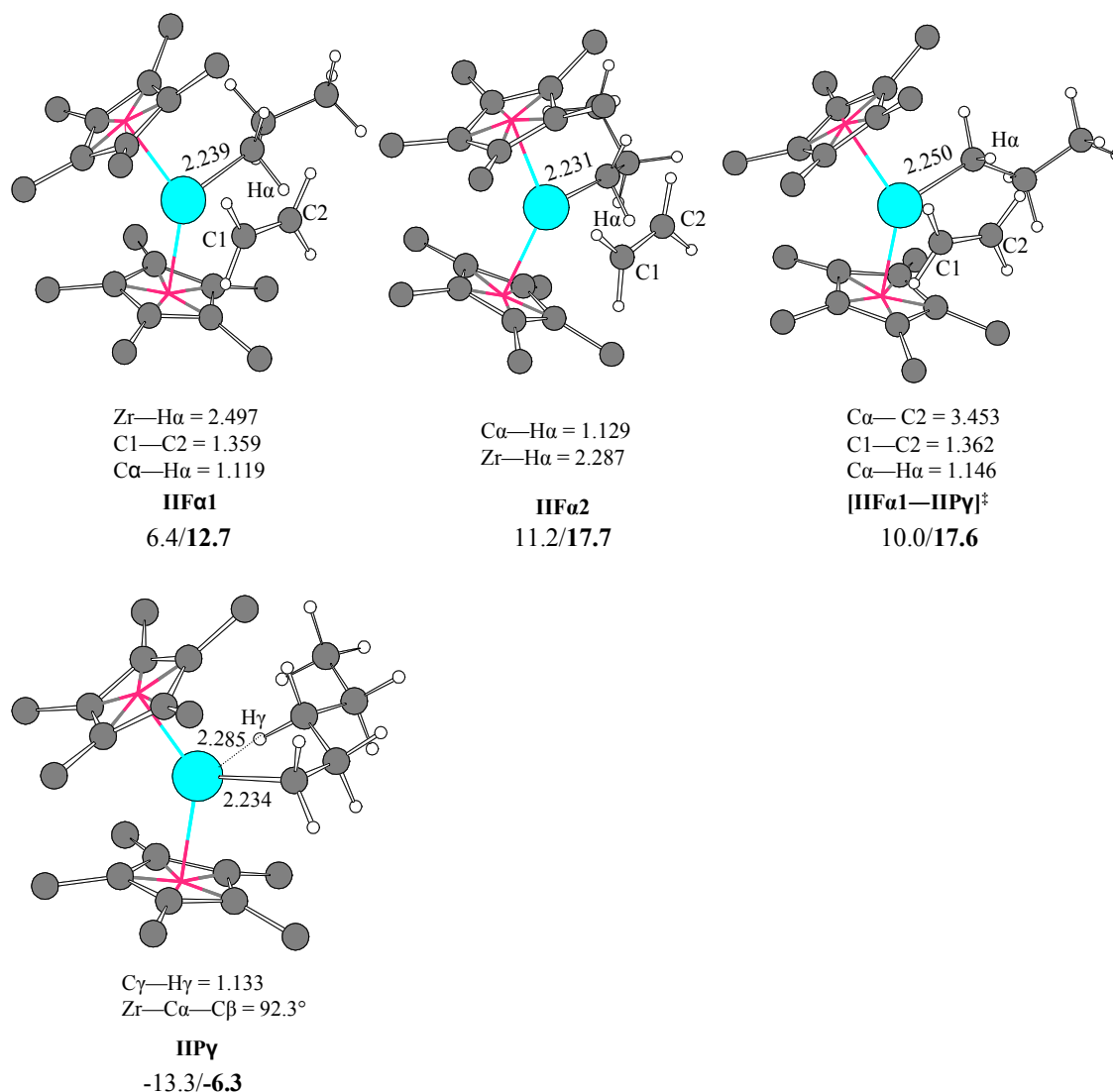


**Figure 6.4.** Transition states and minima along the pathway of frontside ethylene coordination and insertion for  $[\text{Cp}^*_2\text{Zr—Pr}]^+$ . Bond distances are given in angstroms, whereas energies are given in kcal/mol ( $\Delta H_{298}/\Delta G_{298}$ ) relative to **IIβ1** and free ethylene. Hydrogen atoms of the  $\text{Cp}^*$  ligands have been omitted for clarity.

### 6.3.3 Backside olefin coordination and insertion.[47]

For sterically less crowded constrained-geometry catalysts, barriers to frontside and backside insertion have been found to be similar,[11] whereas for metallocenes, backside approach seems to be unimportant. Lohrenz *et al.*[52] noted already 10 years ago that “Backside insertion, although feasible, has a higher activation barrier than the frontside propagation, and is entropically disfavored.” Similar results were reached both for  $L = \text{Cp}$  and  $\text{Cp}^*$  in the comparative study of ethylene polymerization with  $[\text{L}_2\text{Zr—R}]^+$  conducted by Thorshaug *et al.*,[9] who noted that “Backside insertion to a  $\beta$ -agostic conformation is very unlikely for  $L = \text{Cp}^*$ .”. These results suggest that it is not worthwhile to investigate the backside approach to  $\beta$ -

or  $\gamma$ -agostic conformations of the alkyl cation over again for the present zirconocenes. On the other hand, since ethylene coordination to the  $\alpha$ -agostic conformation is most favorable for the bulky system,  $L=Cp^*$ , one may expect the backside approach to be feasible in this case. We indeed find that such backside approach of ethylene to the pentamethyl-substituted zirconocene results in direct insertion (*i.e.*, not passing through a  $\pi$ -complex) with a barrier relative to **II $\beta$ 1** which is less than 1 kcal/mol higher than that estimated for frontside insertion. The TS occurs much earlier than typical 4-center transition states of olefin insertion, see structure **[II $\alpha$ 2—II $\Pi\gamma$ ] $^\ddagger$**  in Figure 6.5. The C—C bond of the inserting ethylene (1.349 Å) is not elongated compared to the bond in free ethylene and the bond to be formed during insertion (C2—C $\alpha$ ) is very long (3.886 Å). Thus, we have located feasible frontside and backside routes of olefin coordination and insertion for the active species  $[Cp^*_2Zr-Pr]^+$ , which in both cases has an  $\alpha$ -agostic conformation of the propyl group.

For the Cp-analogue, the feasibility of backside ethylene approach to an  $\alpha$ -agostic conformation seems more questionable, see Figure 6.6. Ethylene coordination to **I $\alpha$ 2** is associated with a substantial free energy barrier (14.2 kcal/mol relative to **I $\beta$ 1**), whereas frontside coordination to **I $\beta$ 1** was found to be practically barrierless. Coordination leads to the formation of a  $\pi$ -complex, **IB $\alpha$ 2** ( $\Delta G_{298}^\ddagger = 7.2$  kcal/mol relative to **I $\beta$ 1**) with the C—C bond of ethylene being far from parallel to the Zr—propyl bond, and not to direct insertion. However, only a tiny barrier from this  $\pi$ -complex ( $\Delta G_{298}^\ddagger = 0.3$  kcal/mol) must be overcome in order for insertion to take place. The high barrier for ethylene coordination, however, excludes this route as part of the propagation mechanism.

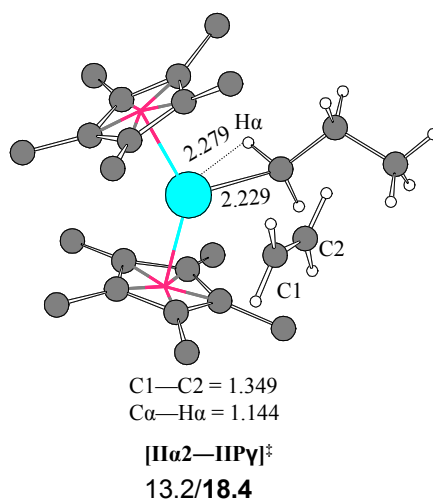


**Figure 6.5.** Transition state for direct backside ethylene insertion for  $[Cp^*_2Zr-Pr]^+$ . Bond distances are given in angstroms, whereas energies are given in kcal/mol ( $\Delta H_{298}/\Delta G_{298}$ ) relative

to the corresponding  $\beta$ -agostic primary alkyl cation (**II $\beta$ 1**) and free ethylene. Hydrogen atoms of the Cp\* ligands have been omitted for clarity.

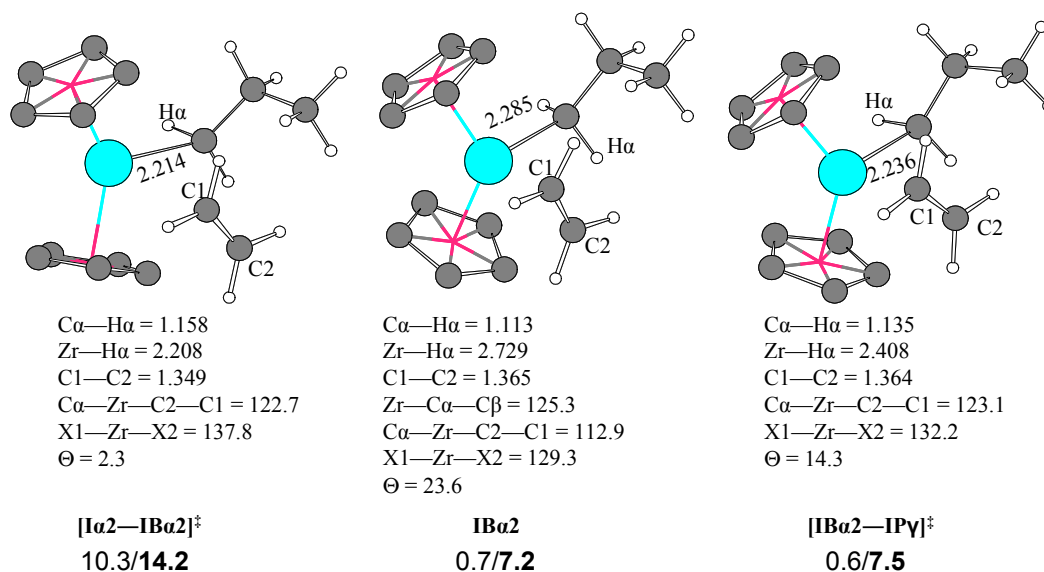


**Figure 6.6.** Transition states and minima along the pathway of backside ethylene coordination and insertion for  $[\text{Cp}_2\text{Zr}-\text{Pr}]^+$ . Bond distances are given in angstroms, whereas energies are given in kcal/mol ( $\Delta H_{298}/\Delta G_{298}$ ) relative to the corresponding  $\beta$ -agostic primary alkyl cation (**II $\beta$ 1**) and free ethylene. Hydrogen atoms of the Cp ligands have been omitted for clarity.

**6.3.4 Comparison to the single-center, two-state model.** So far, we have assumed that both the slow and fast states of the catalyst, if they exist, are to be found among the conformations formed by the *n*-propyl group with the zirconocene fragment,  $\text{L}_2\text{Zr}$ . For  $\text{L} = \text{Cp}$ , our calculations show that the most stable of the ethylene-free complexes is also the most reactive state with respect to ethylene coordination, a pattern which is clearly not commensurate with that required for the single-center, two-state model (Scheme 6.1).

For  $\text{L} = \text{Cp}^*$ , the situation looks better at first glance. We have already pointed out that a propagation involving fast rearrangement from the kinetic product of ethylene insertion, **II $\gamma$ 1**, to the  $\alpha$ -agostic species, may be a viable route since the corresponding formation of the more stable **II $\beta$ 1** conformer involves a higher barrier. Now it turns out that ethylene coordination preferably takes place to the  $\alpha$ -agostic reactant for  $\text{L} = \text{Cp}^*$ , which further seems to strengthen the idea that the  $\gamma$ -agostic conformation of the alkyl cation may be a candidate for the fast state. The transformation  $\text{C}_{\text{fast}} \rightarrow \text{C}_{\text{slow}}$  would then correspond to rearrangement from the  $\gamma$ - to the  $\beta$ -agostic, and from the  $\alpha$ - to the  $\beta$ -agostic conformation, with barriers amounting to 4.1 and 2.0 kcal/mol, respectively. These reactions should be slower than that of fast propagation according to point 3 among the requirements of the kinetic model (*vide supra*). However, as

explained above, the calculated propagation barriers for ethylene polymerization with  $[\text{Cp}^*_2\text{Zr}—\text{Pr}]^+$  are estimated to be in the range 17—18 kcal/mol (frontside approach) and 18—19 kcal/mol (backside approach) relative to the most stable,  $\beta$ -agostic, conformation of the propyl cation, or 9—10 kcal/mol and 12—13 kcal/mol, respectively, relative to the  $\alpha$ -agostic conformation. The differences between the barriers for  $\text{C}_{\text{fast}} \rightarrow \text{C}_{\text{slow}}$  and propagation thus appear far too large for the corresponding rates to become comparable as a result of high monomer concentration.

One should keep in mind, of course, that the computed free energy change resulting from ethylene binding to the metal complex is associated with inaccuracies. The largest of these inaccuracies is the entropic cost of ethylene capture as obtained in our gas-phase calculations, which has been corrected (reduced) by the ethylene solvation entropy as described under Computational Details. It is difficult to see how a further (reasonable) reduction of the entropic cost or other corrections could reduce the propagation barriers of ethylene coordination and insertion enough to be comparable with the barriers to formation of the  $\beta$ -agostic conformation from the  $\gamma$ - and  $\alpha$ -agostic conformations, *i.e.*, with the barriers for  $\text{C}_{\text{fast}} \rightarrow \text{C}_{\text{slow}}$ .

**6.3.5 Comparison to experiment.** Our gas-phase calculations thus suggest that the  $\beta$ -agostic alkyl cation can be regarded as a resting state for both catalysts, but that the preferred pathways of ethylene approach are different in the two cases. For  $\text{L} = \text{Cp}$ , ethylene coordinates to the  $\beta$ -agostic resting state, whereas ethylene complexation for  $\text{L} = \text{Cp}^*$  preferably involves an  $\alpha$ -agostic conformation. Thorshaug *et al.*[9] reported observed activation energies corrected by kinetic modeling in order to separate effects from propagation and deactivation, but the resulting barriers to propagation of 14.6 kcal/mol for  $\text{L} = \text{Cp}$  and 4.1 kcal/mol for  $\text{L} = \text{Cp}^*$  were found to differ from their computed DFT barriers of 2—5 and 6—8 kcal/mol, respectively.[9] According to our present DFT calculations, insertion does not require enthalpic activation for  $\text{L} = \text{Cp}$ , whereas there is an enthalpic insertion barrier of *ca.* 9—10 kcal/mol for the bulkier catalyst with  $\text{L} = \text{Cp}^*$ . Compared with the corrected experimental activation energies,[9] the available two sets of computed DFT barriers are thus too low by 10—15 kcal/mol for  $\text{L} = \text{Cp}$ , and too high by 2—6 kcal/mol for  $\text{L} = \text{Cp}^*$ . Looking for an explanation, we note that the  $\text{Cp}^*$  ligands should afford a better separation of the catalyst—co-catalyst ion pairs in solution than the smaller  $\text{Cp}$  rings, and therefore gas-phase model calculations are expected to be more realistic (smaller errors) for  $\text{L} = \text{Cp}^*$ . It is reasonable to believe[9] that the poor agreement for  $\text{L} = \text{Cp}$  in the gas phase calculations results from the lack of counterion and solvent. Nifant'ev *et al.*[16] have reported a thorough comparison of the

energy coordination and insertion profiles for the naked zirconocene ethyl cation with those including two different borate anions for the system  $[\text{Cp}_2\text{ZrEt}^+\text{A}]^-$  ( $\text{A}^-$  = counterion). For the least nucleophilic borate,  $\text{A}^- = [\text{B}(\text{C}_6\text{F}_5)_4]^-$ , which is expected to show similarities to methyl aluminoxane (MAO), their enthalpic propagation barrier, corresponding to ethylene coordination to  $[\text{Cp}_2\text{ZrEt}^+\text{A}]^-$ , is also close to zero and thus far from the experimental activation energy for  $\text{Cp}_2\text{ZrCl}_2/\text{MAO}$ . It appears that a more realistic modeling of metallocene-catalyzed polymerization, through inclusion of counterion, solvent, and dynamic effects,[4,15-17] will be required to clarify these discrepancies.

**6.3.6 Isomerization of the primary alkyl cations.** As discussed above, our calculations suggest that equilibria between the different conformers of the *n*-propyl chain do not correspond to the fast and slow states appearing in the kinetic model of Fait *et al.*, [28] mainly because the rearrangements from the  $\gamma$ - and  $\alpha$ -agostic conformations to the more stable  $\beta$ -agostic conformations are associated with low barriers. The existence of an active state more stable than the  $\beta$ -agostic conformer, *i.e.*, an alternative  $\text{C}_{\text{slow}}$ , however, may lead to a pattern consistent with the single-center, two-state model. There are of course many possible structures that may turn out to have lower energies than the  $\beta$ -agostic state, and the present study will be limited to isomerization reactions of the Zr—alkyl cation that have already been reported to lead to structures with stabilities comparable to the  $\beta$ -agostic conformation.

One possible isomerization is initiated by  $\beta$ -hydrogen transfer from the alkyl chain to the metal. Subsequent rotation of the thus formed olefin and reinsertion into the metal—hydrogen bond affords a tertiary metal—alkyl species. Based on hybrid DFT/MM calculations on propene polymerization with the catalyst *rac*- $\text{Me}_2\text{C}(\text{3-}^t\text{Bu-Ind})_2\text{ZrCl}_2/\text{MAO}$ , Moscardi *et al.* claimed[5] that the zirconocene complex with a tertiary alkyl group represents a suitable model for the catalyst resting state, *i.e.*, for the slow state. Given that a broken rate order has been observed for a large variety of polymerization catalysts (and monomers), it is reasonable to believe that these catalysts should have similar fast and slow states. We thus decided to investigate the stability of complexes with an *iso*-propyl group, *i.e.*,  $[\text{L}_2\text{Zr}-\text{C}(\text{CH}_3)_2]^+$  ( $\text{L} = \text{Cp}, \text{Cp}^*$ ), relative to **I $\beta$ 1** and **II $\beta$ 1**. Moscardi *et al.* found that their tertiary alkyl species, with two  $\beta$ -agostic hydrogen atoms, was 1 kcal/mol more stable than the corresponding primary  $\beta$ -agostic alkyl. In contrast, we observe a preference for the primary alkyl complex over tertiary alkyl complexes with one and two  $\beta$ -agostic hydrogen atoms, by 3 kcal/mol for  $\text{L} = \text{Cp}$  (*cf.* Figure 6.7), and 5—6 kcal/mol for  $\text{L} = \text{Cp}^*$  (Figure 6.8). Our results for the relative stability of primary and tertiary zirconium—alkyl species thus agree with those reported by several other



authors,[7,9,53] and it seems doubtful whether secondary or tertiary alkyl species of early transition metals can be more stable than primary ones except in very special cases.[53]

Margl *et al.*[8] observed the formation of a stable titanium—dihydrogen complex while performing an *ab initio* molecular dynamics study of  $\beta$ -hydrogen elimination from the alkyl chain to titanium in a constrained-geometry catalyst. Subsequent elimination of  $H_2$  leads to a cationic metal—allyl complex that is also suggested to have considerable stability.[8,17,20,54] For  $L = Cp$ , the present calculations suggest that the zirconium—olefin hydride complex (**IIH1**, the product of the first hydrogen elimination to the metal), and the metal—allyl dihydrogen complex (**IIH2**) are of similar free energy, approximately 9 kcal/mol less stable than **I $\beta$ 1**, whereas the metal—allyl complex (**IA**) is *ca.* 7 kcal/mol less stable than **I $\beta$ 1**. The increased steric bulk of the  $Cp^*$  ligands results in destabilization of the hydride and dihydrogen structures **IIH1** and **IIH2** with respect to both the  $\beta$ -agostic structure **II $\beta$ 1** and the allyl-complex **IIA**. The latter structure still remains *ca.* 6 kcal/mol less stable than the  $\beta$ -agostic resting state in terms of free energy where the entropy change associated with elimination of  $H_2$  has been corrected (reduced) by 40% as described under Computational Details. If one adopts the uncorrected gas-phase entropy change, the allyl complex is only 2 kcal/mol less stable than the  $\beta$ -agostic resting state, **II $\beta$ 1**. The slight preference for the  $\beta$ -agostic complex over the allyl structure is confirmed with a hybrid method (B3LYP), which predicts a 1 kcal/mol larger energy difference. The applicability of density functional methods at describing relative stabilities between agostic metal—alkyl species and corresponding metal—allyl complexes was furthermore confirmed in validation calculations on model reaction (2).



The reaction energy calculated for (6.2) with the standard functional used in the present work (BPW91) is slightly lower than that obtained with a high-level *ab initio* method (CCSD(T)).[55]

Finally, one may argue that the fine balance between the alkyl and allyl complexes could shift due to influence of the co-catalyst anion and we have thus investigated also models of catalyst—co-catalyst adducts of **I $\beta$ 1** and **IA**. Zurek and Ziegler[30] have investigated a series of different adducts between  $[Cp_2ZrMe]^+$ , trimethyl aluminum (TMA) and a model of methylated methyl aluminoxane,  $[MeMAO]^-$  (where MAO is modeled as the hexagonal cage structure  $(MeAlO)_6$ ). We have adapted their most likely candidate for the active polymerizing species,  $[Cp_2ZrMe]^+TMA[MeMAO]^-$  (structure C),[30] as starting points for optimization of the current alkyl and allyl zirconium complexes,  $[Cp_2Zr(\eta^1-C_3H_7)]^+TMA[MeMAO]^-$  and

$[\text{Cp}_2\text{Zr}(\eta^3\text{-C}_3\text{H}_5)]^+\text{TMA}[\text{MeMAO}]^-$ . In the starting structure of  $[\text{Cp}_2\text{Zr}(\eta^1\text{-C}_3\text{H}_7)]^+\text{TMA}[\text{MeMAO}]^-$  a  $\beta$ -agostic conformation was used for the alkyl chain, which, however, relaxed to give  $\alpha$ -agostic conformation in the optimized structure (**I $\alpha$ 1-M** in Figure 6.9). The allyl structure,  $[\text{Cp}_2\text{Zr}(\eta^3\text{-C}_3\text{H}_5)]^+\text{TMA}[\text{MeMAO}]^-$ , retained the hapticity of the metal-bound allyl during optimization (**IA-M** in Figure 6.9). The catalyst—co-catalyst adducts investigated here show a clearer preference for the alkyl isomer, **I $\alpha$ 1-M**, than the naked cations do (*vide supra*). **IA-M** is more than 13 kcal/mol less stable than **I $\alpha$ 1-M** in terms of free energy. In summary, our calculations involving different conformers and isomers of the zirconium—alkyl species have not revealed structures that are predicted to be more stable than the  $\beta$ -agostic alkyl complexes, **I $\beta$ 1** and **II $\beta$ 1**. This further strengthens the hypothesis that dormant, or “slow”, states originate from particularly stable configurations of catalyst—co-catalyst complexes.[29,30]

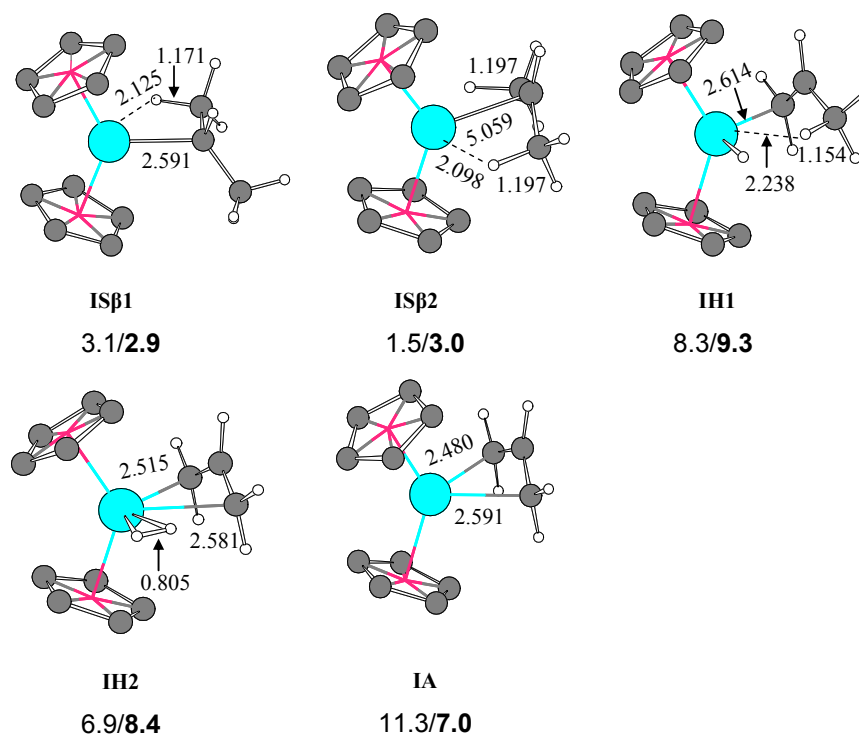


**Figure 6.7.** Minima resulting from isomerization of  $[\text{Cp}_2\text{Zr—Pr}]^+$ . Bond distances are given in angstroms, whereas energies are given in kcal/mol ( $\Delta H_{298}/\Delta G_{298}$ ) relative to the corresponding  $\beta$ -agostic primary alkyl cation (**I $\beta$ 1**) and free ethylene. Hydrogen atoms of the Cp ligands have been omitted for clarity.

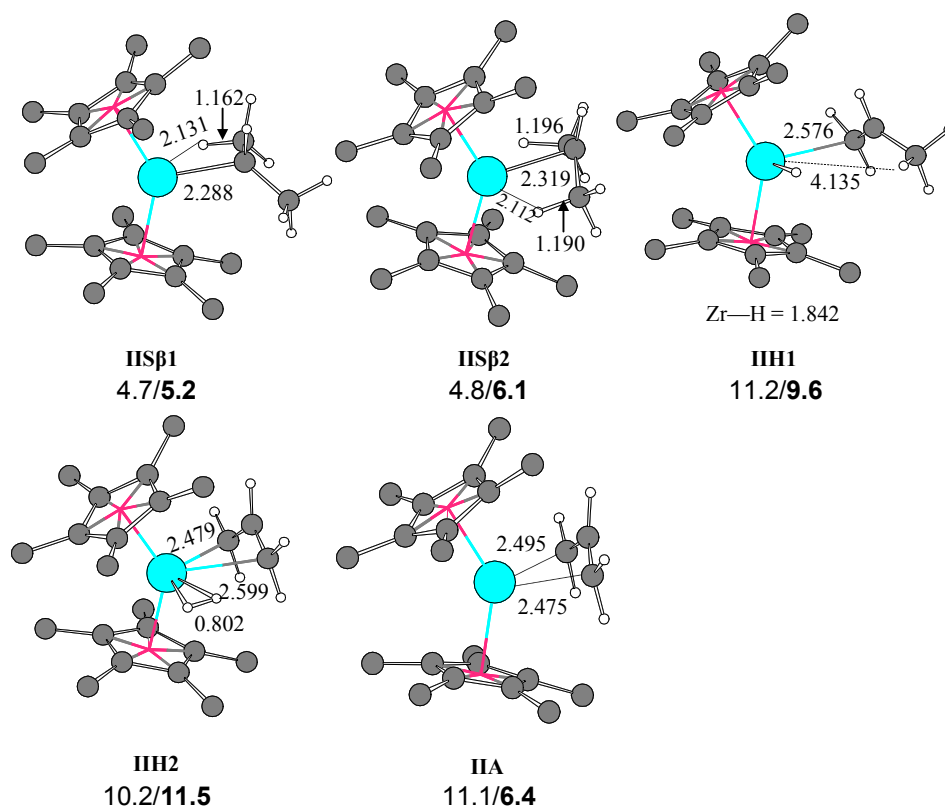


**Figure 6.8.** Minima resulting from isomerization of  $[\text{Cp}^*_2\text{Zr—Pr}]^+$ . Bond distances are given in angstroms, whereas energies are given in kcal/mol ( $\Delta H_{298}/\Delta G_{298}$ ) relative to the corresponding  $\beta$ -agostic primary alkyl cation (**II $\beta$ 1**) and free ethylene. Hydrogen atoms of the  $\text{Cp}^*$  ligands have been omitted for clarity.

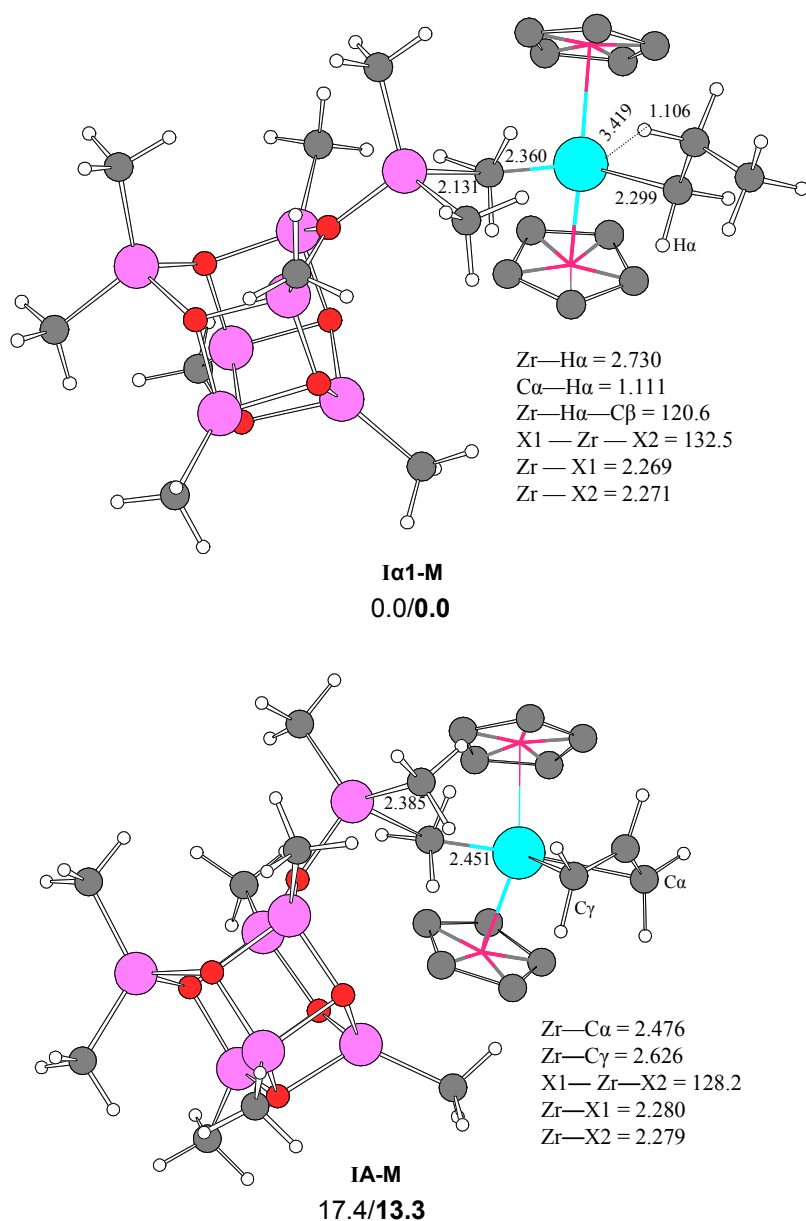


**Figure 6.9.**  $[\text{Cp}_2\text{Zr}(\eta^1\text{-C}_3\text{H}_7)]^+\text{TMA}[\text{MeMAO}]^-$  (**Ia1-M**) and  $[\text{Cp}_2\text{Zr}(\eta^3\text{-C}_3\text{H}_5)]^+\text{TMA}[\text{MeMAO}]^-$  (**IA-M**). Bond distances are given in angstroms, whereas energies are given in kcal/mol ( $\Delta H_{298}/\Delta G_{298}$ ) relative to the primary alkyl (**Ia1-M**). The energy of **IA-M** also includes  $\text{H}_2$ . Hydrogen atoms of the Cp ligands have been omitted for clarity.

## 6.4 Conclusion

Density functional theory calculations on equilibria involving different conformations for zirconium alkyl cations  $[L_2Zr-Pr]^+$  ( $L = Cp, Cp^*$ ;  $Pr = n$ -propyl) and subsequent insertion into the zirconium—propyl bond have not revealed a pattern matching that described for the single-center, two-state model.[28] For  $[Cp_2Zr-Pr]^+$ , the most stable of the ethylene-free complexes, the  $\beta$ -agostic conformer, is also the most reactive state with respect to ethylene coordination. For  $[Cp^*_2Zr-Pr]^+$ , the most facile route involves the  $\gamma$ - and  $\alpha$ -agostic conformations of the alkyl complex, which thus at first glance appear to be candidate fast states,  $C_{fast}$ , but the barriers to rearrangement to the more stable  $\beta$ -agostic conformation are significantly lower than those of propagation.

Several isomerization reactions involving the propyl group of the  $[L_2Zr-Pr]^+$  cation have been investigated in order to look for candidate slow states. For the most promising candidate slow state, these studies have also included a model of the MAO cocatalyst anion and high-level ab initio validation calculations. However, no structure was found to be of lower energy than the  $\beta$ -agostic conformation, and the latter thus takes the role of the resting state for both catalysts in the present study. This suggests that dormant, or “slow”, states originate from particularly stable configurations of catalyst—co-catalyst complexes, and not from the equilibria of the alkyl group as investigated here.

The preferred pathways for the approach of ethylene are different in the two catalysts. For  $L = Cp$ , ethylene coordinates to the  $\beta$ -agostic resting state, whereas for  $L = Cp^*$ , the favored propagation route involves ethylene approach to an  $\alpha$ -agostic conformation. We anticipate that future studies will confirm the role of  $\alpha$ -agostic or non-agostic conformations of the polymer chain in reducing the steric hindrance experienced by the incoming olefin, also in the case of other polymerization catalysts.

## 6.5 Supporting Information

### Contents:

**Table 6.S1.** Total energies, enthalpies and Gibbs free energies (hartree) as obtained in the DFT calculations.

**Table 6.S1.** Total energies, enthalpies and uncorrected Gibbs free energies (hartree) as obtained in the DFT calculations.

Entry	E <sub>e</sub>	H <sub>298</sub>	G <sub>298</sub>
<b>Iβ1</b>	-552.0696211	-551.798686	-551.857254
<b>Iα1</b>	-552.055856	-551.784472	-551.843770
<b>Iγ1</b>	-552.062115	-551.790294	-551.848070
<b>Iα2</b>	-552.055200	-551.783793	-551.842855
<b>IH1</b>	-552.053657	-551.785427	-551.842493
<b>IH2</b>	-552.054433	-551.787640	-551.843901
<b>IA</b>	-550.866581	-550.617255	-550.673988
<b>ISβ2</b>	-552.066324	-551.796328	-551.852454
<b>ISβ1</b>	-552.064845	-551.793766	-551.852619
<b>[Iβ1—Iα1]<sup>‡</sup></b>	-552.051061	-551.780905	-551.840301
<b>[Iγ1—Iα1]<sup>‡</sup></b>	-552.050466	-551.780465	-551.839428
<b>[Iγ1—Iβ1]<sup>‡</sup></b>	-552.055795	-551.784818	-551.841570
<b>[Iα1—Iα2]<sup>‡</sup></b>	-552.051713	-552.781363	-551.838878
<b>[Iα1—IFα1]<sup>‡</sup></b>	-630.663707	-630.337439	-630.411058
<b>[Iβ1—IFβ1]<sup>‡</sup></b>	-630.675125	-630.349250	-630.425417
<b>[Iγ1—IFα2]<sup>‡</sup></b>	-630.665049	-630.337830	-630.405383
<b>IFα1</b>	-630.681542	-630.353550	-630.421433
<b>IFα2</b>	-630.673296	-630.345312	-630.412718
<b>IFβ1</b>	-630.684595	-630.356035	-630.421444
<b>[IFβ1—IFα1]<sup>‡</sup></b>	-630.678413	-630.351322	-630.417340
<b>[IFα1—IPγ]<sup>‡</sup></b>	-630.677461	-630.350736	-630.417125
<b>IPγ</b>	-630.703925	-630.373742	-630.438195
<b>[Iα2—IBα2]<sup>‡</sup></b>	-630.658311	-630.332472	-630.405533
<b>IBα2</b>	-630.676181	-630.347755	-630.414097
<b>[IBα2—IPγ]<sup>‡</sup></b>	-630.674624	-630.347921	-630.413245
<b>IIβ1</b>	-945.191458	-944.629483	-944.723168
<b>IIγ1</b>	-945.182300	-944.619981	-944.713013
<b>IIα2</b>	-945.177320	-944.615774	-944.713084
<b>IISβ1</b>	-945.183826	-944.621931	-944.714942
<b>IISβ2</b>	-945.182343	-944.621842	-944.713467
<b>IIA</b>	-943.987798	-943.448257	-943.541126
<b>IIH2</b>	-945.170298	-944.613225	-944.704788

<b>IIH1</b>	-945.170123	-944.611639	-944.707814
<b>[IIβ1–IIα2]<sup>‡</sup></b>	-945.175106	-944.614513	-944.709990
<b>[IIγ1–IIα2]<sup>‡</sup></b>	-945.176350	-944.615329	-944.710541
<b>[IIγ1–IIβ1]<sup>‡</sup></b>	-945.175277	-944.613792	-944.706362
<b>[IIβ1–IIFβ1]<sup>‡</sup></b>	-1023.785656	-1023.167954	-1023.268529
<b>[IIα2–IIPγ]<sup>‡</sup></b>	-1023.775132	-1023.158580	-1023.263604
<b>IIFα1</b>	-1023.787908	-1023.1695	-1023.271499
<b>IIFβ1</b>	-1023.788002	-1023.169110	-1023.267940
<b>IIFα2</b>	-1023.780374	-1023.16187	-1023.263148
<b>[IIα2–IIFα1]<sup>‡</sup></b>	-1023.78226	-1023.165258	-1023.272122
<b>[IIFα1–IIPγ]<sup>‡</sup></b>	-1023.78109	-1023.1637	-1023.262356
<b>IIPγ</b>	-1023.821675	-1023.200860	-1023.300934
<b>Iα1–M</b>	-1417.859763	-1417.15942	-1417.308129
<b>IA–M</b>	-1416.646813	-1415.96821	-1416.112913



## Bibliography

- [1] (a) R. F. Jordan, W. E. Dasher, S. F. Echols, "Reactive Cationic Dicyclopentadienylzirconium(IV) Complexes." *J. Am. Chem. Soc.* **1986**, *108*, 1718-1719. (b) R. F. Jordan, "Chemistry of Cationic Dicyclopentadienyl Group 4 Metal-Alkyl Complexes." *Adv. Organomet. Chem.* **1991**, *32*, 325-387.
- [2] I. Silanes, J. M. Ugalde, "Comparative Study of Various Mechanisms for Metallocene-Catalyzed  $\alpha$ -Olefin Polymerization." *Organometallics* **2005**, *24*, 3233-3246.
- [3] (a) A. K. Rappé, W. M. Skiff, C. J. Casewit, "Modeling Metal-Catalyzed Olefin Polymerization." *Chem. Rev.* **2000**, *100*, 1435-1456. (b) M. Borrelli, V. Busico, R. Cipullo, S. Ronca, P. H. M. Budzelaar, "Selectivity of Metallocene-Catalyzed Olefin Polymerization: A Combined Experimental and Quantum Mechanical Study. 1. Nonchiral Bis(cyclopentadienyl) Systems." *Macromolecules* **2002**, *35*, 2835-2844. (c) M. Borrelli, V. Busico, R. Cipullo, S. Ronca, P. H. M. Budzelaar, "Selectivity of Metallocene-Catalyzed Olefin Polymerization: A Combined Experimental and Quantum Mechanical Study. The *ansa*-Me<sub>2</sub>Si(Ind)<sub>2</sub>Zr and *ansa*-Me<sub>2</sub>C(Cp)(Flu)Zr Systems." *Macromolecules* **2003**, *36*, 8171-8177. (d) E. Aitola, M. Surakka, T. Repo, M. Linnolahti, K. Lappalainen, K. Kervinen, M. Klinga, T. Pakkanen, M. Leskela, "Polymerization of ethene with zirconocene catalysts: an experimental and quantum chemical study of the influence of para-substituent in benzyl in bis  $\eta^5$ -(1-benzyl)indenyl zirconium dichlorides." *J. Organomet. Chem.* **2005**, *690*, 773-783. (e) S. H. Yang, J. Huh, J. S. Yang, W. H. Jo, "A Density Functional Study on the Stereoselectivity of Styrene Polymerization with *ansa*-Metallocene Catalyst." *Macromolecules* **2004**, *37*, 5741-5751. (f) E. -G. Kim, M. L. Klein, "Density Functional Study of Ethylene-Norbornene Copolymerization via Metallocene and Constrained-Geometry Catalysts." *Organometallics* **2004**, *23*, 3319-3326. (g) P. H. M. Budzelaar, "CO/Ethene Copolymerization at Zirconocene Centers?" *Organometallics* **2004**, *23*, 855-860. (h) S. H. Yang, W. H. Jo, S. K. Noh, "Density functional study of the insertion mechanism for ethylene-styrene copolymerization with constrained geometry catalysts." *J. Chem. Phys.* **2003**, *119*, 1824-1837. (i) H. Wigum, K. A. Solli, J. A. Støvneng, E. Rytter, "Structure-property transition-state model for the copolymerization of ethene and 1-hexene with experimental and theoretical applications to novel disilylene-bridged zirconocenes." *J. Polym. Sci., Part A: Polym. Chem.* **2003**, *41*, 1622-1631. (j) S. Martinez, V. Cruz, A. Munoz-Escalona, J. Martinez-Salazar, "Copolymerization of ethylene and styrene by homogeneous metallocene catalysts. 1. Theoretical studies with *rac*-ethylenebis-(tetrahydroindenyl)MCl<sub>2</sub> [M = Ti, Zr] systems." *Polymer* **2003**, *44*, 295-306. (k) G. Talarico, A. N. J. Blok, T. K. Woo, L.

Cavallo, "Comparison of ab Initio and DFT Methods for Studying Chain Propagation and Chain Termination Processes with Group 4 Polymerization Catalysts. 1. The *ansa*-Bis(cyclopentadienyl)zirconium Catalyst." *Organometallics* **2002**, *21*, 4939-4949. (l) M. Hölscher, H. Keul, H. Höcker, "Explanation of the Different Reaction Behaviors of Bridged and Unbridged Cationic Single Component Zirconocene Catalysts in MMA Polymerizations: a Density Functional Study." *Macromolecules* **2002**, *35*, 8194-8202. (m) R. Blom, O. Swang, R. H. Heyn, "Semi-batch polymerizations of ethylene with metallocene catalysts in the presence of hydrogen, 3 – Correlation between hydrogen sensitivity and molecular parameters." *Macromol. Chem. Phys.* **2002**, *203*, 381-387. (n) M. J. Young, C. C. M. Ma, C. Ting, "Activation energy and transition state determination of the olefin insertion process of metallocene catalysts using a semiempirical molecular orbital calculation." *Russ. J. Coord. Chem.* **2002**, *28*, 25-31. (o) G. Lanza, I. Fragala, T. J. Marks, "Metal and Ancillary Ligand Structural Effects on Ethylene Insertion Processes at Cationic Group 4 Centers. A Systematic, Comparative Quantum Chemical Investigation at Various ab Initio Levels." *Organometallics* **2001**, *20*, 4006-4017. (p) M. Linnolahti, T. A. Pakkanen, "Theoretical Study on the Factors Controlling the Accessibility of Cationic Metal Centers in Zirconocene Polymerization Catalysts." *Macromolecules* **2000**, *33*, 9205-9214. (q) I. E. Nifant'ev, L. Y. Ustynyuk, D. N. Laikov, "A DFT study of ethylene polymerization by zirconocene catalysts. 1. Model system  $[\text{Cp}_2\text{ZrEt}]^+ + \text{C}_2\text{H}_4$ ." *Russ. Chem. Bull.* **2000**, *49*, 1164-1173. (r) L. Petitjean, D. Pattou, M. F. Ruiz-Lopez, "Theoretical Study of the Mechanisms of Ethylene Polymerization with Metallocene-Type Catalysts." *J. Phys. Chem. B* **1999**, *103*, 27-35. (s) L. Deng, T. Ziegler, T. K. Woo, P. Margl, L. Fan, "Computer Design of Living Olefin Polymerization Catalysts: A Combined Density Functional Theory and Molecular Mechanics Study." *Organometallics* **1998**, *17*, 3240-3253. (t) T. K. Woo, P. M. Margl, T. Ziegler, P. E. Blöchl, "Static and ab Initio Molecular Dynamics Study of the Titanium(IV)-Constrained Geometry Catalyst  $(\text{CpSiH}_2\text{NH})\text{Ti-R}^+$ . 2. Chain Termination and Long Chain Branching." *Organometallics* **1997**, *16*, 3454-3468. (u) D. G. Musaev, R. D. J. Froese, K. Morokuma, "Transition-metal-catalyzed olefin polymerization reactions: A theoretical comparison of mechanisms for diimine-Mn(II) (M = Ni, Pd, and Pt) and zirconocene catalysts." *New J. Chem.* **1997**, *21*, 1269-1282. (v) M. H. Prosenc, H. -H. Brintzinger, "Zirconium-Alkyl Isomerizations in Zirconocene-Catalyzed Olefin Polymerization: A Density Functional Study." *Organometallics* **1997**, *16*, 3889-3894. (w) J. A. Støvneng, E. Rytter, "Influence of rotation between agostic structures on ethene interaction with a zirconocene polymerization site." *J. Organomet. Chem.* **1996**, *519*, 277-280. (x) P. Margl, J. C. W. Lohrenz, T. Ziegler, P. E. Blöchl, "A Dynamical Density Functional Study on the Reaction of Ethylene with  $\text{Cp}_2\text{Zr}(\text{C}_2\text{H}_5)^+$ ." *J. Am. Chem. Soc.* **1996**, *118*, 4434-

4441. (y) T. Yoshida, N. Koga, K. Morokuma, "A Combined ab Initio MO-MM Study on Isotacticity Control in Propylene Polymerization with Silylene-Bridged Group 4 Metallocenes.  $C_2$  Symmetrical and Asymmetrical Catalysts." *Organometallics* **1996**, *15*, 766-777. (z) T. Yoshida, N. Koga, K. Morokuma, "Ab Initio Theoretical Study on Ethylene Polymerization with Homogeneous Silylene-Bridged Group 4 Metallocene Catalysts. Ethylene Insertion and  $\beta$ -Elimination." *Organometallics* **1995**, *14*, 746-758. (aa) J. C. W. Lohrenz, T. K. Woo, L. Y. Fan, T. Ziegler, "A density functional study on the insertion mechanism and chain termination in Kaminsky-type catalysts; comparison of frontside and backside attack." *J. Organomet. Chem.* **1995**, *497*, 91-104. (ab) V. R. Jensen, K. J. Børve, N. Westberg, M. Ystenes, "Titanium-Ethylene Complexes Proposed To Be Intermediates in Ziegler-Natta Catalysis. Can They Be Detected through Vibrational Spectroscopy?" *Organometallics* **1995**, *14*, 4349-4358. (ac) E. P. Bierwagen, J. E. Bercaw, W. A. Goddard, III. "Theoretical Studies of Ziegler-Natta Catalysis: Structural Variations and Tacticity Control." *J. Am. Chem. Soc.* **1994**, *116*, 1481-1489. (ad) T. K. Woo, L. Fan, T. Ziegler, "A Density Functional Study of Chain Growing and Chain Terminating Steps in Olefin Polymerization by Metallocene and Constrained Geometry Catalysts." *Organometallics* **1994**, *13*, 2252-2261. (ae) H. Kawamura-Kuribayashi, N. Koga, K. Morokuma, "An ab Initio MO and MM study of Homogeneous Olefin Polymerization with Silylene-Bridged Zirconocene Catalyst and Its Regio- and Stereoselectivity." *J. Am. Chem. Soc.* **1992**, *114*, 8687-8694. (af) H. Kawamura-Kuribayashi, N. Koga, K. Morokuma, "An ab Initio MO Study on Ethylene and Propylene Insertion into the Ti-CH<sub>3</sub> Bond in CH<sub>3</sub>TiCl<sub>2</sub><sup>+</sup> as a Model of Homogeneous Olefin Polymerization." *J. Am. Chem. Soc.* **1992**, *114*, 2359-2366. (ag) C. A. Jolly, D. S. Marynick, "The Direct Insertion Mechanism in Ziegler-Natta Polymerization: A Theoretical Study of Cp<sub>2</sub>TiCH<sub>3</sub><sup>+</sup> + C<sub>2</sub>H<sub>4</sub> → Cp<sub>2</sub>TiC<sub>3</sub>H<sub>7</sub><sup>+</sup>." *J. Am. Chem. Soc.* **1989**, *111*, 7968-7974.

[4] K. Vanka, Z. T. Xu, T. Ziegler, "A density functional study of ethylene insertion into the M-methyl (M = Ti, Zr) bond for different catalysts, with a QM/MM model for the counterion, B(C<sub>6</sub>F<sub>5</sub>)<sub>3</sub>CH<sub>3</sub><sup>-</sup>." *Israeli. J. Chem.* **2002**, *42*, 403-415.

[5] G. Moscardi, L. Resconi, L. Cavallo, "Propene Polymerization with the Isospecific, Highly Regioselective rac-Me<sub>2</sub>C(3-t-Bu-1-Ind)<sub>2</sub>ZrCl<sub>2</sub>/MAO Catalyst. 2. Combined DFT/MM Analysis of Chain Propagation and Chain Release Reactions." *Organometallics* **2001**, *20*, 1918-1931.

[6] (a) K. Angermund, G. Fink, V. R. Jensen, R. Kleinschmidt, "Toward Quantitative Prediction of Stereospecificity of Metallocene-Based Catalysts for  $\alpha$ -Olefin Polymerization."

*Chem. Rev.* **2000**, *100*, 1457-1470. (b) K. Angermund, G. Fink, V. R. Jensen, R. Kleinschmidt, "The role of intermediate chain migration in propene polymerization using substituted  $\{^i\text{Pr}(\text{CpFlu})\}\text{ZrCl}_2/\text{MAO}$  catalysts." *Macromol. Rapid Commun.* **2000**, *21*, 91-97.

[7] J. C. W. Lohrenz, M. Bühl, M. Weber, W. Thiel, "A Density Functional Study on the Formation of Stereoerrors in the Stereoselective Propene Polymerization with Zirconocene Catalysts." *J. Organomet. Chem.* **1999**, *592*, 11-21.

[8] P. M. Margl, T. K. Woo, P. E. Blöchl, T. Ziegler, "Evidence for a Stable Ti(IV) Metallocene Dihydrogen Complex from ab Initio Molecular Dynamics." *J. Am. Chem. Soc.* **1998**, *120*, 2174-2175.

[9] K. Thorshaug, J. A. Støvneng, E. Rytter, "Ethene Polymerization Catalyzed by Monoalkyl-Substituted Zirconocenes. Possible Effects of Ligand-Metal Agostic Interaction." *Macromolecules* **2000**, *33*, 8136-8145.

[10] *Erratum.*: Reference [9]

[11] T. K. Woo, P. M. Margl, J. C. W. Lohrenz, P. E. Blöchl, T. Ziegler, "Combined Static and Dynamic Density Functional Study of the Ti(IV) Constrained Geometry Catalyst  $(\text{CpSiH}_2\text{NH})\text{TiR}^+$ . 1. Resting States and Chain Propagation." *J. Am. Chem. Soc.* **1996**, *118*, 13021-13030.

[12] (a) P. Cossée, "Ziegler-Natta Catalysis I. Mechanism of Polymerization of  $\alpha$ -Olefins with Ziegler-Natta Catalyst." *J. Catal.* **1964**, *3*, 80-88. (b) E. J. Arlman, "Ziegler-Natta Catalysis II. Surface Structure of Layer-Lattice Transition Metal Chlorides." *J. Catal.* **1964**, *3*, 89-98. (c) E. J. Arlman, P. Cossée, "Ziegler-Natta Catalysis III. Stereospecific Polymerization of Propene with the catalyst system  $\text{TiCl}_3\text{-AlEt}_3$ ." *J. Catal.* **1964**, *3*, 99-104.

[13] (a) J. A. Ewen, "Symmetry Rules and Reaction Mechanisms of Ziegler-Natta Catalysts." *J. Mol. Catal. A-Chem.* **1998**, *128*, 103-109. (b) H. -H. Brintzinger, D. Fischer, R. Mülhaupt, B. Rieger, R. M. Waymouth, "Stereospecific olefin polymerization with chiral metallocene catalysts." *Angew. Chem., Int. Ed. Engl.* **1995**, *34*, 1143-1170. (c) L. Resconi, L. Cavallo, A. Fait, F. Piemontesi, "Selectivity in Propene Polymerization with Metallocene Catalysts" *Chem. Rev.* **2000**, *100*, 1253-1345.

[14] (a) E. Y. X. Chen, T. J. Marks, "Cocatalysts for Metal-Catalyzed Olefin Polymerization: Activators, Activation Processes, and Structure-Activity Relationships." *Chem. Rev.* **2000**, *100*, 1391-1434. (b) L. Jia, X. Yang, C. L. Stern, T. J. Marks, "Cationic Metallocene Polymerization Catalysts Based on Tetrakis(pentafluorophenyl)borate and Its

Derivatives. Probing the Limits of Anion “Noncoordination” via a Synthetic, Solution Dynamic, Structural, and Catalytic Olefin Polymerization Study.” *Organometallics* **1997**, *16*, 842-857.

- [15] (a) K. Vanka, Z. T. Xu, T. Ziegler, “A combined density functional theory and molecular mechanics (QM/MM) study of single site ethylene polymerization catalyzed by  $[\text{Cp}\{\text{NC}(\text{tBu})_2\}\text{TiR}^+]$  in the presence of the counterion,  $\text{CH}_3\text{B}(\text{C}_6\text{F}_5)_3^-$ .” *Macromol. Symp.* **2004**, *213*, 275-286. (b) P. G. Belelli, M. M. Branda, N. J. Castellani, “DFT studies of zirconocene/MAO interaction.” *J. Mol. Catal. A-Chem.* **2003**, *192*, 9-24. (c) Z. Xu, K. Vanka, T. Firman, A. Michalak, E. Zurek, C. Zhu, T. Ziegler, “Theoretical Study of the Interactions between Cations and Anions in Group IV Transition-Metal Catalysts for Single-Site Homogeneous Olefin Polymerization.” *Organometallics* **2002**, *21*, 2444-2453. (d) I. I. Zakharov, V. A. Zakharov, “A DFT Quantum-Chemical Study of Ion-Pair Formation for the Catalyst  $\text{Cp}_2\text{ZrMe}_2/\text{MAO}$ .” *Macromol. Theor. Simul.* **2002**, *11*, 352-358. (e) G. Lanza, I. L. Fragala, T. J. Marks, “Energetic, Structural, and Dynamic Aspects of Ethylene Polymerization Mediated by Homogeneous Single-Site “Constrained Geometry Catalysts” in the Presence of Cocatalyst and Solvation: An Investigation at the ab Initio Quantum Chemical Level.” *Organometallics* **2002**, *21*, 5594-5612. (f) F. Schaper, A. Geyer, H. -H. Brintzinger, “Displacement of  $\text{H}_3\text{CB}(\text{C}_6\text{F}_5)_3^-$  Anions from Zirconocene Methyl Cations by Neutral Ligand Molecules: Equilibria, Kinetics, and Mechanisms.” *Organometallics* **2002**, *21*, 473-483. (g) G. Lanza, I. L. Fragala, T. J. Marks, “Ligand Substituent, Anion, and Solvation Effects on Ion Pair Structure, Thermodynamics Stability, and Structural Mobility in “Constrained Geometry” Olefin Polymerization Catalysts: an Ab Initio Quantum Chemical Investigation.” *J. Am. Chem. Soc.* **2000**, *122*, 12764-12777. (h) K. Vanka, M. S. W. Chan, C. C. Pye, T. Ziegler, “A Density Functional Study of Ion-Pair Formation and Dissociation in the Reaction between Boron- and Aluminium-Based Lewis Acids with  $(1,2\text{-Me}_2\text{Cp})_2\text{ZrMe}_2$ .” *Organometallics* **2000**, *19*, 1841-1849. (i) D. Braga, F. Grepioni, E. Tedesco, M. J. Calhorda, “Zirconocene catalysts: Ion-pairs, zwitterions, or weakly bound molecules?” *Z. Anorg. Allg. Chem.* **2000**, *626*, 462-470. (j) V. A. Zakharov, E. P. Talzi, I. I. Zakharov, D. E. Babushkin, N. V. Semikolenova, “Structure of methylaluminoxane and the mechanism of active center formation in the zirconocene/methylaluminoxane catalytic system.” *Kinet. Catal.* **1999**, *40*, 836-850. (k) S. Beck, M. H. Prosenc, H. -H. Brintzinger, “Displacement of weakly coordinating anions from zirconocene alkyl cations by trialkyl phosphines: A model for olefin coordination in homogeneous Ziegler-Natta catalysis.” *J. Mol. Catal. A-Chem.* **1998**, *128*, 41-52. (l) R. Fusco, L. Longo, A. Proto, F. Masi, F. Garbassi, “Ethylene polymerization catalyzed by

metallocene/methylaluminoxane systems: quantum-mechanical study on the role of olefin separated ion pairs (OSIP) in the polymerization mechanism.” *Macromol. Rapid Commun.* **1998**, *19*, 257-262. (m) R. Fusco, L. Longo, F. Masi, F. Garbassi, “Olefin Polymerization with Homogeneous Ziegler-Natta Catalysts: A DFT Quantum-Mechanical Study of the Reactions of  $\text{Cp}_2\text{MtCH}_3\text{Cl}$  Complexes (Mt = Ti, Zr) with  $\text{Al}(\text{CH}_3)_3$  and MAO.” *Macromolecules* **1997**, *30*, 7673-7685. (n) R. Fusco, L. Longo, F. Masi, F. Garbassi, “Ethylene polymerization with homogeneous Ziegler-Natta catalysts: theoretical study on the role of ion pairs in the polymerization mechanism.” *Macromol. Rapid Commun.* **1997**, *18*, 433-441.

[16] I. E. Nifant'ev, L. Y. Ustynyuk, D. N. Laikov, “DFT Study of Ethylene Polymerization by Zirconocene-Boron Catalytic Systems. Effect of Counterion on the Kinetics and Mechanism of the Process.” *Organometallics* **2001**, *20*, 5375-5393.

[17] S. Lieber, M. -H. Prosenc, H. -H. Brintzinger, “Zirconocene Allyl Complexes: Dynamics in Solution, Reaction with Aluminum Alkyls,  $\text{B}(\text{C}_6\text{F}_5)_3$ -Induced Propene Insertion, and Density-Functional Calculations on Possible Formation and Reaction Pathways.” *Organometallics* **2000**, *19*, 377-387.

[18] (a) V. R. Jensen, K. J. Børve, M. Ystenes, “Ziegler-Natta Ethylene Insertion Reaction for a Five-Coordinate Titanium Chloride Complex Bridged to an Aluminum Hydride Cocatalyst.” *J. Am. Chem. Soc.* **1995**, *117*, 4109-4117. (b) O. Novaro, E. Blaisten-Barojas, E. Clementi, G. Giunchi, M. E. Ruiz-Vizcaya, “Theoretical study on a reaction pathway of Ziegler-Natta-type catalysis.” *J. Chem. Phys.* **1978**, *68*, 2337-2351. (c) D. R. Armstrong, P. G. Perkins, J. J. P. Stewart, “A Theoretical Investigation of Ziegler-type Catalysis. Part I. Soluble Catalyst Systems.” *J. Chem. Soc., Dalton Trans.* **1972**, 1972-1980.

[19] (a) X. M. Yang, C. L. Stern, T. J. Marks, “Cationic Zirconocene Olefin Polymerization Catalysts Based on the Organo-Lewis Acid Tris(pentafluorophenyl)borane. A Synthetic, Structural, Solution Dynamic, and Polymerization Catalytic Study.” *J. Am. Chem. Soc.* **1994**, *116*, 10015-10031. (b) X. M. Yang, C. L. Stern, T. J. Marks, “Cation-like homogeneous olefin polymerization catalysts based upon zirconocene alkyls and tris(pentafluorophenyl)borane.” *J. Am. Chem. Soc.* **1991**, *113*, 3623-3625.

[20] (a) C. G. Brandow, A. Mendiratta, J. E. Bercaw, “Ancillary Ligand and Olefin Substituent Effects on Olefin Dissociation for Cationic Zirconocene Complexes Bearing a Coordinated Pendant Olefin.” *Organometallics* **2001**, *20*, 4253-4261. (b) G. Erker, “Homogeneous Single-Component Betaine Ziegler-Natta Catalysts Derived from (Butadiene)zirconocene Precursors.” *Acc. Chem. Res.* **2001**, *34*, 309-317. (c) M. Dahlmann, G.

Erker, K. Bergander, "Experimental Characterization of the Alkene-Addition/-Insertion Energy Profile at Homogeneous Group 4 Metal Ziegler-Type Catalysts." *J. Am. Chem. Soc.* **2000**, *122*, 7986-7998.

[21] (a) C. P. Casey, D. W. Carpenetti, II. "Measurement of Barriers for Alkene Dissociation and for Inversion at Zirconium in a  $d^0$  Zirconium-Alkyl-Alkene Complex." *Organometallics* **2000**, *19*, 3970-3977. (b) Z. Wu, R. F. Jordan, J. L. Petersen, "Models for the Elusive  $Cp_2Zr(R)(olefin)^+$ . Characterization of the  $d^0$  Metal Olefin Complex  $Cp_2Zr(OCMe_2CH_2CH_2CH=CH_2)^+$ ." *J. Am. Chem. Soc.* **1995**, *117*, 5867-5868. (c) B. Temme, G. Erker, J. Karl, H. Luftmann, R. Fröhlich, S. Kotila, "Reaction of (butadiene)zirconocene with tris(pentafluorophenyl)borane – A novel way of generating methylalumoxane-free homogeneous Ziegler-type catalysts." *Angew. Chem., Int. Ed. Engl.* **1995**, *34*, 1755-1757.

[22] (a) J. A. Ewen, M. J. Elder, R. L. Jones, S. Curtis, H. N. Cheng, In *Catalytic Olefin Polymerization*; T. Keii, K. Soga, Eds.; Kodansha: Tokyo, **1990**, page 439. (b) N. Herfert, G. Fink, "Hemiisotactic poly(propylene) through propene polymerization with the  $iPr[3-MeCpFlu]ZrCl_2/MAO$  catalyst system: A kinetic and microstructural analysis." *Macromol. Symp.* **1993**, *66*, 157-178. (c) G. Fink, N. Herfert, P. Montag, "The Relationship between Kinetics and Mechanisms." *Ziegler Catalysts*, G. Fink, R. Mülhaupt, H. -H. Brintzinger, Eds., Springer Verlag, Berlin, **1995**, page 159. (d) J. C. W. Chien, Z. Yu, M. M. Marques, J. C. Flores, M. D. Rausch, "Polymerization of Olefins and Diolefins Catalyzed by Monocyclopentadienyltitanium Complexes Containing a (Dimethylamino)ethyl Substituent and Comparison with *ansa*-Zirconocene Systems." *J. Polym. Sci., Part A: Polym. Chem.* **1998**, *36*, 319-328. (e) L. Oliva, C. Pellecchia, P. Cinquina, A. Zambelli, "Preliminary kinetic investigation on syndiotactic polymerization of styrene." *Macromolecules* **1989**, *22*, 1642-1645. (f) P. Pino, B. Rotzinger, E. Vonachenbach, "The role of some bases in the stereospecific polymerization of propylene with titanium catalysts supported on magnesium-chloride." *Makromol. Chem-Macromolecular chemistry and physics* **1985**, *Suppl. 13*, 105-122.

[23] S. Jüngling, R. Mülhaupt, U. Stehling, H. -H. Brintzinger, D. Fischer, F. Langhauser, "The role of dormant sites in propene polymerization using methylalumoxane activated metallocene catalysts." *Macromol. Symp.* **1995**, *97*, 205-216.

[24] S. Jüngling, R. Mülhaupt, U. Stehling, H. -H. Brintzinger, D. Fischer, F. Langhauser, "Propene Polymerization Using Homogeneous MAO-Activated Metallocene Catalysts:  $Me_2Si(Benz[e]Indenyl)_2ZrCl_2/MAO$  vs.  $Me_2Si(2-Me-Benz[e]Indenyl)_2ZrCl_2/MAO$ ." *J. Polym. Sci., Part A: Polym. Chem.* **1995**, *33*, 1305-1317.

- [25] F. Schaper, H. -H. Brintzinger, R. Kleinschmidt, Y. van der Leek, M. Reffke, G. Fink, "Organometallic Catalysts and Olefin Polymerization." R. Blom, A. Follestad, E. Rytter, M. Tilset, M. Ystenes, Eds., Springer-Verlag, Oslo, Norway, **2000**, page 46.
- [26] (a) M. Ystenes, "The trigger mechanism for polymerization of  $\alpha$ -olefins with Ziegler-Natta catalysts: A new model based on interaction of two monomers at the transition state and monomer activation of the catalytic centers." *J. Catal.* **1991**, *129*, 383-401. (b) M. Ystenes, "Predictions from the Trigger Mechanism for Ziegler-Natta Polymerization of  $\alpha$ -olefins." *Macromol. Symp.* **1993**, *66*, 71-81. (c) M. M. Marques, C. Costa, F. Lemos, F. R. Ribeiro, A. R. Dias, "A kinetic approach to homogeneous Ziegler type polymerization. Steady state." *React. Kinet. Catal. Lett.* **1997**, *62*, 9-15. (d) A. Muñoz-Escalona, J. Ramos, V. Cruz, J. Martínez-Salazar, "Effect of a Second Ethylene Molecule on the Insertion of Ethylene in Zirconocene Catalyst Systems: A QM Semiempirical Study." *J. Polym. Sci., Part A: Polym. Chem.* **2000**, *38*, 571-582.
- [27] M. H. Prosenc, F. Schaper, H. -H. Brintzinger, "Metalorganic Catalysts for Synthesis and Polymerization." W. Kaminsky, Ed., Springer Verlag, Berlin, **1999**, page 223.
- [28] A. Fait, L. Resconi, G. Guerra, P. Corradini, "A Possible Interpretation of the Nonlinear Propagation Rate Laws for Insertion Polymerizations: A Kinetic Model Based on a Single-Center, Two-State Catalyst." *Macromolecules* **1999**, *32*, 2104-2109.
- [29] (a) E. Zurek, T. Ziegler, "Theoretical studies of the structure and function of MAO (methylaluminoxane)." *Prog. Polym. Sci.* **2004**, *29*, 107-148. (b) E. Zurek, T. Ziegler, "A theoretical study of the insertion barrier of MAO (methylaluminoxane)-activated,  $\text{Cp}_2\text{ZrMe}_2$ -catalyzed ethylene polymerization: further evidence for the structural assignment of active and dormant species." *Faraday Discuss.* **2003**, *124*, 93-109.
- [30] E. Zurek, T. Ziegler, "Toward the Identification of Dormant and Active Species in MAO (Methylaluminoxane)-Activated, Dimethylzirconocene-Catalyzed Olefin Polymerization." *Organometallics* **2002**, *21*, 83-92.
- [31] E. Kaminski, G. Fink; personal communication.
- [32] S. H. Vosko, L. Wilk, M. Nusair, "Accurate spin-dependent electron liquid correlation energies for local spin density calculations: a critical analysis." *Can. J. Phys.* **1980**, *58*, 1200-1211.
- [33] A. D. Becke, "Density-functional exchange-energy approximation with correct asymptotic behaviour." *Phys. Rev. A* **1988**, *38*, 3098-3100.



- [34] J. P. Perdew, Y. Wang, "Accurate and simple analytic representation of the electron-gas correlation energy." *Phys. Rev. B* **1992**, *45*, 13244-13249.
- [35] Gaussian 98, Revision A.6, M. J. Frisch, G. W. Trucks, H. B. Schlegel, G. E. Scuseria, M. A. Robb, J. R. Cheeseman, V. G. Zakrzewski, J. A. Montgomery, Jr., R. E. Stratmann, J. C. Burant, S. Dapprich, J. M. Millam, A. D. Daniels, K. N. Kudin, M. C. Strain, O. Farkas, J. Tomasi, V. Barone, M. Cossi, R. Cammi, B. Mennucci, C. Pomelli, C. Adamo, S. Clifford, J. Ochterski, G. A. Petersson, P. Y. Ayala, Q. Cui, K. Morokuma, D. K. Malick, A. D. Rabuck, K. Raghavachari, J. B. Foresman, J. Cioslowski, J. V. Ortiz, B. B. Stefanov, G. Liu, A. Liashenko, P. Piskorz, I. Komaromi, R. Gomperts, R. L. Martin, D. J. Fox, T. Keith, M. A. Al-Laham, C. Y. Peng, A. Nanayakkara, C. Gonzalez, M. Challacombe, P. M. W. Gill, B. Johnson, W. Chen, M. W. Wong, J. L. Andres, C. Gonzalez, M. Head-Gordon, E. S. Replogle, and J. A. Pople, Gaussian, Inc., Pittsburgh PA, **1998**.
- [36] Gaussian 03, Revision B.01, M. J. Frisch, G. W. Trucks, H. B. Schlegel, G. E. Scuseria, M. A. Robb, J. R. Cheeseman, J. A. Montgomery, Jr., T. Vreven, K. N. Kudin, J. C. Burant, J. M. Millam, S. S. Iyengar, J. Tomasi, V. Barone, B. Mennucci, M. Cossi, G. Scalmani, N. Rega, G. A. Petersson, H. Nakatsuji, M. Hada, M. Ehara, K. Toyota, R. Fukuda, J. Hasegawa, M. Ishida, T. Nakajima, Y. Honda, O. Kitao, H. Nakai, M. Klene, X. Li, J. E. Knox, H. P. Hratchian, J. B. Cross, C. Adamo, J. Jaramillo, R. Gomperts, R. E. Stratmann, O. Yazyev, A. J. Austin, R. Cammi, C. Pomelli, J. W. Ochterski, P. Y. Ayala, K. Morokuma, G. A. Voth, P. Salvador, J. J. Dannenberg, V. G. Zakrzewski, S. Dapprich, A. D. Daniels, M. C. Strain, O. Farkas, D. K. Malick, A. D. Rabuck, K. Raghavachari, J. B. Foresman, J. V. Ortiz, Q. Cui, A. G. Baboul, S. Clifford, J. Cioslowski, B. B. Stefanov, G. Liu, A. Liashenko, P. Piskorz, I. Komaromi, R. L. Martin, D. J. Fox, T. Keith, M. A. Al-Laham, C. Y. Peng, A. Nanayakkara, M. Challacombe, P. M. W. Gill, B. Johnson, W. Chen, M. W. Wong, C. Gonzalez, and J. A. Pople, Gaussian, Inc., Pittsburgh PA, **2003**.
- [37] V. R. Jensen, K. J. Børve, "An Investigation of the Quantum Chemical Description of the Ethylenic Double Bond in Reactions: II. Insertion of Ethylene into a Titanium-Carbon Bond." *J. Comput. Chem.* **1998**, *19*, 947-960.
- [38] A. D. Becke, "Density-functional thermochemistry. III. The role of exact exchange." *J. Chem. Phys.* **1993**, *98*, 5648-5652.
- [39] (a) J. Cizek, "On the use of the cluster expansion and the technique of diagrams in calculations of correlation effects in atoms and molecules." *Adv. Chem. Phys.* **1969**, *14*, 35-89.  
(b) G. D. Purvis III, R. J. Bartlett, "A full coupled-cluster singles and doubles model: The

- inclusion of disconnected triples.” *J. Chem. Phys.* **1982**, 76, 1910-1918. (c) G. E. Scuseria, C. L. Janssen, H. F. Schaefer III, “An efficient reformulation of the closed-shell coupled cluster single and double excitation (CCSD) equations.” *J. Chem. Phys.* **1988**, 89, 7382-7387. (d) J. A. Pople, M. Head-Gordon, K. Raghavachari, “Quadratic configuration interaction. A general technique for determining electron correlation energies.” *J. Chem. Phys.* **1987**, 87, 5968-5975.
- [40] P. J. Hay, W. R. Wadt, “Ab initio effective core potentials for molecular calculations. Potentials for K to Au including the outermost core orbitals.” *J. Chem. Phys.* **1985**, 82, 299-310.
- [41] W. R. Wadt, P. J. Hay, “Ab initio effective core potentials for molecular calculations. Potentials for main group elements Na to Bi.” *J. Chem. Phys.* **1985**, 82, 284-298.
- [42] T. H. Dunning, P. J. Hay, “Methods of Electronic Structure Theory.” H. F. Schaefer, Ed., Plenum Press, New York, **1977**, page 1-27.
- [43] S. Tobisch, T. Ziegler, “Catalytic Oligomerization of Ethylene to Higher Linear  $\alpha$ -Olefins Promoted by the Cationic Group 4  $[\eta^2\text{-Cp}-(\text{CMe}_2\text{-bridge})\text{-Ph}]\text{M}^{\text{II}}(\text{ethylene})_2]^+$  (M = Ti, Zr, Hf) Active Catalysts: A Density Functional Investigation of the Influence of the Metal on the Catalytic Activity and Selectivity.” *J. Am. Chem. Soc.* **2004**, 126, 9059-9071
- [44] E. Wilhelm, R. Battino, “Thermodynamic Functions of the Solubilities of Gases in Liquids at 25°C” *Chem. Rev.* **1973**, 73, 1-9.
- [45] R. Pou-Amérigo, M. Merchán, I. Nebot-Gil, P. -O. Widmark, B. O. Roos, “Density matrix averaged atomic natural orbital (ANO) basis sets for correlated molecular wave functions III. First row transition metal atoms.” *Theor. Chim. Acta* **1995**, 92, 149-181.
- [46] The deviation from planarity for the three-coordinate metal complex,  $[\text{L}_2\text{Zr}-\text{Pr}]^+$ , is defined by the angle  $\Theta = 360^\circ - \text{L}^1\text{ZrL}^2 - \text{L}^1\text{ZrPr} - \text{L}^2\text{ZrPr}$ .
- [47] Frontside and backside attack refer to the approach of the ethylene molecule syn and anti to the agostic hydrogen atom of the alkyl cation, respectively.
- [48] No transition state on the potential energy surface of frontside coordination of ethylene to **1a** could be found. However, there exists a barrier (entropic in nature) on the free energy surface and an estimate of its magnitude was obtained by stepwise geometry optimization and vibrational analysis with a constrained Zr-C(ethylene) distance in order to locate the maximum on the free energy curve of ethylene coordination.

[49] Transition states of ethylene coordination may have slightly lower energies than those of separated reactants (propyl cation and free ethylene) due to the existence of weak charge-induced-dipole complexes at long Zr-ethylene distances. Even if the electronic energies of these complexes may be below the reactant asymptote, thermal and entropic corrections in practice render their enthalpies and free energies equal to or higher than the asymptote. These weak complexes are thus not important for the propagation kinetics of the title zirconocenes and their structures and energies are therefore not reported.

[50] For  $L = Cp^*$ , a propyl chain conformation similar to that in **I $\alpha$ 1** is not stable for the naked cations. However, there exist weak charge-induced-dipole complexes with this conformation. Rotation around the  $C\alpha-C\beta$  bond to interconvert between **I $\alpha$ 1** and **I $\alpha$ 2** was found to be associated with a low barrier. For  $L = Cp^*$  such a rotation may take place, for example in the weak pre-coordination complex, prior to the TS of ethylene coordination (**[II $\alpha$ 2—IIF $\alpha$ 1] $^\ddagger$** ).

[51] A. Döhring, V. R. Jensen, P. W. Jolly, W. Thiel, J. C. Weber, "Donor-ligand-substituted cyclopentadienylchromium(III) complexes: A new class of alkene polymerization catalyst. 2. Phosphinoalkyl-substituted systems." *Organometallics* **2001**, 20, 2234-2245.

[52] J. C. W. Lohrenz, T. K. Woo, T. Ziegler, "A Density Functional Study on the Origin of the Propagation Barrier in the Homogeneous Ethylene Polymerization with Kaminsky-Type Catalysts." *J. Am. Chem. Soc.* **1995**, 117, 12793-12804.

[53] J. N. Harvey, "Electronic Effects on the Stability of Isomeric Alkyl Transition Metal Compounds." *Organometallics* **2001**, 20, 4887-4895.

[54] M. Hill, G. Erker, G. Kehr, R. Fröhlich, O. Kataeva, "Exploring CH-Activation Pathways in Bifunctional Zirconocene/Borane Systems." *J. Am. Chem. Soc.* **2004**, 126, 11046-11057.

[55] Using BPW91 (CCSD(T)) in connection with TZD2P basis sets,  $\Delta E = 28.0$  (30.0) kcal/mol for reaction (6.2). The geometries were optimized using the BPW91 functional







## Regiocontrolled Ru-catalyzed addition of carboxylic acids to alkynes: practical protocols for the synthesis of vinyl esters.

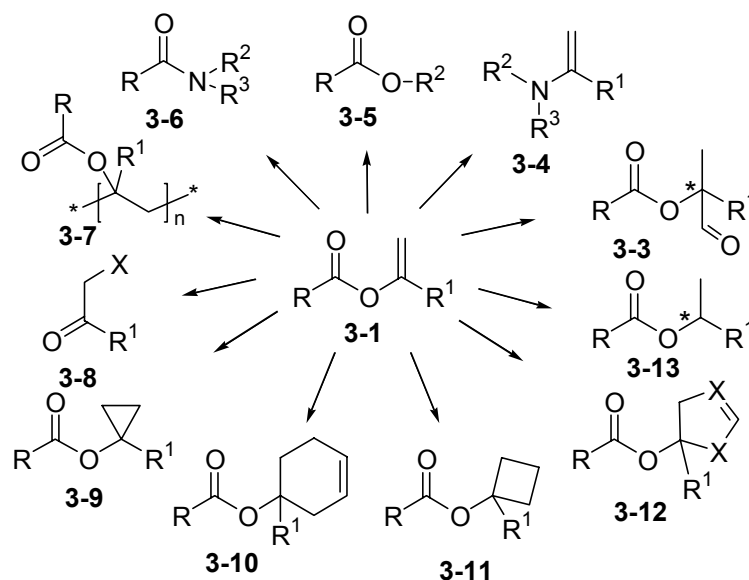
*The grandest as well as the most correct views are those that have been gained by minute observation, and by the application of all the more precise and accurate methods in science.*

(Sir Humphry Davy, The Collected Works of Sir Humphry Davy, Volume I, Memories of the Life of Sir Humphry Davy, Chapter III, page 153)

### 7.1 Introduction

Enol esters have been shown to be useful precursors in organic synthesis, especially for the regio- and stereo-selective generation of enolates.[1] Enol esters such as vinyl **3-1** ( $R^1 = H$ ) and isopropenyl ester **3-1** ( $R^1 = Me$ ) are mild acylating reagents for synthesis of esters **3-5** and amides **3-6**. [2] Furthermore, these reactions are often used in lipase catalyzed kinetic resolutions of racemic alcohols (Scheme 7.1). [3]

**Scheme 7.1. Synthetic routes from enol esters**

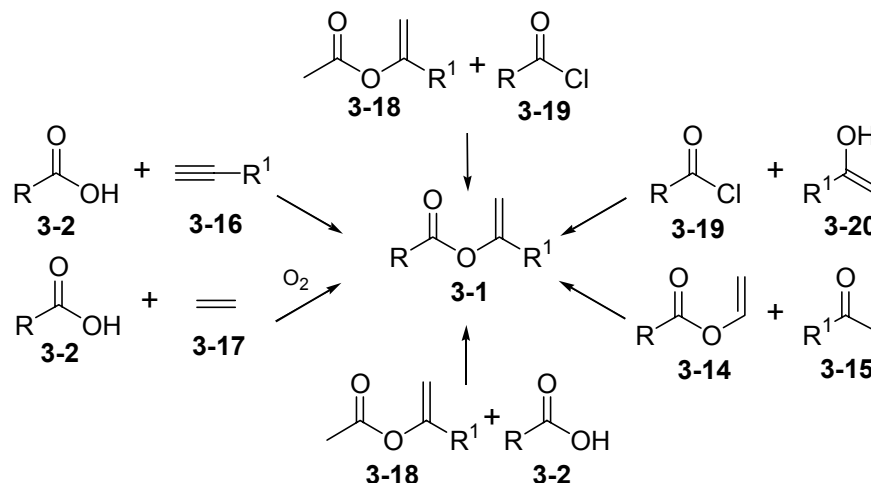


Enol esters **3-1** possess a strongly activated double bond due to the +M-effect of the bonded oxygen atom. Enol esters are useful intermediates for carbon-carbon and carbon-heteroatom bond formation. Vinyl esters such as vinyl acetates, acetoxystyrenes and vinylhaloacetates are important substrates for polymerization reactions.[4] Other applications include

cyclopropanations,[5] [2 + 4]-, [2 + 2]-, and 1,3-dipolar cycloadditions,[6] asymmetric hydrogenation[7] and hydroformylation[8] reactions and the conversion to enamides.[9]

In the laboratory, enol esters are usually prepared *via* O-acylation of enolate **3-20** with acid chloride **3-19** (Scheme 7.2).

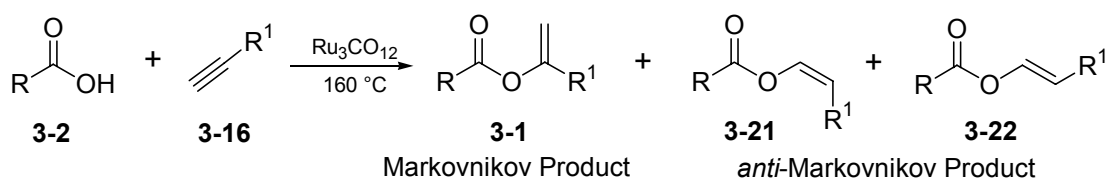
**Scheme 7.2. Routes for enol ester synthesis**



The most popular method for preparation of vinyl or isopropenyl esters is the transesterification of a nonvolatile carboxylic acid **3-2** with vinylacetate **3-18** ( $R^1 = H$ ) or isopropenyl acetate **3-18** ( $R^1 = Me$ ) in the presence of Lewis acid as catalyst. During the reaction the byproducts acetone or acetaldehyde are continuously distilled out from the reaction vessel. Another way of synthesizing enol ester is *via* the reaction of vinyl ester **3-14** and nonvolatile ketones **3-15**, as shown in Scheme 7.2.[10]

Rotem *et al.* used  $Ru_3(CO)_{12}$  as well as  $[Ru(CO)_2(O_2CCH_3)]_n$  as catalyst precursors for the addition of aliphatic and aromatic carboxylic acids to di- and monosubstituted acetylenes under harsh conditions, (Scheme 7.3) resulting mainly in Markovnikov products.[11] In the groups of Mitsudo and Dixneuf,[12,13] the reaction was further developed and more active catalysts were discovered, *e.g.* *bis*(cyclooctadienyl)Ru-phosphine-maleic anhydride or  $Ru(\text{methallyl})_2$ -phosphine combinations. It was also found that bidentate phosphines on the ruthenium reverse the selectivity of the addition, so that instead of alk-1-en-2-yl esters **3-1**, the (*Z*)-alk-1-en-1-yl esters **3-21** are predominantly formed.[13]

**Scheme 7.3. Rotem and Shvo method for addition of alkyne to carboxylic acids**



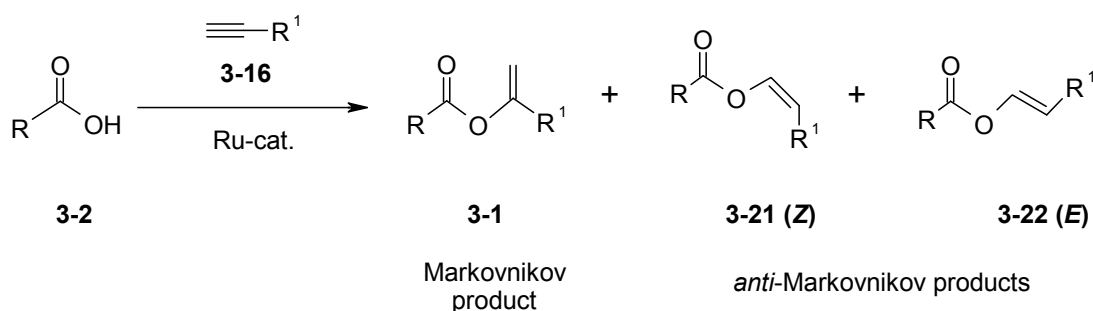


However, the practical value of this elegant transformation remained limited for organic chemists, since the catalytic activity of readily available ruthenium compounds is rather low,[14] and sufficiently active catalysts have to be especially synthesized from sensitive organometallic compounds (*i.e.* *bis*(cyclooctadienyl)Ru).[12]

It was our target to devise a new catalytic system that is highly effective, yet consists solely of easy to handle, commercially available components and is thus particularly practical for applications in synthetic chemistry. Jens Paetzold[15] and myself were assigned to synthesize the Markovnikov and *anti*-Markovnikov product, respectively (Scheme 7.4).

Our model system constitutes the reaction of benzoic acid **3-2a** (R = phenyl) with 1-hexyne **3-16a** (R<sup>1</sup> = *n*-butyl), which is represented in Scheme 7.4. We have screened various ruthenium complexes in order to identify factors that influence their catalytic activity. Selected results are summarized in Table 7.1.

### Scheme 7.4. Addition of carboxylic acids to terminal alkynes



At 60 °C, the commercially available ruthenium compounds show no reactivity for the desired transformation (Table 7.1, Entries 1-3). However, in the presence of a catalyst generated *in situ* from ((*p*-cumene)RuCl<sub>2</sub>)<sub>2</sub> **3-23** and PPh<sub>3</sub>, the addition proceeds with high selectivity for the Markovnikov product **3-1a**, though in modest yields (Table 7.1, Entry 4).

**Table 7.1. Ruthenium-catalyzed addition of benzoic acid (3-2a) to hexyne (3-16a).**

Entry	Ru-Precursor	Ligand	Additive	Conv. (%) <sup>a</sup>	Sel. <b>3-1</b> (%)	Sel. <b>3-21</b> (%)
1	RuCl <sub>3</sub>	—	—	<1	—	—
2	RuCl <sub>3</sub> (PPh <sub>3</sub> ) <sub>3</sub>	—	—	<1	—	—
3	[( <i>p</i> -Cymol)RuCl <sub>2</sub> ] <sub>2</sub>	—	—	<1	—	—
4	[( <i>p</i> -Cymol)RuCl <sub>2</sub> ] <sub>2</sub>	PPh <sub>3</sub>	—	10	97	2
5	[( <i>p</i> -Cymol)RuCl <sub>2</sub> ] <sub>2</sub>	PCy <sub>3</sub>	—	10	80	15
6	[( <i>p</i> -Cymol)RuCl <sub>2</sub> ] <sub>2</sub>	P( <i>p</i> -Cl-C <sub>6</sub> H <sub>4</sub> ) <sub>3</sub>	—	10	97	2
7	[( <i>p</i> -Cymol)RuCl <sub>2</sub> ] <sub>2</sub>	P(Fur) <sub>3</sub>	—	15	97	2

Entry	Ru-Precursor	Ligand	Additive	Conv. (%) <sup>a</sup>	Sel. <b>3-1</b> (%)	Sel. <b>3-21</b> (%)
8	[( <i>p</i> -Cymol)RuCl <sub>2</sub> ] <sub>2</sub>	P(Fur) <sub>3</sub>	AgNO <sub>3</sub>	85	95	4
9	[( <i>p</i> -Cymol)RuCl <sub>2</sub> ] <sub>2</sub>	P(Fur) <sub>3</sub>	AgClO <sub>4</sub>	5	90	n.d.
10	[( <i>p</i> -Cymol)RuCl <sub>2</sub> ] <sub>2</sub>	P(Fur) <sub>3</sub>	AgSbF <sub>6</sub>	<1	—	—
11	[( <i>p</i> -Cymol)RuCl <sub>2</sub> ] <sub>2</sub>	P(Fur) <sub>3</sub>	NaF	50	97	2
12	[( <i>p</i> -Cymol)RuCl <sub>2</sub> ] <sub>2</sub>	P(Fur) <sub>3</sub>	PhCOONa	95	97	2
13	[( <i>p</i> -Cymol)RuCl <sub>2</sub> ] <sub>2</sub>	P(Fur) <sub>3</sub>	Na <sub>2</sub> CO <sub>3</sub>	95	97	2
14 <sup>a</sup>	[( <i>p</i> -Cymol)RuCl <sub>2</sub> ] <sub>2</sub>	P(Fur) <sub>3</sub>	Na <sub>2</sub> CO <sub>3</sub>	95	97	2
15	[( <i>p</i> -Cymol)RuCl <sub>2</sub> ] <sub>2</sub>	P(Fur) <sub>3</sub>	2,6-lutidine	<1	—	—
16	[( <i>p</i> -Cymol)RuCl <sub>2</sub> ] <sub>2</sub>	P(Fur) <sub>3</sub>	pyridine	20	<1	98
17	[( <i>p</i> -Cymol)RuCl <sub>2</sub> ] <sub>2</sub>	P(Fur) <sub>3</sub>	DMAP	20	<1	98
18	[( <i>p</i> -Cymol)RuCl <sub>2</sub> ] <sub>2</sub>	PPPh <sub>3</sub>	DMAP	45	<1	99
19	[( <i>p</i> -Cymol)RuCl <sub>2</sub> ] <sub>2</sub>	P( <i>p</i> -Cl-C <sub>6</sub> H <sub>4</sub> ) <sub>3</sub>	DMAP	65	<1	99
20 <sup>b</sup>	[( <i>p</i> -Cymol)RuCl <sub>2</sub> ] <sub>2</sub>	P( <i>p</i> -Cl-C <sub>6</sub> H <sub>4</sub> ) <sub>3</sub>	DMAP	90	<1	99
21 <sup>c</sup>	[( <i>p</i> -Cymol)RuCl <sub>2</sub> ] <sub>2</sub>	P(Fur) <sub>3</sub>	Na <sub>2</sub> CO <sub>3</sub>	95	97	2
22 <sup>d</sup>	[( <i>p</i> -Cymol)RuCl <sub>2</sub> ] <sub>2</sub>	P(Fur) <sub>3</sub>	Na <sub>2</sub> CO <sub>3</sub>	<1	—	—
23 <sup>e</sup>	[( <i>p</i> -Cymol)RuCl <sub>2</sub> ] <sub>2</sub>	P(Fur) <sub>3</sub>	Na <sub>2</sub> CO <sub>3</sub>	95	97	2

Conditions: 1.00 mmol benzoic acid, 1.30 mmol 1-hexyne, 0.01 mmol Ru-precursor, 0.02 mmol ligand, 0.04 mmol additive, toluene, 60 °C, 16 h. <sup>a</sup>10 mmol water, no argon, 25 °C, 72 h. <sup>b</sup>0.03 mmol ligand. <sup>c</sup>1,2-Dichloroethane. <sup>d</sup>NMP. <sup>e</sup>Nonanoic acid, no solvent.

Better yields are obtained when using phosphines with strong  $\pi$ -acceptor ability such as tri-2-furyl phosphine (= P(Fur)<sub>3</sub>) (Table 7.1, Entries 5-7).

It was then investigated whether the addition of silver salts with non-coordinating counterions would generate more active cationic catalysts.[12] However, among the silver salts tested, solely AgNO<sub>3</sub> showed an accelerating effect (Table 7.1, Entries 8-10).

Since in the catalytic cycle the carboxylate attacks the alkyne coordinated to the ruthenium[2], we thought that the presence of catalytic amounts of base would facilitate the reaction. Indeed, simply by adding few mol% of sodium benzoate, the yields were drastically increased. Addition of inorganic bases to the reaction mixture had the same accelerating effect and the best results were obtained using sodium carbonate (Table 7.1, Entries 11-13). The reaction is insensitive to both air and water—a great advantage for preparative applications (Table 7.1, Entry 14).

The Markovnikov product **3-1a** was formed predominantly in presence of inorganic bases. However, this selectivity was reversed when organic bases *e.g.* pyridines, were added (Table

7.1, Entries 15-17). In the presence of (4-dimethylamino)pyridine (DMAP), the selectivity for the (*Z*)-*anti*-Markovnikov product **3-21a** was 98 to 99%. For the *anti*-Markovnikov reaction variant, P(*p*-Cl-C<sub>6</sub>H<sub>4</sub>)<sub>3</sub> was slightly more effective than P(Fur)<sub>3</sub> (Table 7.1, Entries 17-20).

Toluene, chloroform and 1,2-dichloroethane are suitable solvents for both reaction variants, while more strongly coordinating solvents lower the turnover rates (Table 7.1, Entries 13, 21 and 22). When using liquid carboxylic acids, the reaction can also be carried out successfully without solvent (Table 7.1, Entry 23).

After having identified highly active catalyst systems for both Markovnikov and *anti*-Markovnikov additions of carboxylic acids to 1-alkynes, we investigated the scope of our protocols using various carboxylic acids in combination with several alkynes. Selected results are displayed in Table 7.2. Electron-rich and electron-poor alkyl, aryl, and heteroaryl carboxylic acids give excellent yields with both catalyst systems. The reaction converts sterically hindered carboxylic acids and is tolerant to variety of functionalities *e.g.* esters, ethers, aldehydes, carbamates, and hydroxyls.

The *N*-protected  $\alpha$ - and  $\beta$ -amino acids undergo Markovnikov addition smoothly, while the  $\alpha$ -amino acids give no conversion in the *anti*-Markovnikov reaction variant. Further experiments suggested that this might be due to the high C—H acidity of  $\alpha$ -amino acids.

Various other terminal alkynes were converted in good yields, even gaseous propyne smoothly reacts at ambient pressure, so that no high-pressure equipment is required for the preparation of the synthetically particularly useful isopropenyl esters.[3]

**Table 7.2. Scope of the Markovnikov and the *anti*-Markovnikov addition.**

R <sup>1</sup>	R <sup>2</sup>	Method	Prod.	Yield (%)	Sel <sup>a</sup> <b>3-1:3-21</b>
Phenyl	<i>n</i> -C <sub>4</sub> H <sub>9</sub>	A	<b>3-1a</b>	93	30:1
		B	<b>3-21a</b>	89	1:50
<i>o</i> -Tolyl	<i>n</i> -C <sub>4</sub> H <sub>9</sub>	A	<b>3-1b</b>	86	35:1
		B	<b>3-21b</b>	93	1:50
<i>p</i> -MeO-C <sub>6</sub> H <sub>4</sub>	<i>n</i> -C <sub>4</sub> H <sub>9</sub>	A	<b>3-1c</b>	88	15:1
		B	<b>3-21c</b>	90	1:50
<i>p</i> -H(CO)-C <sub>6</sub> H <sub>4</sub>	<i>n</i> -C <sub>4</sub> H <sub>9</sub>	A <sup>b</sup>	<b>3-1d</b>	87	10:1
		B <sup>c</sup>	<b>3-21d</b>	80	1:50
2-Thienyl	<i>n</i> -C <sub>4</sub> H <sub>9</sub>	A	<b>3-1e</b>	94	30:1
		B	<b>3-21e</b>	87	1:50
1-Me-pyrrol-2-yl	<i>n</i> -C <sub>4</sub> H <sub>9</sub>	A	<b>3-1f</b>	95	24:1

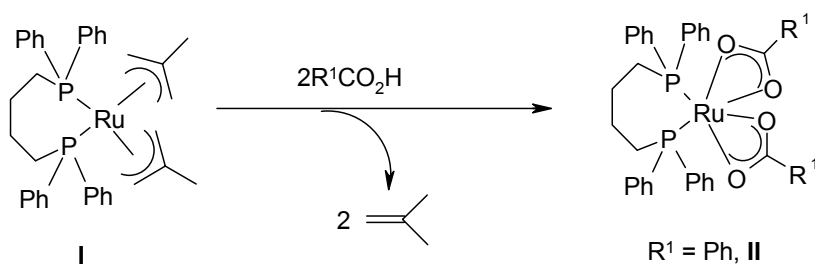
		B	<b>3-21f</b>	94	1:50
HO- <i>n</i> -C <sub>11</sub> H <sub>22</sub>	<i>n</i> -C <sub>4</sub> H <sub>9</sub>	A <sup>b</sup>	<b>3-1g</b>	61	15:1
		B	<b>3-21g</b>	72	1:50
<i>m</i> -AcO-C <sub>6</sub> H <sub>4</sub>	<i>n</i> -C <sub>4</sub> H <sub>9</sub>	A	<b>3-1i</b>	86	50:1
		B	<b>3-21i</b>	86	1:50
C <sub>6</sub> H <sub>5</sub> -C <sub>2</sub> H <sub>4</sub>	<i>n</i> -C <sub>4</sub> H <sub>9</sub>	A	<b>3-1j</b>	83	22:1
		B	<b>3-21j</b>	74	1:50
<i>p</i> -CF <sub>3</sub> -C <sub>6</sub> H <sub>4</sub>	<i>n</i> -C <sub>4</sub> H <sub>9</sub>	A	<b>3-1k</b>	95	30:1
		B <sup>c</sup>	<b>3-21k</b>	78	1:50
Cbz-NHCH <sub>2</sub> CH <sub>2</sub>	<i>n</i> -C <sub>4</sub> H <sub>9</sub>	A <sup>b</sup>	<b>3-1l</b>	70	14:1
		B	<b>3-21l</b>	46	1:50
Cbz-NHCH <sub>2</sub>	<i>n</i> -C <sub>4</sub> H <sub>9</sub>	A <sup>b</sup>	<b>3-1m</b>	82	14:1
		B	<b>3-21m</b>	<5	n.d.
Phenyl	Phenyl	A <sup>d</sup>	<b>3-1n</b>	88	3:2
		B	<b>3-21n</b>	99	1:50
Phenyl	CH <sub>3</sub>	A	<b>3-1o</b>	99	22:1
		B	<b>3-21o</b>	76	1:50
Phenyl	<i>t</i> -Butyl	A	<b>3-1p</b>	88	10:1
		B <sup>c</sup>	<b>3-21p</b>	68	1:50

Conditions: A: 5.00 mmol acid, 6.50 mmol alkyne, 0.02 mmol **6**, 0.04 mmol P(Fur)<sub>3</sub>, 0.08 mmol Na<sub>2</sub>CO<sub>3</sub>, toluene, 50 °C, 16 h; B: 5.00 mmol acid, 6.50 mmol alkyne, 0.05 mmol ((*p*-cumene)RuCl<sub>2</sub>)<sub>2</sub> **3-23**, 0.15 mmol P(*p*-Cl-C<sub>6</sub>H<sub>4</sub>)<sub>3</sub>, 0.20 mmol DMAP, toluene, 60 °C, 16 h. <sup>a</sup> Isomer **3-22** < 1 %. <sup>b</sup> In CHCl<sub>3</sub>. <sup>c</sup> In 1,2-dichloroethane, 80 °C. <sup>d</sup> 70 °C.

## 7.2 Mechanism

A number of ruthenium complexes catalyze the reaction such as Ru<sub>3</sub>(CO)<sub>12</sub>, [(arene)RuCl<sub>2</sub>]<sub>2</sub> or even RuCl<sub>3</sub>·xH<sub>2</sub>O, but the yields are low and almost no selectivity is observed. The presence of phosphorus ligands coordinated to the ruthenium center increases the rate, yield and selectivity of the reaction. Doucet *et al.* discussed the mechanism of this catalytic reaction on the basis of the complex **I**.<sup>[13]</sup> Initially, the ruthenium-catalyst undergoes ligand substitution to afford the (η<sup>2</sup>-carboxylate)Ru(II)complex (**II**) which had already been reported and isolated by the same authors (Scheme 7.5).

## Scheme 7.5



The probable catalytic cycle for this transformation (Scheme 7.4) is displayed in Scheme 7.6. Bruneau *et al.* ruled out the possibility of alkyne insertion into the (carboxylate)O—ruthenium bond. The initially formed adduct **IV** is postulated to yield the ruthenacyclopentene **V2** (with resonance form **V2'**) or the vinylidene tautomer **V1**, depending on the coordinated ligands. The addition of carboxylic acid to the electrophilic C atom of the alkyne will afford either intermediate **VII** or **VI2**. Subsequent protonolysis of the ruthenium—C bond, or protonation of the ruthenium center followed by reductive elimination, will liberate the alkenyl ester.

The regioselectivity of the reaction may depend on the electron deficiency of the coordinated triple bond. The formation of the tautomeric ruthenium—vinylidene moiety **V1**, formed from a terminal alkyne and ruthenium(II) catalysts, would favor the addition of the carboxylate at the electrophilic C(1) of the terminal alkyne.

In order to get further information on the mechanism of this interesting transformation, the reaction mixtures of both the Markovnikov- and the *anti*-Markovnikov-selective protocol were investigated by *in situ* ESI-MS.

In the ESI-MS study of the reaction mixture, the Markovnikov-selective protocol does not show any signal for a ruthenium-complex which contains the carbonate base (Figure 7.2). In contrast, the mixture containing DMAP shows a signal for ruthenium-*p*-cymene-benzoate-hexyne-DMAP complex at  $m/z = 561.3$  (Figure 7.1). This suggests that in this case both the *p*-cymene and DMAP base are coordinated to the ruthenium center. The coordinated DMAP tunes the electronic environment at the metal center, which subsequently triggers a regioselective attack to the coordinated triple bond. Moreover, the strong coordination of hexyne to ruthenium suggests that a vinylidene isomer of the type **V1** is formed (Figure 7.1). In the Markovnikov protocol both the  $P(\text{Fur})_3$  and benzoic acid are coordinated to the ruthenium center ( $m/z = 589.2$ ). The coordination of hexyne to **3-43** will afford an  $\eta^2$ -type complex (Scheme 7.6, **V2**) which will give rise to the Markovnikov product after the nucleophilic attack of the benzoate.

**Scheme 7.6.** The catalytic cycle for both Markovnikov and *anti*-Markovnikov product.

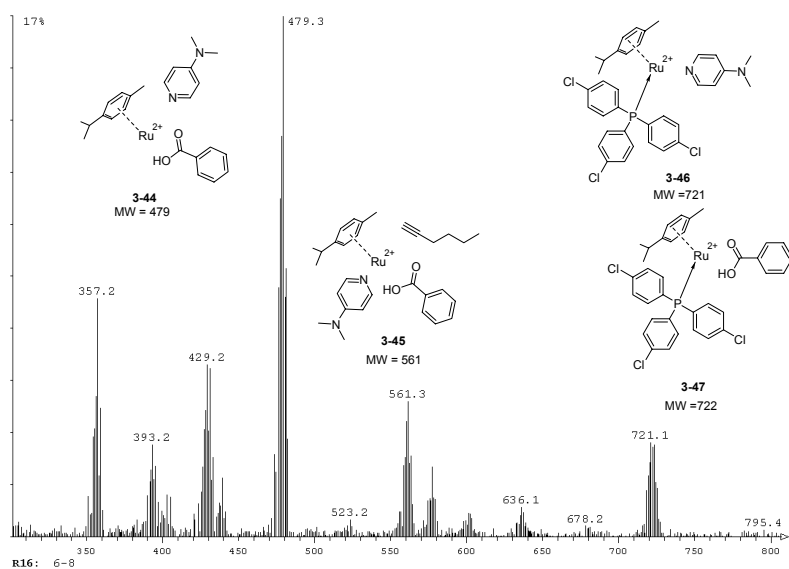
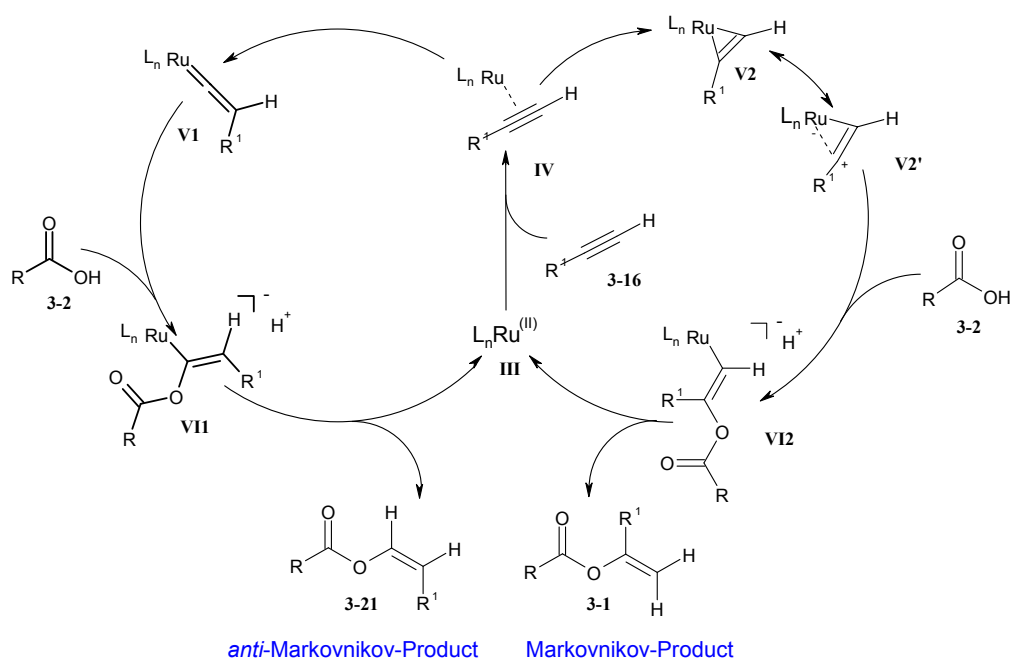


**Figure 7.1.** ESI-MS spectrum for the *anti*-Markovnikov addition in presence of DMAP.

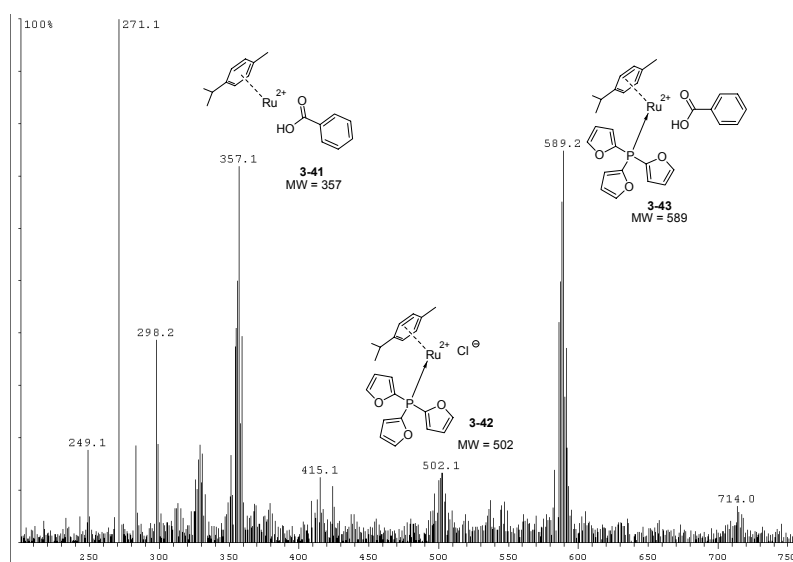


**Figure 7.2.** ESI-MS spectrum for the Markovnikov addition as represented in Scheme 4.

### 7.3 Conclusion

Overall, we have developed highly efficient catalyst systems for both the Markovnikov and the *anti*-Markovnikov addition of carboxylic acids to terminal alkynes. The catalysts are generated *in situ* from air- and water-stable compounds that are commercially available at low cost. Thus, important drawbacks of this elegant transformation have been overcome. We propose a plausible catalytic cycle for these transformations which is supported by *in situ* ESI-MS measurements.

## 7.4 Experimental Section.

**General Methods:** All reagents were obtained from commercial sources and used without further purification. The solvents were dried and degassed using standard procedures. NMR-spectra were recorded in  $\text{CDCl}_3$  with TMS as the internal standard. The mass spectra were measured on a MAT 95 (70 eV) instrument. Column chromatography was performed on silica gel (230-400 mesh; Kieselgel 60 “Merck”) or on basic aluminum oxide (0.05-0.15 mm; 5016A “Merck”).

### General procedure for the preparation of Vinyl Esters.

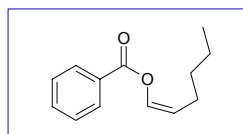
#### Method A:

Benzoic acid (588 mg, 5.00 mmol) and  $\text{Na}_2\text{CO}_3$  (9.40 mg, 0.08 mmol) were suspended in toluene (16 ml). Subsequently, a solution of  $((p\text{-cumene})\text{RuCl}_2)_2$  (12.2 mg, 0.02 mmol) and tri(2-furyl)phosphine (9.20 mg, 0.04 mmol) in toluene (4 ml), and 1-hexyne (710  $\mu\text{l}$ , 6.50 mmol) were added. The reaction mixture was heated to 50  $^\circ\text{C}$ . After complete conversion (GC), usually 16 h, the mixture was cooled and filtered over a small plug of silica gel. The solvent was removed and the crude mixture was purified by Kugelrohr distillation at 120  $^\circ\text{C}$ /0.1 mbar, yielding product **3-1a** (950 mg, 93%, isomeric purity > 96%) as a colorless liquid.[14]

See the Dissertation of Dr. Jens Paetzold, “Carbonsäuren als Startmaterialien in der Übergangsmetallkatalyse.” for further details.

#### Method B:

##### 1) Benzoic acid hex-1-enyl ester (**3-1a**):



A solution of  $((p\text{-cumene})\text{RuCl}_2)_2$  (30.6 mg, 0.05 mmol), tri(*p*-Cl- $\text{C}_6\text{H}_4$ )phosphine (54.8 mg, 0.15 mmol) and DMAP (24.4 mg, 0.20 mmol) in dry toluene (4 ml) was added to a solution of benzoic acid (588 mg, 5.00 mmol) and 1-hexyne (712  $\mu\text{l}$ , 6.50 mmol) in dry toluene (16 ml). The mixture was stirred for 16 h at 60  $^\circ\text{C}$ . After complete conversion (GC), usually 16 h, the mixture was cooled and filtered over a small plug of silica gel. The solvent was removed and the crude mixture was purified by kugelrohr distillation at 128  $^\circ\text{C}$ /0.1 mbar, yielding **1a** (908 mg, 89%, isomeric purity > 98%).

Beilstein Registry No: 6175354.



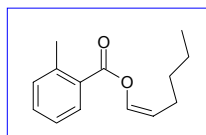
**<sup>1</sup>H-NMR** (300 MHz, CDCl<sub>3</sub>): δ = 0.95 (t, 3H, <sup>3</sup>J = 7.16 Hz), 1.45-1.36 (m, 4H), 2.28-2.29 (m, 2H), 5.00 (dd, 1H, <sup>3</sup>J = 6.97 and 7.25 Hz), 7.25 (d, 1H, <sup>3</sup>J = 6.9 Hz), 7.6 (d, 2H, <sup>3</sup>J = 4 Hz), 7.8 (d, 2H, <sup>3</sup>J = 4.2 Hz), 8.20 (d, 2H, <sup>3</sup>J = 4.1 Hz) ppm.

**<sup>13</sup>C-NMR** (75 MHz, CDCl<sub>3</sub>): δ = 13.9; 22.2; 24.3; 31.3; 114.9; 128.5; 129.5; 133.4; 134.1; 163.6 ppm.

**MS** (EI, 70 eV, Evaporation Temperature -7°C): m/z (%) = 204 (4, [M]<sup>+</sup>), 105 (100), 77 (26), 51 (6), 50 (1.5), 41 (2), 39 (1.6), 29 (1.6), 27 (2.3).

**HRMS** (EI): calcd. for C<sub>13</sub>H<sub>16</sub>O<sub>2</sub> [M]<sup>+</sup>: 204.115030, found: 204.115092.

## 2) 2-Methyl-benzoic acid hex-1-enyl ester (**3-1b**):



This enol ester was obtained following the general procedure from 2-Methylbenzoic acid **3-2a** (680.8 mg, 5.00 mmol) and 1-hexyne **3-16a** (712 μL, 6.50 mmol) in toluene as solvent. Boiling point 130 °C/ 0.1 mbar. Yield: 1013.7 mg (93%), a colorless liquid. Isomeric ratio i/n = 1/50.

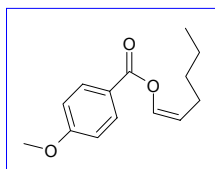
**<sup>1</sup>H-NMR** (300.1 MHz, CDCl<sub>3</sub>, 25 °C, TMS): δ = 0.94 (t, 3H, <sup>3</sup>J = 7.16 Hz), 1.45-1.36 (m, 4H), 2.27-2.29 (m, 2H), 2.64 (s, 1H), 5.02 (dd, 1H, <sup>3</sup>J = 6.53 and 7.32 Hz), 7.22 (m, 3H), 7.45 (dd, 1H, <sup>3</sup>J = 7.37 and 7.83 Hz), 8.00 (d, 1H, <sup>3</sup>J = 7.83 Hz) ppm.

**<sup>13</sup>C-NMR** (75.5 MHz, CDCl<sub>3</sub>, 25 °C, TMS): δ = 13.9; 21.9; 22.7; 24.5; 31.4; 114.6; 125.8; 128.7; 130.9; 131.3; 132.5; 134.1; 140.9; 164.4 ppm.

**MS** (EI, 70 eV, Evaporation Temperature 1 °C): m/z (%) = 218 (2.6, [M]<sup>+</sup>), 119 (100), 91 (27), 90 (1.9), 89 (2.3), 65 (8.5), 41 (2.6), 39 (2.8), 27 (1.7).

**HRMS** (EI): calcd. for C<sub>14</sub>H<sub>19</sub>O<sub>2</sub> [M]<sup>+</sup>: 219.138505, found: 219.138344.

## 3) 4-Methoxy-benzoic acid hex-1-enyl ester (**3-1c**):



This enol ester was obtained following the general procedure from *p*-methoxybenzoic acid **3-2c** (760.8 mg, 5.00 mmol) and 1-hexyne **3-16a** (712  $\mu$ L, 6.50 mmol) in toluene as solvent. Boiling point 120  $^{\circ}$ C/ 0.1 mbar. Yield: 1054.35 mg (90%), a light yellowish color liquid. Isomeric ratio i/n = 1/50.

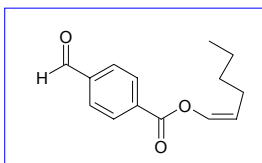
**$^1\text{H-NMR}$**  (300.1 MHz,  $\text{CDCl}_3$ , 25 $^{\circ}$ C, TMS):  $\delta$  = 0.94 (t, 3H,  $^3J$  = 6.98 Hz), 1.56-1.32 (m, 4H), 2.29-2.22 (m, 2H), 3.86 (s, 1H), 4.99 (dd, 1H,  $^3J$  = 6.53 and 7.32 Hz), 6.92 (d, 1H,  $^3J$  = 6.53 Hz), 7.23 (d, 2H,  $^3J$  = 4.0 Hz), 8.04 (d, 2H,  $^3J$  = 4.0 Hz) ppm.

**$^{13}\text{C-NMR}$**  (75.5 MHz,  $\text{CDCl}_3$ , 25  $^{\circ}$ C, TMS):  $\delta$  = 13.8; 22.2; 24.3; 31.7; 55.4; 113.4; 114.3; 121.8; 131.9; 134.2; 145.0; 163.3; 163.7 ppm.

**MS** (EI, 70 eV, Evaporation Temperature 30  $^{\circ}$ C):  $m/z$  (%) = 234 (3,  $[\text{M}]^+$ ), 135 (100), 107 (5.5), 92 (7), 77 (9), 64 (3).

**HRMS** (EI): calcd for  $\text{C}_{14}\text{H}_{18}\text{O}_3$   $[\text{M}]^+$ : 234.125595, found: 234.125341.

#### 4) 4-(1-Hex-1-enyloxy-vinyl)-benzaldehyde (**3-1d**):



This enol ester was obtained following the general procedure from terephthalaldehyde acid **3-2d** (750.7 mg, 5.00 mmol) and 1-hexyne **3-16a** (712  $\mu$ L, 6.50 mmol) in toluene as solvent. Boiling point 150  $^{\circ}$ C/ 0.1 mbar. Yield: 929 mg (80%), a colorless liquid. Isomeric ratio i/n = 1/50.

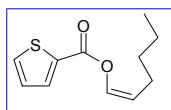
**$^1\text{H-NMR}$**  (300.1 MHz,  $\text{CDCl}_3$ , 25  $^{\circ}$ C, TMS):  $\delta$  = 0.92 (t, 3H,  $^3J$  = 6.99 Hz), 1.45-1.37 (m, 4H), 2.29-2.27 (m, 2H), 5.01 (dd, 1H,  $^3J$  = 6.50 and 7.01 Hz), 7.25 (d, 1H,  $^3J$  = 6.50 Hz), 8.01 (d, 1H,  $^3J$  = 3.50 Hz), 8.31 (d, 1H,  $^3J$  = 3.50 Hz), 10.13 (s, 1H) ppm.

**$^{13}\text{C}$ -NMR** (75.5 MHz,  $\text{CDCl}_3$ , 25 °C, TMS):  $\delta$  = 13.8; 22.2; 24.3; 31.2; 115.7; 129.6; 134.0; 134.4; 139.4; 162.5; 191.4 ppm.

**MS** (EI, 70 eV, Evaporation Temperature 30 °C):  $m/z$  (%) = 232 (4,  $[\text{M}]^+$ ), 133 (100), 105 (13), 104 (3), 82 (1.6), 77 (11), 76 (3), 51 (6), 50 (2), 41 (3), 29 (2), 27 (2).

**HRMS** (EI): calcd for  $\text{C}_{14}\text{H}_{16}\text{O}_3$   $[\text{M}]^+$ : 232.109945, found: 232.110014.

#### 5) Thiophene-2-carboxylic acid pent-1-enyl ester (**3-1e**):



This enol ester was obtained following the general procedure from Thiophen-2-carboxylic acid **3-2e** (640.8 mg, 5.00 mmol) and 1-hexyne **3-16a** (712  $\mu\text{L}$ , 6.50 mmol) in toluene as solvent. Boiling point 120 °C/ 0.1 mbar. Yield: 914.8 mg (87%), a colorless liquid. Isomeric ratio i/n = 1/50.

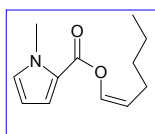
**$^1\text{H}$ -NMR** (300.1 MHz,  $\text{CDCl}_3$ , 25 °C, TMS):  $\delta$  = 0.94 (t, 3H,  $^3J$  = 7.11 Hz), 1.45-1.35 (m, 4H), 2.28-2.30 (m, 2H), 5.00 (dd, 1H,  $^3J$  = 6.53 and 7.36 Hz), 7.12 (d, 1H,  $^3J$  = 6.53 Hz), 7.23 (t, 1H,  $^3J$  = 3.76 and 5.00 Hz), 7.62 (d, 1H,  $^3J$  = 5.00 Hz), 7.78 (d, 1H,  $^3J$  = 3.76 Hz) ppm.

**$^{13}\text{C}$ -NMR** (75.5 MHz,  $\text{CDCl}_3$ , 25 °C, TMS):  $\delta$  = 13.8; 22.2; 24.3; 31.3; 114.9; 127.9; 132.8; 133.2; 133.9; 134.1; 159.2 ppm.

**MS** (EI, 70 eV, Evaporation Temperature 2 °C):  $m/z$  (%) = 210 (5.8,  $[\text{M}]^+$ ), 113 (4.7), 111 (100), 83 (5.4), 82 (2), 57 (1.9), 41 (2.5), 39 (12), 29 (1.8), 27 (2).

**HRMS** (EI): calcd for  $\text{C}_{11}\text{H}_{14}\text{O}_2\text{S}_1$   $[\text{M}]^+$ : 210.071453, found: 210.071609.

#### 6) N-Methyl-pyrrole-2-carboxylic acid hex-1-enyl ester (**3-1f**):



This enol ester was obtained following the general procedure from N-methylpyrrol-2-carboxylic acid **3-2f** (625.6 mg, 5.00 mmol) and 1-hexyne **3-16a** (712  $\mu$ L, 6.50 mmol) in toluene as solvent. Boiling point 110 °C/ 0.1 mbar. Yield: 908.3 mg (94%), a colorless liquid. Isomeric ratio i/n = 1/50.

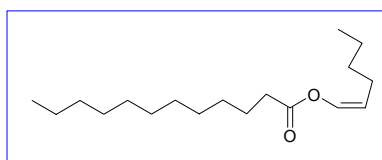
**$^1\text{H-NMR}$**  (300.1 MHz,  $\text{CDCl}_3$ , 25 °C, TMS):  $\delta$  = 0.92 (t, 3H,  $^3J$  = 7.01 Hz), 1.45-1.32 (m, 4H), 2.28-2.30 (m, 2H), 3.94 (s, 1H), 5.02 (dd, 1H,  $^3J$  = 6.53 and 7.33 Hz), 6.13 (dd, 1H,  $^3J$  = 4.01 and 2.38 Hz), 6.82 (d, 1H,  $^3J$  = 2.38 Hz), 7.03 (d, 1H,  $^3J$  = 6.53 Hz), 7.16 (d, 1H,  $^3J$  = 4.01 Hz) ppm.

**$^{13}\text{C-NMR}$**  (75.5 MHz,  $\text{CDCl}_3$ , 25 °C, TMS):  $\delta$  = 13.8; 22.2; 24.3; 31.4; 36.8; 106.5; 113.7; 118.8; 121.6; 130.3; 133.6; 158.2 ppm.

**MS** (EI, 70 eV, Evaporation Temperature -4 °C):  $m/z$  (%) = 207 (8,  $[\text{M}]^+$ ), 135 (3), 108 (100), 80 (5.6), 53 (9), 39 (7.2), 27 (2.4).

**HRMS** (EI): calcd for  $\text{C}_{12}\text{H}_{17}\text{N}_1\text{O}_2$   $[\text{M}]^+$ : 207.125929, found: 207.125617.

#### 7) Dodecanoic acid hex-1-enyl ester (**3-1g**):



This enol ester was obtained following the general procedure from 12-hydroxydodecanoic acid **3-2g** (1081.6 mg, 5.00 mmol) and 1-hexyne **3-16a** (712  $\mu$ L, 6.50 mmol) in toluene as solvent. Boiling point 160 °C/ 0.1 mbar. Yield: 1017 mg (72%), a yellow liquid. Isomeric ratio i/n = 1/50.

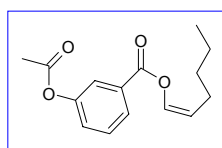
**$^1\text{H-NMR}$**  (300.1 MHz,  $\text{CDCl}_3$ , 25 °C, TMS):  $\delta$  = 0.94 (t, 3H,  $^3J$  = 6.78 Hz), 1.50-1.22 (m, 10H), 1.55-1.80 (m, 2H), 2.51 (t, 2H,  $^3J$  = 6.75 Hz), 3.05 (s, 1H), 3.67 (t, 2H,  $^3J$  = 6.52 Hz), 4.98 (t, 1H,  $^3J$  = 6.53 and 7.33 Hz), 7.01 (d, 1H,  $^3J$  = 6.53 Hz) ppm.

**$^{13}\text{C-NMR}$**  (75.5 MHz,  $\text{CDCl}_3$ , 25 °C, TMS):  $\delta$  = 13.8; 22.1; 24.0; 24.7; 25.7; 29.3; 29.5; 31.3; 32.8; 34.0; 63.0; 99.7; 114.1; 133.9; 195.9 ppm.

**MS** (EI, 70 eV, Evaporation Temperature 60°C):  $m/z$  (%) = 298 (1,  $[M]^+$ ), 199 (59), 182 (10.5), 181 (52), 169 (6), 163 (43), 143 (5), 125 (20), 122 (3), 121 (10), 115 (7.5), 101 (8), 100 (8), 98 (10), 95 (17.6), 83 (55.6), 82 (11), 81 (21), 80 (2), 79 (4), 73 (3), 67 (17), 59 (3), 58 (3), 57 (36), 55 (100), 54 (6), 44 (3), 43 (39), 42 (13), 39 (5), 31 (9).

**HRMS** (EI): calcd for  $C_{18}H_{34}O_3$   $[M]^+$ : 298.250795, found: 298.250660.

8) **3-Acetoxy-benzoic acid hex-1-enyl ester (3-1i):**



This enol ester was obtained following the general procedure from m-acetoxybenzoic acid **3-2i** (900.8 mg, 5.00 mmol) and 1-hexyne **3-16a** (712  $\mu$ L, 6.50 mmol) in toluene as solvent. Boiling point 140 °C/ 0.1 mbar. Yield: 1128 mg (86%), a colorless liquid. Isomeric ratio i/n = 1/50.

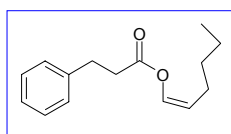
**$^1H$ -NMR** (300.1 MHz,  $CDCl_3$ , 25 °C, TMS):  $\delta$  = 0.94 (t, 3H,  $^3J$  = 6.80 Hz), 1.42-1.32 (m, 4H), 2.31-2.23 (m, 2H), 2.32 (s, 1H), 5.01 (dd, 1H,  $^3J$  = 6.50 and 7.38 Hz), 7.21 (d, 1H,  $^3J$  = 6.50 Hz), 7.45 (d, 1H,  $^3J$  = 4.03 Hz), 7.56 (t, 1H,  $^3J$  = 3.81 and 4.03 Hz), 7.86 (s, 1H), 8.02 (d, 1H,  $^3J$  = 3.81 Hz) ppm.

**$^{13}C$ -NMR** (75.5 MHz,  $CDCl_3$ , 25 °C, TMS):  $\delta$  = 13.9; 21.0; 22.2; 24.3; 31.3; 115.3; 123.0; 126.8; 128.2; 129.6; 131.0; 134.0; 150.7; 162.7; 169.1 ppm.

**MS** (EI, 70 eV, Evaporation Temperature 35°C):  $m/z$  (%) = 262 (5.5,  $[M]^+$ ), 163 (100), 121 (58), 120 (4.2), 93 (12), 92 (7), 65 (7), 64 (4), 63 (2.6), 43 (9), 41 (2), 39 (3), 27 (1.5).

**HRMS** (EI): calcd for  $C_{15}H_{18}O_4$   $[M]^+$ : 262.120510, found: 262.120657.

9) **3-Phenyl-propionic acid hex-1-enyl ester (3-1j):**



This enol ester was obtained following the general procedure from phenylpropionic acid **3-2j** (750.9 mg, 5.00 mmol) and 1-hexyne **3-16a** (712  $\mu$ L, 6.50  $\mu$ mol) in toluene as solvent. Boiling point 120 °C/ 0.1 mbar. Yield: 859.6 mg (74%), a colorless liquid. Isomeric ratio i/n = 1/50.

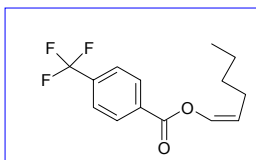
**$^1\text{H-NMR}$**  (300.1 MHz,  $\text{CDCl}_3$ , 25 °C, TMS):  $\delta$  = 0.90 (t, 3H,  $^3J$  = 6.70 Hz), 1.38-1.28 (m, 4H), 2.20-2.06 (m, 2H), 2.80 (t, 2H,  $^3J$  = 7.01 Hz), 3.22 (t, 2H,  $^3J$  = 7.01 Hz), 4.98 (dd, 1H,  $^3J$  = 6.50 and 7.33 Hz), 5.28 (s, 1H), 7.01 (t, 1H,  $^3J$  = 6.50 Hz), 7.20-7.01 (m, 5H) ppm.

**$^{13}\text{C-NMR}$**  (75.5 MHz,  $\text{CDCl}_3$ , 25 °C, TMS):  $\delta$  = 13.8; 22.1; 24.0; 31.1; 39.5; 53.4; 114.4; 126.1; 128.4; 140.2; 143.5; 170.0 ppm.

**MS** (EI, 70 eV, Evaporation Temperature 10°C):  $m/z$  (%) = 232 (8.5,  $[\text{M}]^+$ ), 150 (2.5), 133 (61.6), 131 (2), 105 (100), 104 (8), 103 (6), 91 (66), 79 (7), 78 (5), 57 (2.6), 55 (3), 51 (4), 41 (5), 39 (4), 29 (3), 27 (5).

**HRMS** (EI): calcd for  $\text{C}_{15}\text{H}_{20}\text{O}_2$   $[\text{M}]^+$ : 232.146330, found: 232.146501.

#### 10) 4-Trifluoromethyl-benzoic acid hex-1-enyl ester (**3-1k**):



This enol ester was obtained following the general procedure from trifluoromethylbenzoic acid **3-2a** (950.6 mg, 5.00 mmol) and 1-hexyne **3-16a** (712  $\mu$ L, 6.50 mmol) in toluene as solvent. Boiling point 120 °C/ 0.1 mbar. Yield: 1062 mg (78%), a colorless liquid. Isomeric ratio i/n = 1/50.

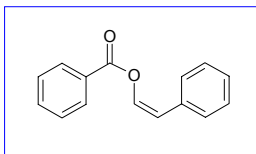
**$^1\text{H-NMR}$**  (300.1 MHz,  $\text{CDCl}_3$ , 25 °C, TMS):  $\delta$  = 0.91 (t, 3H  $^3J$  = 7.12 Hz), 1.46-1.33 (m, 4H), 2.29-2.30 (m, 2H), 5.06 (dd, 1H,  $^3J$  = 6.44 and 7.36 Hz), 7.23 (d, 1H,  $^3J$  = 6.44 Hz), 7.49 (d, 1H,  $^3J$  = 4.33 Hz), 8.18 (d, 1H,  $^3J$  = 4.33 Hz) ppm.

**$^{13}\text{C-NMR}$**  (75.5 MHz,  $\text{CDCl}_3$ , 25 °C, TMS):  $\delta$  = 13.8; 22.2; 24.3; 31.2; 115.6; 125.5; 125.6; 130.2; 130.5; 132.7; 134.0; 134.6; 135.0; 162.4 ppm.

**MS** (EI, 70 eV, Evaporation Temperature -10 °C):  $m/z$  (%) = 272 (3,  $[\text{M}]^+$ ), 253 (2), 173 (100), 145 (24), 126 (2), 125 (2), 95 (3), 82 (3), 41 (2), 27 (2).

**HRMS** (EI): calcd for  $C_{14}H_{15}F_3O_2$   $[M]^+$ : 272.102416, found: 272.102510.

**11) Benzoic acid-2-phenylvinyl ester (3-1n):**



This enol ester was obtained following the general procedure from benzoic acid **3-2a** (588 mg, 5.00 mmol) and phenylacetylene **3-16b** (714  $\mu$ L, 6.50 mmol) in toluene as solvent. Yield: 1100 mg (99%), a colorless liquid. Isomeric ratio i/n = 1/50.

**$^1H$ -NMR** (300.1 MHz,  $CDCl_3$ , 25°C, TMS):  $\delta$  = 5.28 (s, 1H), 5.86 (d, 1H,  $^3J$  = 7.12 Hz), 7.32 (d, 2H,  $^3J$  = 4.80 Hz), 7.46 (d, 2H,  $^3J$  = 4.66 Hz), 7.52-(m, 2H) ppm.

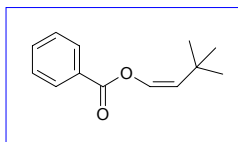
**$^{13}C$ -NMR** (75.5 MHz,  $CDCl_3$ , 25°C, TMS):  $\delta$  = 112.6; 127.3; 128.4; 128.5; 128.7; 128.9; 129.2; 130.1; 133.7; 134.1; 134.2; 163.4 ppm.

**MS** (EI, 70 eV, Evaporation Temperature 30°C): m/z (%) = 224 (10,  $[M]^+$ ), 105 (100), 90 (2), 89 (2), 77 (32), 51 (8), 50 (2), 39 (2).

**HRMS** (EI): calcd for  $C_{15}H_{12}O_2$   $[M]^+$ : 224.083730, found: 224.083619.

CAS Registry Number: [86846-84-6]

**12) Benzoic acid 3,3-dimethyl-but-1-enyl ester (3-1p):**



This enol ester was obtained following the general procedure from benzoic acid **3-2a** (588 mg, 5.00 mmol) and 3,3-dimethylbut-1-yne **3-16a** (750  $\mu$ L, 6.50 mmol) in Toluene as solvent. Boiling point 120 °C/ 0.1 mbar. Yield: 694.5 mg (68%), a colorless liquid. Isomeric ratio i/n = 1/50

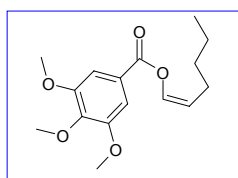
**<sup>1</sup>H-NMR** (300.1 MHz, CDCl<sub>3</sub>, 25 °C, TMS):  $\delta$  = 1.24 (s, 9H), 4.89 (d, 1H, <sup>3</sup>*J* = 6.66 Hz), 7.12 (d, 1H, <sup>3</sup>*J* = 6.66 Hz), 7.49 (t, 1H, <sup>3</sup>*J* = 3.45 and 4.01 Hz), 7.56 (d, 1H, <sup>3</sup>*J* = 3.45 Hz), 8.11 (d, 1H, <sup>3</sup>*J* = 4.01 Hz) ppm.

**<sup>13</sup>C-NMR** (75.5 MHz, CDCl<sub>3</sub>, 25 °C, TMS):  $\delta$  = 27.8; 30.6; 32.0; 123.8; 128.4; 128.8; 130.1; 133.2; 133.4; 134.5; 163.5 ppm.

**MS** (EI, 70 eV, Evaporation Temperature -6°C): *m/z* (%) = 204 (4.5, [M]<sup>+</sup>), 122 (1), 105 (100), 77 (21), 76 (1), 51 (5), 50 (1), 43 (1), 41 (2), 39 (1), 29 (1), 27 (1).

**HRMS** (EI): calcd for C<sub>13</sub>H<sub>16</sub>O<sub>2</sub> [M]<sup>+</sup>: 204.115030, found: 204.115117.

### 13) 3,4,5-Trimethoxy-benzoic acid hex-1-enyl ester.



This enol ester was obtained following the general procedure from trimethoxybenzoic acid (1061.0 mg, 5.00 mmol) and 1-hexyne **3-16a** (712  $\mu$ L, 6.50 mmol) in Toluene as solvent. Boiling point 150 °C/ 0.1 mbar. Yield: 1142 mg (98%), a colorless liquid. Isomeric ratio *i/n* = 1/50.

**<sup>1</sup>H-NMR** (300.1 MHz, CDCl<sub>3</sub>, 25 °C, TMS):  $\delta$  = 0.92 (t, 3H, <sup>3</sup>*J* = 6.72 Hz), 1.50-1.32 (m, 4H), 2.27-2.25 (m, 2H), 3.90 (s, 9H), 5.01 (dd, 1H, <sup>3</sup>*J* = 6.53 and 7.36 Hz), 7.22 (d, 1H, <sup>3</sup>*J* = 6.53 Hz), 7.34 (s, 2H) ppm.

**<sup>13</sup>C-NMR** (75.5 MHz, CDCl<sub>3</sub>, 25 °C, TMS):  $\delta$  = 13.8; 22.2; 24.3; 31.2; 56.2; 60.9; 67.6; 107.1; 114.8; 124.3; 134.3; 153.0 ppm.

**MS** (EI, 70 eV, Evaporation Temperature 40 °C): *m/z* (%) = 294 (6.5, [M]<sup>+</sup>), 195 (100), 167 (3), 152 (4.5), 137 (3), 122 (2.4), 109 (2), 81 (3), 77 (2.4), 66 (2.4), 53 (1.6).

**HRMS** (EI): calcd for C<sub>16</sub>H<sub>22</sub>O<sub>5</sub> [M]<sup>+</sup>: 294.146725, found: 294.146848.





## Bibliography

- [1] (a) S. Rozen, O. Lerman, "A New Approach towards the Synthesis and Chemistry of Fluoroxy Compounds." *J. Am. Chem. Soc.* **1979**, *101*, 2782-2784. (b) A. Wexler, R. J. Balchunis, J. S. Swenton, "A Photochemical Synthon for the 5-Uracil Carbanion. Application to the Direct Functionalization of Unprotected Uracils." *J. Chem. Soc., Chem. Commun.* **1975**, 601-602. (c) H. O. House, "Modern Synthetic Reactions", W. A. Benjamin, Ed., 2<sup>nd</sup> Edition, Menlo Park, CA, **1972**, page 313. (d) J. Tsuji, I. Minami, I. Shimizu, "Allylation of ketones via their enol acetates catalyzed by palladium-phosphine complexes and organotin compounds." *Tetrahedron Lett.* **1983**, *24*, 4713-4714.
- [2] C. Bruneau, M. Neveux, Z. Kabouche, C. Ruppin, P. H. Dixneuf, "Ruthenium-Catalysed Additions to Alkynes: Synthesis of Activated Esters and Their Use in Acylation Reactions." *Synlett* **1991**, 755-763.
- [3] T. Ema, S. Maeno, Y. Takaya, T. Sakai, M. Utaoka, "Kinetic Resolution of Racemic 2-Substituted 3-Cyclopenten-1-ols by Lipase-Catalyzed Transesterifications: A Rational Strategy To Improve Enantioselectivity." *J. Org. Chem.* **1996**, *61*, 8610-8616.
- [4] J. P. Monthéard, M. Camps, G. Seytre, J. Guillet, J. C. Dubois, "Propriétés des esters d'énols I. Polymérisation d'acétoxyalcènes et études diélectriques des polymères obtenus." *Angew. Makromol. Chem.* **1978**, *72*, 45-55.
- [5] (a) A. Demonceau, E. Saive, Y. de Froidmont, A. F. Noels, A. J. Hubert, "Olefin cyclopropanations reactions catalysed by novel ruthenacarborane clusters" *Tetrahedron Lett.* **1992**, *33*, 2009-2012. (b) W. B. Motherwell, L. R. Roberts, "A Practical Cyclopropanation Method using Direct Generation of Organozinc Carbenoids from Carbonyl Compounds." *J. Chem. Soc., Chem. Commun.* **1992**, 1582-1583.
- [6] (a) M. E. Jung, J. P. Hudspeth, "Anionic Oxy-Cope Rearrangements with Aromatic Substrates in Bicyclo[2.2.1]heptene Systems. Facile Synthesis of *cis*-Hydrindanone Derivatives, Including Steroid Analogues." *J. Am. Chem. Soc.* **1978**, *100*, 4309-4311. (b) L. F. Tietze, A. Montenbruck, C. Schneider, "De-Novo Synthesis of Enantiopure Carbohydrates: Preparation of Ethyl  $\beta$ -D- and  $\beta$ -L-Mannopyranosides by an Asymmetrically Induced Hetero Diels-Alder Reaction." *Synlett* **1994**, 509-510. (c) M. C. Pirrung, Y. R. Lee, "Dipolar

cycloaddition of rhodium carbenoids with vinyl esters. Total synthesis of pongamol and lanceolatin B.” *Tetrahedron Lett.* **1994**, 35, 6231-6234.

[7] K. E. Koenig, G. L. Bachman, B. D. Vineyard, “Asymmetric Hydrogenation of Geminal-Substituted Vinyl Acetates.” *J. Org. Chem.* **1980**, 45, 2362-2365.

[8] (a) N. Sakai, K. Nozaki, K. Mashima, H. Takaya, “Asymmetric Hydroformylation of Vinyl Acetate By Use of Chiral Bis(triarylphosphite)–Rhodium(I) Complexes.” *Tetrahedron: Asymmetry* **1992**, 3, 583-586. (b) C. G. Arena, F. Nicolo, D. Drommi, G. Bruno, F. Faraone, “Enantioselective Hydroformylation with the Chiral Bidentate *P,N*-Ligand 2-[1-(1*S*,2*S*,5*R*)-(–)menthoxydiphenylphosphino]pyridine Cationic Rhodium(I) Complexes.” *J. Chem. Soc., Chem. Commun.* **1994**, 2251-2252.

[9] (a) P. H. Dixneuf, C. Bruneau, S. Dérien, “Smart ruthenium catalysts for the selective catalytic transformations of alkynes.” *Pure Appl. Chem.* **1998**, 70, 1065-1070. (b) H. Doucet, C. Bruneau, P. H. Dixneuf, “Novel Two-Step Stereoselective Synthesis of (*E*)-Enamines and 1-Amino-1,3-dienes from Terminal Alkynes.” *Synlett* **1997**, 807-808.

[10] (a) D. S. Noyce, R. M. Pollack, “The Two Mechanisms for the Acid-Catalyzed Hydrolysis of Enol Acetates.” *J. Am. Chem. Soc.* **1969**, 91, 119-124. (b) S. D. Nelson, D. J. Kasparian, W. F. Trager, “The Reaction of  $\alpha$ -Nitro Ketones with the Ketene-Generating Compounds, Isopropenyl Acetate and  $\alpha$ -Acetoxystyrene. Synthesis of 3-Acetyl- and 3-Benzoyl-5-Substituted Isoxazoles.” *J. Org. Chem.* **1972**, 37, 2686-2688.

[11] M. Rotem, Y. Shvo, “Addition of Carboxylic Acids to Alkynes Catalyzed by Ruthenium Complexes. Vinyl Ester Formation.” *Organometallics* **1983**, 2, 1689-1691.

[12] (a) T. Mitsudo, Y. Hori, Y. Watanabe, “Selective Addition of Unsaturated Carboxylic Acids to Terminal Acetylenes Catalyzed by Bis( $\eta^5$ -cyclooctadienyl)ruthenium(II)–Tri-*n*-butylphosphine. A Novel Synthesis of Enol Esters.” *J. Org. Chem.* **1985**, 50, 1566-1568. (b) T. Mitsudo, Y. Hori, Y. Yamakawa, Y. Watanabe, “Ruthenium-Catalyzed Selective Addition of Carboxylic Acids to Alkynes. A Novel Synthesis of Enol Esters.” *J. Org. Chem.* **1987**, 52, 2230-2239.

[13] (a) H. Doucet, J. Höfer, C. Bruneau, P. H. Dixneuf, “Stereoselective Synthesis of *Z*-Enol Esters catalysed by [Bis(disphenylphosphino)alkane]bis(2-methylpropenyl)ruthenium Complexes.” *J. Chem. Soc., Chem. Commun.* **1993**, 850-851. (b) H. Doucet, B. Martin-Vanca,

C. Bruneau, P. H. Dixneuf, "General Synthesis of (*Z*)-Alk-1-en-1-yl Esters via Ruthenium-Catalyzed *anti*-Markovnikov *trans*-Addition of Carboxylic Acids to Terminal Alkynes." *J. Org. Chem.* **1995**, *60*, 7247-7255.

[14] (a) H. Doucet, N. Derrien, Z. Kabouche, C. Bruneau, P. H. Dixneuf, "Powerful control by organoruthenium catalysts of the regioselective addition to C(1) or C(2) of the prop-2-ynyl ethers C≡C triple bond." *J. Organomet. Chem.* **1997**, *551*, 151-157. (b) C. Bruneau, M. Neveux-Duflos, P. H. Dixneuf, "Utilization of an industrial feedstock without separation: Ruthenium-catalysed hydrocarboxylation of propadiene and propyne." *Green Chem.* **1999**, *1*, 183-185.

[15] (a) PhD Dissertation of Dr. Jens Paetzold, "Carbonsäuren als Startmaterialien in der Übergangsmetallkatalyse." Ruhr-Universität Bochum, **2004**. (b) L. J. Gooßen, J. Paetzold, D. Koley, "Regiocontrolled Ru-catalyzed addition of carboxylic acids to alkynes: practical protocols for the synthesis of vinyl esters." *Chem. Commun.* **2003**, *6*, 706-707.





## CHAPTER 8

## SUMMARY

DFT calculations have been performed for several transition-metal catalyzed reactions using the gradient-corrected BP86 functional and occasionally also the hybrid B3LYP functional. Our standard basis set was 6-31G\* combined with a small-core pseudopotential LANL2DZ basis for the transition metal. Single-point energy evaluations were done with a larger basis of triple- $\zeta$  quality, and bulk solvation effects were taken into account by the COSMO continuum model. Full catalytic cycles were computed, with complete optimization of all intermediates and transition states, followed by frequency analysis and – if necessary – by IRC calculations. In the following, we summarize the main results of these computational studies from a chemical point of view.

Concerning the mechanism of oxidative addition of aryl halides to palladium(0) complexes, we confirm the presence of three-coordinate anionic palladium(0) species as proposed by Amatore and Jutand, as a starting point for catalytic reactions. However we did not see any evidence for the existence of the proposed five-coordinate palladium(II) complexes (Chapter 2). Instead, we find a stable minimum for an entirely different structure, in which the aryl iodide linearly coordinates to palladium *via* the iodine atom. The formation of this linear, four-coordinate intermediate occurs without any significant energy barrier. From this adduct, there are two energetically feasible reaction pathways for the actual C—X cleavage, confirming that such hypervalent halide species may indeed be the initial intermediates formed in catalytic reactions. Both reaction pathways lead to the formation of *cis*-configured palladium(II) complexes. Since a subsequent *cis-trans* isomerization of these complexes to the isolable *trans* complexes requires significant energy, we consider catalytic cycles consisting solely of *cis*-configured intermediates to be favorable in palladium chemistry (Chapter 2).

The cross-coupling of phenylboronic acid with acetic anhydride may proceed *via* two mechanistically and energetically plausible catalytic cycles, using either the neutral  $\text{Pd}(\text{PMe}_3)_2$  or the anionic  $[\text{Pd}(\text{PMe}_3)_2\text{OAc}]^-$  complex as a starting point. The calculations show that both the neutral and anionic pathways give rise to *cis*-configured palladium(II) diphosphine intermediates in the oxidative addition step. They suggest that the higher catalytic activity of  $[\text{Pd}(\text{PMe}_3)_2\text{OAc}]^-$  arises from the ability to coordinate to carbon electrophiles. During the transmetalation process,

dissociation of one of the phosphine occurs which is consistent with experimental findings in related reactions (Chapter 3).

The same cross-coupling reaction can also be catalyzed by the two-coordinate anionic  $[\text{Pd}(\text{PMe}_3)\text{OAc}]^-$  complex. Multiple interconnected reaction pathways are considered that start from the neutral  $\text{Pd}(\text{PMe}_3)_2$  molecule, the two-coordinate anionic  $[\text{Pd}(\text{PMe}_3)\text{OAc}]^-$  complex, and the three-coordinate anionic  $[\text{Pd}(\text{PMe}_3)_2\text{OAc}]^-$  complex. Oxidative addition of acetic anhydride to either of the two anionic species leads to the formation of anionic palladium(II) monophosphine complexes with two acetate ligands oriented either *cis* or *trans* to each other. As a consequence, there are two competing anionic pathways for the transmetalation reaction with phenylboronic acid which involve only monophosphine complexes. Both pathways are energetically feasible, with a slight preference for the *cis*-variant. Overall, the anionic pathways are favored over the neutral pathways in our model system (Chapter 4).

After these mechanistic investigations on palladium-catalyzed cross-coupling reactions, the structural and electronic properties of Staab-type proton sponges and their palladium complexes are addressed. DFT calculations yield realistic geometries for both Alder-type and Staab-type proton sponges. In agreement with experiment the Staab-type proton sponges are computed to have higher proton affinities. Their extremely high basicity is rationalized in terms of the calculated strain energies and hydrogen-bond energies. The palladium(II) complexes of the Staab-type proton sponges are much more stable than the corresponding palladium(0) complexes (Chapter 5). The unusual out-of plane distortion of the proton sponge ligand is well reproduced in the palladium(II) complexes. The calculations predict an unsymmetrical geometry of palladium(0) complexes where the metal is coordinated to two nitrogen atoms and one additional carbon atom. The involvement of such palladium(0) complexes in Heck olefination reactions is supported by the computed relative energies of the intermediates in a plausible catalytic cycle (Chapter 5).

A previously proposed single-center, two-state kinetic model for olefin polymerization has been explored by considering different conformers and isomers of the propyl group in alkyl cations  $[\text{L}_2\text{Zr}-\text{Pr}]^+$  ( $\text{L} = \text{Cp}, \text{Cp}^*$ ;  $\text{Pr} = n\text{-propyl}$ ), corresponding to two catalysts with different observed rate orders ( $n$ ) for ethylene polymerization. For  $\text{L} = \text{Cp}$  ( $n \approx 1$ ), the  $\beta$ -agostic conformer is found to be the most stable structure and also the most reactive with respect to ethylene coordination, which is commensurate with unity rate order. For  $\text{L} = \text{Cp}^*$  ( $n \approx 1.4$ ), the favored propagation route involves the  $\gamma$ - and  $\alpha$ -agostic conformations of the alkyl complex, with coordination taking place to an  $\alpha$ -agostic conformation in order to minimize the steric hindrance experienced by the



incoming ethylene. The barriers to rearrangement from the  $\alpha$ - and  $\gamma$ -agostic conformers to the more stable  $\beta$ -agostic structure are significantly lower than those of propagation. Moreover, no structure was found to be lower than the  $\beta$ -agostic conformer, and the latter thus takes the role of the resting state for both catalysts in the present study. Hence our calculations suggest that dormant, or “slow”, states originate from particularly stable configurations of catalyst—co-catalyst complexes, and not from the equilibria involving the alkyl groups as investigated here (Chapter 6).

In the experimental work on the Ru-catalyzed addition of carboxylic acids to terminal alkynes, novel and highly efficient catalysts have been developed which can undergo both the Markovnikov and *anti*-Markovnikov addition reactions. The catalysts are generated *in situ* from air- and water-stable compounds that are available commercially, at low cost. The availability of these catalysts facilitates the use of this elegant transformation in chemical synthesis. The proposed catalytic cycle is supported by *in situ* ESI-MS measurements (Chapter 7).

**Publications based on this thesis:**

- [1] L. J. Gooßen, J. Paetzold, D. Koley, "Regiocontrolled Ru-catalyzed addition of carboxylic acids to alkynes: practical protocols for the synthesis of vinyl esters." *Chem. Commun.* **2003**, 706-707.
- [2] L. J. Gooßen, D. Koley, H. L. Hermann, W. Thiel, "The mechanism of the oxidative addition of aryl halides to Pd-catalysts: a DFT investigation." *Chem Commun.* **2004**, 2141-2143.
- [3] L. J. Gooßen, D. Koley, H. L. Hermann, W. Thiel, "Mechanistic pathways for oxidative addition of aryl halides to palladium(0) complexes: A DFT study." *Organometallics* **2005**, 24, 2398-2410.
- [4] L. J. Gooßen, D. Koley, H. L. Hermann, W. Thiel, "The palladium-catalyzed cross-coupling reaction of carboxylic anhydrides with arylboronic acids: a DFT study." *J. Am. Chem. Soc.* **2005**, ASAP article.
- [5] V. R. Jensen, D. Koley, M. N. Jagadeesh, W. Thiel, "DFT investigation of the single-center, two-state model for the broken rate order of transition metal catalyzed olefin polymerization." *Macromolecules* submitted.
- [6] L. J. Gooßen, D. Koley, H. L. Hermann, W. Thiel, "Palladium monophosphine intermediates in catalytic cross-coupling reactions: A DFT study." *J. Am. Chem. Soc.* submitted.





## **List of Abbreviations and Symbols**

---

COSMO	conductor-like screening model
CPCM	conductor-like polarized continuum mode
DFT	density functional theory
DMAP	dimethylamino pyridine
ECP	effective core potential
ESI-MS	electrospray ionization mass spectrometry
GGA	generalized gradient approximation
HF	Hartree-Fock
HOMO	highest occupied molecular orbital
IRC	intrinsic reaction coordinate
KS-MO	Kohn-Sham molecular orbital
LANL2DZ	Los Alamos double zeta basis
LCAO	linear combination of atomic orbitals
LDA	local density approximation
LST	linear synchronous transit
LUMO	lowest unoccupied molecular orbital
MAO	methylalumoxane
MEP	minimum energy path
NAO	natural atomic orbital
NBO	natural bond orbital
NHO	natural hybrid orbital
NMP	1-methylpyrrolidin-2-one
NPA	natural population analysis
PA	proton affinity
PCM	polarized continuum model
QST	quadratic synchronous transit
SCRF	self-consistent reaction field
SE	strain energy
STQN	synchronous transit-guided quasi-Newton
THF	tetrahydrofuran
TMA	trimethylaluminum
UAKS	united-atom Kohn-Sham

WBI	Wiberg bond indices
$H$	Hamiltonian
$\Psi$	molecular wavefunction
$\nabla^2$	$\partial^2/\partial x^2 + \partial^2/\partial y^2 + \partial^2/\partial z^2$ ('del-squared')
$H^{core}$	core Hamiltonian operator
$F$	Fock operator
$J_i$	Coulomb operator
$K_i$	exchange operator
$S$	overlap matrix
$F$	Fock matrix
$\mu$	Lagrange multiplier
$r_{ij}$	distance between two particles i and j
$P$	density matrix
$\alpha, \beta$	spin functions ('spin up' and 'spin down')

---

**Conversion factors for energy units.**

Name of unit		Conversions	
Hartree	1 E <sub>h</sub>	≈ 2625.5 kJ/mol	≈ 627.5 kcal/mol
Electronvolt	1 eV	≈ 96.5 kJ/mol	≈ 23.1 kJ/mol
Kilojoule per mole	1 kJ/mol	≈ 1.036 × 10 <sup>-2</sup> eV	≈ 4.18 kcal/mol
Kilocalorie per mole	1 kcal/mol	≈ 4.336 × 10 <sup>-2</sup> eV	≈ 0.239 kJ/mol

---







## ERKLÄRUNG

Hiermit erkläre ich, Debasis Koley, geboren am 08.09.1977 in Uttarpara, dass ich diese Arbeit eigenständig verfasst und ohne unerlaubte Hilfe angefertigt und diese in der vorgelegten oder ähnlichen Form noch keiner anderen Institution eingereicht habe.

Mülheim an der Ruhr, den 26.07.2005



---



